

ABSTRACT AND Applied Analysis

SCALING, SELF-SIMILARITY, AND SYSTEMS OF FRACTIONAL ORDER

GUEST EDITORS: CARLO CATTANI, MARTIN EHLER, MING LI, ZHIWU LIAO,
AND MOHAMMADREZA HOOSHMANDASL





Scaling, Self-Similarity, and Systems of Fractional Order

Abstract and Applied Analysis

Scaling, Self-Similarity, and Systems of Fractional Order

Guest Editors: Carlo Cattani, Martin Ehler, Ming Li, Zhiwu Liao, and Mohammadreza Hooshmandasl



Copyright © 2014 Hindawi Publishing Corporation. All rights reserved.

This is a special issue published in "Abstract and Applied Analysis." All articles are open access articles distributed under the Creative Commons Attribution License, which permits unrestricted use, distribution, and reproduction in any medium, provided the original work is properly cited.

Editorial Board

- Ravi P. Agarwal, USA
Bashir Ahmad, KSA
M. O. Ahmedou, Germany
Nicholas D. Alikakos, Greece
Debora Amadori, Italy
Pablo Amster, Argentina
Douglas R. Anderson, USA
Jan Andres, Czech Republic
Giovanni Anello, Italy
Stanislav Antontsev, Portugal
Mohamed Kamal Aouf, Egypt
Narcisa C. Apreutesei, Romania
Natig M. Atakishiyev, Mexico
Ferhan M. Atici, USA
Ivan G. Avramidi, USA
Soohyun Bae, Korea
Chuanzhi Bai, China
Zhanbing Bai, China
D. Baleanu, Turkey
Józef Banaś, Poland
Gerassimos Barbatis, Greece
Martino Bardi, Italy
Roberto Barrio, Spain
Feyzi Başar, Turkey
Abdelghani Bellouquid, Morocco
Daniele Bertaccini, Italy
Lucio Boccardo, Italy
Igor Boglaev, New Zealand
Martin J. Bohner, USA
Geraldo Botelho, Brazil
Elena Braverman, Canada
Romeo Brunetti, Italy
Janusz Brzdek, Poland
Detlev Buchholz, Germany
Sun-Sig Byun, Korea
Fabio M. Camilli, Italy
Jinde Cao, China
Anna Capietto, Italy
Jianqing Chen, China
Wing-Sum Cheung, Hong Kong
Michel Chipot, Switzerland
Changbum Chun, Korea
Soon Y. Chung, Korea
Jaeyoung Chung, Korea
Silvia Cingolani, Italy
- Jean M. Combes, France
Monica Conti, Italy
Diego Córdoba, Spain
Juan Carlos Cortes, Spain
Graziano Crasta, Italy
Bernard Dacorogna, Switzerland
Vladimir Danilov, Russia
Mohammad T. Darvishi, Iran
Luis Pinheiro de Castro, Portugal
T. Diagana, USA
Jesús I. Díaz, Spain
Josef Diblík, Czech Republic
Fasma Diele, Italy
Tomas Dominguez, Spain
Alexander Domoshnitsky, Israel
Marco Donatelli, Italy
Bo-Qing Dong, China
Ondřej Došlý, Czech Republic
Wei-Shih Du, Taiwan
Luiz Duarte, Brazil
Roman Dwilewicz, USA
Paul W. Eloe, USA
Ahmed El-Sayed, Egypt
Luca Esposito, Italy
Jose A. Ezquerro, Spain
Khalil Ezzinbi, Morocco
Dashan Fan, USA
Angelo Favini, Italy
Márcia Federson, Brazil
J. Fernandez Bonder, Argentina
S. Filippas, Equatorial Guinea
Alberto Fiorenza, Italy
Ilaria Fragala, Italy
Bruno Franchi, Italy
Xianlong Fu, China
Massimo Furi, Italy
Giovanni P. Galdi, USA
Isaac Garcia, Spain
Jesús García Falset, Spain
José A. García-Rodríguez, Spain
Leszek Gasinski, Poland
György Gát, Hungary
Vladimir Georgiev, Italy
Lorenzo Giacomelli, Italy
Jaume Giné, Spain
- Valery Y. Glizer, Israel
Laurent Gosse, Italy
Jean P. Gossez, Belgium
Jose L. Gracia, Spain
Maurizio Grasselli, Italy
Qian Guo, China
Yuxia Guo, China
Chaitan P. Gupta, USA
Uno Hämarik, Estonia
Ferenc Hartung, Hungary
Behnam Hashemi, Iran
Norimichi Hirano, Japan
Jiaxin Hu, China
Zhongyi Huang, China
Chengming Huang, China
Gennaro Infante, Italy
Ivan Ivanov, Bulgaria
Hossein Jafari, Iran
Jaan Janno, Estonia
Aref Jeribi, Tunisia
Un Cig Ji, Korea
Zhongxiao Jia, China
L. Jódar, Spain
Jong Soo Jung, Republic of Korea
Henrik Kalisch, Norway
Hamid Reza Karimi, Norway
Satyanad Kichenassamy, France
Tero Kilpeläinen, Finland
Sung Guen Kim, Republic of Korea
Ljubisa Kocinac, Serbia
Andrei Korobeinikov, Spain
Pekka Koskela, Finland
Victor Kovtunenکو, Austria
Ren-Jieh Kuo, Taiwan
Pavel Kurasov, Sweden
Mirosław Lachowicz, Poland
Kunquan Lan, Canada
Ruediger Landes, USA
Irena Lasiecka, USA
Matti Lassas, Finland
Chun-Kong Law, Taiwan
Ming-Yi Lee, Taiwan
Gongbao Li, China
Elena Litsyn, Israel
Yansheng Liu, China

Shengqiang Liu, China
Carlos Lizama, Chile
Milton C. Lopes Filho, Brazil
Julian López-Gómez, Spain
Guozhen Lu, USA
Jinhu Lü, China
Grzegorz Lukaszewicz, Poland
Shiwang Ma, China
Wanbiao Ma, China
Nazim I. Mahmudov, Turkey
Eberhard Malkowsky, Turkey
Salvatore A. Marano, Italy
Cristina Marcelli, Italy
Paolo Marcellini, Italy
Jesús Marín-Solano, Spain
Jose M. Martell, Spain
Mieczysław Mastły, Poland
Ming Mei, Canada
Taras Melnyk, Ukraine
Anna Mercaldo, Italy
Changxing Miao, China
Stanislaw Migorski, Poland
Mihai Mihăilescu, Romania
Feliz Minhós, Portugal
Dumitru Motreanu, France
Roberta Musina, Italy
G. M. N'Guérékata, USA
Maria Grazia Naso, Italy
Sylvia Novo, Spain
Micah Osilike, Nigeria
Mitsuharu Ôtani, Japan
Turgut Öziş, Turkey
Nikolaos S. Papageorgiou, Greece
Sehie Park, Korea
Alberto Parmeggiani, Italy
Kailash C. Patidar, South Africa
Kevin R. Payne, Italy
Ademir Fernando Pazoto, Brazil
Josip E. Pečarić, Croatia
Shuangjie Peng, China
Sergei V. Pereverzyev, Austria
Maria Eugenia Perez, Spain
Josefina Perles, Spain
Allan Peterson, USA
Andrew Pickering, Spain
Cristina Pignotti, Italy

Somyot Plubtieng, Thailand
Milan Pokorný, Czech Republic
Sergio Polidoro, Italy
Ziemowit Popowicz, Poland
Maria M. Porzio, Italy
Enrico Priola, Italy
Vladimir S. Rabinovich, Mexico
I. Rachůnková, Czech Republic
Maria Alessandra Ragusa, Italy
Simeon Reich, Israel
Abdelaziz Rhandi, Italy
Hassan Riahi, Malaysia
Juan P. Rincón-Zapatero, Spain
Luigi Rodino, Italy
Yuriy Rogovchenko, Norway
Julio D. Rossi, Argentina
Wolfgang Ruess, Germany
Bernhard Ruf, Italy
Marco Sabatini, Italy
Satit Saejung, Thailand
Stefan G. Samko, Portugal
Martin Schechter, USA
Javier Segura, Spain
Sigmund Selberg, Norway
Valery Serov, Finland
Naseer Shahzad, KSA
Andrey Shishkov, Ukraine
Stefan Siegmund, Germany
Abdel-Maksoud Soliman, Egypt
Pierpaolo Soravia, Italy
Marco Squassina, Italy
Svatoslav Staněk, Czech Republic
Stevo Stević, Serbia
Antonio Suárez, Spain
Wenchang Sun, China
Robert Szalai, UK
Sanyi Tang, China
Chun-Lei Tang, China
Youshan Tao, China
Gabriella Tarantello, Italy
Nasser-eddine Tatar, KSA
Gerd Teschke, Germany
Bevan Thompson, Australia
Sergey Tikhonov, Spain
Claudia Timofte, Romania
Thanh Tran, Australia

Juan J. Trujillo, Spain
Gabriel Turinici, France
Milan Tvrđy, Czech Republic
Mehmet Ünal, Turkey
Csaba Varga, Romania
Carlos Vazquez, Spain
Jesus Vigo-Aguiar, Spain
Yushun Wang, China
Qing-Wen Wang, China
Shawn X. Wang, Canada
Youyu Wang, China
Jing Ping Wang, UK
Peixuan Weng, China
Noemi Wolanski, Argentina
Ngai-Ching Wong, Taiwan
Patricia J. Y. Wong, Singapore
Yonghong Wu, Australia
Zili Wu, China
Shanhe Wu, China
Tie-cheng Xia, China
Xu Xian, China
Yanni Xiao, China
Gongnan Xie, China
Fuding Xie, China
Naihua Xiu, China
Daoyi Xu, China
Xiaodong Yan, USA
Zhenya Yan, China
Norio Yoshida, Japan
Beong In Yun, Korea
Vjacheslav Yurko, Russia
Agacik Zafer, Turkey
Jianming Zhan, China
Meirong Zhang, China
Chengjian Zhang, China
Weinian Zhang, China
Zengqin Zhao, China
Sining Zheng, China
Tianshou Zhou, China
Yong Zhou, China
Qiji J. Zhu, USA
Chun-Gang Zhu, China
Malisa R. Zizovic, Serbia
Wenming Zou, China

Contents

Scaling, Self-Similarity, and Systems of Fractional Order, Carlo Cattani, Martin Ehler, Ming Li, Zhiwu Liao, and Mohammadreza Hooshmandasl
Volume 2014, Article ID 843018, 2 pages

ε -Coverings of Hölder-Zygmund Type Spaces on Data-Defined Manifolds, Martin Ehler and Frank Filbir
Volume 2014, Article ID 402918, 6 pages

Linear Total Variation Approximate Regularized Nuclear Norm Optimization for Matrix Completion, Xu Han, Jiasong Wu, Lu Wang, Yang Chen, Lotfi Senhadji, and Huazhong Shu
Volume 2014, Article ID 765782, 8 pages

Applying Data Clustering Feature to Speed Up Ant Colony Optimization, Chao-Yang Pang, Ben-Qiong Hu, Jie Zhang, Wei Hu, and Zheng-Chao Shan
Volume 2014, Article ID 545391, 8 pages

Nonrigid Registration of Monomodal MRI Using Linear Viscoelastic Model, Jian Yang, Yang Chen, Jingfan Fan, and Songyuan Tang
Volume 2014, Article ID 792194, 8 pages

A New Definition of Fractional Derivatives Based on Truncated Left-Handed Grünwald-Letnikov Formula with $0 < \alpha < 1$ and Median Correction, Zhiwu Liao
Volume 2014, Article ID 914386, 9 pages

Theory Analysis of Left-Handed Grünwald-Letnikov Formula with $0 < \alpha < 1$ to Detect and Locate Singularities, Shaoxiang Hu and Ping Liang
Volume 2014, Article ID 157542, 7 pages

Mathematical Models Arising in the Fractal Forest Gap via Local Fractional Calculus, Chun-Ying Long, Yang Zhao, and Hossein Jafari
Volume 2014, Article ID 782393, 6 pages


A Discretized Tikhonov Regularization Method for a Fractional Backward Heat Conduction Problem, Zhi-Liang Deng and Xiao-Mei Yang
Volume 2014, Article ID 964373, 12 pages

Construction of Fusion Frame Systems in Finite Dimensional Hilbert Spaces, Jinsong Leng and Tingzhu Huang
Volume 2014, Article ID 836731, 9 pages

Similarity Solution for Fractional Diffusion Equation, Jun-Sheng Duan, Ai-Ping Guo, and Wen-Zai Yun
Volume 2014, Article ID 548126, 5 pages

On the (p, q) th Relative Order Oriented Growth Properties of Entire Functions, Luis Manuel Sánchez Ruiz, Sanjib Kumar Datta, Tanmay Biswas, and Golok Kumar Mondal
Volume 2014, Article ID 826137, 8 pages

Local Fractional Z-Transforms with Applications to Signals on Cantor Sets, Kai Liu, Ren-Jie Hu, Carlo Cattani, Gong-Nan Xie, Xiao-Jun Yang, and Yang Zhao
Volume 2014, Article ID 638648, 6 pages



Nonlinear Methodologies for Identifying Seismic Event and Nuclear Explosion Using Random Forest, Support Vector Machine, and Naive Bayes Classification, Longjun Dong, Xibing Li, and Gongnan Xie
Volume 2014, Article ID 459137, 8 pages

Hybrid Bernstein Block-Pulse Functions Method for Second Kind Integral Equations with Convergence Analysis, Mohsen Alipour, Dumitru Baleanu, and Fereshteh Babaei
Volume 2014, Article ID 623763, 8 pages

Picard Successive Approximation Method for Solving Differential Equations Arising in Fractal Heat Transfer with Local Fractional Derivative, Ai-Min Yang, Cheng Zhang, Hossein Jafari, Carlo Cattani, and Ying Jiao
Volume 2014, Article ID 395710, 5 pages

A Note on Certain Modular Equations about Infinite Products of Ramanujan, Hong-Cun Zhai
Volume 2013, Article ID 826472, 5 pages

On Local Fractional Continuous Wavelet Transform, Xiao-Jun Yang, Dumitru Baleanu, H. M. Srivastava, and J. A. Tenreiro Machado
Volume 2013, Article ID 725416, 5 pages

Editorial

Scaling, Self-Similarity, and Systems of Fractional Order

Carlo Cattani,¹ Martin Ehler,² Ming Li,³ Zhiwu Liao,⁴ and Mohammadreza Hooshmandasl⁵

¹ *Department of Mathematics, University of Salerno, Via Giovanni Paolo II, 84084 Fisciano, Italy*

² *Faculty of Mathematics, University of Vienna, Oskar-Morgenstern-Platz 1, 1090 Vienna, Austria*

³ *Institute of Systems Science, East China Normal University, Shanghai 200241, China*

⁴ *Visual Computing and Virtual Reality Key Laboratory of Sichuan Province, Sichuan Normal University, Chengdu 610101, China*

⁵ *Faculty of Mathematics, Yazd University, Yazd, Iran*

Correspondence should be addressed to Carlo Cattani; ccattani@unisa.it

Received 3 August 2014; Accepted 3 August 2014; Published 31 August 2014

Copyright © 2014 Carlo Cattani et al. This is an open access article distributed under the Creative Commons Attribution License, which permits unrestricted use, distribution, and reproduction in any medium, provided the original work is properly cited.

Scaling (power-type) laws and self-similarity reveal some featuring properties of physical-chemical objects and can be easily noticed in nature. Moreover, also some mathematical abstract objects, such as nondifferentiable functions and fractals, enjoy scaling and self-similarity. Experimental data often show some characteristic power law and self-similarity. A self-similar (scaling) object repeats itself at different scales in space or time. The property of self-similarity gives us a better opportunity to study phenomena from all analytical and computational aspects.

Scale dependence and multiscale analysis are peculiar properties of some families of special functions and can be observed in nature. A continuous scale transformation from one scale to another implies a generalization and suitable extension of differential operator, as it happens with fractional derivatives.

Dynamical processes and systems of fractional order attract researchers from many areas of sciences and technologies, ranging from mathematics and physics to computer science. From analytical point of view, these kinds of problems often lead us to deal with the concepts of scales, fractals, and fractional operators. For instance, medical images nowadays play an essential role in detection and diagnosis of numerous diseases and a suitable scale-dependent interpretation of the images is a fundamental aspect of the clinical investigation. Nonlinear analysis of data, collected by modern devices, offers still unsolved analytical problems related to not only complex physics and abstract mathematical theories but also nonlinear science.

The focus of this special issue is on both the abstract mathematical models on scaling and self-similarity and the applied computations on those dynamical processes and systems of fractional order towards the applications in all aspects of theoretical and practical study in analysis.

Scaling and self-similarity characterize several mathematical topics:

- (1) self-similar analytical problems: scale-depending theoretical and applied analytical problems;
- (2) fractals, nondifferentiable functions: theoretical and applied analytical problems of fractal type;
- (3) $1/f$ process, fractional Brownian motion, fractional Gaussian noise, self-similar processes, long memory processes, heavy-tailed random processes, and power law systems;
- (4) fractional differential/integral equations, fractional operators: systems of fractional order;
- (5) complex systems, nonlinear processing;
- (6) wavelets;
- (7) scaling and self-similarity in applications by focusing on theoretical and analytical aspects arising, for example, in nonlinear analysis of data, image analysis, data science, and system science.

This special issue contains 17 papers.

In the category of scale-depending problems, fractals and self-similarity there are many papers devoted to interesting problem.

H. Zhai proposes some discussion on certain modular equations about infinite products of Ramanujan. The paper of J. Leng and T. Huang deals with the “*Construction of fusion frame systems in finite dimensional Hilbert spaces.*” The fractional order, in particular “*On the (p, q) th relative order oriented growth properties of entire functions,*” has been investigated in the paper of L. M. S. Ruiz et al. The convergence analysis of the numerical approximation of second kind integral equations by hybrid Bernstein block-pulse functions has been proposed by M. Alipour et al. The paper of C. Pang et al deals with the complex problem of “*Applying data clustering feature to speed up ant colony optimization.*”

In their paper, S. Hu, and P. Liang propose a smart model to detect and locate singularities by using the theory analysis of left-handed Grünwald-Letnikov formula with $0 < \alpha < 1$.

J. Yang et al. investigate the “*Nonrigid registration of monomodal MRI using linear viscoelastic model.*” The “*Linear total variation approximate regularized nuclear norm optimization for matrix completion*” has been discussed in the paper of X. Han et al. The “ *ε -coverings of Hölder-Zygmund type spaces on data defined manifolds*” are the main topics of the paper of M. Ehler and F. Filbir. In the paper of L. Dong et al., “*Nonlinear methodologies for identifying seismic event and nuclear explosion using random forest, support vector machine, and naive bayes classification*” are studied.

Several papers are dealing more specifically with fractional calculus-systems of fractional order.

Transforms within the theory of local fractional calculus are considered, respectively, in the paper of X. Yang et al. by focusing on the continuous wavelet transform and the paper of K. Liu et al. which is dealing with the “*Local fractional Z transforms with applications to signals on cantor sets.*”

Approximate solution of fractional differential equations is considered in the paper “*Picard successive approximation method for solving differential equations arising in fractal heat transfer with local fractional derivative*” proposed by A. Yang et al. and in the paper of J. Duan et al. dealing with the “*Similarity solution for fractional diffusion equation.*”

A new definition of fractional derivatives based on truncated left-handed Grünwald-Letnikov formula with $0 < \alpha < 1$ and median correction has been investigated by Z. Liao.

Z. Deng and X. Yang propose a “*Discretized Tikhonov regularization method for a fractional backward heat conduction problem.*”

Mathematical models arising in the fractal forest gap via local fractional calculus are studied in the paper of C. Long et al.

Of the 36 submissions, 17 papers are accepted in this special issue (with the acceptance rate being 47.2%). All papers are dealing with current problems in the topics; however, they are not an exhaustive representation of the area of fractional order systems where the concepts of scale, self-similarity, and fractional order interact. In all papers, the authors have focused on the main aspects of the theory and although they have proposed some solutions and models, most problems remain open, thus giving the opportunity to readers for further research and discussions in this field.

Acknowledgment

Thanks to the excellent authors' contributions, all of the key aspects raised have been addressed. The authors would also thank the reviewers in helping improvement of the papers and the publisher for continuous professional assistance. One editor (Ming Li) acknowledges the supports in part by the National Natural Science Foundation of China under the Project Grants nos. 61272402, 61070214, and 60873264.

Carlo Cattani

Martin Ehler

Ming Li

Zhiwu Liao

Mohammadreza Hooshmandasl

Research Article

ε -Coverings of Hölder-Zygmund Type Spaces on Data-Defined Manifolds

Martin Ehler¹ and Frank Filbir^{2,3}

¹ Department of Mathematics, University of Vienna, Oskar-Morgenstern-Platz 1, 1090 Vienna, Austria

² Faculty of Mathematics, Technische Universität München, Boltzmannstraße 3, 85748 Garching, Germany

³ Helmholtz Zentrum München, Ingolstädter Landstraße 1, 85764 Neuherberg, Germany

Correspondence should be addressed to Martin Ehler; martin.ehler@univie.ac.at

Received 13 February 2014; Accepted 19 May 2014; Published 17 June 2014

Academic Editor: Carlo Cattani

Copyright © 2014 M. Ehler and F. Filbir. This is an open access article distributed under the Creative Commons Attribution License, which permits unrestricted use, distribution, and reproduction in any medium, provided the original work is properly cited.

We first determine the asymptotes of the ε -covering numbers of Hölder-Zygmund type spaces on data-defined manifolds. Secondly, a fully discrete and finite algorithmic scheme is developed providing explicit ε -coverings whose cardinality is asymptotically near the ε -covering number. Given an arbitrary Hölder-Zygmund type function, the nearby center of a ball in the ε -covering can also be computed in a discrete finite fashion.

1. Introduction

Data processing in the digital era often deals with finitely many high-dimensional data chunks stemming from measurements that obey some continuous physical model. The implementation and numerical evaluation require estimates on the accuracy of the discretization with respect to the underlying model. As an elementary tool providing accuracy guarantees, we will address ε -coverings of some function spaces related to information theory and machine learning.

As a standard concept in discrete mathematics, the ε -covering number $n_\varepsilon(Y)$ is the minimal number of balls of radius ε that cover a compact metric space Y . An arbitrary element in Y can be represented by a nearby center preserving precision up to ε . As such, ε -coverings are also an integral part of approximation theory, especially if Y is some function space. Covering numbers capture the complexity of Y and the approximation aspects are used in many fields such as information theory, statistics, nonparametric density estimation, and machine learning. There are estimates on the asymptotics of the ε -covering numbers of the standard function spaces (cf. [1, 2]), but some fields such as machine learning involve data lying on some manifold, so that target functions are naturally defined on this manifold. To clarify the terminology, we consider smoothness spaces on manifolds as somewhat

nonstandard function spaces. It may be possible that the covering number of a function space on some compact Riemannian manifold can be assembled by covering numbers of standard function spaces on Euclidian spaces derived from the charts. However, it is also important to derive explicit ε -coverings whose cardinality is near the benchmark given by the ε -covering number. We believe that explicit coverings may be harder to construct using the charts due to interface problems, and therefore we will not pursue this direction and, instead, we will follow a more global approach.

In general, there is still demand for computing coverings of many discrete and continuous spaces [3]. As an important additional requirement, any covering of a function space needs to come with an algorithmic scheme to determine some function's nearby center in an effective manner. At first sight, the latter seems simple enough as we can take the center whose distance is minimal. However, determining the distance between two functions is eventually a continuous operation, and one is particularly interested in finite methods.

In this paper, we first determine the asymptotics of the ε -covering number for the unit ball of some Hölder-Zygmund type space $Y = \mathcal{C}^s(\mathbb{X})$ on an underlying smooth compact Riemannian manifold \mathbb{X} (without boundary and with nonnegative Ricci curvature). In fact, we determine the asymptotics of the metric entropy $\log_2(n_\varepsilon(Y))$, which is

the number of bits needed to enumerate the ε -covering (cf. [1]). Moreover, we compute an explicit ε -covering, such that

$$\frac{\log_2(\widehat{n}_\varepsilon)}{\log_2(n_\varepsilon)} \leq \left(1 + \log_2\left(\frac{1}{\varepsilon}\right)\right), \quad (1)$$

where \widehat{n}_ε is the cardinality of the constructed covering and \leq means that the left-hand side can be bounded by a generic constant times the right-hand side. Hence, our covering is optimal up to a logarithmic factor by means of the metric entropy. We allow the underlying manifold to be unknown in our scheme and, instead, to be represented through a finite sampling. This sampling must be chosen carefully and is the key to obtaining a finite scheme. The centers of our ε -covering can then be determined through a finite process, and we can measure any function's distance to these centers in a finite manner.

For constructions of ε -coverings on periodic smoothness spaces, for instance, we refer to [4, 5]. The concept of ε -entropy is also closely related to entropy numbers; see [6–8].

The outline of this paper is as follows. In Section 2 we introduce the setting, define the Hölder-Zygmund type space $\mathcal{E}^s(\mathbb{X})$, and determine the metric entropy for its unit ball. An explicit covering is computed in Section 3.

2. Covering Numbers for Hölder-Zygmund Type Spaces

We first fix the setting and list some technical assumptions used throughout the paper. Let $\mathbb{X} \subset \mathbb{R}^d$ be an α -dimensional compact and connected Riemannian manifold without boundary and with nonnegative Ricci curvature, geodesic distance ρ , and μ being the normalized Riemannian volume measure on \mathbb{X} ; $\{\varphi_k\}_{k=0}^\infty$ are the eigenfunctions of the Laplacian on \mathbb{X} , and $\{-\lambda_k^2\}_{k=0}^\infty$ are the corresponding eigenvalues arranged in nonincreasing order, so that $0 = \lambda_0 \leq \lambda_1 \leq \dots$. Readers who are not familiar with some terms from differential geometry that are used here may simply think of a “nice” manifold without boundary, such as the sphere, the real projective space, the (real) Grassmann manifold, or more generally compact homogeneous spaces. The above properties ensure certain estimates on the heat kernel on \mathbb{X} (see [9, 10]), which were used in a series of papers [9, 11–13] to develop approximation schemes for smooth functions on the manifold. Here, we will make use of those approximation schemes, but we will keep the technical details at a minimum level.

Let N be a positive integer and most of the time we will restrict ourselves to $N = 2^j$, where j is some nonnegative integer. The space of *diffusion polynomials* up to degree N is

$$\Pi_N := \text{span} \{\varphi_k : \lambda_k \leq N\}. \quad (2)$$

Later, we will use the fact that the above conditions imply the following estimate on the Christoffel function:

$$\sum_{\lambda_k \leq N} |\varphi_k(x)|^2 \asymp N^\alpha, \quad x \in \mathbb{X}, \quad N > 0 \quad (3)$$

(cf. [9–11]), so that integration and orthonormality yield $\dim(\Pi_N) \asymp N^\alpha$. Here, the symbol \asymp indicates that each side is bounded by a generic positive constant times the other side.

In traditional scenarios, the accuracy of approximation by polynomials is closely related to the smoothness of the function. Therefore, the accuracy of approximation itself is nowadays considered to be a measurement of smoothness. This viewpoint is particularly useful in our setting because defining smoothness in a classical manner would require more technical details. Here, we define the *Hölder-Zygmund type space* of order $s > 0$ by $\mathcal{E}^s(\mathbb{X}) = \{f \in L_\infty(\mathbb{X}) : \|f\|_{\mathcal{E}^s(\mathbb{X})} < \infty\}$, where its norm is given by

$$\|f\|_{\mathcal{E}^s(\mathbb{X})} := \|f\|_{L_\infty(\mathbb{X})} + \sup_{N \geq 1} N^s E(f, \Pi_N, L_\infty(\mathbb{X})), \quad (4)$$

with $E(f, \Pi_N, L_\infty(\mathbb{X})) := \inf_{g \in \Pi_N} \|f - g\|_{L_\infty(\mathbb{X})}$. Hence, $f \in L_\infty(\mathbb{X})$ is contained in the Hölder-Zygmund type space if and only if it can be approximated by Π_N at rate N^{-s} . Since the eigenfunctions $\{\varphi_k\}_{k=0}^\infty$ are known to be smooth and we consider the L_∞ -norm, each function in $\mathcal{E}^s(\mathbb{X})$ has a continuous representative and point evaluation makes sense. The unit ball in $\mathcal{E}^s(\mathbb{X})$ is denoted by $\overline{\mathcal{E}^s(\mathbb{X})} := \{f \in L_\infty(\mathbb{X}) : \|f\|_{\mathcal{E}^s(\mathbb{X})} \leq 1\}$. To compute its covering number, we first establish compactness. Since $\mathcal{E}^s(\mathbb{X})$ is not finite-dimensional, $\overline{\mathcal{E}^s(\mathbb{X})}$ is not compact in the Hölder-Zygmund type space, but we consider it as a subspace of $L_\infty(\mathbb{X})$.

Lemma 1. *The set $\overline{\mathcal{E}^s(\mathbb{X})}$ is compact in $L_\infty(\mathbb{X})$.*

The compactness of this embedding can be derived from (4) by abstract arguments involving Kolmogorov numbers (cf. [6]). Here, we provide a simple elementary proof for the sake of completeness.

Proof. We aim to verify that any sequence $(f_j)_{j=1}^\infty \subset \overline{\mathcal{E}^s(\mathbb{X})}$ must have an accumulation point in this set. Since each space Π_N is finite-dimensional, there are $g_{j,N} \in \Pi_N$, such that $\|f_j\|_{L_\infty(\mathbb{X})} + \sup_{N \geq 1} N^s \|f_j - g_{j,N}\|_{L_\infty(\mathbb{X})} \leq 1$. The latter implies that $\|g_{j,N}\|_{L_\infty(\mathbb{X})}$ is bounded for all j and N . Thus, there is $g_1 \in \Pi_1$ such that the subsequence $(g_{\pi_1(j),1})_{j=1}^\infty$ converges towards g_1 . For any $N = 1, 2, \dots$, we can recursively construct $g_N \in \Pi_N$ such that

$$g_{\pi_N(j),k} \longrightarrow g_k, \quad \forall k = 1, \dots, N, \quad (5)$$

and $(g_{\pi_N(j),k})_{n=1}^\infty$ is a subsequence of $(g_{\pi_{N-1}(j),k})_{n=1}^\infty$. For $N' \geq N$, this construction yields that $(g_{\pi_{N'}(j),N})_{j=1}^\infty$ is a subsequence of $(g_{\pi_N(j),N})_{j=1}^\infty$, so that we derive

$$\begin{aligned} \|g_N - g_{N'}\|_{L_\infty(\mathbb{X})} &= \lim_{n \rightarrow \infty} \|g_{\pi_{N'}(j),N} - g_{\pi_{N'}(j),N'}\|_{L_\infty(\mathbb{X})} \\ &\leq \lim_{n \rightarrow \infty} \|g_{\pi_{N'}(j),N} - f_{\pi_{N'}(j)}\|_{L_\infty(\mathbb{X})} \\ &\quad + \|f_{\pi_{N'}(j)} - g_{\pi_{N'}(j),N'}\|_{L_\infty(\mathbb{X})} \\ &\leq N^{-s} + N'^{-s}. \end{aligned} \quad (6)$$

Therefore, $(g_N)_{N=1}^\infty$ is a Cauchy sequence and, hence, converges towards some $g \in L_\infty(\mathbb{X})$. Standard calculations reveal that g is an accumulation point of $(f_j)_{j=1}^\infty$ and is contained in $\overline{\mathcal{E}^s}(\mathbb{X})$, which concludes the proof. \square

We can now derive the asymptotes of the ε -covering number of $\overline{\mathcal{E}^s}(\mathbb{X})$ in $L_\infty(\mathbb{X})$.

Theorem 2. *If $s > 0$ is fixed and $0 < \varepsilon \leq 1$, then*

$$\log_2 \left(n_\varepsilon \left(\overline{\mathcal{E}^s}(\mathbb{X}) \right) \right) \asymp \varepsilon^{-\alpha/s} \quad (7)$$

holds, where the generic constants do not depend on ε .

Analogous results can be derived for similar concepts such as different types of n -widths of functions spaces (cf. [14–16]). Theorem 2 and its proof are rather classical and can be derived from [17]. To guide the interested reader, we will provide the outline of the proof that is based on a general Banach space result and is also used in [18, Theorem 4.1]. Let X be a Banach space and let $\{\phi_k\}_{k=1}^\infty \subset X$ be a sequence of linearly independent elements whose linear span is dense in X , and define $X_k := \text{span}\{\phi_1, \dots, \phi_k\}$ with $X_0 = \{0\}$. Let $\{\delta_k\}_{k=0}^\infty$ be a nonincreasing sequence of positive numbers with $\lim_{k \rightarrow \infty} \delta_k = 0$. The full approximation space is

$$\begin{aligned} \mathcal{A} \left(X; \{\delta_k\}_{k=0}^\infty, \{\phi_k\}_{k=1}^\infty \right) \\ := \{f \in X : E(f, X_k, X) \leq \delta_k, \text{ for } k = 0, 1, \dots\}. \end{aligned} \quad (8)$$

A proof similar to Lemma 1 yields that this space is compact, and we can formulate the result from Banach space theory that goes back to Lorentz in [17].

Theorem 3 (see [19, Theorem 3.3]). *Let $\{\delta_k\}_{k=0}^\infty$ be a nonincreasing sequence of positive numbers such that $\delta_{2k} \leq c\delta_k$, for $k = 1, 2, \dots$ and some constant $c \in (0, 1)$. For $\ell \geq 0$, let $M_\ell := \min\{k : \delta_k \leq e^{-\ell}\}$. If n_ε denotes the ε -covering number of $\mathcal{A}(X; \{\delta_k\}_{k=0}^\infty, \{\phi_k\}_{k=1}^\infty)$ in X , then one has, for $0 < \varepsilon \leq 1$,*

$$\log_2(n_\varepsilon) \asymp \sum_{\ell=1}^L M_\ell, \quad (9)$$

where $L := 2 + \lceil \log(1/\varepsilon) \rceil$.

At this point our preparations are complete.

Proof of Theorem 2. We aim to apply Theorem 3 with the function system $\{\varphi_k\}_{k=0}^\infty$ and with X being the closure of $\bigcup_{N=1}^\infty \Pi_N$ in $L_\infty(\mathbb{X})$. There, the index set is supposed to start with $k = 1$, so we set $\phi_k = \varphi_{k-1}$, $k = 1, 2, \dots$. To define the sequence $\{\delta_k\}_{k=0}^\infty$, we need some preparations. As pointed out before, integrating (3) over \mathbb{X} yields $\dim(\Pi_N) \asymp N^\alpha$. By using $X_k := \text{span}\{\varphi_0, \dots, \varphi_{k-1}\}$, we derive, for $N^\alpha \leq k \leq (2N)^\alpha$,

$$(2N)^s E(f, \Pi_{2N}, X) \leq k^{s/\alpha} E(f, X_k, X) \leq N^s E(f, \Pi_N, X). \quad (10)$$

Therefore, there are constants $C_i \geq 1$, for $i = 1, 2$, such that the definitions $\delta_{1;0} = 1/2$, $\delta_{1;k} := (2C_1)^{-1} k^{-s/\alpha}$, and $\delta_{2;0} = C_2$, $\delta_{2;k} := C_2 k^{-s/\alpha}$, lead to

$$\begin{aligned} \mathcal{A} \left(X; \{\delta_{1;k}\}_{k=0}^\infty, \{\phi_k\}_{k=1}^\infty \right) \\ \subset \overline{\mathcal{E}^s}(\mathbb{X}) \subset \mathcal{A} \left(X; \{\delta_{2;k}\}_{k=0}^\infty, \{\phi_k\}_{k=1}^\infty \right), \end{aligned} \quad (11)$$

which also yields

$$\begin{aligned} n_\varepsilon \left(\mathcal{A} \left(X; \{\delta_{1;k}\}_{k=0}^\infty, \{\phi_k\}_{k=1}^\infty \right) \right) \\ \leq n_\varepsilon \left(\overline{\mathcal{E}^s}(\mathbb{X}) \right) \leq n_\varepsilon \left(\mathcal{A} \left(X; \{\delta_{2;k}\}_{k=0}^\infty, \{\phi_k\}_{k=1}^\infty \right) \right). \end{aligned} \quad (12)$$

Since $\delta_{i;2k} \leq c\delta_{i;k}$, for $c := 2^{-s/\alpha} \in (0, 1)$, we can apply Theorem 3. According to [18, Lemma 4.1], $\sum_{\ell=1}^L M_\ell \asymp e^{L\alpha/s}$, so that the choice of L in (9) implies (7). \square

Remark 4. The proof of Theorem 2 discovers that (7) also holds under much weaker conditions, and we have only used the fact that there is a sequence of linearly independent functions $\{\varphi_k\}_{k=0}^\infty$, so that the polynomial spaces in (2) satisfy $\dim(\Pi_N) \asymp N^\alpha$.

3. Near Optimal Covering

This section is dedicated to constructing our covering of the unit ball in the Hölder-Zygmund type space, which is based on localized summation kernels as developed in a series of papers [9, 11–13]. We first need some preparations. A Borel probability measure ν on \mathbb{X} is called a *quadrature measure* of order N if

$$\int_{\mathbb{X}} f(x) g(x) d\mu(x) = \int_{\mathbb{X}} f(x) g(x) d\nu(x), \quad \forall f, g \in \Pi_N. \quad (13)$$

Note that our setting yields that there is a constant $a > 0$ such that $f \cdot g \in \Pi_{aN}$ for all $f, g \in \Pi_N$ and all N (cf. [11, Theorem A.1]); see also [20] for homogeneous spaces. The existence of quadrature measures with finite support is proved for fairly general smooth Riemannian manifolds in [11], where a construction procedure is outlined. In fact, the support of ν can be chosen to be contained in any sufficiently dense finite sampling $\{x_\ell\}_{\ell=1}^m$ of \mathbb{X} , so that ν can be identified with $\{x_\ell\}_{\ell=1}^m$ and nonnegative weights $\{\omega_\ell\}_{\ell=1}^m$ satisfying $\nu(\{x_\ell\}) = \omega_\ell$. Examples on the sphere, for instance, are given in [21].

The results in [11] yield that we can even choose a sequence $(\nu_N)_{N=1}^\infty$ of quadrature measures of order N , respectively, such that $\#\text{supp}(\nu_N) \leq N^\alpha$. For the remaining part of the paper, we will suppose that this estimate holds and we define, for $N = 2^j$,

$$\sigma_N(f) := \int_{\mathbb{X}} f(y) K_N(\cdot, y) d\nu_N(y), \quad (14)$$

$$\text{where } K_N(x, y) = \sum_{k=0}^\infty h\left(\frac{\lambda_k}{N}\right) \varphi_k^*(y) \varphi_k(x),$$

where $h : \mathbb{R}_{\geq 0} \rightarrow \mathbb{R}$ is an infinitely often differentiable and nonincreasing function with $h(t) = 1$ for $t \leq 1/2$ and $h(t) = 0$ for $t \geq 1$. Although we will not explicitly use it in the present paper, we want to point out that many advantageous properties of σ_N are steered by the so-called localization of the kernel K_N ; that is, for fixed $S > \alpha$ and all $x \neq y$ with $N = 1, 2, \dots$,

$$|K_N(x, y)| \leq \frac{N^{\alpha-s}}{\rho(x, y)^S}. \quad (15)$$

See [12, 13]. Later, we will apply

$$\sup_{x \in \mathbb{X}} \int_{\mathbb{X}} |K_N(x, y)| d|\nu_N|(y) \leq 1 \quad (16)$$

(cf. [11]). Those estimates are used in [12, 13] to characterize the Hölder-Zygmund type smoothness by means of σ_N .

Theorem 5. *Assume that $(\nu_N)_{N=1}^\infty$ is a family of quadrature measures of order N , respectively. Then, for all $f \in \mathcal{C}^s(\mathbb{X})$, one has*

$$\|f - \sigma_N(f)\|_{L_\infty(\mathbb{X})} \leq N^{-s} \|f\|_{\mathcal{C}^s(\mathbb{X})}, \quad (17)$$

where the generic constants do not depend on N or f . On the other hand, if, for $f \in L_p(\mathbb{X})$, there are generic constants not depending on N such that $\|f - \sigma_N(f)\|_{L_\infty(\mathbb{X})} \leq N^{-s}$ holds, then $f \in \mathcal{C}^s(\mathbb{X})$.

Next, by using $h(\lambda_k/N)h(\lambda_k/2N) = h(\lambda_k/N)$ and applying the quadrature property of ν_N , a straightforward calculation yields

$$\sigma_N(f, x) = \int_{\mathbb{X}} \sigma_N(f, y) K_{2N}(x, y) d\nu_N(y). \quad (18)$$

For some fixed $S > 1$, we define the actual approximation by

$$\begin{aligned} \sigma_N^\circ(f, x) &:= \int_{\mathbb{X}} I_N(f, y) K_{2N}(x, y) d\nu_N(y), \\ \text{where } I_N(f, y) &= N^{-S} \lfloor N^S \sigma_N(f, y) \rfloor. \end{aligned} \quad (19)$$

In other words, we replace $\sigma_N(f, y)$ in (18) with a number on the grid $(1/N^S)\mathbb{Z}$. We define the following collection:

$$\mathcal{M}_{S,N} := \{\sigma_N^\circ(f) : f \in \overline{\mathcal{C}^s(\mathbb{X})}\}, \quad (20)$$

which induces a covering of $\overline{\mathcal{C}^s(\mathbb{X})}$ in $L_\infty(\mathbb{X})$.

Theorem 6. *For fixed $s > 0$ and $S > \max(1, s)$, one applies the discretization (19). Then, there is a constant $c > 0$ such that, for all $f \in \overline{\mathcal{C}^s(\mathbb{X})}$, $\|f - \sigma_N^\circ(f)\|_{L_\infty(\mathbb{X})} \leq cN^{-s}$ holds. Thus, for $cN^{-s} = \varepsilon \leq 1$, the collection $\mathcal{M}_{S,N}$ induces an ε -covering of $\overline{\mathcal{C}^s(\mathbb{X})}$ in $L_\infty(\mathbb{X})$. Its cardinality \hat{n}_ε satisfies*

$$\log_2(\hat{n}_\varepsilon) \leq \varepsilon^{-\alpha/s} (1 - \log_2(\varepsilon)), \quad (21)$$

where the generic constant does not depend on ε .

Proof of Theorem 6. The triangle inequality yields

$$\begin{aligned} \|f - \sigma_N^\circ(f)\|_{L_\infty(\mathbb{X})} &\leq \|f - \sigma_N(f)\|_{L_\infty(\mathbb{X})} \\ &\quad + \|\sigma_N(f, \nu_N) - \sigma_N^\circ(f)\|_{L_\infty(\mathbb{X})}. \end{aligned} \quad (22)$$

Since Theorem 5 implies $\|f - \sigma_N(f)\|_{L_\infty(\mathbb{X})} \leq N^{-s} \|f\|_{\mathcal{C}^s(\mathbb{X})} = N^{-s}$, we only need to take care of the term on the farmost right. The quantization (19) immediately yields

$$|\sigma_N(f, y) - I_N(f, y)| \leq N^{-s}, \quad \forall y \in \text{supp}(\nu_N), \quad (23)$$

so that (18) and (16) imply

$$\begin{aligned} \|\sigma_N(f) - \sigma_N^\circ(f)\|_{L_\infty(\mathbb{X})} &= \left\| \int_{\mathbb{X}} (\sigma_N(f, y) - I_N(f, y)) K_N(\cdot, y) d\nu_N(y) \right\|_{L_\infty(\mathbb{X})} \\ &\leq N^{-s} \leq N^{-s}. \end{aligned} \quad (24)$$

Hence, we have derived the estimate on $\|f - \sigma_N^\circ(f)\|_{L_\infty(\mathbb{X})}$.

To tackle (21), we apply (23), which yields

$$|I_N(f, y)| \leq \|\sigma_N(f)\|_{L_\infty(\mathbb{X})}. \quad (25)$$

According to [13, Theorem 5.1], $\|\sigma_N(f)\|_{L_\infty(\mathbb{X})} \leq \|f\|_{L_\infty(\mathbb{X})}$ holds. Since f is contained in the ball of radius 1, we see that

$$|I_N(f, y)| \leq 1. \quad (26)$$

Thus, the number of possible values of $I_N(f, y)$ for fixed y is at most $c_1 N^S$, where $c_1 \geq 1$ is a positive constant. Note that we can assume that $c_1 N^S \geq 1$ because, otherwise, $I_N(f, y)$ would be zero. Since $\#\text{supp}(\nu_N) \leq N^\alpha$, we have $\#\{I_N(f, y) : y \in \text{supp}(\nu_N)\} \leq N^\alpha$. Therefore, we have $\hat{n}_\varepsilon \leq (c_1 N^S)^{c_2 N^\alpha}$, for some positive constant c_2 . By using $cN^{-s} = \varepsilon \leq 1$, we obtain

$$\begin{aligned} \log_2(\hat{n}_\varepsilon) &= c_2 c^{\alpha/s} \varepsilon^{-\alpha/s} \log_2 \left(c_1 \left(\frac{c}{\varepsilon} \right)^{S/s} \right) \\ &\leq \varepsilon^{-\alpha/s} \log_2 \left(\frac{(c_1)^{S/s} c}{\varepsilon} \right) \\ &\leq \varepsilon^{-\alpha/s} \log_2 \left(\frac{(c_1/\varepsilon)^{S/s} c}{\varepsilon} \right) \\ &\leq \varepsilon^{-\alpha/s} \left(1 + \log_2 \left(\frac{1}{\varepsilon} \right) \right), \end{aligned} \quad (27)$$

which concludes the proof. \square

According to Theorems 2 and 6, the ε -covering number n_ε of $\overline{\mathcal{C}^s(\mathbb{X})}$ and the number \hat{n}_ε of ε -balls induced by $\mathcal{M}_{S,N}$ satisfy

$$\frac{\log_2(\hat{n}_\varepsilon)}{\log_2(n_\varepsilon)} \leq \left(1 + \log_2 \left(\frac{1}{\varepsilon} \right) \right). \quad (28)$$

Therefore, our scheme is optimal up to a logarithmic factor by means of the metric entropy.

Our results are also related to the field of manifold learning, in which a function must be reconstructed from finite training data (cf. [22–25]). When actually applying our scheme, we first acquire a set of samples $\{x_\ell\}_{\ell=1}^m$ sufficiently well covering \mathbb{X} and we also need the function values $\{f(x_\ell)\}_{\ell=1}^m$, which altogether build the training data. Next, we compute a quadrature measure ν_N for some maximal N such that $\text{supp}(\nu_N) \subset \{x_\ell\}_{\ell=1}^m$; see [11, 21] for an algorithm. Here, we need that the sample points $\{x_\ell\}_{\ell=1}^m$ are well distributed and larger N require more samples. An element in $\mathcal{M}_{S,N}$ that is ε -close to f is simply given by $\sigma_N^\circ(f)$, whose computation only requires knowledge of f and $\{\varphi_k : \lambda_k \leq N\}$ on the finite set $\text{supp}(\nu_N)$; see (14) and (19). In other words, we do not need to know the entire manifold but only the finite sampling of the training data $\{x_\ell\}_{\ell=1}^m$, the sampling of the target function $\{f(x_\ell)\}_{\ell=1}^m$, and, more delicately, the sampling of the eigenfunctions $\{\varphi_k(x_\ell) : \lambda_k \leq N, \ell = 1, \dots, m\}$ of the Laplacian. Those eigenfunctions, however, are not explicitly known except for few special cases, such as the sphere, projective space, the Grassmann manifold, and few more. Fortunately, approximation of those eigenfunctions is a common procedure in manifold learning. Computational schemes are based on the graph Laplacian to be built from the training data and, at least under suitable assumptions, converging towards the Laplacian on the manifold when the cardinality of the data increases (cf. [26–28] and references therein). Those schemes approximately sample the first few eigenfunctions on the training data. Thus, our proposed approach is indeed fully discrete and computationally feasible even if the eigenfunctions $\{\varphi_k\}_{k=0}^\infty$ are not explicitly known. In fact, the manifold itself can be unknown. As long as \mathbb{X} satisfies the theoretical assumptions, it is simply represented by means of a finite sample.

Remark 7. The technical assumptions on the manifold \mathbb{X} and the function system $\{\varphi_k\}_{k=0}^\infty$ imply certain estimates on the heat kernel on \mathbb{X} (see [9, 10]), mainly used to ensure that the localization property (15) holds (cf. [12, 13]). Our assumptions also imply the existence of quadrature measures ν_N and that $f \cdot g \in \Pi_{aN}$ for all $f, g \in \Pi_N$ and some constant $a > 0$. These items lead to the characterization of the Hölder-Zygmund type space by means of σ_N in Theorem 5. Moreover, the family $(\nu_N)_{N=1}^\infty$ can be chosen with finite support, in fact with $\#\text{supp}(\nu_N) \leq N^\alpha$ (cf. [11]). Theorem 5 and $\#\text{supp}(\nu_N) \leq N^\alpha$ are indeed the two main ingredients of the proof of our results in Theorem 6.

Remark 8. The reader familiar with the approximation scheme developed in [9, 11–13] may expect that the presented results can be generalized to a wider class of Besov spaces on metric spaces. This is indeed true but requires more technical details and does not lead to a fully discrete scheme in the end. Here, we intended to emphasize the main ideas by keeping technical details at a minimum level and to focus on the development of a fully discrete covering algorithm. The more general approach will be described elsewhere.

Conflict of Interests

The authors declare that there is no conflict of interests regarding the publication of this paper.

Acknowledgments

Martin Ehler has been funded by the Vienna Science and Technology Fund (WWTF) through Project VRG12-009. The research of Frank Filbir was partially funded by the Deutsche Forschungsgemeinschaft Grant FI 883/3-1. Both authors thank H. N. Mhaskar for many fruitful discussions.

References

- [1] A. N. Kolmogorov and V. M. Tihomirov, “ ε -entropy and ε -capacity of sets in function spaces,” *Uspekhi Matematicheskikh Nauk*, vol. 14, no. 2, pp. 3–86, 1959, English translation in American Mathematical Society, vol. 17, pp. 277–364, 1961.
- [2] A. G. Vituškin, *Theory of the Transmission and Processing of Information*, Pergamon, 1961.
- [3] A. Schürmann and F. Vallentin, “Computational approaches to lattice packing and covering problems,” *Discrete & Computational Geometry*, vol. 35, no. 1, pp. 73–116, 2006.
- [4] D. Dung, “Non-linear approximations using sets of finite cardinality or finite pseudo-dimension,” *Journal of Complexity*, vol. 17, no. 2, pp. 467–492, 2001.
- [5] V. N. Temlyakov, “Estimates for the asymptotic characteristics of classes of functions with bounded mixed derivative or difference,” *Proceedings of the Steklov Institute of Mathematics*, vol. 189, pp. 161–197, 1990.
- [6] B. Carl and I. Stephani, *Entropy, Compactness and the Approximation of Operators*, Cambridge University Press, Cambridge, UK, 1990.
- [7] D. E. Edmunds and H. Triebel, *Function Spaces, Entropy Numbers, Differential Operators*, vol. 120, Cambridge University Press, Cambridge, UK, 1996.
- [8] D. D. Haroske and H. Triebel, *Distributions, Sobolev Spaces, Elliptic Equations*, European Mathematical Society, 2008.
- [9] C. K. Chui and H. N. Mhaskar, “Smooth function extension based on high dimensional unstructured data,” *Mathematics of Computation*, 2013.
- [10] E. B. Davies, “ L^p spectral theory of higher-order elliptic differential operators,” *The Bulletin of the London Mathematical Society*, vol. 29, no. 5, pp. 513–546, 1997.
- [11] F. Filbir and H. N. Mhaskar, “Marcinkiewicz-Zygmund measures on manifolds,” *Journal of Complexity*, vol. 27, no. 6, pp. 568–596, 2011.
- [12] M. Maggioni and H. N. Mhaskar, “Diffusion polynomial frames on metric measure spaces,” *Applied and Computational Harmonic Analysis*, vol. 24, no. 3, pp. 329–353, 2008.
- [13] H. N. Mhaskar, “Eignets for function approximation on manifolds,” *Applied and Computational Harmonic Analysis*, vol. 29, no. 1, pp. 63–87, 2010.
- [14] D. Düng and T. Ullrich, “ n -widths and ε -dimensions for high-dimensional approximations,” *Foundations of Computational Mathematics*, vol. 13, no. 6, pp. 965–1003, 2013.
- [15] E. Novak, “Optimal recovery and n -widths for convex classes of functions,” *Journal of Approximation Theory*, vol. 80, no. 3, pp. 390–408, 1995.

- [16] A. Pinkus, *n-Widths in Approximation Theory*, Springer, Berlin, Germany, 1985.
- [17] G. G. Lorentz, "Metric entropy and approximation," *Bulletin of the American Mathematical Society*, vol. 72, pp. 903–937, 1966.
- [18] H. N. Mhaskar, "On the representation of smooth functions on the sphere using finitely many bits," *Applied and Computational Harmonic Analysis*, vol. 18, no. 3, pp. 215–233, 2005.
- [19] G. G. Lorentz, M. V. Golitschek, and Y. Makovoz, *Constructive Approximation, Advanced Problems*, Springer, New York, NY, USA, 1996.
- [20] D. Geller and I. Z. Pesenson, "Band-limited localized Parseval frames and Besov spaces on compact homogeneous manifolds," *Journal of Geometric Analysis*, vol. 21, no. 2, pp. 334–371, 2011.
- [21] Q. T. Le Gia and H. N. Mhaskar, "Localized linear polynomial operators and quadrature formulas on the sphere," *SIAM Journal on Numerical Analysis*, vol. 47, no. 1, pp. 440–466, 2009.
- [22] M. Belkin and P. Niyogi, "Semi-supervised learning on riemannian manifolds," *Machine Learning*, vol. 56, no. 1–3, pp. 209–239, 2004.
- [23] M. Belkin, P. Niyogi, and V. Sindhwani, "Manifold regularization: a geometric framework for learning from labeled and unlabeled examples," *Journal of Machine Learning Research*, vol. 7, pp. 2399–2434, 2006.
- [24] M. Gavish, B. Nadler, and R. R. Coifman, "Multiscale wavelets on trees, graphs and high dimensional data: theory and applications to semi supervised learning," in *Proceedings of the 27th International Conference on Machine Learning (ICML '10)*, pp. 367–374, June 2010.
- [25] A. D. Szlam, M. Maggioni, and R. R. Coifman, "Regularization on graphs with function-adapted diffusion processes," *Journal of Machine Learning Research*, vol. 9, pp. 1711–1739, 2008.
- [26] M. Belkin and P. Niyogi, "Convergence of Laplacian eigenmaps," in *Proceedings of the NIPS*, B. Schölkopf, J. C. Platt, and T. Hoffman, Eds., pp. 129–136, MIT Press, 2006.
- [27] B. Nadler, S. Lafon, R. R. Coifman, and I. G. Kevrekidis, "Diffusion maps, spectral clustering and Eigen functions of Fokker-Planck operators," in *Advances in Neural Information Processing Systems*, Y. Weiss, B. Schölkopf, and J. Platt, Eds., vol. 18, MIT Press, Cambridge, Mass, USA, 2006.
- [28] U. von Luxburg, M. Belkin, and O. Bousquet, "Consistency of spectral clustering," *The Annals of Statistics*, vol. 36, no. 2, pp. 555–586, 2008.

Research Article

Linear Total Variation Approximate Regularized Nuclear Norm Optimization for Matrix Completion

**Xu Han,^{1,2} Jiasong Wu,^{1,2,3,4} Lu Wang,^{2,3,4} Yang Chen,^{1,2,3}
Lotfi Senhadji,^{2,3,4} and Huazhong Shu^{1,2}**

¹ *Laboratory of Image Science and Technology, Southeast University, Nanjing 210096, China*

² *Centre de Recherche en Information Médicale Sino-français (CRIBs), France*

³ *INSERM, U1099, Rennes 35000, France*

⁴ *Université de Rennes 1, LTSI, Rennes 35042, France*

Correspondence should be addressed to Xu Han; xuhan@seu.edu.cn

Received 15 February 2014; Accepted 7 May 2014; Published 28 May 2014

Academic Editor: Zhiwu Liao

Copyright © 2014 Xu Han et al. This is an open access article distributed under the Creative Commons Attribution License, which permits unrestricted use, distribution, and reproduction in any medium, provided the original work is properly cited.

Matrix completion that estimates missing values in visual data is an important topic in computer vision. Most of the recent studies focused on the low rank matrix approximation via the nuclear norm. However, the visual data, such as images, is rich in texture which may not be well approximated by low rank constraint. In this paper, we propose a novel matrix completion method, which combines the nuclear norm with the local geometric regularizer to solve the problem of matrix completion for redundant texture images. And in this paper we mainly consider one of the most commonly graph regularized parameters: the total variation norm which is a widely used measure for enforcing intensity continuity and recovering a piecewise smooth image. The experimental results show that the encouraging results can be obtained by the proposed method on real texture images compared to the state-of-the-art methods.

1. Introduction

The problem of matrix completion, which can be seen as the extension of recently developed compressed sensing (CS) theory [1–3], plays an important role in the field of signal and image processing [4–11]. This problem occurs in many real applications in computer vision and pattern recognition, such as image inpainting [12, 13], video denoising [14], and recommender systems [15, 16]. Reconstruction algorithms for matrix completion have received much attention. Cai et al. [17] proposed an algorithm, namely, the singular value thresholding (SVT) algorithm for matrix completion and related nuclear norm minimization problems. In [18], a simple and fast singular value projection (SVP) algorithm for rank minimization with affine constraints is exploited. Keshavan et al. [19] dealt with the matrix completion based on singular value decomposition followed by local manifold optimization. In order to achieve a better approximation of the rank of matrix, Hu et al. [11] presented an approach based on the truncated nuclear norm regularization (TNNR), which is defined by the difference between the nuclear norm

and the sum of the largest few singular values. Since most of the existing matrix completion models aim to solve the low rank optimization via nuclear norm, we recall here this model. For an incomplete matrix $\mathbf{M} \in \mathbb{R}^{m \times n}$ of rank r , the model can be described as follows:

$$\min_{\mathbf{X}} \text{rank}(\mathbf{X}) \quad \text{s.t. } \mathbf{X}_{\Omega} = \mathbf{M}_{\Omega}, \quad (1)$$

where $\mathbf{X} \in \mathbb{R}^{m \times n}$ and $\mathbf{M}_{\Omega} = \mathbf{M}_{ij}$, $(i, j) \in \Omega$, and Ω is the set of locations corresponding to the observed entries.

Unfortunately, the rank minimization problem in (1) is an NP-hard one, so the following convex relaxation is widely used:

$$\min_{\mathbf{X}} \|\mathbf{X}\|_* \quad \text{s.t. } \mathbf{X}_{\Omega} = \mathbf{M}_{\Omega}, \quad (2)$$

where $\|\cdot\|_*$ is the nuclear norm given by

$$\|\mathbf{X}\|_* = \sum_{k=1}^{\min(m,n)} \sigma_k, \quad (3)$$

where σ_k denotes the k th largest singular value of \mathbf{X} .

In this paper, our objective is to exploit the intrinsic geometry of the data distribution and incorporate it as an additional regularization term to deal with the images which are rich in texture. The total variation (TV) norm has demonstrated its usefulness as a graph regularizer in the field of image processing, so we propose here a method that combines the nuclear norm with the linear TV approximate norm to solve the problem of matrix completion. We call it the linear total variation approximate regularized nuclear norm (LTVNN) minimization problem. This combination optimization problem will be solved by simple and efficient optimization scheme based on the alternating direction method of multipliers (ADMM) model [20, 21].

The paper is organized as follows. In the next section, we introduce the proposed LTVNN model and we describe the optimization schemes. In Section 3, we establish the convergence results for the iterations given in Section 2. Experimental results on a set of images are provided in Section 4. Finally, we draw some conclusions in Section 5.

2. Proposed Method

2.1. Some Preliminaries. The total variation along the vertical and horizontal directions can be described as

$$D_{j,k}^v(\mathbf{X}) = \begin{cases} \mathbf{X}_{j,k} - \mathbf{X}_{j+1,k}, & 1 \leq j < m \\ 0, & j = m, \end{cases} \quad (4)$$

$$D_{j,k}^h(\mathbf{X}) = \begin{cases} \mathbf{X}_{j,k} - \mathbf{X}_{j,k+1}, & 1 \leq k < n \\ 0, & k = n. \end{cases} \quad (5)$$

So the total variation of \mathbf{X} is the summation for the magnitude of the gradient of each pixel [22]:

$$\|\mathbf{X}\|_{\text{TV}} = \sum_{j,k} \sqrt{(D_{j,k}^v \mathbf{X})^2 + (D_{j,k}^h \mathbf{X})^2}. \quad (6)$$

And the equivalent total variation formula as follows:

$$\|\mathbf{X}\|_{\text{TV}} = \sum_{j,k} (|D_{j,k}^v \mathbf{X}| + |D_{j,k}^h \mathbf{X}|). \quad (7)$$

Here, we use the linear total variation approximate of (7) to approximate the second kind of total variation; that is,

$$\|\mathbf{X}\|_{\text{LTV}} = \sum_{j,k} ((D_{j,k}^v \mathbf{X})^2 + (D_{j,k}^h \mathbf{X})^2). \quad (8)$$

2.2. Proposed Model. As mentioned above, the key point of the proposed approach is the combination of the nuclear norm and the linear total variation approximate norm; therefore, the optimization problem is described as

$$\min_{\mathbf{X}} (1 - \gamma) \|\mathbf{X}\|_* + \gamma \|\mathbf{X}\|_{\text{LTV}} \quad \text{s.t. } \mathbf{X}_\Omega = \mathbf{M}_\Omega, \quad (9)$$

where $0 \leq \gamma \leq 1$ is a penalty parameter, $\|\mathbf{X}\|_*$ is the nuclear norm defined in (3), and $\|\mathbf{X}\|_{\text{LTV}}$ is linear total variation

norm approximate defined in (8), which can be reformulated as

$$\begin{aligned} \|\mathbf{X}\|_{\text{LTV}} &= \text{Tr} [(\mathbf{X} - \mathbf{X}\phi_1)(\mathbf{X} - \mathbf{X}\phi_1)^T] \\ &\quad + \text{Tr} [(\mathbf{X} - \phi_2\mathbf{X})(\mathbf{X} - \phi_2\mathbf{X})^T] \\ &= \|\mathbf{X} - \mathbf{X}\phi_1\|_F^2 + \|\mathbf{X} - \phi_2\mathbf{X}\|_F^2, \end{aligned} \quad (10)$$

where “Tr” means the trace of the matrix, $\|\cdot\|_F$ denotes the Frobenius norm of the matrix, and ϕ_1 and ϕ_2 are, respectively, the column and row transform matrix given by

$$\begin{aligned} \phi_1 &= \begin{bmatrix} 0 & 0 & 0 & \cdots & 0 \\ 1 & 0 & \cdots & 0 & 0 \\ 0 & 1 & 0 & 0 & 0 \\ \vdots & \vdots & \ddots & \vdots & \vdots \\ 0 & 0 & \cdots & 1 & 1 \end{bmatrix}_{n \times n}, \\ \phi_2 &= \begin{bmatrix} (m-1) \times (m-1) \\ 0 & 1 & 0 & \cdots & 0 \\ 0 & 0 & 1 & 0 & 0 \\ 0 & \vdots & \vdots & \ddots & \vdots \\ \vdots & 0 & 0 & \cdots & 1 \\ 0 & 0 & 0 & \cdots & 1 \end{bmatrix}_{m \times m}. \end{aligned} \quad (11)$$

So, the problem in (9) can be rewritten as

$$\begin{aligned} \min_{\mathbf{X}} (1 - \gamma) \|\mathbf{X}\|_* + \gamma \|\mathbf{X} - \mathbf{X}\phi_1\|_F^2 \\ + \gamma \|\mathbf{X} - \phi_2\mathbf{X}\|_F^2 \\ \text{s.t. } \mathbf{X}_\Omega = \mathbf{M}_\Omega. \end{aligned} \quad (12)$$

2.3. The Optimization Scheme. The alternating direction method of multipliers-ADMM [20, 21] is an efficient and scalable optimization model which exploits the structure of the optimization problem. In this section, we use ADMM to deal with the problem in (12), which can be reformulated as

$$\begin{aligned} \min_{\mathbf{X}, \mathbf{W}} (1 - \gamma) \|\mathbf{X}\|_* + \gamma \|\mathbf{W} - \mathbf{W}\phi_1\|_F^2 \\ + \gamma \|\mathbf{W} - \phi_2\mathbf{W}\|_F^2 \\ \text{s.t. } \mathbf{X} = \mathbf{W}, \quad \mathbf{W}_\Omega = \mathbf{M}_\Omega, \end{aligned} \quad (13)$$

where $\|\mathbf{W} - \mathbf{W}\phi_1\|_F^2$ and $\|\mathbf{W} - \phi_2\mathbf{W}\|_F^2$ are the indicator functions. The augmented Lagrange function of (13) is

$$\begin{aligned} \mathcal{L}(\mathbf{X}, \mathbf{Y}, \mathbf{W}, \lambda) &= (1 - \gamma) \|\mathbf{X}\|_* + \gamma \|\mathbf{W} - \mathbf{W}\phi_1\|_F^2 \\ &\quad + \gamma \|\mathbf{W} - \phi_2\mathbf{W}\|_F^2 + \frac{\lambda}{2} \|\mathbf{W} - \mathbf{X}\|_F^2 \\ &\quad + \text{Tr}(\mathbf{Y}^T(\mathbf{W} - \mathbf{X})), \end{aligned} \quad (14)$$

where $\lambda > 0$ is the penalty parameter and \mathbf{Y} is the multiplier. The solution can be obtained by incorporating the solutions

of each regularization problem separately which are defined as follows.

Row TV is as follows:

$$\begin{aligned} \mathcal{L}_R(\mathbf{X}\mathbf{R}, \mathbf{Y}\mathbf{R}, \mathbf{W}\mathbf{R}, \lambda) &= (1 - \gamma) \|\mathbf{X}\mathbf{R}\|_* + \gamma \|(\mathbf{W}\mathbf{R} - \phi_2 \mathbf{W}\mathbf{R})\|_F^2 \\ &\quad + \frac{\lambda}{2} \|\mathbf{W}\mathbf{R} - \mathbf{X}\mathbf{R}\|_F^2 + \text{Tr}(\mathbf{Y}\mathbf{R}^T (\mathbf{W}\mathbf{R} - \mathbf{X}\mathbf{R})), \end{aligned} \quad (15)$$

where $\mathbf{X}\mathbf{R}$ denotes the optimization result along the vertical direction of the total variation defined in (4).

Column TV is as follows:

$$\begin{aligned} \mathcal{L}_C(\mathbf{X}\mathbf{C}, \mathbf{Y}\mathbf{C}, \mathbf{W}\mathbf{C}, \lambda) &= (1 - \gamma) \|\mathbf{X}\mathbf{C}\|_* + \gamma \|(\mathbf{W}\mathbf{C} - \mathbf{W}\mathbf{C}\phi_1)\|_F^2 \\ &\quad + \frac{\lambda}{2} \|\mathbf{W}\mathbf{C} - \mathbf{X}\mathbf{C}\|_F^2 + \text{Tr}(\mathbf{Y}\mathbf{C}^T (\mathbf{W}\mathbf{C} - \mathbf{X}\mathbf{C})), \end{aligned} \quad (16)$$

where $\mathbf{X}\mathbf{C}$ denotes the optimization result along the horizontal direction of the total variation defined in (5).

We deal with column linear TV optimization problem in (16) by the following steps in each iteration.

Step 1 (initial setting). $\mathbf{X}\mathbf{C}_1 = \mathbf{M}_\Omega$, $\mathbf{W}\mathbf{C}_1 = \mathbf{X}\mathbf{C}_1$, $\mathbf{Y}\mathbf{C}_1 = \mathbf{X}\mathbf{C}_1$, with the tolerance ε .

Step 2 (computing $\mathbf{X}\mathbf{C}_{k+1}$). Fix $\mathbf{W}\mathbf{C}_k$ and $\mathbf{Y}\mathbf{C}_k$, and minimize (16) for obtaining $\mathbf{X}\mathbf{C}_{k+1}$ as

$$\begin{aligned} \mathbf{X}\mathbf{C}_{k+1} &= \arg \min_{\mathbf{X}} (1 - \gamma) \|\mathbf{X}\mathbf{C}\|_* + \gamma \|(\mathbf{W}\mathbf{C}_k - \mathbf{W}\mathbf{C}_k\phi_1)\|_F^2 \\ &\quad + \frac{\lambda}{2} \|\mathbf{W}\mathbf{C}_k - \mathbf{X}\mathbf{C}_k\|_F^2 + \text{Tr}(\mathbf{Y}\mathbf{C}_k^T (\mathbf{W}\mathbf{C}_k - \mathbf{X}\mathbf{C}_k)). \end{aligned} \quad (17)$$

Ignoring the constant terms, (17) can be rewritten as

$$\begin{aligned} \mathbf{X}\mathbf{C}_{k+1} &= \arg \min_{\mathbf{X}} (1 - \gamma) \|\mathbf{X}\mathbf{C}\|_* \\ &\quad + \frac{\lambda}{2} \left\| \mathbf{X}\mathbf{C} - \left(\mathbf{W}\mathbf{C}_k + \frac{1}{\lambda} \mathbf{Y}\mathbf{C}_k \right) \right\|_F^2. \end{aligned} \quad (18)$$

To solve (18), Cai et al. [17] introduce the soft-thresholding operator \mathcal{D}_τ which is defined as follows:

$$\begin{aligned} \mathcal{D}_\tau(\mathbf{X}) &:= \mathbf{U}\mathcal{D}_\tau(\Sigma)\mathbf{V}^T, \\ \mathcal{D}_\tau(\Sigma) &= \text{diag}\{\max(\sigma_i - \tau, 0)\}, \end{aligned} \quad (19)$$

where $t_+ = \max(0, t)$.

Using the operator \mathcal{D}_τ in (19), the solution of (18) can be obtained as

$$\mathbf{X}\mathbf{C}_{k+1} = \mathcal{D}_{(1-\gamma)/\lambda} \left(\mathbf{W}\mathbf{C}_k + \frac{1}{\lambda} \mathbf{Y}\mathbf{C}_k \right). \quad (20)$$

Step 3 (computing $\mathbf{W}\mathbf{C}_{k+1}$). Fix $\mathbf{X}\mathbf{C}_{k+1}$ and $\mathbf{Y}\mathbf{C}_k$ and calculate $\mathbf{W}\mathbf{C}_{k+1}$ as follows:

$$\mathbf{W}\mathbf{C}_{k+1} = \arg \min_{\mathbf{W}} \mathcal{L}(\mathbf{X}\mathbf{C}_{k+1}, \mathbf{Y}\mathbf{C}_k, \mathbf{W}\mathbf{C}, \lambda) \quad (21)$$

which is a quadratic function of $\mathbf{W}\mathbf{C}$ and can be easily solved by setting the derivation of $\mathcal{L}(\mathbf{X}\mathbf{C}_{k+1}, \mathbf{Y}\mathbf{C}_k, \mathbf{W}\mathbf{C}, \lambda)$ to zeros, and then we get

$$\begin{aligned} \mathbf{W}\mathbf{C}_{k+1} &= (\lambda \mathbf{X}\mathbf{C}_{k+1} - \mathbf{Y}\mathbf{C}_k) \\ &\quad \times [2\gamma(\mathbf{I} - \phi_1 - \phi_1^T + \phi_1^T \phi_1) + \lambda \mathbf{I}_{m \times n}]^{-1}. \end{aligned} \quad (22)$$

Then we fix the values at the observed entries:

$$\mathbf{W}\mathbf{C}_{k+1} = (\mathbf{W}\mathbf{C}_{k+1})_{\Omega_m} + \mathbf{M}_\Omega, \quad (23)$$

where Ω_m denotes the set of the missing entries.

Step 4 (computing $\mathbf{Y}\mathbf{C}_{k+1}$). Fix $\mathbf{X}\mathbf{C}_{k+1}$ and $\mathbf{W}\mathbf{C}_{k+1}$ and calculate $\mathbf{Y}\mathbf{C}_{k+1}$ as follows:

$$\mathbf{Y}\mathbf{C}_{k+1} = \mathbf{Y}\mathbf{C}_k + \lambda (\mathbf{W}\mathbf{C}_{k+1} - \mathbf{X}\mathbf{C}_{k+1}). \quad (24)$$

Until the stop condition: $\|\mathbf{X}\mathbf{C}_{k+1} - \mathbf{X}\mathbf{C}_k\|_F \leq \varepsilon$.

Row TV problem defined by (15) can be solved in a similar way to that of column TV problem. The only difference is the $\mathbf{W}\mathbf{R}_{k+1}$ in the second step, which is given by

$$\begin{aligned} \mathbf{W}\mathbf{R}_{k+1} &= [2\gamma(\mathbf{I} - \phi_2 - \phi_2^T + \phi_2^T \phi_2) + \lambda \mathbf{I}_{m \times m}]^{-1} \\ &\quad \times (\lambda \mathbf{X}\mathbf{R}_{k+1} - \mathbf{Y}\mathbf{R}_k). \end{aligned} \quad (25)$$

And the stop condition is $\|\mathbf{X}\mathbf{R}_{k+1} - \mathbf{X}\mathbf{R}_k\|_F \leq \varepsilon$.

Finally, we obtained \mathbf{X}_{k+1} as the average of $\mathbf{X}\mathbf{C}_{k+1}$ and $\mathbf{X}\mathbf{R}_{k+1}$; that is,

$$\mathbf{X}_{k+1} = \frac{\mathbf{X}\mathbf{C}_{k+1} + \mathbf{X}\mathbf{R}_{k+1}}{2}. \quad (26)$$

3. Convergence Analysis

In this section, we give the proof of the convergence of column total variation (16) and the convergence of row total variation is similar to the column total variation. Here, the objection function (16) about column variation is as follows:

$$\begin{aligned} \min_{\mathbf{X}} f_\tau(\mathbf{X}) \\ \text{s.t. } \mathbf{X}_\Omega = \mathbf{M}_\Omega \\ f_\tau(\mathbf{X}) = \tau \|\mathbf{X}\|_* + \frac{1}{2} \text{Tr}[(\mathbf{X} - \mathbf{X}\phi_1)(\mathbf{X} - \mathbf{X}\phi_1)^T], \\ \tau = \frac{1 - \gamma}{2\gamma}. \end{aligned} \quad (27)$$

Lemma 1. Let $\mathbf{Z} \in \partial f_\tau(\mathbf{X})$ and $\mathbf{Z}' \in \partial f_\tau(\mathbf{X}')$. Then

$$\langle \mathbf{Z} - \mathbf{Z}', \mathbf{X} - \mathbf{X}' \rangle \geq \|\mathbf{X} - \mathbf{X}'\|_F^2. \quad (28)$$

The details of the proof can be found in [17].



FIGURE 1: The recovered results with 60% random mask and word mask for $\gamma = 0, 0.5$ and 1 by LTVNN.

Theorem 2. Assuming that the sequence of step size obeys $0 < \inf \lambda_k < \sup \lambda_k < (2\alpha/\beta)$, $\alpha = \langle (\mathbf{X}^k - \mathbf{X}^*)(\mathbf{I} - \phi_1 - \phi_1^T + \phi_1\phi_1^T), \mathbf{X}^k - \mathbf{X}^* \rangle$ and $\beta = \|\mathbf{X}^k - \mathbf{X}^*\|_F^2$. Here, \mathbf{X}^* denotes the optimization result and \mathbf{X}^k denotes the k th iteration object variable; then by the iteration procedure defined in Section 2.3, we can obtain the unique optimization result, that is, \mathbf{X}^* . And the details of the proof can be found in the Appendix.

4. Experiments

In this section, we test the proposed method on a set of images. The algorithm was implemented with MATLAB programming language on a PC machine, which sets up

Microsoft Windows 7 operating system and has an Intel Core I5 CPU with speed of 2.79 GHz and 2 GB RAM.

We deal with three channels (r, g, b) of color images separately and combine the results together to get the final outcome. We use peak signal-to-noise ratio (PSNR) values to evaluate the performance:

$$\text{PSNR} = 10 \times \log_{10} \left(\frac{255^2}{\text{MSE}} \right), \quad (29)$$

where MSE denotes mean squared error,

$$\text{MSE} = \frac{1}{3mn} [\text{error}^2(r) + \text{error}^2(g) + \text{error}^2(b)]. \quad (30)$$

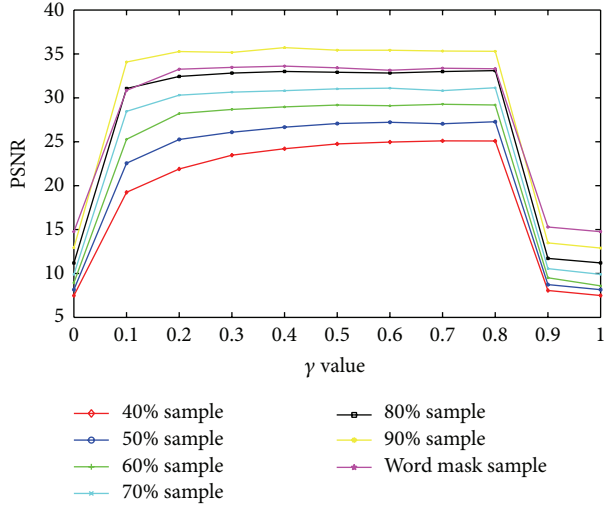


FIGURE 2: The recovered PSNR for Pepper under different random sample ratio and word mask sample with γ from 0 to 1 by LTVNN.

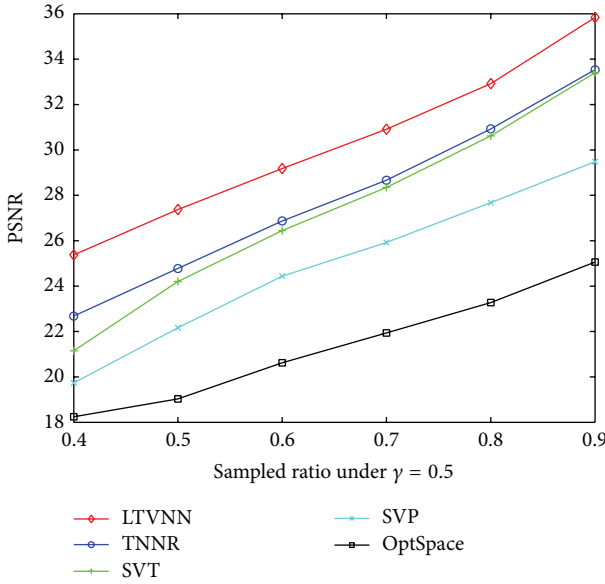


FIGURE 3: Recovered PSNR for Pepper under $\gamma = 0.5$ with different random sample ratio by LTVNN, TNNR, SVT, SVP, and OptSpace.

In the experiments, we consider two situations: random mask sample and word mask sample. Figure 1 describes the recovered results with 60% random mask and word mask for $\gamma = 0, 0.5$ and 1 by LTVNN. Figure 2 shows the recovered PSNR for Pepper under different random sample ratios and word mask sample for γ from 0 to 1 with step of 0.1 by LTVNN. It can be observed from these two figures that the best result is obtained for the value of γ near to 0.5, which corresponds to the case where the two norms (nuclear and LTV) are equivalently used in (9). For the two extreme cases: $\gamma = 0$ (only the nuclear norm is taken into consideration) and $\gamma = 1$ (only the linear total variation approximate norm is considered), the algorithm loses its efficiency.

We also compare our method (LTVNN) with other matrix completion methods including TNNR [10, 11], SVT [12], SVP [13], and OptSpace [14]. Figure 3 plots the recovered PSNR for Pepper for $\gamma = 0.5$ with different random sample ratios (from 40% to 90%) by LTVNN and other four methods (TNNR, SVT, SVP, and OptSpace). It can be seen from Figure 3 that the proposed LTVNN method achieves much higher PSNR than the other methods. Figure 4 shows the comparison of PSNR of recovered methods for Lena under word mask with $\gamma = 0.5$ by LTVNN and the other methods. Table 1 lists the PSNR results under word mask sample with $\gamma = 0.5$ for different images by LTVNN and the other methods. From Figure 4 and Table 1, we can see that the proposed method outperforms the other matrix completion methods under word mask for different images.

5. Conclusion

In this paper, we have proposed a new model that combines the nuclear norm and total variation norm for the matrix completion problem, which was then solved by ADMM model. Experimental results demonstrate the effectiveness of the proposed algorithm compared to other methods.

Appendix

Before we give the proof of Theorem 2, we supplement one proof about

$$\langle (\mathbf{X} - \mathbf{X}')(\mathbf{I} - \phi_1 - \phi_1^T + \phi_1\phi_1^T), \mathbf{X} - \mathbf{X}' \rangle \geq 0. \quad (\text{A.1})$$

Without loss of generality, we take an example matrix $\xi = (\mathbf{X} - \mathbf{X}') \in \mathbb{R}^{4 \times 4}$ and the corresponding transform matrix $(\mathbf{I} - \phi_1 - \phi_1^T + \phi_1\phi_1^T) = \begin{bmatrix} 2 & -1 & 0 & 0 \\ -1 & 2 & -1 & 0 \\ 0 & -1 & 2 & 0 \\ 0 & 0 & 0 & 0 \end{bmatrix}$. Then,

$$\begin{aligned} & \text{Tr} \left[(\mathbf{I} - \phi_1 - \phi_1^T + \phi_1\phi_1^T) \xi^T \xi \right] \\ &= 2 \left(\xi_{1,1}^2 + \xi_{2,1}^2 + \xi_{3,1}^2 + \xi_{4,1}^2 \right) \\ & \quad - (\xi_{1,1}\xi_{1,2} + \xi_{2,1}\xi_{2,2} + \xi_{3,1}\xi_{3,2} + \xi_{4,1}\xi_{4,2}) \\ & \quad + 2 \left(\xi_{1,2}^2 + \xi_{2,2}^2 + \xi_{3,2}^2 + \xi_{4,2}^2 \right) \\ & \quad - (\xi_{1,1}\xi_{1,2} + \xi_{2,1}\xi_{2,2} + \xi_{3,1}\xi_{3,2} + \xi_{4,1}\xi_{4,2}) \\ & \quad - (\xi_{1,2}\xi_{1,3} + \xi_{2,2}\xi_{2,3} + \xi_{3,2}\xi_{3,3} + \xi_{4,2}\xi_{4,3}) \\ & \quad + 2 \left(\xi_{1,3}^2 + \xi_{2,3}^2 + \xi_{3,3}^2 + \xi_{4,3}^2 \right) \\ & \quad - (\xi_{1,2}\xi_{1,3} + \xi_{2,2}\xi_{2,3} + \xi_{3,2}\xi_{3,3} + \xi_{4,2}\xi_{4,3}) \\ &= (\xi_{1,1}^2 + \xi_{2,1}^2 + \xi_{3,1}^2 + \xi_{4,1}^2) + (\xi_{1,1} - \xi_{1,2})^2 \\ & \quad + (\xi_{2,1} - \xi_{2,2})^2 + (\xi_{3,1} - \xi_{3,2})^2 + (\xi_{4,1} - \xi_{4,2})^2 \\ & \quad + (\xi_{1,2} - \xi_{1,3})^2 + (\xi_{2,2} - \xi_{2,3})^2 + (\xi_{3,2} - \xi_{3,3})^2 \\ & \quad + (\xi_{4,2} - \xi_{4,3})^2 + (\xi_{1,3}^2 + \xi_{2,3}^2 + \xi_{3,3}^2 + \xi_{4,3}^2) \\ & \geq 0, \end{aligned} \quad (\text{A.2})$$



FIGURE 4: Comparison of PSNR of recovered methods for Lena under word mask with $\gamma = 0.5$ by LTVNN, TNNR, SVT, SVP, and OptSpace.

TABLE 1: PSNR results under word mask sample with $\gamma = 0.5$ for different images by LTVNN, TNNR, SVT, SVP, and OptSpace.

	LTVNN	TNNR [10, 11]	SVT [12]	SVP [13]	OptSpace [14]
Mandrill (256 × 256)	29.495	27.845	27.736	18.881	26.264
Pepper (256 × 256)	33.421	31.019	30.188	23.648	27.141
Barbara (240 × 192)	31.170	29.261	29.352	22.901	23.427
Barbara (512 × 512)	32.680	30.682	28.855	22.113	26.872
Girl (256 × 256)	36.797	34.298	33.848	27.128	30.977
Couple (256 × 256)	36.916	35.176	35.241	29.649	32.815
Airplane (512 × 512)	31.883	30.083	25.506	19.573	26.222
House (256 × 256)	34.340	33.288	32.646	22.374	27.505
Sailboat (512 × 512)	30.858	29.103	27.079	26.778	20.891

so the term $\langle (\mathbf{X} - \mathbf{X}')(\mathbf{I} - \phi_1 - \phi_1^T + \phi_1\phi_1^T), \mathbf{X} - \mathbf{X}' \rangle \geq 0$. The proof of Theorem 2 is as follows.

Proof. Let $(\mathbf{X}^*, \mathbf{Y}^*)$ be primal-dual optimization for the problem (27). The optimality conditions give

$$\begin{aligned} \mathbf{0} &= \mathbf{Z}^k - \mathcal{P}_\Omega(\mathbf{Y}^{k-1}), \\ \mathbf{0} &= \mathbf{Z}^* - \mathcal{P}_\Omega(\mathbf{Y}^*), \end{aligned} \quad (\text{A.3})$$

where $\mathbf{Z}^k \in \partial f_\tau(\mathbf{X}^k)$ and $\mathbf{Z}^* \in \partial f_\tau(\mathbf{X}^*)$. Then from (A.3), we deduce that

$$(\mathbf{Z}^k - \mathbf{Z}^*) - \mathcal{P}_\Omega(\mathbf{Y}^{k-1} - \mathbf{Y}^*) = \mathbf{0} \quad (\text{A.4})$$

and combine (A.4) with Lemma 1 that

$$\begin{aligned} &\langle \mathbf{X}^k - \mathbf{X}^*, \mathcal{P}_\Omega(\mathbf{Y}^{k-1} - \mathbf{Y}^*) \rangle \\ &= \langle \mathbf{Z}^k - \mathbf{Z}^*, \mathbf{X}^k - \mathbf{X}^* \rangle \\ &\geq \langle (\mathbf{X}^k - \mathbf{X}^*)(\mathbf{I} - \phi_1 - \phi_1^T + \phi_1\phi_1^T), \mathbf{X}^k - \mathbf{X}^* \rangle. \end{aligned} \quad (\text{A.5})$$

We observe (23) that $\mathcal{P}_\Omega \mathbf{X}^* = \mathcal{P}_\Omega \mathbf{W}$,

$$\begin{aligned} &\|\mathcal{P}_\Omega(\mathbf{Y}^k - \mathbf{Y}^*)\|_F \\ &= \|\mathcal{P}_\Omega(\mathbf{Y}^{k-1} - \mathbf{Y}^*) + \lambda_k \mathcal{P}_\Omega(\mathbf{W} - \mathbf{X}^k)\|_F \\ &= \|\mathcal{P}_\Omega(\mathbf{Y}^{k-1} - \mathbf{Y}^*) + \lambda_k \mathcal{P}_\Omega(\mathbf{X}^* - \mathbf{X}^k)\|_F. \end{aligned} \quad (\text{A.6})$$

Here, we set $r_k = \|\mathcal{P}_\Omega(\mathbf{Y}^k - \mathbf{Y}^*)\|_F$; then

$$\begin{aligned} r_k^2 &= r_{k-1}^2 - 2\lambda_k \langle \mathcal{P}_\Omega(\mathbf{Y}^{k-1} - \mathbf{Y}^*), \mathbf{X}^k - \mathbf{X}^* \rangle \\ &\quad + \lambda_k^2 \|\mathcal{P}_\Omega(\mathbf{X}^* - \mathbf{X}^k)\|_F^2 \\ &\leq r_{k-1}^2 - 2\lambda_k \langle (\mathbf{X}^k - \mathbf{X}^*)(\mathbf{I} - \phi_1 - \phi_1^T + \phi_1\phi_1^T), \mathbf{X}^k - \mathbf{X}^* \rangle \\ &\quad + \lambda_k^2 \|\mathbf{X}^k - \mathbf{X}^*\|_F^2 \\ &= r_{k-1}^2 - (2\lambda_k \boldsymbol{\alpha} - \lambda_k^2 \boldsymbol{\beta}), \end{aligned} \quad (\text{A.7})$$

where $\boldsymbol{\alpha} = \langle (\mathbf{X}^k - \mathbf{X}^*)(\mathbf{I} - \phi_1 - \phi_1^T + \phi_1\phi_1^T), \mathbf{X}^k - \mathbf{X}^* \rangle \geq 0$, $\boldsymbol{\beta} = \|\mathbf{X}^k - \mathbf{X}^*\|_F^2 \geq 0$.

Based on (A.7), when $(2\lambda_k \boldsymbol{\alpha} - \lambda_k^2 \boldsymbol{\beta}) > 0$, that is, $\lambda_k \in (0, 2\boldsymbol{\alpha}/\boldsymbol{\beta})$, the term $\|\mathcal{P}_\Omega(\mathbf{Y}^k - \mathbf{Y}^*)\|_F$ is nonincreasing and converges to limit. The parameter λ_k is very easy for satisfying this condition when λ_k is smaller constant. And we can obtain other properties as follows.

Let $\lambda_k = \boldsymbol{\alpha}/\boldsymbol{\beta}$, and then $2\lambda_k \boldsymbol{\alpha} - \lambda_k^2 \boldsymbol{\beta} = \boldsymbol{\alpha}^2/\boldsymbol{\beta}$. Due to the fact that $\boldsymbol{\alpha}^2/\boldsymbol{\beta}$ converges to zero, so $\boldsymbol{\alpha}^2$ is infinite small about $\boldsymbol{\beta}$ and converges to zero. Now we reconsider (A.2); evidently the first column in ξ converges to zero; that is, $\xi_{1,1} \rightarrow 0$, $\xi_{2,1} \rightarrow 0$, $\xi_{3,1} \rightarrow 0$, $\xi_{4,1} \rightarrow 0$. The second column converges to the first column and then converges to zero; that is, $\xi_{1,2} \rightarrow \xi_{1,1} \rightarrow 0$, $\xi_{2,2} \rightarrow \xi_{2,1} \rightarrow 0$, $\xi_{3,2} \rightarrow \xi_{3,1} \rightarrow 0$, $\xi_{4,2} \rightarrow$

$\xi_{4,1} \rightarrow 0$. The third column converges to the second column and then converges to zero; that is, $\xi_{1,3} \rightarrow \xi_{1,2} \rightarrow 0$, $\xi_{2,3} \rightarrow \xi_{2,2} \rightarrow 0$, $\xi_{4,3} \rightarrow \xi_{4,2} \rightarrow 0$, $\xi_{1,2} \rightarrow \xi_{1,1} \rightarrow 0$, so through the iteration \mathbf{X}^k converges to \mathbf{X}^* except the last column due to the definition in (4) and (5); the last column and the last row are set to zero.

Fortunately, this problem does not have side effect for global result. Theorem 2 is established. \square

Conflict of Interests

The authors declare that there is no conflict of interests regarding the publication of this paper.

Acknowledgments

This work was supported by the National Basic Research Program of China under Grant 2011CB707904, by the National Natural Science Foundation of China under Grants 61201344, 61271312, and 61073138, by the Ministry of Education of China under Grants 20110092110023 and 20120092120036, the Key Laboratory of Computer Network and Information Integration (Southeast University), Ministry of Education, and by Natural Science Foundation of Jiangsu Province under Grant BK2012329. This work is supported by INSERM postdoctoral fellowship.

References

- [1] E. J. Candès, J. Romberg, and T. Tao, "Robust uncertainty principles: exact signal reconstruction from highly incomplete frequency information," *IEEE Transactions on Information Theory*, vol. 52, no. 2, pp. 489–509, 2006.
- [2] D. L. Donoho, "Compressed sensing," *IEEE Transactions on Information Theory*, vol. 52, no. 4, pp. 1289–1306, 2006.
- [3] E. J. Candès, J. K. Romberg, and T. Tao, "Stable signal recovery from incomplete and inaccurate measurements," *Communications on Pure and Applied Mathematics*, vol. 59, no. 8, pp. 1207–1223, 2005.
- [4] E. J. Candès and B. Recht, "Exact matrix completion via convex optimization," *Foundations of Computational Mathematics*, vol. 9, no. 6, pp. 717–772, 2008.
- [5] E. J. Candès and T. Tao, "The power of convex relaxation: near-optimal matrix completion," *IEEE Transactions on Information Theory*, vol. 56, no. 5, pp. 2053–2080, 2009.
- [6] A. Eriksson and A. van den Hengel, "Efficient computation of robust low-rank matrix approximations in the presence of missing data using the L1 norm," in *Proceedings of the IEEE Computer Society Conference on Computer Vision and Pattern Recognition (CVPR '10)*, pp. 771–778, June 2010.
- [7] H. Ji, C. Liu, Z. Shen, and Y. Xu, "Robust video denoising using Low rank matrix completion," in *Proceedings of the IEEE Computer Society Conference on Computer Vision and Pattern Recognition (CVPR '10)*, pp. 1791–1798, June 2010.
- [8] J. Liu, P. Musialski, P. Wonka, and J. Ye, "Tensor completion for estimating missing values in visual data," in *Proceedings of the IEEE 12th International Conference on Computer Vision (ICCV '09)*, pp. 2114–2121, Kyoto, Japan, 2009.
- [9] T. Okatani, T. Yoshida, and K. Deguchi, "Efficient algorithm for low-rank matrix factorization with missing components and

- performance comparison of latest algorithms,” in *Proceedings of the IEEE International Conference on Computer Vision (ICCV '11)*, pp. 842–849, Barcelona, Spain, November 2011.
- [10] D. Zhang, Y. Hu, J. Ye, X. Li, and X. He, “Matrix completion by truncated nuclear norm regularization,” in *Proceedings of the IEEE Conference on Computer Vision and Pattern Recognition (CVPR '12)*, pp. 2192–2199, 2012.
- [11] Y. Hu, D. Zhang, J. Ye, X. Li, and X. He, “Fast and accurate matrix completion via truncated nuclear norm regularization,” *IEEE Transactions on Pattern Analysis and Machine Intelligence*, vol. 35, no. 9, pp. 2117–2130, 2013.
- [12] N. Komodakis and G. Tziritas, “Image completion using global optimization,” in *Proceedings of the IEEE Conference on Computer Vision and Pattern Recognition (CVPR '06)*, vol. 1, pp. 442–452, 2006.
- [13] C. Rasmussen and T. Korah, “Spatiotemporal inpainting for recovering texture maps of partially occluded building facades,” in *Proceedings of the IEEE International Conference on Image Processing (ICIP '05)*, vol. 3, pp. 125–128, September 2005.
- [14] H. Ji, C. Liu, Z. Shen, and Y. Xu, “Robust video denoising using Low rank matrix completion,” in *Proceedings of the IEEE Conference on Computer Vision and Pattern Recognition (CVPR '10)*, pp. 1791–1798, June 2010.
- [15] Y. Koren, “Factorization meets the neighborhood: a multi-faceted collaborative filtering model,” in *Proceedings of the 14th ACM SIGKDD International Conference on Knowledge Discovery and Data Mining*, pp. 426–434, Las Vegas, Nev, USA, August 2008.
- [16] H. Steck, “Training and testing of recommender systems on data missing not at random,” in *Proceedings of the 16th ACM SIGKDD International Conference on Knowledge Discovery and Data Mining (KDD '10)*, pp. 713–722, Washington, DC, USA, July 2010.
- [17] J.-F. Cai, E. J. Candès, and Z. Shen, “A singular value thresholding algorithm for matrix completion,” *SIAM Journal on Optimization*, vol. 20, no. 4, pp. 1956–1982, 2010.
- [18] P. Jain, R. Meka, and I. Dhillon, “Guaranteed rank minimization via Singular Value Projection,” in *Proceedings of the 24th Annual Conference on Neural Information Processing Systems (NIPS '10)*, Vancouver, Canada, December 2010.
- [19] R. H. Keshavan, A. Montanari, and S. Oh, “Matrix completion from a few entries,” *IEEE Transactions on Information Theory*, vol. 56, no. 6, pp. 2980–2998, 2010.
- [20] Z. Lin, R. Liu, and Z. Su, “Linearized alternating direction method with adaptive penalty for low-rank representation,” in *Proceedings of the 25th Annual Conference on Neural Information Processing Systems (NIPS '11)*, December 2011.
- [21] J. Yang and X. Yuan, “Linearized augmented Lagrangian and alternating direction methods for nuclear norm minimization,” *Mathematics of Computation*, vol. 82, no. 281, pp. 301–329, 2013.
- [22] L. I. Rudin, S. Osher, and E. Fatemi, “Nonlinear total variation based noise removal algorithms,” *Physica D: Nonlinear Phenomena*, vol. 60, pp. 259–268, 1992.

Research Article

Applying Data Clustering Feature to Speed Up Ant Colony Optimization

Chao-Yang Pang,¹ Ben-Qiong Hu,² Jie Zhang,³ Wei Hu,⁴ and Zheng-Chao Shan⁵

¹ College of Computer Science, Sichuan Normal University, Chengdu 610101, China

² College of Management Science, Chengdu University of Technology, Chengdu 610059, China

³ Department of Control Engineering, Chengdu University of Information Technology, Chengdu 610225, China

⁴ North Sichuan Preschool Educators College, Guangyuan 628000, China

⁵ The Personnel Department of Sichuan Normal University, Chengdu 610068, China

Correspondence should be addressed to Ben-Qiong Hu; hbq402@126.com

Received 23 January 2014; Accepted 4 April 2014; Published 5 May 2014

Academic Editor: Zhiwu Liao

Copyright © 2014 Chao-Yang Pang et al. This is an open access article distributed under the Creative Commons Attribution License, which permits unrestricted use, distribution, and reproduction in any medium, provided the original work is properly cited.

Ant colony optimization (ACO) is often used to solve optimization problems, such as traveling salesman problem (TSP). When it is applied to TSP, its runtime is proportional to the squared size of problem N so as to look less efficient. The following statistical feature is observed during the authors' long-term gene data analysis using ACO: when the data size N becomes big, local clustering appears frequently. That is, some data cluster tightly in a small area and form a class, and the correlation between different classes is weak. And this feature makes the idea of divide and rule feasible for the estimate of solution of TSP. In this paper an improved ACO algorithm is presented, which firstly divided all data into local clusters and calculated small TSP routes and then assembled a big TSP route with them. Simulation shows that the presented method improves the running speed of ACO by 200 factors under the condition that data set holds feature of local clustering.

1. Introduction

1.1. Introduction of Ant Colony Optimization (ACO). In 1991, ant colony optimization (ACO) was presented firstly by Colormi et al. [1] and applied to solve TSP firstly by Dorigo et al. [1–3]. Dorigo et al. created a new research topic which is studied by many scholars now.

ACO is essentially a system based on agents that simulate the natural behavior of ants, in which real ants are able to find the shortest route from a food source to their nest, without using visual cues by exploiting pheromone information [2]. Pheromone is deposited when ants are walking on a route. It provides heuristic information for other ants to choose their routes. The more dense the pheromone trail of a route is, the more possibly the route is selected by ants. At last, nearly all ants select the route that has the most dense pheromone trail, and it is the shortest route potentially.

ACO has been applied to solve optimization problems widely and successfully, such as TSP [1–4], quadratic

assignment problem [5], image processing [6], data mining [7], classification or clustering analysis [8], and biology [9]. The application of ACO leads the theoretic study of ACO. Gutijahr firstly analyzes the convergence property of ACO [10]. Stutzle and Dorigo prove the important conclusion that if the running time of ACO is long enough, ACO can find optimal solution possibly [11]. The other interesting property is revealed currently by Birattari et al. that the sequence of solutions of some algorithms does not depend on the scale of problem instance [12].

ACO is especially well suited for solving difficult optimization problems, where traditional optimization methods are less efficient. However, ACO is not very efficient in solving large problems because running time is too long and the quality of solution is still low. To solve the two main problems, the configuration of the parameters is discussed [2, 3]. To further improve ACO, many approaches have been proposed. Among these approaches, parallel computation and other methods are used to accelerate ACO [13]. In this study,

we design a novel clustering algorithm named special local clustering algorithm (SLC), which is applied to classify and find the solution for TSP problem. Moreover, a colony of ants acts on each class to get a local TSP path. And we use the convergence of route length as termination criterion of ACO. The experimental results indicated that the improved ACO speeds up and its quality becomes higher for testing problems. It is more robust than comparative approaches.

1.2. Clustering Correlates to the Running Time of ACO. One of study focuses of ACO is to cut down running time. The running time of ACO is $O(t_{\max}MN^2)$, and $M = \lceil N/1.5 \rceil$ in general, where t_{\max} , M , and N denote the iteration number, number of ants, and number of cities, respectively [4]. The running time is proportional to N^2 . Cutting down the number of cities N is the key to reduce running time. Therefore, classifying all cities into different classes and letting ACO act on each class will reduce running time heavily. Hu and Huang used this method to improve the running speed of ACO [14], which is named ACO-K-Means. It is faster than ACO by factors of 5–15 approximately. Simulations show that ACO-K-Means algorithm is valid only to the set of cities that has evident clustering feature and invalid to more general situation. ACO-K-Means implies that using clustering method to improve the running speed of ACO is possible.

1.3. Introduction of Local Clustering Algorithm. Clustering is classifying objects of a set (named training set) into different clusters (or groups), so that the data in each class (ideally) share some common traits. One of the most popular clustering algorithms is K-Means clustering algorithm [15, 16]. K-Means clustering algorithm assigns each point to the cluster whose center (i.e., centroid) is nearest to it and then updates the centroid. Repeat this process until termination criterion is satisfied [16].

During the t th iteration of K-Means algorithm, the i th class has distortion that is defined as the average distance of each point and the class centroid, which is denoted by $D_i^{(t)}$ ($1 \leq i \leq m$), where m is the number of classes. Pang proves that for each i the distortion sequence $\{D_i^{(t)}\}$ is convergent if the i th class is separated from other classes evidently [16]. That is, distortion sequence is convergent locally. According to this property, an algorithm named local clustering algorithm (LC) is presented [17], and its essential idea is introduced as below.

Step 1. K-Means is applied to a given training set to generate classes.

Step 2. The class whose distortion $D_i^{(t)}$ is convergent first is deleted from training set. Then, update training set such that it is comprised of residual points. Go to Step 1.

Repeat the process of Steps 1 and 2 until all data is classified.

LC algorithm is faster than K-Means algorithm by factors of 4–13 approximately.

Suppose that the i th class is $R_i^{(t)}$ during the t th iteration of K-Means algorithm. Set $R_i^{(t)}$ has entropy $H(R_i^{(t)})$, where

$H(R_i^{(t)}) = -\sum_{a \in R_i^{(t)}} p(a) \log_2 p(a)$ and $p(a)$ is the probability of data a . It is proved that entropy sequence $\{H(R_i^{(0)}), H(R_i^{(1)}), \dots, H(R_i^{(t)}), \dots\}$ is convergent [16]. That is, the convergent criterion of K-Means algorithm can be replaced by the convergence of entropy sequence [18]. The K-Means with convergent criterion of entropy convergence is fast by factors of 2 at least [18, 19].

2. Improve Local Clustering Algorithm to Generate Compact Class

2.1. Compact Set and the Method of Generation. For any subset of Euclidean space R^n , every sequence in this subset has a convergent subsequence, the limit point of which belongs to the set. This subset is called *compact set*. The conception of compact set (or compactness) is a topology conception. To understand it easily, compactness can be described visually as the phenomenon where many points cluster tightly in a small region, while noncompact set is the set of which most of points cluster loosely in a big region.

K-Means clustering, LC, or other algorithms aim to partition a training set into classes. Some classes are compact and some are not. The most common situation is that a class contains a compact subset and some loose points, and points of the compact subset are around the center of the class. That is, the central part of class is compact possibly. To extract compact subset from a class, the following 3δ -principle is introduced.

For Gauss distribution, suppose that δ denotes the deviation of random data. It is the 3δ -principle that there is more than 99% probability that a random point falls into the central region of data set whose radius is 3δ [16]. The central region contains more than 99% points. Thus, if radius 3δ is small enough and the number of points is big enough, the central region is compact. If the central region with radius 3δ is not compact, shortening the radius of central region to $3\delta/4$, $3\delta/16$, and so on will make it compact. For Gauss distribution which is comprised of enough points, the compact central region always exists. In general, for a class generated by clustering algorithm, all distances of points from class centroid comprise a similar gauss distribution. Therefore, the central region of a class is compact possibly.

Suppose that the i th class is $R_i^{(t)}$ at the t th iteration of K-Means or LC algorithm. With the increase of iteration, class sequence $\{R_i^{(0)}, R_i^{(1)}, \dots, R_i^{(t)}, R_i^{(t+1)}, \dots\}$ ($1 \leq i \leq m$) appears, where m denotes the number of classes. Let

$$D_i^{(t)} = \frac{1}{|R_i^{(t)}|} \sum_{x \in R_i^{(t)}} d(x, c_i^{(t)}), \quad (1)$$

where $|R_i^{(t)}|$ denotes the number of elements in $R_i^{(t)}$ and $d(x, c_i^{(t)})$ denotes distance.

Consider

$$\delta_i^{(t)} = \frac{1}{|R_i^{(t)}|} \sum_{x \in R_i^{(t)}} |d(x, c_i^{(t)}) - D_i^{(t)}|. \quad (2)$$

Clearly, $D_i^{(t)}$ is the distortion of class $R_i^{(t)}$ and $\delta_i^{(t)}$ is the approximation of deviation of $D_i^{(t)}$.

Consider

$$K_i^{(t)} = \left\{ x \mid d(x, c_i^{(t)}) \leq \frac{1}{4p} (D_i^{(t)} + 3\delta_i^{(t)}), \right. \\ \left. x \in R_i^{(t)} (p \geq 0) \right\}. \quad (3)$$

$K_i^{(t)}$ is the central region of class $R_i^{(t)}$. Parameter p is used to shorten the radius of central region $K_i^{(t)}$ and makes it compact. Figure 1 illustrates the 3δ -principle and compact subset $K_i^{(t)}$.

2.2. Subroutine 1: Local Clustering Algorithm with 3δ -Principle. The local clustering algorithm with 3δ -principle is used to classify points into classes and to extract compact central region of classes. Its essential idea is described as below.

Firstly, apply LC algorithm to cluster data. And apply the criterion of entropy convergence (i.e., $|H(R_i^{(t)}) - H(R_{i+1}^{(t+1)})|/H(R_i^{(t)}) \rightarrow 0$) to mark the stable class $R_i^{(t)}$.

Secondly, extract compact central region $K_i^{(t)}$ from class $R_i^{(t)}$ and preserve it as a genuine class. Remove $R_i^{(t)}$ from training set and update it. Repeat the above two steps until all compact central regions are extracted. The details are described in Algorithm 1.

2.3. Special LC Algorithm to Generate Compact Classes (SLC). Note that above subroutine 1 is not a partition of training set. Subroutine 1 extracts only compact central regions of all classes and the residual points are unclassified. The residual points comprise a new training set. And it is possible that some of residual points cluster together tightly and comprise some small compact subsets again. These small compact subsets are new classes. To obtain these new classes and classify all points, SLC algorithm is described in Algorithm 2.

2.4. The Clustering for Mixture Distribution (SLC-Mixture). The clustering algorithm SLC presented above generates spherical classes only. However, for a general distribution, some classes are of spherical shape, some classes are of chain shape in which points cluster closely around a curve (or a line), and some classes contain isolated points. This common distribution is called mixture distribution. For a large-scale TSP, the distribution of cities is mixture distribution in general. The clustering method for mixture distribution is proposed as below.

2.4.1. The Simple Maker to Distinguish Spherical Class from Chain-Shaped Class. The position of city on a map is two-dimensional point. A given class can be divided into 8 areas along the 4 directions of the north-south and west-east and two diagonal lines through the centroid of the class. If the class is spherical, the percentage of points in each area is close to 1/8 and is the same approximately. If the class is chain-shaped class (or part of chain-shaped class), it is impossible that the percentage of every area is close to 1/8 at the same

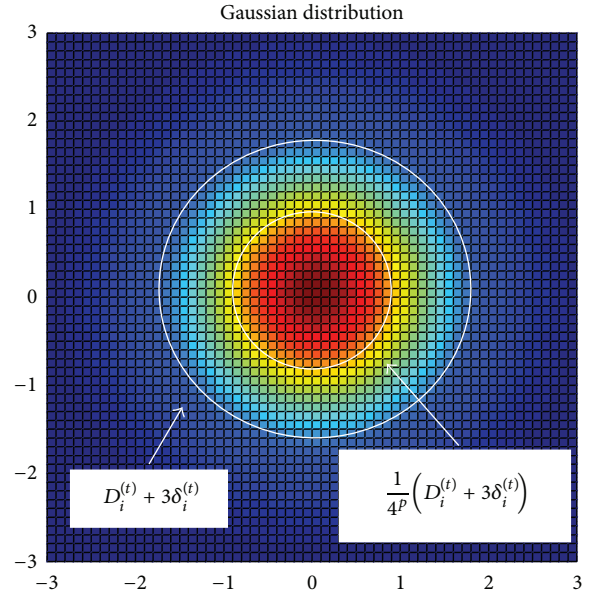


FIGURE 1: The illustration of compact central region of a class. In a class $R_i^{(t)}$, most of points cluster around their centroid and few points are far away from the centroid. Subset $K_i^{(t)}$ (i.e., the shadow part) is the central region of class $R_i^{(t)}$. Compact set is the set where many points cluster in a small region tightly. Increasing parameter p will shorten radius and make $K_i^{(t)}$ compact.

time. Therefore, the percentage of points in each area is the maker of spherical class. Figure 2 illustrates the marker.

2.4.2. Applying SLC to Process Mixture Distribution (SLC-Mixture). At first, apply SLC to classify all data of training set. Secondly, apply the marker presented above to distinguish spherical classes and extract them from the training set. Then all residual points comprise a new set named residual set. The residual set contains only chain-shaped classes and isolated points. Thirdly, apply the method presented in [20] to classify all residual points of residual set into different chain-shaped classes or marked as isolated points. The method presented in [20] is named chain-shaped clustering algorithm.

The clustering method presented in this section is called SLC-Mixture algorithm, which processes the mixture distribution of spherical classes, chain-shaped classes, and isolated points.

3. Apply SLC to ACO

3.1. The Termination Criterion of ACO. Suppose ACO acts on a compact class and let L_t denote the minimum route length that is generated at the t th iteration of computation. There is sequence $\{L_1, L_2, \dots, L_t, L_{t+1}, \dots\}$ and it is convergent under ideal condition. The convergent criterion $|L_t - L_{t+1}|/L_t \leq \epsilon$ is proposed as the termination criterion of ACO in this paper.

In the following discussion, ACO refers to the algorithm whose termination criterion is $(|L_t - L_{t+1}|/L_t) \leq \epsilon$.

3.2. Apply SLC to Improve the Running Speed of ACO (ACO-SLC). In this section, the clustering algorithm SLC will be

Input parameters:
T: Training Set
m: The number of classes
 ε : The stop threshold for clustering.
 $C^{(0)} = \{c_i^0 (1 \leq i \leq m)\}$: Initial centroids set.
p: A parameter to adjust the size of compact subsets $K_i^{(t)}$ ($p \geq 0$).
Output:
 $\varphi(T) = \{K_1^{(t)}, K_2^{(t)}, \dots, K_i^{(t)}, \dots, K_m^{(t)}\}$ (i.e., the set of co-compact subset, see Figure 1)
 $\sigma(T) = \{B_1^{(t)}, B_2^{(t)}, \dots, B_i^{(t)}, \dots, B_m^{(t)}\}$, where $B_i^{(t)} = R_i^{(t)} - K_i^{(t)}$, and it is comprised by dispersive points ($1 \leq i \leq m$, see Figure 1)
Void Subroutine 1 ($T, m, \varepsilon, C^{(0)}, p, \varphi(T), \sigma(T)$)
{
Step 1. Initialization: Let iteration number $t = 0$. Let *Counter* = m . Let $\varphi(T) = \phi$ and $\sigma(T) = \phi$, where ϕ denotes empty set. According to initial centroids set $C^{(0)}$, generate initial partition of training set $\varphi^0 = \{R_i^0 \mid R_i^0 \subset T, 1 \leq i \leq m\}$.
Step 2. While (*Counter* > 0) {
 Step 2.1. Generate new centroids set $C^{(t+1)} = \{c_i^{(t+1)} \mid 1 \leq i \leq m\}$ and new partition $\varphi^{(t+1)} = \{R_i^{(t+1)} \mid 1 \leq i \leq m\}$
 /* Note: Check whether entropy sequence $H_i^{(0)}, H_i^{(1)}, \dots, H_i^{(t)}, H_i^{(t+1)}, \dots$ is convergent. If it is convergent, let the convergent marker $\text{StableMarker}(R_i^{(t+1)}) = \text{True}$ */
 Step 2.2. For ($i = 1; i \leq \text{Counter}; i++$) {
 Estimate the entropy of class $R_i^{(t+1)}$, that is, $H(R_i^{(t+1)}) = \log_2 |R_i^{(t+1)}|$.
 If $\left(\frac{|H(R_i^{(t)}) - H(R_i^{(t+1)})|}{H(R_i^{(t)})} < \varepsilon \right) \{ \text{StableMarker}(R_i^{(t+1)}) = \text{True}; \}$
 Else $\{ \text{StableMarker}(R_i^{(t+1)}) = \text{False} \}$
 }
 /* Note: Extract the data around the centroid of class as a genuine class */
 Step 2.3. For ($i = 1; i \leq \text{Counter}; i++$) {
 If $(\text{StableMarker}(R_i^{(t+1)}) = \text{True})$ {
 Calculate compact central region $K_i^{(t)}$ according to formula (3)
 Calculate $B_i^{(t)}$: $B_i^{(t)} = R_i^{(t+1)} - K_i^{(t)}$
 Let $\varphi(T) = \varphi(T) \cup K_i^{(t)}$
 Let $\sigma(T) = \sigma(T) \cup B_i^{(t)}$
 Update Training Set: $T = T - R_i^{(t)}$
 Update centroids set: $C^{(t+1)} = C^{(t+1)} - \{c_i^{(t+1)}\}$
 Counter = *Counter* - 1
 }
 }
 t = *t* + 1
} }
}

ALGORITHM 1

applied to improve the running speed of ACO. The method is named ACO-SLC and it is described as below.

Input parameter:

T: set of cities.

Output: the shortest TSP route obtained by the algorithm.

ACO-SLC Algorithm.

Step 1. Apply SLC algorithm to partition set *T*. The classes are $B_1, B_2, \dots, B_i, \dots,$ and B_{Num} , and their centroids are $b_1, b_2, \dots, b_i, \dots,$ and b_{Num} , respectively.

Step 2. Construct graph G' : centroids $b_1, b_2, \dots, b_i, \dots,$ and b_{Num} are regarded as virtual cities, respectively, and the virtual cities are regarded as the vertices of graph G' . For a pair of classes B_i and B_j , if there exist two cities that belong to B_i and B_j , respectively, and they join each other, use an edge to join the two corresponding vertices b_i and b_j . The weight of edge is the minimum distance between two classes; that is,

$$d(B_i, B_j) = \min \{d(x_i, x_j) \mid x_i \in B_i, x_j \in B_j\}. \quad (4)$$

Step 3. Calculate a TSP route of graph G' to generate the traveling order of all classes: let ACO algorithm act on graph G' to find a TSP route denoted by $b_{j_1}, b_{j_2}, \dots, b_{j_{\text{Num}}}$, where

Input parameters:
 T_0 : Training Set
 m_0 : The initial number of classes.
 ε : The stop threshold for clustering.
 Output:
 Num: The final number of classes.
 CLS: The partition of T_0 , in which each class is com-pact.
 SLC Algorithm:
 Step 1. Initialization: Let $T = T_0$, $m = m_0$, $CLS = \phi$, and $p = 0$.
 Step 2. For ($i = 0$; $i < \lceil \log_2 m \rceil$; $i++$) /*Note: $\lceil \log_2 m \rceil$ denotes the integer */
 { Step 2.1. Generate initial centroids set $C^0 = \{c_i^{(0)} \mid 1 \leq i \leq m\}$.
 Step 2.2. Call Subroutine1 ($T, m, C^{(0)}, \varepsilon, p, \varphi(T), \sigma(T)$)
 Step 2.3. $CLS = CLS \cup \varphi(T)$;
 Step 2.4. $T = \sigma(T)$;
 /* Note: Increase p to get smaller compact class */
 Step 2.5. $m = \lfloor \frac{m}{2} \rfloor$; $p = p + 1$
 }
 Step 3. Every residual point x in the last set $\sigma(T)$ is regarded as a class $\{x\}$. And let $CLS = CLS \cup \{x\}$.
 Let Num denote the number of classes contained in CLS. The two outputs are CLS and Num.

ALGORITHM 2

j_1, j_2, \dots, j_{Num} , is a permutation of sequence $1, 2, \dots, Num$. The pair of classes B_{j_i} and $B_{j_{(i+1)}}$ is called neighbor class.

Step 4. Choose an edge as the bridge to join a pair of neighbor classes, and this edge is named bridge edge. Assume that the two neighbor classes are B_{j_1} and B_{j_2} . If there exists an edge such that

$$d(x_u, x_v) = \min \{d(a, b) \mid a \in B_{j_1}, b \in B_{j_2}\}, \quad (5)$$

edge (x_u, x_v) is the bridge edge, x_u and x_v are called border cities, where vertices a and b should be not used to join other neighbor classes.

Step 5. Calculate a local TSP route for every class B_i ($1 \leq i \leq Num$): add a new edge to join the two border cities in the class and mark the edge as necessary edge of the local TSP route. This edge is named pseudoedge. Let the ACO algorithm with convergence criterion $(|L_t - L_{t+1}|/L_t) \leq \varepsilon$ act on the class to generate a local TSP route.

Step 6. Construct a TSP route: walk along the traveling order obtained at Step 3; for every pair of neighbor classes, delete the pseudoedge of each class such that the local route is not close. Then let the local route of each class and the bridge edge between these two classes be joined.

Figure 3 illustrates the processing of ACO-SLC algorithm.

3.3. Using the Method of Little-Window and Removing Cross-Edge to Improve ACO-SLC (ACO-SLC-LWCR). Clustering may cause the error of solution although it improves the running speed of ACO heavily. If all classes are compact and separated clearly, the quality of solution of ACO-SLC should be very good. However, in fact, the border between two neighbor classes is fuzzy. The fuzzy border will cause the

inaccuracy of solution, and much longer route will appear. And recognizing the longer part and removing it will generate better solution possibly. It is well known that the shortest route is always at the surface of a convex hull. Thus, the longer part should be at the inner of a convex hull and two longer edges intersect. In other words, intersection of two edges is a marker of longer part of a route possibly. According to the marker, removing longer edges is called *removing cross-edge* or *removing intersection edges*, which is similar to the method in [4]. (Notice: in [4], before executing ACO, the long and crossed edges are removed to improve the running speed of ACO, not to improve the solution quality.)

Figure 4 illustrates the method of removing cross-edge.

In addition, a simple method named *little-window strategy* is proposed to improve the running speed of ACO in [21]. Construct a set S_i that is comprised by w accessible and short edges which join the i th city, where w is a preassigned constant. The ant which has arrived at i th city will select an edge from window set S_i only to arrive at its next city and not select an edge from all neighbor edges of this vertex. So, this method improves the running speed of ACO.

The ACO-SLC with little-window strategy and cross-edges removing is called *ACO-SLC-LWCR*.

3.4. The ACO-SLC for Mixture Distribution (ACO-SLC-Mixture). ACO-SLC is suitable for the spherical shape distribution only, and the low quality of solution will appear possibly when ACO-SLC is applied to process mixture distribution. To process mixture distribution, the following method named ACO-SLC-Mixture is proposed in this paper.

Firstly, apply SLC-Mixture at Section 2.4.2 to partition the set of cities into spherical classes, chain-shaped classes, or isolated points. Secondly, apply ACO-SL-C-LWCR to each class and generate a TSP route.

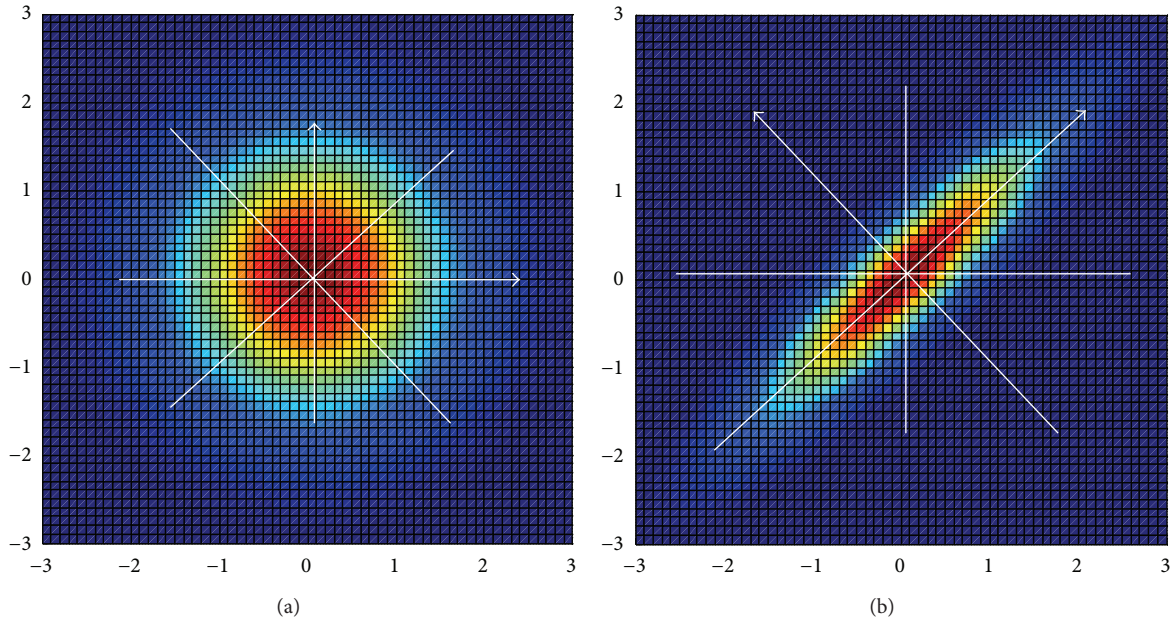


FIGURE 2: The illustration of distinguishing spherical class from chain-shaped class. A given class is divided into 8 parts along the 8 lines through the centroid of the class. If the class is spherical, the percentage of each part is close to threshold $\varepsilon = 1/8$. If the class is chain-shaped class (or part of chain-shaped class), there are 2–4 parts whose percentage is far less than $1/8$. Therefore, the percentage of each part is the marker of spherical class. $\varepsilon = 0.058$ in this paper because some classes are elliptical.

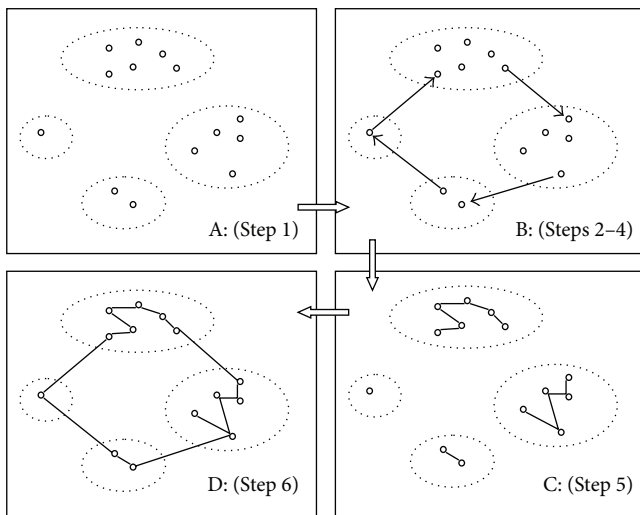


FIGURE 3: The schematic diagram of ACO-SLC. Firstly, classify all points into compact classes. Secondly, the centroid of each class is regarded as a virtual city; calculate a virtual TSP route. Then along the virtual route, join all classes. Thirdly, let ACO act on each class to get a local TSP route. Fourthly, join all local TSP routes along the virtual route to form the last route.

4. Simulation

In this section, five related algorithms ACO, ACO-K-Means, ACO-SLC, ACO-SLC-LWCR, and ACO-SLC-Mixture are tested and compared. In the following simulation, ACO refers to ant-cycle presented by Colorni et al., which is very typical [1].

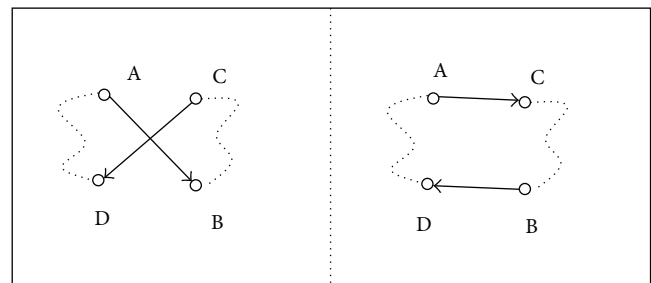


FIGURE 4: The schematic diagram of ACO-SLC. Firstly, classify all points into compact classes. Secondly, the centroid of each class is regarded as a virtual city. And calculate a virtual TSP route. Then along the virtual route, join all classes. Thirdly, let ACO act on each class to get a local TSP route. Fourthly, join all local TSP routes along the virtual route to form the last route. The illustration of removing cross-edges from TSP route: at the left figure, AB and CD intersect each other. There is a principle that the shortest route is at the surface of a convex hull. Thus, edges AB and CD are the longer part of route and should be removed. Removing these two edges will generate shorter route (see right figure).

All test data in this paper is downloaded from <http://www.iwr.uni-heidelberg.de/groups/comopt/software/TSPLIB95/tsp/>. All algorithms in this paper run on personal computer (CPU: 1.80 GHz; memory: 480 M; software: Matlab). The parameters are listed as below. Initialize pheromone trails $\tau_{ij}(0) = 1$, iteration number 1000, $\varepsilon = 0.001$, $\alpha = 1$, $\beta = 10$, $\rho = 0.4$, $Q = 300$, and $m = \lceil N/1.5 \rceil$. Two performance items are tested. One item is the running time, which is defined as $Ratio = Time(ACO)/Time(Algorithm)$. The bigger the ratio is, the faster

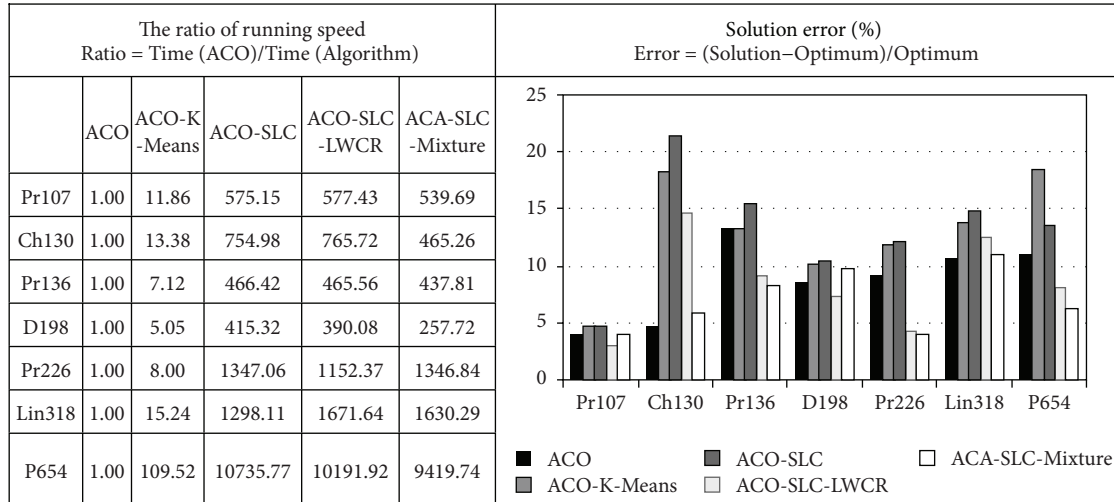


FIGURE 5: The performance comparison with five algorithms. The figure shows that ACO-SLC algorithm, ACO-SLC, ACO-SLC-LWCR, and ACO-SLC-Mixture are faster than ACO by 415 ~ 10736, 390 ~ 10192, and 257~9419 of factors, respectively! However, some solutions of ACO-K-Means and ACO-SLC have low quality. ACO-SLC-Mixture can process mixture distribution and its inaccuracy ratio is less than ACO in most cases and is bigger than ACO by 2% at most. It should be noted that under the condition where the data set holds feature of local clustering significantly, the quality of solution is good.

the algorithm is. In addition, the advantage of the ratio is that the subtle infection of other processes to runtime is evaded as possible, and it is more accurate than raw measured runtime because the value caused by other processes gives little contribution to the ratio. The other item is the quality of solution, which is defined as the percentage of error $Error = (Solution-Optimum)/Optimum$, where $Optimum$ denotes the best solution known currently. The smaller the error is, the better the quality of solution is.

The performances of the five algorithms are listed in Figure 5. It shows that ACO-SLC, ACO-SLC-LWCR, and ACO-SLC-Mixture are faster than ACO by 415 ~ 10736, 390 ~ 101~92, and 257~9419 of factors, respectively! However, some solutions of ACO-K-Means and ACO-SLC have low quality. The inaccuracy ratio of ACO-SLC-Mixture is less than ACO in most cases and is bigger than ACO by 2% at most.

The Defect of ACO-SLC. (1) From Figure 5, it should be noted that only under the condition that the data set holds feature of local clustering significantly, the quality of solution is good. (2) The simulations of this paper show that the quality of ACO-SLC solution depends on the quality of clustering and clustering quality of SLC is sensitive to the initial centroids just like K-Mean algorithm. This is the main defect of ACO-SLC.

5. Conclusion

Time Complexity of ACO. ACO is the algorithm that is inspired by the foraging behavior of ant colonies and has been applied to solve many optimization problems. The typical application of ACO is the application at traveling salesman problem (TSP). The running time of ACO is $O(t_{max}MN^2)$, where t_{max} , M , and N denote the iteration number, number

of ants, and number of cities, respectively. Parameter m is an experiential value and is set to $\lfloor N/1.5 \rfloor$ in general. Parameter N is the key factor of running time because running time is proportional to its square. Parameter t_{max} and N are available, and decreasing parameter t_{max} and N will cut down running time.

Focus of ACO Study. ACO can generate solution with high quality in general. But its shortage is that running time is too long. Cutting down running time is one of study focuses of ACO, and one way is to decrease parameters t_{max} and N , especially N .

Basic Idea for this Study Focus. For this study focus, the following basic idea is presented in this paper.

Firstly, all cities are classified into compact classes, where compact class is the class where all cities in this class cluster tightly in a small region. Secondly, let ACO act on every class to get a local TSP route. Thirdly, all local TSP routes are joined to form solution. Fourthly, the inaccuracy of solution caused by clustering is eliminated.

Realization of Basic Idea. The realization of above idea is based on a novel clustering algorithm presented in this paper, which is named special local clustering algorithm (SLC). The running time of SLC is far less than the time of ACO. SLC generates compact classes, while current popular clustering algorithm such as K-Means does not generate compact classes in general. The compactness of class makes the length of TSP route L_t at every iteration convergent; the convergence of L_t (i.e., $(|L_t - L_{t+1}|/L_t) \rightarrow 0$) is proposed as the termination criterion of ACO in this paper. Thus, parameter t_{max} is cut down to improve the running speed of ACO. In addition, every class has small size; ACO acting on small class makes parameter N cut down, and running speed is improved.

According to this analysis, ACO-SLC algorithm is presented in this paper. Simulation shows that ACO-SLC is faster than ACO by 415 ~ 10736 of factors!

Elimination of the Solution Inaccuracy Caused by Clustering. Although the running speed is improved in this paper, the inaccuracy of solution is heavy. Two factors causing the inaccuracy are found in this paper. One is the cross-edges (see Section 3.3) and the other factor is the unmatching between ACO-SLC and mixture distribution (see Section 3.4). According to these two factors, ACO-SLC-LWCR and ACO-SLC-Mixture are presented in this paper, which is the improvement of ACO-SLC. Simulation shows that ACO-SLC-LWCR and ACO-SLC-Mixture are faster than ACO by 390 ~ 101-92 and 257-9419 of factors, respectively! The inaccuracy ratio of ACO-SLC-Mixture is less than ACO in most cases and is bigger than ACO by 2% at most.

Conflict of Interests

The authors declare that there is no conflict of interests regarding the publication of this paper.

Acknowledgments

The work is supported by Aeronautical Science Foundation of China (no. 2012ZD11) and partially by the Education Department of Sichuan Province (no. 12zA134 and no. 09zz028).

References

- [1] A. Colorni, M. Dorigo, and V. Maniezzo, "Distributed optimization by ant colonies," in *Proceedings of the 1st European Conference on Artificial Life*, pp. 134-142, Paris, France, 1991.
- [2] M. Dorigo and L. M. Gambardella, "Ant colony system: a cooperative learning approach to the traveling salesman problem," *IEEE Transactions on Evolutionary Computation*, vol. 1, no. 1, pp. 53-66, 1997.
- [3] M. Dorigo, V. Maniezzo, and A. Colorni, "Ant system: optimization by a colony of cooperating agents," *IEEE Transactions on Systems, Man, and Cybernetics B: Cybernetics*, vol. 26, no. 1, pp. 29-41, 1996.
- [4] H. B. Duan, *Ant Colony Algorithms: Theory and Applications*, Science Publisher, Beijing, China, 2005.
- [5] V. Maniezzo and A. Colorni, "The ant system applied to the quadratic assignment problem," *IEEE Transactions on Knowledge and Data Engineering*, vol. 11, no. 5, pp. 769-778, 1999.
- [6] S. Meshoul and M. Batouche, "Ant colony system with extremal dynamics for point matching and pose estimation," in *Proceeding of the 16th International Conference on Pattern Recognition*, pp. 823-826, Quebec, Canada, 2002.
- [7] R. S. Parpinelli, H. S. Lopes, and A. A. Freitas, "Data mining with an ant colony optimization algorithm," *IEEE Transactions on Evolutionary Computation*, vol. 6, no. 4, pp. 321-332, 2002.
- [8] X. Li, X. H. Luo, and J. H. Zhang, "Codebook design by a hybridization of ant colony with improved LBG algorithm," in *Proceedings of the International Conference on Neural Networks and Signal Processing (ICNNSP '03)*, pp. 469-472, Nanjing, China, December 2003.
- [9] P. Meksangsouy and N. Chaiyaratana, "DNA fragment assembly using an ant colony system algorithm," in *Proceedings of the Congress on Evolutionary Computation*, pp. 1756-1763, Canberra, Australia, 2003.
- [10] W. J. Gutjahr, "Graph-based ant system and its convergence," *Future Generation Computer Systems*, vol. 16, no. 8, pp. 873-888, 2000.
- [11] T. Stutzle and M. Dorigo, "A short convergence proof for a class of ant colony optimization algorithms," *IEEE Transactions on Evolutionary Computation*, vol. 6, no. 4, pp. 358-365, 2002.
- [12] M. Birattari, P. Pellegrini, and M. Dorigo, "On the invariance of ant colony optimization," *IEEE Transactions on Evolutionary Computation*, vol. 11, no. 6, pp. 732-742, 2007.
- [13] B. Bullnheimer, G. Kotsis, and C. Strauß, "Parallelization strategies for the ant system," in *High Performance and Algorithms and Software in Nonlinear Optimization*, vol. 24 of *Applied Optimization*, pp. 87-100, 1998.
- [14] X.-B. Hu and X.-Y. Huang, "Solving TSP with characteristic of clustering by ant colony algorithm," *Journal of System Simulation*, vol. 16, no. 12, pp. 55-58, 2004.
- [15] Y. Linde, A. Buzo, and R. M. Gray, "An algorithm for vector quantization design," *IEEE transactions on communications systems*, vol. 28, no. 1, pp. 84-95, 1980.
- [16] C. Y. Pang, *Quantization and image compression [Ph.D. thesis]*, University of Electronic Science and Technology of China, Chengdu, China, 2002.
- [17] P. Chaoyang, S. Shixin, P. Ye, and G. Haiying, "A fast codebook training algorithm using local clustering," *Journal of Electronics and Information Technology*, vol. 9, pp. 1282-1286, 2002.
- [18] C.-Y. Pang and S.-X. Sun, "Codebook training algorithm by the convergence of entropy sequence for vector quantization," *Systems Engineering and Electronics*, vol. 24, no. 1, pp. 83-85, 2002.
- [19] X. Li, X. H. Luo, and J. H. Zhang, "Modeling of vector quantization image coding in an Ant colony system," *Chinese Journal of Electronics*, vol. 13, no. 2, pp. 305-307, 2004.
- [20] X. Huang, J. Wang, and Y. Zhang, "Adaptive K near neighbor clustering algorithm for data with non-spherical-shape distribution," *Computer Engineering*, vol. 29, pp. 21-22, 2003.
- [21] Y. Xiao and B. Li, "Ant colony algorithm based on little window," *Computer Engineering*, vol. 29, pp. 143-145, 2003.

Research Article

Nonrigid Registration of Monomodal MRI Using Linear Viscoelastic Model

Jian Yang,¹ Yang Chen,² Jingfan Fan,¹ and Songyuan Tang¹

¹ Beijing Engineering Research Center of Mixed Reality and Advanced Display, School of Optics and Electronics, Beijing Institute of Technology, Beijing 100081, China

² Laboratory of Image Science and Technology, Southeast University, Nanjing 210096, China

Correspondence should be addressed to Songyuan Tang; sytang@bit.edu.cn

Received 14 January 2014; Accepted 22 March 2014; Published 22 April 2014

Academic Editor: Zhiwu Liao

Copyright © 2014 Jian Yang et al. This is an open access article distributed under the Creative Commons Attribution License, which permits unrestricted use, distribution, and reproduction in any medium, provided the original work is properly cited.

This paper describes a method for nonrigid registration of monomodal MRI based on physical laws. The proposed method assumes that the properties of image deformations are like those of viscoelastic matter, which exhibits the properties of both an elastic solid and a viscous fluid. Therefore, the deformation fields of the deformed image are constrained by both sets of properties. After global registration, the local shape variations are assumed to have the properties of the Maxwell model of linear viscoelasticity, and the deformation fields are constrained by the corresponding partial differential equations. To speed up the registration, an adaptive force is introduced according to the maximum displacement of each iteration. Both synthetic datasets and real datasets are used to evaluate the proposed method. We compare the results of the linear viscoelastic model with those of the fluid model on the basis of both the standard and adaptive forces. The results demonstrate that the adaptive force increases in both models and that the linear viscoelastic model improves the registration accuracy.

1. Introduction

A current major topic in computational neuroanatomy is the development of nonrigid image registration algorithms. Nonrigid image registration has many potential applications. It can be applied to building atlases, segmentation, quantifying local morphological differences, comparing the variance of different population, and detecting pathological changes [1–4]. Various methods have been developed to deal with nonrigid image registration. The methods are usually classified into two categories: feature-based and intensity-based [5]. The former first needs to build a geometric model and identify a number of anatomic characters in the model. These characters include point landmarks, curves, and surfaces [6–8]. The anatomical characters are then parameterized. The aim of the registration is to find the optimal combinations of the model parameters. These methods are critically dependent on feature extraction quality. However, the anatomical structures are complex, making it difficult to extract them accurately. Usually, human interaction is required during registration, thereby making the process inconvenient and

time consuming. The intensity-based method is used to match regional intensity patterns based on mathematical or statistical criteria [9–13]. This method reduces the need for direct feature extraction or segmentation, can be automatic, and can obtain satisfactory results and is thus widely used. Fluid registration uses physics models and assumes that the deformation obeys fluid mechanics laws. These methods allow flexible deformation with large freedom and are used in many applications.

In the early 1980s, the elastic model was proposed as a means to match images [14]. Brain images are modeled as an elastic solid and the deformations are calculated from elastic mechanic equations [15, 16]. However, this model is only suitable for small deformations. To address this problem, the properties of brain images were assumed to be like those of viscous fluid, and the viscous fluid model was proposed [17], where the deformations are driven by forces that are equal to the gradient of the sum of squared intensity difference (SSD) metrics. The orientation and magnitude of deformation fields are computed using the fluid-dynamical Navier-Stokes equation. This method allows large deformations and serious



FIGURE 1: Maxwell model is made of springs (E) and dashpots (η) in series, and the forces acting on two parts are equal.

localized distortions, but with increased likelihood of misregistration [18]. The Navier-Stokes equation is solved by means of the relaxation method and requires much time. To reduce the computation cost, Bro-Nielson proposed a convolution filter method to solve the equation quickly [19]. However, Wollny et al. [20] obtained unsatisfactory results when using a small filter width in the convolution filter methods. However, if the filter width is large, the computational costs are not more advantageous than when using iterative methods. Thus the relaxation method is currently the best method. The brain images are also modeled as diffusions [21–23] and have been shown to be similar to the method proposed by Bro-Nielsen et al. [19].

In this study, we try to use the properties of both elastic solids and viscous fluids to register images. Linear viscoelastic matter has these properties. The deformation properties of brain images are assumed to be similar to those of viscoelastic matter and obey viscoelastic laws [24, 25]. As the Maxwell model has the abilities to describe linear viscoelastic deformation [26], this study hence utilizes the Maxwell model to represent and capture large deformation of the brain images. When a force acts on the Maxwell model, the motion of the fluid component relaxes over time, allowing large displacements. The deformation fields are constrained by both elastic and fluid components. To speed up the algorithm, an adaptive force is introduced. Given our aim of monomodal anatomic image registration, the SSD is used as a similarity metric in the registration. Both synthetic and real images are used to demonstrate the performance of the proposed method. The performances of both models (Maxwell and fluid) with both forces (standard and adaptive) are compared with each other. The fluid model with adaptive forces (FMAF) has the fastest registration speed, the Maxwell model with adaptive force (MMAF) is the second, the Maxwell model with standard force (MMSF) is the third, and the fluid model with standard force (FMSF) is the slowest. The ranking of registration accuracy from high to low is as follows: MMAF, MMSE, FMAF, and FMSE.

2. Materials and Methods

2.1. Maxwell Model. The Maxwell model [26] is made of a spring and a dashpot in series (Figure 1), which is perfectly elastic and viscous. Since the deformation process is assumed to be quasistatic, inertia can be neglected and the force or stress is the same in both parts. The total deformation is the sum deformations of both parts. If the displacement of spring or dashpot is \vec{u}^s or \vec{u}^d , the total displacement \vec{u} is

$$\vec{u} = \vec{u}^s + \vec{u}^d. \quad (1)$$

If E is Young's modulus of the spring and η is the viscosity of the dashpot, σ_s and σ_d are the stresses of the spring and the dashpot. The stresses are

$$\sigma_s = E\vec{u}^s, \quad \sigma_d = \eta\dot{\vec{u}}^d, \quad \sigma_s = \sigma_d. \quad (2)$$

Given that the force on the spring and the dashpot is equal at any given time, the two parts can be processed independently.

2.2. Reference Frame. Two kinds of reference frames are used to describe deformations in a floating image that is deformed to a target image. One is the Lagrangian reference frame, which describes the deformations by observing changes in the positions and velocities of definite particles. The other is the Eulerian reference frame, which describes the deformations by observing velocity changes at fixed points. The Eulerian reference frame is suitable for large deformations because it does not trace the motion of the particles [27]. Therefore, the Eulerian reference frame is used to track the deformations in our method. Voxel grids are used as the fixed points. A particle at grid position \vec{x} in floating image $I_1(\vec{x})$ at time t is originated at the position $\vec{x}(t) - \vec{u}(\vec{x}, t)$, where $\vec{u}(\vec{x}, t)$ is the displacement field. The corresponding velocity field $\vec{v}(\vec{x}, t)$ is expressed as

$$\vec{v}(\vec{x}, t) = \frac{\partial \vec{u}(\vec{x}, t)}{\partial t} + \sum_{j=1}^3 v_j \frac{\partial \vec{u}(\vec{x}, t)}{\partial x_j}, \quad (3)$$

where $\vec{v} = [v_1, v_2, v_3]$. It comes from the derivative of the displacement field about time. The second term in (3) represents the nonlinearities of the displacement field.

2.3. The Viscoelastic Fluid Algorithm. We extend the Maxwell model to three dimensions. The spring becomes an elastic solid, and the dashpot becomes a viscous fluid. Therefore, the total deformation is similar to that in (1), where $\vec{u}^s = [u_1^s, u_2^s, u_3^s]$ and $\vec{u}^d = [u_1^d, u_2^d, u_3^d]$ are displacements of the elastic solid part and the viscous fluid part, respectively. The force of the two parts is equal and is expressed as

$$\vec{f}^s = \vec{f}^d, \quad (4)$$

where \vec{f}^s and \vec{f}^d are the forces acting on the elastic solid part and the viscous fluid part, respectively.

We used the continuum mechanics method to compute the displacements. The elastic solid displacements are described by the following partial differential equations:

$$\mu^s \nabla^2 \vec{u}^s + (\lambda^s + \mu^s) \nabla (\nabla \cdot \vec{u}^s) + \vec{f}^s = 0, \quad (5)$$

where μ^s and λ^s are Lamé's elastic coefficients and $\vec{u}^s = [u_1^s(x, t), u_2^s(x, t), u_3^s(x, t)]$. The velocity of the viscous fluid part is determined using the following equation:

$$\mu^d \nabla^2 \vec{v}^d + (\lambda^d + \mu^d) \nabla (\nabla \cdot \vec{v}^d) + \vec{f}^d = 0, \quad (6)$$

where $\vec{v}^d = [v_1^d(x, t), v_2^d(x, t), v_3^d(x, t)]$ and μ^d and λ^d are the viscosity constants.

The velocity field of viscous fluid in an Eulerian reference frame can be determined by the following equation:

$$\vec{v}^d(\vec{x}, t) = \frac{\partial \vec{u}^d(\vec{x}, t)}{\partial t} + \sum_{j=1}^3 v_j^d \frac{\partial \vec{u}^d(\vec{x}, t)}{\partial x_j}. \quad (7)$$

The displacement fields \vec{u}^d are updated iteratively over time step Δt and are determined as follows:

$$\vec{u}^d(t + \Delta t) = \vec{u}^d(t) + \Delta t [\vec{v}^d(t) - \nabla \vec{u}^d(t) \vec{v}^d(t)]. \quad (8)$$

Time step Δt is chosen according to the perturbation of the deformation field; we have

$$\Delta t = \max \left(\left\| \vec{v}^d(\vec{x}, t) - \sum_{i=1}^3 v_i^d(\vec{x}, t) \left[\frac{\partial \vec{u}^d(\vec{x}, t)}{\partial x_i} \right] \right\| \right). \quad (9)$$

The boundary conditions $\vec{u}^s(\vec{x}, t) = 0$ and $\vec{v}^d(\vec{x}, t) = 0$, and the total displacements on the boundary are set to zero. The elastic equation (5) and fluid equation (6) are solved simultaneously to obtain the total deformation.

2.4. The Adaptive Force. The motivation of the adaptive force is to speed up the registration. In the proposed method, the key parts of the partial differential equations (PDEs) (5) and (6) are the forces that drive the floating image to deform to the target image $I_2(\vec{x})$. The gradient of the SSD metrics is used as these forces. The standard force is defined as

$$f = -\alpha (I_1(\vec{x} - \vec{u}(\vec{x}, t)) - I_2(\vec{x})) \nabla I_1(\vec{x})|_{\vec{x} - \vec{u}(\vec{x}, t)}, \quad (10)$$

where α is a constant.

The $\nabla I_1(\vec{x})|_{\vec{x} - \vec{u}(\vec{x}, t)}$ is the gradient of the floating image at $\vec{x} - \vec{u}(\vec{x}, t)$. $I_1(\vec{x} - \vec{u}(\vec{x}, t)) - I_2(\vec{x})$ is the difference in intensity between the deformed floating image and the target image and weighs the $\nabla I_1(\vec{x})|_{\vec{x} - \vec{u}(\vec{x}, t)}$. The force is minimized at the location where the floating image and the target image are aligned.

As the registration progresses, the forces become smaller and the corresponding velocities also become smaller which lead to very small deformation in the iteration. Therefore, more iterations are needed to reach the final deformations. To speed up the registration, the forces should increase in the next iteration. Hence, an adaptive force is introduced to solve the problem in the proposed method. The maximum of the displacements should not stay below a specific threshold. When the maximum of the displacements is below the threshold at the current iteration, the forces are adjusted automatically to increase the maximum of the displacements in the next iteration. In our method, an empirical formula is used to define the adaptive force. The adaptive force in the Eulerian reference frame is expressed as

$$\begin{aligned} \vec{f}_{n+1} &= \vec{f}_{n+1}^s(\vec{x}, \vec{u}(\vec{x}, t)) = \vec{f}_{n+1}^d(\vec{x}, \vec{u}(\vec{x}, t)) \\ &= -\alpha_{n+1} \times (I_1(\vec{x} - \vec{u}(\vec{x}, t)) - I_2(\vec{x})) \nabla I_1(\vec{x})|_{\vec{x} - \vec{u}(\vec{x}, t)}, \end{aligned} \quad (11)$$

where $n + 1$ is the next iteration and α_{n+1} is the function with respect to the maximum displacements of the current iteration. It is described as

$$\alpha_{n+1} = \begin{cases} \alpha_n (1 + \beta (\gamma - \max(\|\vec{u}(\vec{x}, t)\|))), & \text{if } (\max(\|\vec{u}(\vec{x}, t)\|)) < \gamma, \\ \alpha_n, & \text{if } (\max(\|\vec{u}(\vec{x}, t)\|)) \geq \gamma, \end{cases} \quad (12)$$

where $\max(\|\vec{u}(\vec{x}, t)\|)$ is the maximum of the displacements of the current iteration.

If the maximum displacement is below the threshold γ , $1 + \beta(\gamma - \max(\|\vec{u}(\vec{x}, t)\|))$ should be larger than one, thereby making α_{n+1} larger than α_n . The parameter α_{n+1} of the next iteration increases automatically. Therefore, the corresponding forces \vec{f}_{n+1} also increase to prevent the displacement from becoming too small.

2.5. Implementation. When the floating image is deformed by the corresponding deformation field in the registration, the topology of the floating image should be preserved. Keeping all Jacobian of the deformation fields positive can preserve the topology. In the implementation, when the minimum of the Jacobian is below 0.5, the transformation is applied to the floating image to produce a new image and the displacement field \vec{u} is set to zero. The new image is then used as the floating image in the subsequent registration. The process continues as long as the SSD decreases. The pseudocode of the algorithm is as follows.

- (1) Let $t = 0$ and $\vec{u}(\vec{x}, 0) = 0$.
- (2) Calculate the force using (10), (11), and (12).
- (3) If the SSD stops decreasing or the maximum number of iterations is reached, then stop.
- (4) Solve PDEs (5) and (6) for displacements $\vec{u}^s(\vec{x}, t)$ and instantaneous velocity $\vec{v}^d(\vec{x}, t)$, respectively.
- (5) Choose time step Δt according to (8) and calculate $\vec{u}^d(\vec{x}, t)$.
- (6) Calculate the total displacement $\vec{u}(\vec{x}, t) = \vec{u}^s(\vec{x}, t) + \vec{u}^d(\vec{x}, t)$.
- (7) If the Jacobian of the transformation is less than 0.5, a new floating image is constructed, and then go to Step 1. Otherwise, update the displacement field according to (4), then set $t = t + \Delta t$, and go to Step 2.

As it has been proved that relaxation is currently the best method [20], we solve PDEs (6) and (7) by means of successive overrelaxation [28].

2.6. Evaluation. The performance of the proposed method is evaluated on the basis of three analyses. The first analysis uses the golden deformation field \vec{T} . We then compare the recovered deformation field \vec{T}' by the root mean square (RMS) error over all voxels:

$$\text{RMS} = \sqrt{\frac{1}{N} \sum (\vec{T}'(\vec{x}) - \vec{T}(\vec{x}))^2}, \quad (13)$$

where N is the number of total voxels in the image.

TABLE 1: Computing time of various methods.

	FMSF (s)	FMAF (s)	MMSF (s)	MMAF (s)
2D simulated data	36	12	26	18
2D MRI data	60	23	41	32
IBSR database	2891	1143	2025	1793
Real data	1256	532	1077	625

The second analysis uses the mean of the SSD. They are defined as

$$\text{SSD} = \frac{1}{N} \sqrt{\sum (I_2(\vec{x}) - T(I_1(\vec{x})))^2}, \quad (14)$$

where N is the number of total voxels in the image, $I_1(\vec{x})$ and $I_2(\vec{x})$ are floating and target images, respectively. While $T(I_1(\vec{x}))$ is the deformed floating image.

The last analysis uses tissue overlaps, which are defined as

$$O = 2 \times \frac{V(I_2(\vec{x}) \cap T(I_1(\vec{x})))}{V(I_2(\vec{x})) + V(I_1(\vec{x}))}, \quad (15)$$

where V is the volume of the tissues.

If the floating image completely matches the target image, the O value would be one, and the RMS or SSD would be minimized. If there is no overlap between the two images, the O value would be zero, and the RMS or SSD would be maximized.

3. Experiments and Results

Four experiments are conducted to demonstrate the proposed method. The first two experiments are about 2D data and the rest 3D volumes. The method is implemented in C and complies with VC++ [29]. The whole image is modeled using a single set of material parameters for simplification purposes. The parameters μ^s , λ^d , μ^d are all set to one and λ^s is set to zero. The parameters α_0 and β are both set to 1, and γ is set to 0.8 voxels. The maximum iteration is set to 200. These parameters are used in all the experiments.

3.1. 2D Synthetic Datasets. The experiment shows that the proposed method can deal with large deformation well. The image sizes are 128×128 pixels, as shown in Figure 2. Figure 2(a) is the floating image, with a rectangular image, and Figure 2(b) is the target image, a C-shape image. The results of FMSF, MMSF, FMAF, and MMAF are all successful to deform the rectangular image to C-shape image. Figure 2(c) shows the results of FMAF. The computing costs are listed in the second row of Table 1. The computing times of FMSF, FMAF, MMSF, and MMAF are 36, 12, 26, and 18 seconds, respectively. The ranking of speed from the fastest to the slowest is as follows: FMAF, MMAF, MMSF, and FMSF.

3.2. 2D Brain MRI Datasets. The second experiment shows the effectiveness of the proposed method when it is applied to brain MRI. The floating image size is 256×256 , as shown in Figure 3(a). This image is registered to a selected image by

TABLE 2: Comparison of RMS and SSD for various methods.

	FMSF	FMAF	MMSF	MMAF
RMS (mm)	0.3783	0.3066	0.2742	0.2412
SSD	0.0381	0.0293	0.0367	0.0293

the finite element method [30] and obtains the deformation fields \vec{T} , which is used as the golden standard. The known deformation fields \vec{T} are applied to the floating image to obtain a target image, as shown in Figure 3(b). The known field is shown in Figure 3(c) using the following equation:

$$T = \sqrt{T_x^2 + T_y^2}, \quad (16)$$

where T_x, T_y are the known deformation fields in the x and y directions, respectively.

The fluid model and the Maxwell model with the standard forces and the adaptive forces are applied to the images. The computing time is listed in the third row of Table 1. The FMAF only costs 23 seconds, which is the fastest. By contrast, the MMAF and the MMSF cost 32 and 41 seconds, respectively, and they are the second and the third in terms of speed. The FMSF is the slowest and costs 60 seconds.

All of these methods can successfully deform the floating image to the target image. However, the matching accuracy is different. Table 2 lists the RMS and SSD acquired by the various methods. The RMS of FMSF, FMAF, MMSF, and MMAF are 0.3783, 0.3066, 0.2742, and 0.2412. According to RMS, MMAF has obtained the best result, followed by the MMSF, then FMAF, and FMSF last.

Figure 4 shows the difference among the known deformation fields obtained using various methods using the following equation:

$$\Delta T = \sqrt{(T'_x - T_x)^2 + (T'_y - T_y)^2}, \quad (17)$$

where ΔT is the difference of the known deformation fields. T'_x, T'_y are the deformation fields of x and y directions, respectively. We find that regardless of which forces act, the differences of the known deformation fields with that of the fluid model (shown in Figures 4(a) and 4(b)) are much larger than that with the Maxwell model (shown in Figures 4(c) and 4(d)). The Maxwell model has obtained better results. Among them, the Maxwell model with the adaptive forces has obtained the best result, whereas the fluid model with the standard forces has the worst results. The SSD of FMSF, FMAF, MMSF, and MMAF are 0.0381, 0.0293, 0.0367, and 0.0293. Based on the SSD, the results of the MMAF and FMAF have the same rank, whereas the results of the MMSF and the FMSF are ranked as third and fourth. It indicates that the adaptive force is superior to the standard force and the Maxwell model is more robust.

3.3. The Internet Brain Segmentation Repository (IBSR) Database. High-resolution 3D MR images are used to evaluate the proposed method. The MRI data are downloaded from the IBSR [31] and include 20 normal MR brain datasets and

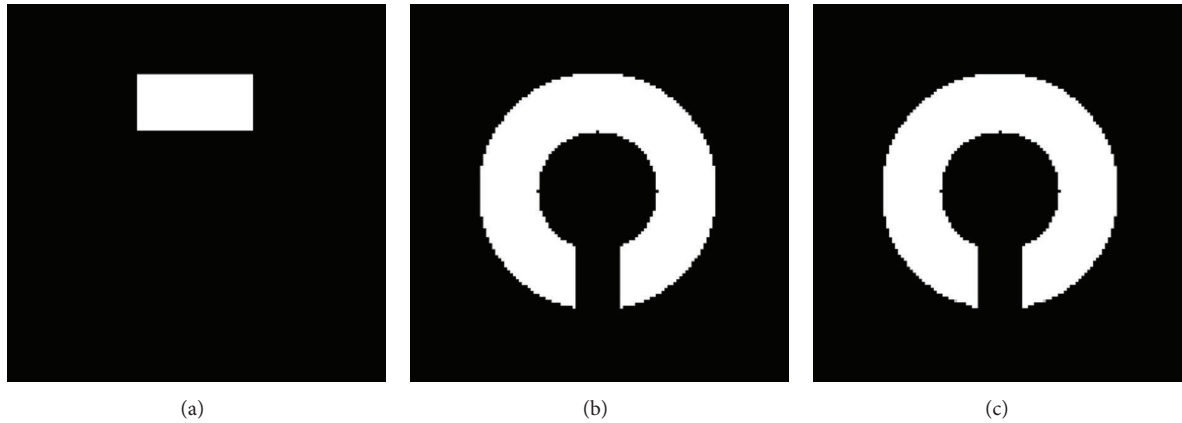


FIGURE 2: Results on 2D simulated datasets: (a) floating image, (b) target image, and (c) the result of Maxwell model with adaptive forces (MMAF).

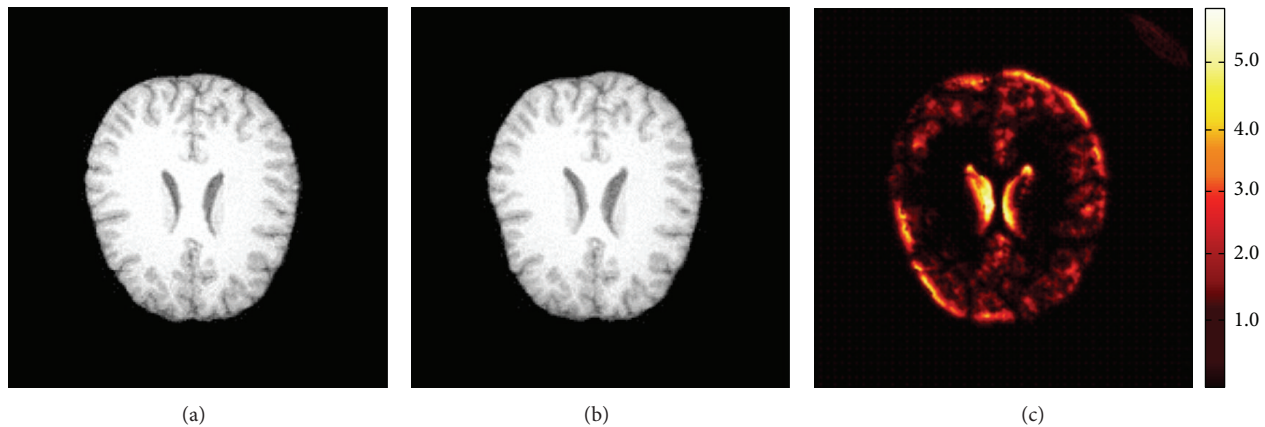


FIGURE 3: (a) Floating image. (b) Target image obtained by deforming the floating image with the known deformation field. (c) The known deformation field is obtained from FEM-based deformable registration method.

the skulls are all stripped. The column and row are 256, and the slice is from 58 to 64. The voxel size is $1 \times 1 \times 3 \text{ mm}^3$. We have randomly selected 30 couples from the data to test the methods. The mean time is listed in the fourth row of Table 1. The computing times of FMSE, FMAF, MMSF, and MMAF are 2891, 1143, 2025, and 1793. The computation time of the fluid model with the adaptive forces is the fastest, the Maxwell model with the adaptive forces is the second, the model with the standard forces is the third, and the fluid model with the standard force is the slowest.

The mean of SSD is listed in the second row of Table 3. The SSD of the FMSE, FMAF, MMSF, and MMAF are 0.0553, 0.0490, 0.0504, and 0.0484, respectively. According to the SSD value, the results obtained by the MMAF and the FMAF are ranked as the first and the second, respectively, and those acquired by the MMSF are the third. The result obtained using the FMSE is the worst. However, finding the difference using visual inspections in the results is difficult. An example is shown in Figure 5.

The average tissue overlap values are listed in the second row of Table 4. The overlap values of FMSE, FMAF, MMSF, and MMAF are 0.8813, 0.8879, 0.8872, and 0.8917. The overlap

values of the Maxwell model are larger than that of the fluid model, and the model with the adaptive forces performs better than that with the standard forces.

3.4. Real Datasets. The real datasets are acquired from the local hospital. The scans are acquired using a SIEMENS TRIO 3 Tesla scanner installed at the Institute of Biophysics of the Chinese Academy of Sciences. These scans are T1 sagittal images (TR = 1730 ms, TE = 3.93 ms, thickness = 1.0 mm, no gap, in-plane resolution = 256×256 , slice = 192, and flip angle = 15). The scans are resampled as $120 \times 120 \times 96 \text{ mm}^3$ and the voxel size is $2.0 \times 2.0 \times 2.0 \text{ mm}^3$. Thirty couples are randomly selected from the datasets. The mean time is listed in the fifth row of Table 1, and the SSD is listed in the third row of Table 3. The computing times of FMSE, FMAF, MMSF, and MMAF are 1256, 532, 1077, and 625, respectively. The SSD of FMSE, FMAF, MMSF, and MMAF are 0.0328, 0.0293, 0.0301, and 0.0279. The computation costs and matching accuracy of the real datasets are similar to those of the IBSR datasets. The overlap values are listed in the third row of Table 4. The overlap values of FMSE, FMAF, MMSF, and MMAF are

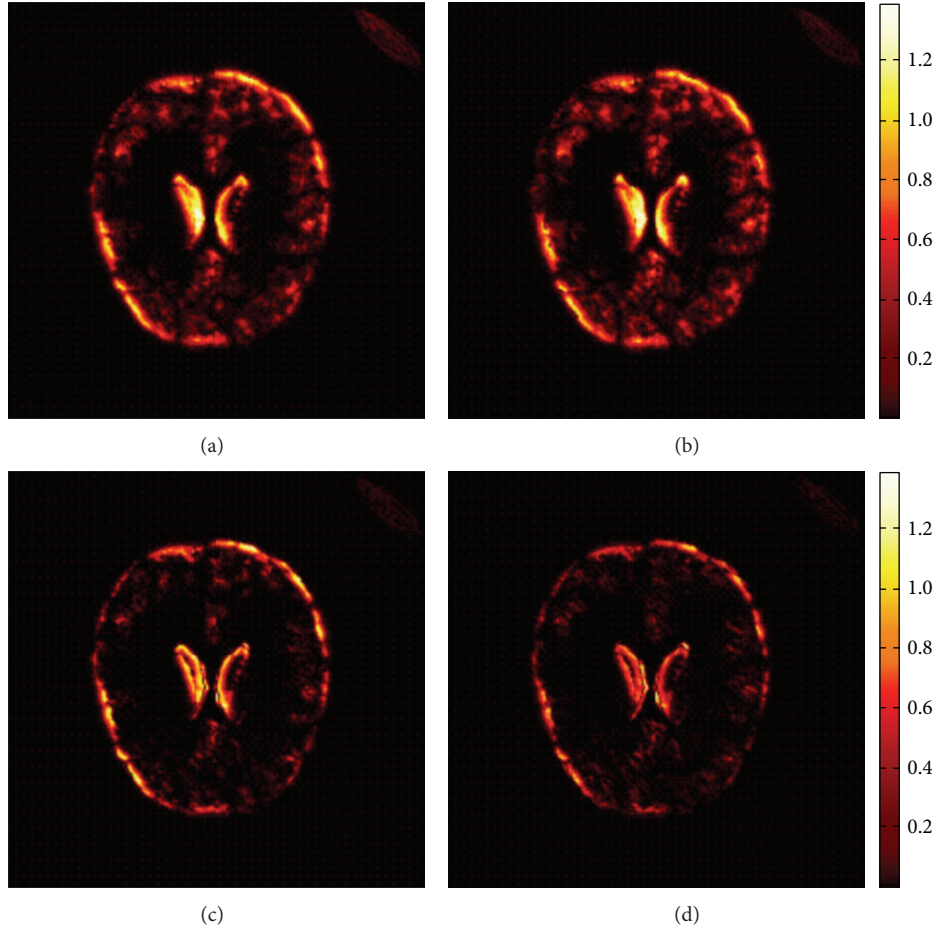


FIGURE 4: The differences of the known deformation fields with those got by various methods. (a) The difference of known deformation field with that obtained by the FMSF. (b) The difference of known deformation field with that obtained by the FMAF. (c) The difference of known deformation field with that obtained by the MMSF. (d) The difference of known deformation field with that obtained by the MMSF.

TABLE 3: Comparison of the mean values of SSD for various databases.

	FMSF	FMAF	MMSF	MMAF
IBSR database	0.0553	0.0490	0.0504	0.0484
Real data	0.0328	0.0293	0.0301	0.0279

TABLE 4: Comparison of the overlap values for various methods.

	FMMI	FMSF	FMAF	MMSF	MMAF
IBSR database	0.8794	0.8813	0.8879	0.8872	0.8917
Real data	0.8801	0.8823	0.8912	0.8892	0.8920

0.8823, 0.8912, 0.8892, and 0.8920. The results are similar to those obtained in Section 3.3. The proposed method is also compared with a method using fluid model and mutual information (FMMI) [32]. As the second column of Table 4 shows, the overlaps of the IBSR dataset and the real dataset from FMMI are the smallest, respectively. This indicates that the SSD is better than mutual information in monomodal images.

4. Conclusions

The proposed method is driven by the fluid and elastic models [15–17], which uses the Maxwell model, a linear viscoelastic model that combines the properties of elastic and fluid models, to represent the image deformation. The proposed method introduces an adaptive force to speed up the registration.

The performances of the elastic and fluid models are compared in [17]. Therefore, we only compare the proposed method with the fluid method in this paper. The successive over relaxation method is used to solve the corresponding PDE, which is not the fastest but the most accurate among the evaluated methods. The computational cost can be reduced if PDEs are solved quickly, such as when using filter convolution [19] with a small filter width and parallel computing. However, the relative computation costs should be the same as those obtained in this paper. Actually, the fluid model is a special case of the linear viscoelastic model. When $\mu^s = 0$ and $\lambda^s = 0$, the linear viscoelastic model becomes a fluid model.

Our experimental results show that the linear viscoelastic model has several potential applications and that adaptive force can greatly reduce the registration time. The proposed

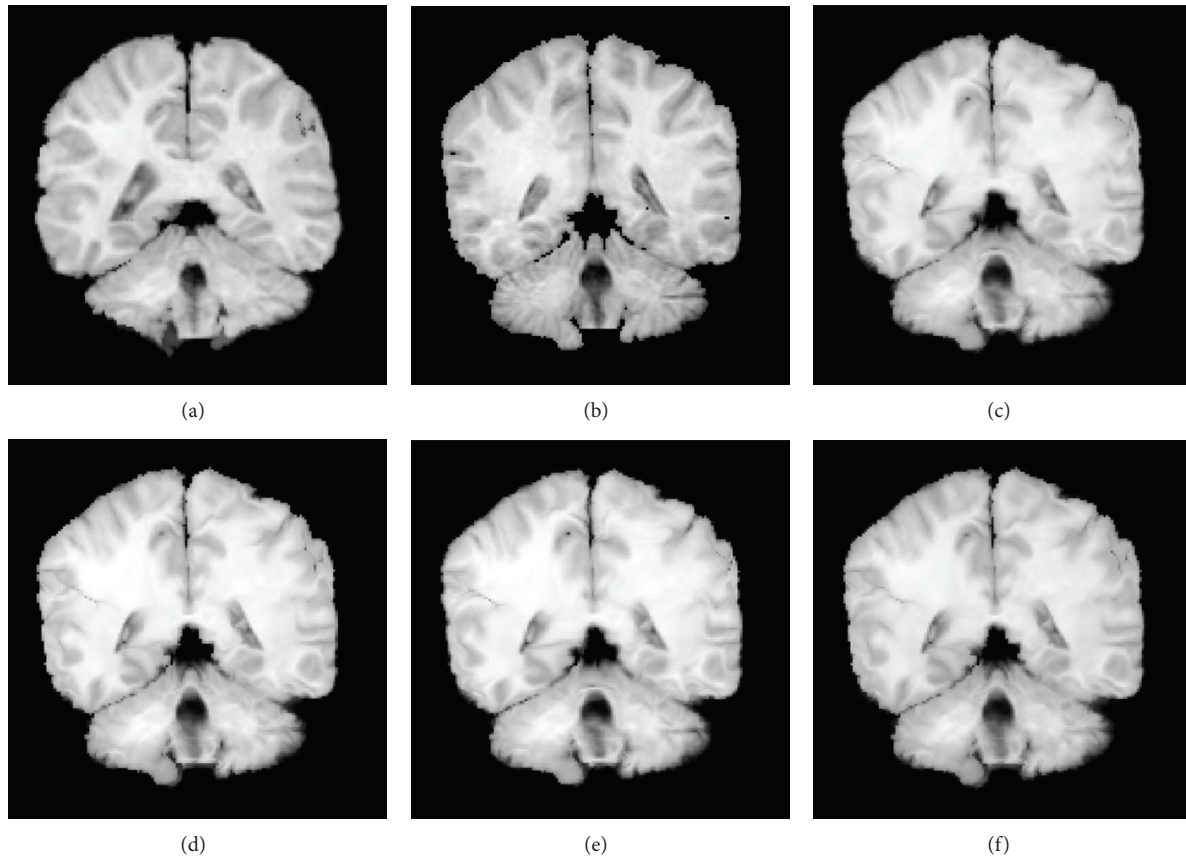


FIGURE 5: An example of the results of the 24th slice with various methods on IBSR Database is shown. (a) Floating image. (b) Target image. (c) The result of the fluid model with standard force (FMSF). (d) The result of the fluid model with adaptive force (FMAF). (e) The result of the Maxwell model with standard force (MMSF). (f) The result of the Maxwell model with adaptive force (MMAF).

method includes many parameters, and these should be analyzed further. We would also like to analyze the characterization of the transformation and how to obtain the optimal parameters for the corresponding transformation in the future.

Conflict of Interests

The authors declare that they have no conflict of interests.

Acknowledgments

This research was supported by the National Basic Research Program of China (2010CB732505 and 2013CB328806), the Key Projects in the National Science & Technology Pillar Program (2013BAI01B01), the National Hi-Tech Research and Development Program (2013AA013703), and the National Natural Science Foundation of China (61272360).

References

- [1] P. Aljabar, R. A. Heckemann, A. Hammers, J. V. Hajnal, and D. Rueckert, "Multi-atlas based segmentation of brain images: atlas selection and its effect on accuracy," *NeuroImage*, vol. 46, no. 3, pp. 726–738, 2009.
- [2] S. Joshi, B. Davis, M. Jomier, and G. Gerig, "Unbiased diffeomorphic atlas construction for computational anatomy," *NeuroImage*, vol. 23, pp. 151–160, 2004.
- [3] S. Tang, Y. Fan, G. Wu, M. Kim, and D. Shen, "RABBIT: rapid alignment of brains by building intermediate templates," *NeuroImage*, vol. 47, no. 4, pp. 1277–1287, 2009.
- [4] J. Burdett, J. Stevens, D. Flügel, E. Williams, J. S. Duncan, and L. Lemieux, "Increased sensitivity to pathological brain changes using co-registration of magnetic resonance imaging scans," *Acta Radiologica*, vol. 47, no. 10, pp. 1067–1072, 2006.
- [5] D. Rueckert and J. A. Schnabel, "Medical image registration," in *Biomedical Image Processing*, pp. 131–154, Springer, Berlin, Germany, 2011.
- [6] H. Chui and A. Rangarajan, "A new point matching algorithm for non-rigid registration," *Computer Vision and Image Understanding*, vol. 89, no. 2-3, pp. 114–141, 2003.
- [7] A. Klein, S. S. Ghosh, B. Avants et al., "Evaluation of volume-based and surface-based brain image registration methods," *NeuroImage*, vol. 51, no. 1, pp. 214–220, 2010.
- [8] P. Wen, "Medical image registration based-on points, contour and curves," in *Proceedings of the International Conference on BioMedical Engineering and Informatics (BMEI '08)*, pp. 132–136, May 2008.
- [9] F. Maes, D. Vandermeulen, and P. Suetens, "Medical image registration using mutual information," *Proceedings of the IEEE*, vol. 91, no. 10, pp. 1699–1721, 2003.

- [10] M. Otte, "Elastic registration of fMRI data using Bezier-spline transformations," *IEEE Transactions on Medical Imaging*, vol. 20, no. 3, pp. 193–206, 2001.
- [11] E. D'Agostino, F. Maes, D. Vandermeulen, and P. Suetens, "A viscous fluid model for multimodal non-rigid image registration using mutual information," *Medical Image Analysis*, vol. 7, no. 4, pp. 565–575, 2003.
- [12] A. Klein, J. Andersson, B. A. Ardekani et al., "Evaluation of 14 nonlinear deformation algorithms applied to human brain MRI registration," *NeuroImage*, vol. 46, no. 3, pp. 786–802, 2009.
- [13] J. Ashburner, "A fast diffeomorphic image registration algorithm," *NeuroImage*, vol. 38, no. 1, pp. 95–113, 2007.
- [14] C. Broit, *Optimal registration of deformed images [M.S. thesis]*, ProQuest, 1981.
- [15] R. Bajcsy and S. Kovacic, "Multiresolution elastic matching," *Computer Vision, Graphics, and Image Processing*, vol. 46, pp. 1–21, 1989.
- [16] M. Miller, G. Christensen, Y. Amit, and U. Grenander, "Mathematical textbook of deformable neuroanatomies," *Proceedings of the National Academy of Sciences of the United States of America*, vol. 90, no. 24, pp. 11944–11948, 1993.
- [17] G. Christensen, R. Rabbitt, and M. Miller, "Deformable templates using large deformation kinematics," *IEEE Transactions on Image Processing*, vol. 5, no. 10, pp. 1435–1447, 1996.
- [18] H. Lester and S. R. Arridge, "A survey of hierarchical non-linear medical image registration," *Pattern Recognition*, vol. 32, no. 1, pp. 129–149, 1999.
- [19] M. Bro-Nielsen and C. Gramkow, "Fast fluid registration of medical images," in *Visualization in Biomedical Computing*, vol. 1131 of *Lecture notes in computer science*, pp. 267–276, Springer, Berlin, Germany, 1996.
- [20] G. Wollny and F. Kruggel, "Computational cost of nonrigid registration algorithms based on fluid dynamics," *IEEE Transactions on Medical Imaging*, vol. 21, no. 8, pp. 946–952, 2002.
- [21] B. Fischer and J. Modersitzki, "Fast diffusion registration," in *Inverse problems, Image Analysis, and Medical Imaging: AMS Special Session on Interaction of Inverse Problems and Image Analysis*, vol. 3, pp. 117–127, American Mathematical Society, New Orleans, La, USA, 2002.
- [22] J. Modersitzki, *Numerical Methods for Image Registration*, Oxford University Press, New York, NY, USA, 2004.
- [23] P. Cachier, E. Bardinet, D. Dormont, X. Pennec, and N. Ayache, "Iconic feature based nonrigid registration: the PASHA algorithm," *Computer Vision and Image Understanding*, vol. 89, no. 2-3, pp. 272–298, 2003.
- [24] M. Hrapko, J. A. W. van Dommelen, G. W. M. Peters, and J. S. H. M. Wismans, "The mechanical behaviour of brain tissue: large strain response and constitutive modelling," *Biorheology*, vol. 43, no. 5, pp. 623–636, 2006.
- [25] M. Shafeian and K. Darvish, "Viscoelastic properties of brain tissue under high-rate large deformation," in *Proceedings of the ASME International Mechanical Engineering Congress and Exposition (IMECE '09)*, pp. 83–85, November 2009.
- [26] R. Lakes, *Viscoelastic Solids*, CRC Press, New York, NY, USA, 1999.
- [27] K. A. Saddi, C. Chef d'Hotel, and F. Cheriet, "Large deformation registration of contrast-enhanced images with volume-preserving constraint," in *Medical Imaging 2007: Image Processing*, Proceedings of SPIE, February 2007, 651203.
- [28] W. H. Press, *Numerical Recipes*, Cambridge University Press, Cambridge, UK, 3rd edition, The Art of Scientific Computing, 2007.
- [29] B. Zaratian, *Microsoft Visual C++ 6.0 Programmer's Guide*, Microsoft Press, 1998.
- [30] L. Ibanez, W. Schroeder, L. Ng, and J. Cates, *The ITK Software Guide*, Citeseer, 2005.
- [31] <http://www.cma.mgh.harvard.edu/ibsr/>.
- [32] X. Huang, *Nonrigid Image Registration Problem using Fluid Dynamics and Mutual Information*, University of Connecticut, Storrs, Conn, USA, 2011.

Research Article

A New Definition of Fractional Derivatives Based on Truncated Left-Handed Grünwald-Letnikov Formula with $0 < \alpha < 1$ and Median Correction

Zhiwu Liao

School of Computer Science, Sichuan Normal University, Chengdu, Sichuan 610101, China

Correspondence should be addressed to Zhiwu Liao; liaoziwu@163.com

Received 10 February 2014; Accepted 23 March 2014; Published 13 April 2014

Academic Editor: Ming Li

Copyright © 2014 Zhiwu Liao. This is an open access article distributed under the Creative Commons Attribution License, which permits unrestricted use, distribution, and reproduction in any medium, provided the original work is properly cited.

We propose a new definition of fractional derivatives based on truncated left-handed Grünwald-Letnikov formula with $0 < \alpha < 1$ and median correction. Analyzing the difficulties to choose the fractional orders and unsatisfied processing results in signal processing using fractional-order partial differential equations and related methods; we think that the nonzero values of the truncated fractional order derivatives in the smooth regions are major causes for these situations. In order to resolve the problem, the absolute values of truncated parts of the G-L formula are estimated by the median of signal values of the remainder parts, and then the truncated G-L formula is modified by replacing each of the original signal value to the differences of the signal value and the median. Since the sum of the coefficients of the G-L formula is zero, the median correction can reduce the truncated errors greatly to approximate G-L formula better. We also present some simulation results and experiments to support our theory analysis.

1. Introduction

Partial differential equations (PDEs) and related methods are very important tools for signal processing [1–13]. Especially, in recent years progress was achieved in the theory of fractional calculus as a useful tool to handle applications in the area of physics, chemistry, and engineering sciences [6–20].

However, unlike integer-order derivatives with zeros or small values in the smooth regions and with big values near singularities, the values of truncated fractional derivatives are with very large absolute values. The direct result is that the derivative values cannot be used to measure the degrees of singularities. That is, small derivative values perhaps relate to singularity regions and big derivative values perhaps relate to smooth regions. Therefore, some integer-order PDE methods cannot be modified to their fractional-order counterparts directly. Hu noticed the problem in 2013 and proposed a new fractional-order PDE with different orders of different parts for fractional-order PM method [13]. However, he did not give the analysis in theory.

In this paper, we study behaviors of fractional-order derivatives of truncated left-handed Grünwald-Letnikov formula with $0 < \alpha < 1$. Based on the analysis, a new fractional derivative formula is proposed based on truncated left-handed Grünwald-Letnikov formula with $0 < \alpha < 1$ and median correction. The median correction is used to reduce the truncated errors of G-L formula.

The rest of this paper is as follows. Section 2 introduces some basic theory backgrounds in fractional derivatives; we also deduce some useful results based on these theory backgrounds. In Section 3 we introduce the truncated G-L formula and its numerical approximation. Section 4 presents the new fractional derivative formula and gives properties and numerical methods for the new fractional definition. The simulation results and experiments are presented in Section 5. We also give conclusions and acknowledgments finally.

2. Fractional Derivatives

In this section, we will introduce some preparations for the new method, that is, Grünwald-Letnikov formula and its matrix approximation.

2.1. Grünwald-Letnikov Formula. Fractional-order derivatives are defined as operators whose orders have been extended to noninteger numbers. There are a number of definitions of fractional derivatives. One usual way of representing the discrete fractional derivatives is by the Grünwald-Letnikov (G-L) formula [21, 22], which is

$$D_{GL}^\alpha u(x) = \lim_{\Delta x \rightarrow 0} \frac{1}{\Delta x^\alpha} \sum_{k=0}^{[(x-a)/\Delta x]} \omega_k^{(\alpha)} u(x - k\Delta x), \quad (1)$$

where $x \in [a, b]$, Δx denotes the uniform space step, and $\omega_k^{(\alpha)} = (-1)^k \binom{\alpha}{k}$ represents the normalized G-L weights which are given by

$$\begin{aligned} \omega_0^{(\alpha)} &= 1, \\ \omega_k^{(\alpha)} &= (-1)^k \frac{\alpha(\alpha-1)\cdots(\alpha-k+1)}{k!} = \frac{\Gamma(k-\alpha)}{\Gamma(-\alpha)\Gamma(k+1)}, \\ &\text{for } k = 1, 2, 3, \dots \end{aligned} \quad (2)$$

For $\alpha = 1$, (1) becomes the classical 1st derivative, and for any $\alpha = n$, $n \in \mathbb{N}$ is a positive integer; they are classical n th derivatives of $u(x)$. Note that for when α is a positive integer, equations are with limit support whose support lengths are $\alpha + 1$. However, for when α is not an integer, fractional derivatives are nonlocal operators. That is, the value of the fractional derivative at a point x depends on the function values at all the points to the left of the point x .

Therefore, in order to handle fractional derivative numerically, it is necessary to compute the coefficients $\omega_k^{(\alpha)}$, where α is the order of the fractional derivative. For that we can use the recurrence relationships:

$$\begin{aligned} \omega_0(\alpha) &= 1; \\ \omega_k^{(\alpha)} &= \left(1 - \frac{\alpha+1}{k}\right) \omega_{k-1}^{(\alpha)}, \quad k = 1, 2, 3, \dots \end{aligned} \quad (3)$$

Some useful properties for left-handed G-L formula are presented as follows.

Lemma 1. *The nonlocal operator defined in (1) is a linear operator.*

Proof. $u(x)$ and $v(x)$ are two functions, and $x \in [a, b]$; λ is a real number. We have

$$\begin{aligned} (1) \quad D_{GL}^\alpha [u(x) + v(x)] &= \lim_{\Delta x \rightarrow 0} \frac{1}{\Delta x^\alpha} \\ &\quad \times \sum_{k=0}^{[(x-a)/\Delta x]} \omega_k^{(\alpha)} [u(x - k\Delta x) + v(x - k\Delta x)] \\ &= \lim_{\Delta x \rightarrow 0} \frac{1}{\Delta x^\alpha} \sum_{k=0}^{[(x-a)/\Delta x]} \omega_k^{(\alpha)} u(x - k\Delta x) \\ &\quad + \lim_{\Delta x \rightarrow 0} \frac{1}{\Delta x^\alpha} \sum_{k=0}^{[(x-a)/\Delta x]} \omega_k^{(\alpha)} v(x - k\Delta x) \\ &= D_{GL}^\alpha u(x) + D_{GL}^\alpha v(x) \\ (2) \quad D_{GL}^\alpha [\lambda u(x)] &= \lim_{\Delta x \rightarrow 0} \frac{1}{\Delta x^\alpha} \sum_{k=0}^{[(x-a)/\Delta x]} \omega_k^{(\alpha)} [\lambda u(x)] \\ &= \lambda \lim_{\Delta x \rightarrow 0} \frac{1}{\Delta x^\alpha} \sum_{k=0}^{[(x-a)/\Delta x]} \omega_k^{(\alpha)} u(x) \\ &= \lambda D_{GL}^\alpha u(x). \end{aligned} \quad (4)$$

□

Lemma 2. $\sum_{k=0}^\infty \omega_k^{(\alpha)} = 0$.

Proof. Since $(1 - z)^\alpha = \sum_{k=0}^\infty \omega_k^{(\alpha)} z^k$, let $k = 1$; we have

$$\sum_{k=0}^\infty \omega_k^{(\alpha)} = (1 - 1)^\alpha = 0. \quad (5)$$

□

Lemma 3. *For $0 < \alpha < 1$, m is a positive integer; one has*

$$\begin{aligned} \omega_k^{(\alpha)} &< 0, \quad k = 1, 2, 3, \dots, \\ \sum_{k=m}^\infty \omega_k^{(\alpha)} &< 0. \end{aligned} \quad (6)$$

Proof. For $k = 1$, $\omega_1^{(\alpha)} = -\alpha < 0$.

Assume that $\omega_k^{(\alpha)} < 0$.

According to (3), we have $\omega_{k+1}^{(\alpha)} = (1 - (\alpha+1)/(k+1))\omega_k^{(\alpha)}$. Since $0 < \alpha < 1$ and $k+1 \geq 2$, $(1 - (\alpha+1)/(k+1)) > 0$. Thus, $\text{sgn}(\omega_{k+1}^{(\alpha)}) = \text{sgn}(\omega_k^{(\alpha)}) < 0$. Here

$$\text{sgn}(x) = \begin{cases} 1, & x \geq 0, \\ -1, & x < 0. \end{cases} \quad (7)$$

Then, we have $\omega_{k+1}^{(\alpha)} < 0$. Thus, $\sum_{k=m}^\infty \omega_k^{(\alpha)} < 0$. □

Lemma 4. For $0 < \alpha < 1$, $m \geq 0$ is an integer. One has

$$\sum_{k=m}^{\infty} \omega_k^{(\alpha)}(-k) > 0. \tag{8}$$

Proof. From Lemma 3, for $0 < \alpha < 1$, $\omega_k^{(\alpha)} < 0$, $k = 1, 2, 3, \dots$

Thus, $\omega_k^{(\alpha)}(-k) > 0$ for $k = 1, 2, 3, \dots$. We have $\sum_{k=m}^{\infty} \omega_k^{(\alpha)}(-k) > 0$, $m \geq 1$.

Since $\omega_0^{(\alpha)}(-0) = 0$, we have $\sum_{k=m}^{\infty} \omega_k^{(\alpha)}(-k) > 0$, $m \geq 0$. \square

2.2. Numerical Method of G-L Formula. For G-L formula in (1) in signal processing, the uniform space step is set to $\Delta x = 1$ for easy description; x is the variant whose support is $[a, b]$. That is, the signal $u(x)$ is compact support. Therefore, equations can be specified as

$$D_{GL}^{\alpha} = \sum_{k=0}^{[x-a]} \omega_k^{(\alpha)} s(x-k). \tag{9}$$

The coefficients can also be obtained recursively from (3). We can discretize (1) into a finite difference on a grid on the x axis, where the 0th lattice is a ; j th lattice is x_j , $j = 1, 2, \dots, n-1$; and the n th lattice is b . That is, n is the length of the signal.

Therefore, using the matrix approximate method, we have

$$D_{GL}^{\alpha} \mathbf{S} = M^{(\alpha)} \mathbf{S}, \tag{10}$$

where TGL represents truncated G-L formula, $\mathbf{S} = [s(x_0), s(x_1), \dots, s(x_n)]^T$, T represents the transposed vector, and $M^{(\alpha)}$ is an $n \times n$ lower triangular strip matrix defined as

$$M^{(\alpha)} = \begin{pmatrix} \omega_0^{(\alpha)} & 0 & \dots & 0 \\ \omega_1^{(\alpha)} & \omega_0^{(\alpha)} & \dots & \vdots \\ \vdots & \vdots & \ddots & 0 \\ \omega_n^{(\alpha)} & \omega_{n-1}^{(\alpha)} & \dots & \omega_0^{(\alpha)} \end{pmatrix}. \tag{11}$$

3. Truncated Grünwald-Letnikov Formula

Fractional integration and fractional differentiation are generalizations of notions of integer-order integration and differentiation and include n th derivatives (n denotes an integer number) as particular cases. One usual way of representing the discrete fractional derivatives is by the Grünwald-Letnikov (G-L) formula introduced in Section 2 (see (1)).

However, for digital signals, we have to discuss truncated G-L formula rather than the G-L formula itself because of the limited supports of digital signals. In this section, the definition of truncated G-L formula and its properties are discussed firstly and then we will give its numerical scheme.

3.1. Truncated Grünwald-Letnikov Formula. The truncated G-L formula is

$$D_{TGL}^{\alpha} s(x) = \sum_{k=0}^t \omega_k^{(\alpha)} s(x-k), \tag{12}$$

where $x \in [a, b]$, the uniform space step is set to 1, t is the length of the support, $\omega_k^{(\alpha)} = (-1)^k \binom{\alpha}{k}$ represents the normalized G-L weights, and their recurrence relationship is given by (3).

Just as above sections, we will discuss some properties of truncated G-L formula.

Lemma 2'. For $0 < \alpha < 1$, $t \geq 0$ is an integer. One has

$$\sum_{k=0}^t \omega_k^{(\alpha)} > 0. \tag{13}$$

Proof. According to Lemma 2, we have

$$0 = \sum_{k=0}^{\infty} \omega_k^{(\alpha)} = \sum_{k=0}^t \omega_k^{(\alpha)} + \sum_{k=t+1}^{\infty} \omega_k^{(\alpha)}. \tag{14}$$

According to Lemma 3, $\sum_{k=t+1}^{\infty} \omega_k^{(\alpha)} < 0$. Therefore, $\sum_{k=0}^t \omega_k^{(\alpha)} > 0$. \square

Lemma 3'. For $0 < \alpha < 1$, m is a positive integer, $t \geq m$. One has

$$\sum_{k=m}^t \omega_k^{(\alpha)} < 0. \tag{15}$$

Proof. For $k = 1$, $\omega_1^{(\alpha)} = -\alpha < 0$.

Assume that $\omega_k^{(\alpha)} < 0$.

According to Lemma 1, we have $\omega_{k+1}^{(\alpha)} = (1 - (\alpha + 1)/(k + 1))\omega_k^{(\alpha)}$. Since $0 < \alpha < 1$ and $k + 1 \geq 2$, $(1 - (\alpha + 1)/(k + 1)) > 0$. Thus, $\text{sgn}(\omega_{k+1}^{(\alpha)}) = \text{sgn}(\omega_k^{(\alpha)}) < 0$. Here

$$\text{sgn}(x) = \begin{cases} 1, & x \geq 0, \\ -1, & x < 0. \end{cases} \tag{16}$$

Then, we have $\omega_{k+1}^{(\alpha)} < 0$. Thus, $\sum_{k=m}^t \omega_k^{(\alpha)} < 0$. \square

Lemma 4'. For $0 < \alpha < 1$, $m \geq 0$ is an integer and t is a positive integer. One has

$$\sum_{k=m}^t \omega_k^{(\alpha)}(-k) > 0. \tag{17}$$

Proof. From Lemma 3, for $0 < \alpha < 1$, $\omega_k^{(\alpha)} < 0$, $k = 1, 2, 3, \dots$

Thus, $\omega_k^{(\alpha)}(-k) > 0$ for $k = 1, 2, 3, \dots, t$. We have $\sum_{k=m}^t \omega_k^{(\alpha)}(-k) > 0$, $m \geq 0$, $t \geq 1$. \square

3.2. Numerical Method of Truncated G-L Formula. We can discretize (12) into a finite difference on a grid on the x axis, where the 0th lattice is a ; j th lattice is x_j , $j = 1, 2, \dots, n-1$; and the n th lattice is b . That is, n is length of signals.

Therefore, using the matrix approximate method, we have

$$D_{GL}^{\alpha} \mathbf{S} \approx D_{TGL}^{\alpha} \mathbf{S} = M_T^{(\alpha)} \mathbf{S}, \tag{18}$$

where $\mathbf{S} = [s(x_0), s(x_1), \dots, s(x_n)]^T$, T represents the transposed vector, and $M_T^{(\alpha)}$ is an $n \times n$ matrix defined as

$$M_T^{(\alpha)} = \begin{pmatrix} \omega_0^{(\alpha)} & 0 & \dots & 0 & 0 & \dots & 0 \\ \omega_1^{(\alpha)} & \omega_0^{(\alpha)} & \dots & \vdots & 0 & \dots & 0 \\ \vdots & \vdots & \ddots & 0 & \vdots & \ddots & \vdots \\ \omega_t^{(\alpha)} & \omega_{t-1}^{(\alpha)} & \dots & \omega_0^{(\alpha)} & 0 & \dots & 0 \\ 0 & \omega_t^{(\alpha)} & \omega_{t-1}^{(\alpha)} & \dots & \omega_0^{(\alpha)} & \dots & 0 \\ \vdots & \vdots & \ddots & \ddots & \ddots & \ddots & \vdots \\ 0 & \dots & 0 & \omega_t^{(\alpha)} & \omega_{t-1}^{(\alpha)} & \dots & \omega_0^{(\alpha)} \end{pmatrix}. \quad (19)$$

Notice that n is the length of the signal and t is the length of the support. That is, $n \geq t$. Since $M_T^{(\alpha)}$ is sparser than $M^{(\alpha)}$ for $n > t$, the computation cost of the truncated G-L formula is lower than that of the G-L formula.

4. New Truncated Grünwald-Letnikov Formula

Although Lemma 2 tells us the values of fractional derivatives for a constant function $s(x) = 1$ defined by G-L formula equal to zeros, for truncated G-L formula, Lemma 2' shows that it is not true.

The main awkwardness for this situation comparing with integer-order derivatives is that the fractional derivatives cannot be used to measure the strength of singularities. Therefore, estimation methods based on the strength of singularities measured by the modula of 1-order derivatives cannot be generalized to their fractional counterparts directly. These estimation methods include many popular and state-of-art frameworks, such as anisotropic diffusion, nonlocal means, and bilateral filtering.

Therefore, in order to generalize fractional derivatives to these frameworks, the truncated G-L formula should be modified as follows: for $s(x) = c$, $c \neq 0$, $D^\alpha s(x) = 0$.

We start from the requirement to obtain the definition and properties of the new truncated G-L formula, and then the numerical method of the new model by matrix is presented.

4.1. Motivations and Definitions. The discussion is from the error of truncated G-L formula.

Definition 5. The error of the truncated G-L formula is

$$\begin{aligned} \text{Err}_{\text{TGL}}(s(x)) &= \sum_{k=0}^{\infty} \omega_k^{(\alpha)} s(x-k) - \sum_{k=0}^t \omega_k^{(\alpha)} s(x-k) \\ &= \sum_{k=t+1}^{\infty} \omega_k^{(\alpha)} s(x-k), \end{aligned} \quad (20)$$

where TGL represents truncated G-L formula, t is the support length, and $s(\cdot)$ is the signal, $0 < \alpha < 1$.

Especially, for $s(x) = 1$, we have

$$\text{Err}_{\text{TGL}}(s(x)) = \sum_{k=t+1}^{\infty} \omega_k^{(\alpha)}, \quad (21)$$

that is, the sum of all terms after t . From Lemma 2', we have $\sum_{k=0}^t \omega_k^{(\alpha)} > 0$, for $t \geq 0$, $0 < \alpha < 1$ and from Lemma 3, we have $\omega_k^{(\alpha)} < 0$, for $k = 1, 2, \dots$, $0 < \alpha < 1$, which implies that the error will become smaller as t becomes bigger.

Moreover, from Lemma 2, we have $\sum_{k=0}^{\infty} \omega_k^{(\alpha)} = 0$; thus, the truncated error can be changed as follows.

Proposition 6. *The truncated error of $s(x) = 1$ is*

$$\text{Err}_{\text{TGL}}(s(x)) = -\sum_{k=0}^t \omega_k^{(\alpha)}. \quad (22)$$

Proof. From Lemma 2 and the above equation,

$$\begin{aligned} 0 &= \sum_{k=0}^{\infty} \omega_k^{(\alpha)} = \sum_{k=0}^t \omega_k^{(\alpha)} + \sum_{k=t+1}^{\infty} \omega_k^{(\alpha)} \\ &= \sum_{k=0}^t \omega_k^{(\alpha)} + \text{Err}_{\text{TGL}}(s(x)). \end{aligned} \quad (23)$$

Thus,

$$\text{Err}_{\text{TGL}}(s(x)) = -\sum_{k=0}^t \omega_k^{(\alpha)}. \quad (24)$$

For $s(x) = c$, c is a constant real number; we can get similar results. \square

Proposition 7. *The truncated error of $s(x) = c \neq 0$ is*

$$\text{Err}_{\text{TGL}}(s(x)) = -c \sum_{k=0}^t \omega_k^{(\alpha)}. \quad (25)$$

Similarly, for $s(x) \neq \text{constant}$, values from $t + 1$ to ∞ are not known and we only know the samples from 0 to t . Thus, we should estimate errors defined in (20) by the values from 0 to t . For $s(x) = \text{constant}$, estimate errors defined in (20) by the values from 0 to t have been accomplished through Proposition 7, which reminds us that the problem can be solved by assuming $s(x)$ a constant. Thus, times the constant and the sum of $\omega_k^{(\alpha)}$, $k = 0, 1, \dots$, k can approximate the error well. This constant also should be estimated from values from 0 to t .

One alternative scheme is that the median of values from 0 to t is used as the estimate value for the constant since median is an estimate with good performance in flexibility and reliability.

Definition 8. The new truncated G-L formula is

$$D_{\text{NTGL}}^\alpha s(x) = \sum_{k=0}^t \omega_k^{(\alpha)} s(x-k) - \text{median}(\mathbf{S}) \sum_{k=0}^t \omega_k^{(\alpha)}, \quad (26)$$

where NTGL represents the new truncated G-L formula, $\text{median}(\mathbf{S})$ is the median of the vector $\mathbf{S} = [s(x), s(x - 1), \dots, s(x - t)]^T$, the uniform space step is set to 1, t is the length of the support, and $\omega_k^{(\alpha)} = (-1)^k \binom{\alpha}{k}$ represents the normalized G-L weights.

4.2. Numerical Method of New Truncated G-L Formula. We can discretize (26) into a finite difference on a grid on the x axis, where the 0th lattice is a ; j th lattice is x_j , $j = 1, 2, \dots, n - 1$; and the n th lattice is b . That is, n is length of signals.

Therefore, using the matrix approximate method, we have

$$D_{\text{GL}}^\alpha \mathbf{S} \approx D_{\text{NTGL}}^\alpha \mathbf{S}_c = M_T \mathbf{S}_c, \tag{27}$$

where NTGL represents new truncated G-L formula, $\mathbf{S} = [s(x_0), s(x_1), \dots, s(x_n)]^T$, and T represents the transposed vector. $\mathbf{S}_c = [s(x_0) - \text{median}(\mathbf{S}), s(x_1) - \text{median}(\mathbf{S}), \dots, s(x_n) - \text{median}(\mathbf{S})]^T$ is the corrected vector of \mathbf{S} by the median of \mathbf{S} , and M_T is an $n \times n$ matrix defined as

$$M_T = \begin{pmatrix} \omega_0^{(\alpha)} & 0 & \dots & 0 & 0 & \dots & 0 \\ \omega_1^{(\alpha)} & \omega_0^{(\alpha)} & \dots & \vdots & 0 & \dots & 0 \\ \vdots & \vdots & \ddots & 0 & \vdots & \vdots & \\ \omega_t^{(\alpha)} & \omega_{t-1}^{(\alpha)} & \dots & \omega_0^{(\alpha)} & 0 & \dots & 0 \\ 0 & \omega_t^{(\alpha)} & \omega_{t-1}^{(\alpha)} & \dots & \omega_0^{(\alpha)} & \dots & 0 \\ \vdots & \vdots & \ddots & \ddots & \ddots & \vdots & \\ 0 & \dots & 0 & \omega_t^{(\alpha)} & \omega_{t-1}^{(\alpha)} & \dots & \omega_0^{(\alpha)} \end{pmatrix} \tag{28}$$

Notice that n is the length of the signal and t is the length of the support. That is, $n \geq t$. Since M_T is sparser than M for $n > t$, the computation cost of the truncated G-L formula is lower than the G-L formula's.

4.3. Properties of the New Truncated G-L Formula. In this subsection, we will give some important properties of the new truncated G-L formula.

Theorem 9. *The nonlocal operator defined in (27) is a linear operator.*

Proof. $u(x)$ and $v(x)$ are two functions, and $x \in [a, b]$; λ is a real number. We have

$$\begin{aligned} (1) \quad D_{\text{NTGL}}^\alpha [u(x) + v(x)] &= D_{\text{NTGL}}^\alpha [\mathbf{U} + \mathbf{V}] \\ &= M_T [\mathbf{U}_c + \mathbf{V}_c] \\ &= M_T \mathbf{U}_c + M_T \mathbf{V}_c \\ &= D_{\text{NTGL}}^\alpha u(x) + D_{\text{NTGL}}^\alpha v(x), \\ (2) \quad D_{\text{NTGL}}^\alpha [\lambda u(x)] &= D_{\text{NTGL}}^\alpha [\lambda \mathbf{U}] \\ &= \lambda M_T \mathbf{U}_c \\ &= \lambda D_{\text{NTGL}}^\alpha u(x). \end{aligned} \tag{29}$$

Here, $\mathbf{U}_c, \mathbf{V}_c$ are corrected vectors of \mathbf{U}, \mathbf{V} , which are defined as the corrected vector in (27). \square

Theorem 10. $M_T^{(\alpha)}$ and $M_T^{(\beta)}$ are two matrixes defined in (27), that is, the approximation matrixes of truncated G-L formula with fractional orders α and β , respectively. Thus,

$$M_T^{(\alpha)} M_T^{(\beta)} = M_T^{(\beta)} M_T^{(\alpha)} = \begin{pmatrix} \gamma_0 & 0 & \dots & 0 & 0 & \dots & 0 \\ \gamma_1 & \gamma_0 & \dots & \vdots & 0 & \dots & 0 \\ \vdots & \vdots & \ddots & 0 & \vdots & \vdots & \\ \gamma_t & \gamma_{t-1} & \dots & \gamma_0 & 0 & \dots & 0 \\ 0 & \gamma_t & \gamma_{t-1} & \dots & \gamma_0 & \dots & 0 \\ \vdots & \vdots & \ddots & \ddots & \ddots & \vdots & \\ 0 & \dots & 0 & \gamma_t & \gamma_{t-1} & \dots & \gamma_0 \end{pmatrix}, \tag{30}$$

where $\gamma_i = \sum_{k=0}^i \omega_k^{(\alpha)} \omega_{i-k}^{(\beta)}$, $i = 0, 1, \dots, t$.

Lemma 12 can be proved easily by times two matrixes. That is, two operators of the truncated G-L formula with different fractional orders are commutative.

We guess the following equations in Guess 1 are correct. However, we cannot prove it.

Guess 1. We have

$$D_{\text{NTGL}}^\alpha D_{\text{NTGL}}^\beta s(x) = D_{\text{NTGL}}^\beta D_{\text{NTGL}}^\alpha s(x) = D_{\text{NTGL}}^{\alpha+\beta} s(x). \tag{31}$$

5. Numerical Simulations

For the numerical approximation, although longer memory is more precise computation for the fractional derivatives, a fixed number for t is adopted for reducing computation complexity, for example, $t = 100$ or $t = 1000$ and so forth. But these truncated forms will lead to some unsatisfied results. In this section, we will give error analysis of truncated G-L formulas firstly and then present experiments using test signals.

5.1. Error Analysis of Truncated G-L Formula. The error analysis of truncated G-L formula is very important in the applications of fractional derivatives. Some efforts discuss the problem in theory [23]. In this subsection we will discuss the truncated errors by considering the signal $s(x) = 1$ since the most serious effect of truncated errors is that the values of fractional derivatives are not equal to zeros when $s(x) = \text{constant}$.

According to Lemma 2, the values of untruncated G-L formula for $s(x) = 1$ are equal to zeros, which are coincident to the 1-order derivatives. For the truncated G-L formula when fractional order α satisfies $0 < \alpha < 1$, according to Lemma 2', the remainder part of $s(x) = 1$ is more than zero. Thus, the truncated part is less than zero. That is, it is a negative number. The truncated errors of truncated G-L formula for $s(x) = 1$ with different support lengths and different fractional-orders α , $0 < \alpha < 1$, are shown in Table 1, which demonstrate the above conclusions.

Moreover, we will compare the changes of absolute values of truncated errors with different α and different support lengths.

Lemma 11. *The absolute values of truncated errors $|\sum_{k=0}^t \omega_k^{(\alpha)}|$, where t is the support length, for $s(x) = 1$, become smaller as the support lengths become larger.*

Proof. According to Lemma 3, $\omega_k^{(\alpha)} < 0$, $0 < \alpha < 1$, for $k \leq 1$ is an integer.

According to Lemma 2', $\sum_{k=0}^t \omega_k^{(\alpha)} > 0$, for $t \geq 0$ is an integer and $0 < \alpha < 1$.

Here, t can be considered as the support length of the truncated G-L formula. When $t_1 > t_2$, where t_1 and t_2 are two support lengths and $t_1 \geq 0$ and $t_2 \geq 0$, we have

$$\sum_{k=0}^{t_1} \omega_k^{(\alpha)} < \sum_{k=0}^{t_2} \omega_k^{(\alpha)}. \tag{32}$$

□

Lemma 12. *The absolute values of truncated errors for $s(x) = 1$ become smaller as the fractional orders $0 < \alpha < 1$ become larger.*

Proof. Since $\omega_0^{(\alpha)} = 1$ and $\omega_1^{(\alpha)} = -\alpha$, for $\alpha_1 > \alpha_2$, $0 < \alpha_1 < 1$, and $0 < \alpha_2 < 1$, where α_1 and α_2 are two fractional orders, we have

$$1 - \alpha_1 > 0, \quad 1 - \alpha_2 > 0, \quad 1 - \alpha_1 < 1 - \alpha_2. \tag{33}$$

According to Lemma 2, then $\omega_k^{(\alpha)} = (1 - (\alpha + 1)/k)\omega_{k-1}^{(\alpha)}$.

For $0 < \alpha < 1$ and $k \geq 2$, we have $0 < (1 - (\alpha + 1)/k) < 1$. Thus,

$$\omega_k^{(\alpha)} < 0, \quad |\omega_k^{(\alpha)}| < |\omega_{k-1}^{(\alpha)}|, \quad \omega_k^{(\alpha)} > \omega_{k-1}^{(\alpha)}, \tag{34}$$

where $|\cdot|$ represents the absolute value. Thus, for $\alpha_1 > \alpha_2$, $0 < \alpha_1 < 1$, and $0 < \alpha_2 < 1$, we have

$$0 < \left(1 - \frac{\alpha_1 + 1}{k}\right) < \left(1 - \frac{\alpha_2 + 1}{k}\right) < 1. \tag{35}$$

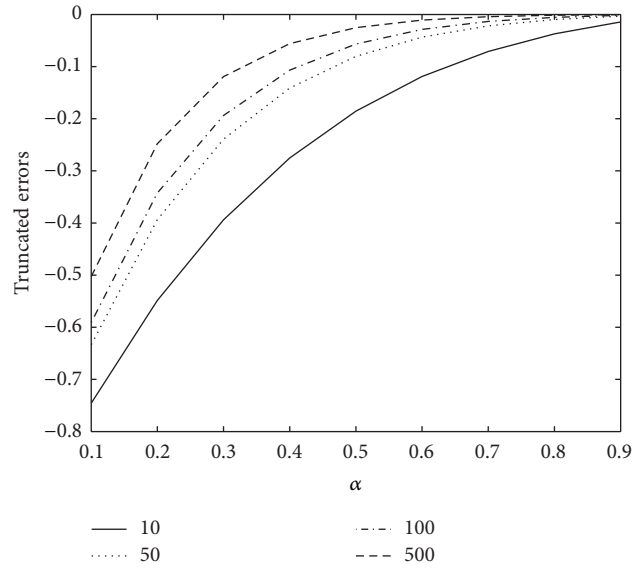


FIGURE 1: Truncated errors of truncated G-L formula with support lengths 10, 50, 100, and 500 and fractional orders α from 0.1 to 0.9.

If $0 > \omega_k^{(\alpha_1)} > \omega_k^{(\alpha_2)}$, for $k \geq 1$, $\alpha_1 > \alpha_2$, $0 < \alpha_1 < 1$, and $0 < \alpha_2 < 1$.

Thus, we can assume that $\alpha_1 = \alpha_2 + c_1$, $1 > c_1 > 0$, and $\omega_k^{(\alpha_1)} = \omega_k^{(\alpha_2)} + c_2$, $c_2 > 0$. We have

$$\begin{aligned} \omega_{k+1}^{(\alpha_1)} &= \omega_k^{(\alpha_1)} \left(1 - \frac{\alpha_1 + 1}{k}\right) \\ &= (\omega_k^{(\alpha_2)} + c_2) \left(1 - \frac{\alpha_2 + 1 + c_1}{k}\right) \\ &= \omega_k^{(\alpha_2)} \left(1 - \frac{\alpha_2 + 1}{k}\right) + \omega_k^{(\alpha_2)} \left(-\frac{c_1}{k}\right) \\ &\quad + c_2 \left(1 - \frac{\alpha_2 + 1 + c_1}{k}\right) \\ &= \omega_{k+1}^{(\alpha_2)} + \omega_k^{(\alpha_2)} \left(-\frac{c_1}{k}\right) + c_2 \left(1 - \frac{\alpha_2 + 1 + c_1}{k}\right) \end{aligned} \tag{36}$$

Since $\omega_k^{(\alpha_2)}(-c_1/k) > 0$ and $c_2(1 - (\alpha_2 + 1 + c_1)/k) > 0$, we have

$$\omega_{k+1}^{(\alpha_1)} > \omega_{k+1}^{(\alpha_2)}. \tag{37}$$

Thus, $\sum_{k=1}^t \omega_k^{(\alpha_2)} < \sum_{k=1}^t \omega_k^{(\alpha_1)} < 0$ and $\sum_{k=0}^t \omega_k^{(\alpha_2)} > \sum_{k=0}^t \omega_k^{(\alpha_1)} > 0$. □

Summary of above two lemmas: we have that the long support and large fractional orders of truncated G-L formulas will have small absolute values of truncated errors. Experiments shown in Table 1 and Figure 1 also support these theory analysis results. Note that the truncated errors are negative numbers. Therefore, discussing their absolute values can show the differences between zeros and errors.

5.2. Experiments. In order to test if the new truncated method can reduce the truncated errors in real signals, two

TABLE 1: Truncated errors of truncated left-handed G-L formula for $s(x) = 1$ with support lengths from 10 to 500 (rows) and fractional-orders α from 0.1 to 0.9 (columns).

Length of support	$\alpha = 0.1$	$\alpha = 0.2$	$\alpha = 0.3$	$\alpha = 0.4$	$\alpha = 0.5$	$\alpha = 0.6$	$\alpha = 0.7$	$\alpha = 0.8$	$\alpha = 0.9$
10	-0.7475	-0.5487	-0.3939	-0.2752	-0.1855	-0.1190	-0.0710	-0.0372	-0.0145
30	-0.6672	-0.4368	-0.2795	-0.1739	-0.1043	-0.0595	-0.0315	-0.0147	-0.0051
50	-0.6335	-0.3937	-0.2392	-0.1412	-0.0804	-0.0435	-0.0219	-0.0097	-0.0032
100	-0.5908	-0.3432	-0.1939	-0.1067	-0.0566	-0.0286	-0.0134	-0.0055	-0.0017
200	-0.5510	-0.2979	-0.1573	-0.0808	-0.0400	-0.0188	-0.0082	-0.0032	-0.0009
500	-0.5027	-0.2479	-0.1194	-0.0559	-0.0253	-0.0108	-0.0043	-0.0015	-0.0004

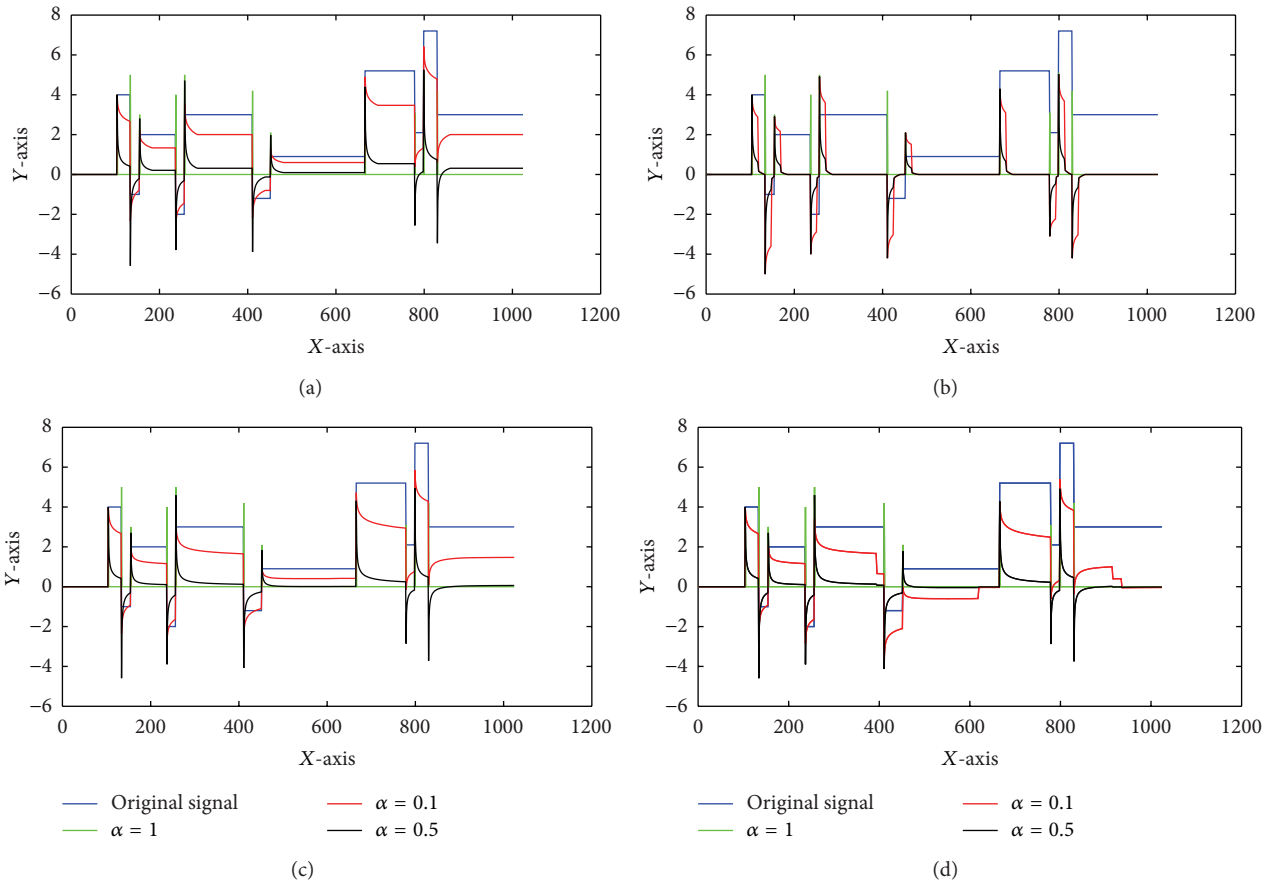


FIGURE 2: The original signal (blocks with 1024 samples, blue lines), its fractional derivatives of truncated G-L with different fractional orders ((a) and (c)), and its fractional derivatives of the new method with different fractional orders ((b) and (d)), where the support length of (a) and (b) is 30 and the support length of (c) and (d) is 500.

test signals, blocks, and bumps, with 1024 samples, are used for analysis of the performance of our new framework (see Figures 2 and 3).

From Figure 2, we can see both integer-order derivatives (green lines) and fractional derivatives ($\alpha = 0.1$ are represented by red lines and $\alpha = 0.5$ are represented by black lines) have the properties that the singularities are related to the local extrema. Just as discussed above, the values of truncated G-L formula are not zeros in smooth regions (see Figures 2(a) and 2(c)). Moreover, coinciding Lemma 11, the signals with longer truncated length will be nearer to zeros

in the smooth segments than the shorter length signals. The bigger fractional orders will also have better performance in sharper impulses in singularities and much more near zeros in the smooth segments than the smaller fractional orders, which coincides Lemma 12 (see Figures 2(a) and 2(c)).

When truncated length $t = 30$ for the new definition of fractional derivatives (see Figure 2(b)), the values of new definition at singularities have very high impulses comparing to the corresponding truncated G-L formula (Figure 2(a)), which is a very impressive nature to detect, locate, and preserve singularities. Moreover, near singularities, the values

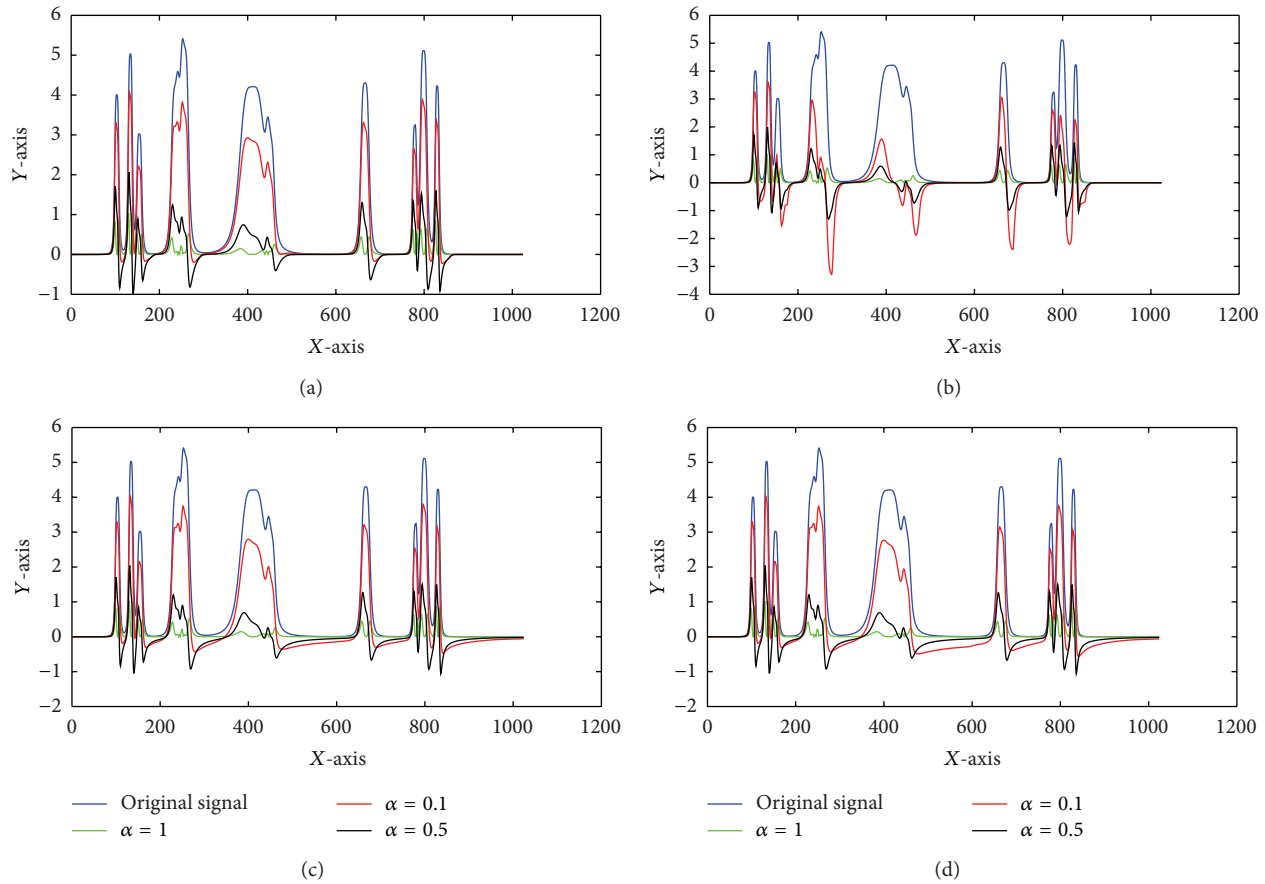


FIGURE 3: The original signal (bumps with 1024 samples, blue line), its fractional derivatives of truncated G-L with different fractional orders ((a) and (c)), and its fractional derivatives of the new method with different fractional orders ((b) and (d)), where the support length of (a) and (b) is 30 and the support length of (c) and (d) is 500.

are decreased/increased gradually to zeros and the values of the smooth segments are zeros. These characters together ensure that the new fractional derivatives can obtain good results in signal processing.

Observing Figure 3, we can find that 1-order derivatives cannot locate “bump like” singularities: (1) there are two extremums of 1-order derivatives even for a very narrow bump, for example, the first bump; (2) some weak singularities cannot be detected, for example, the left singularity of the fifth bump.

Fortunately, all fractional derivatives have better performance in above two sides. That is, each narrow bump only has one extremum of the fractional derivatives.

The best performance of the new definition for block signal is the derivative with truncated length $t = 30$ and fractional order $\alpha = 0.1$, which also has the best natures for the bump signal. That is, it has very high impulses in singularities and equals to zeros in smooth segments. Weak singularity in the left of the fifth bump has a very obvious high impulse, which can be detected and located easily. It is very interesting thing that the weak impulses in two signals using truncated G-L formula are enhanced by new definitions of

fractional derivatives with small α and t by comparing Figures 2(a) and 2(b) and Figures 3(a) and 3(b).

In summary, from the simulation results of two test signals, we can conclude that the new definition of fractional derivatives has the best performance in three type derivatives including 1-order derivatives, truncated G-L formula and themselves.

6. Conclusions

In this paper, we study errors of truncated Grünwald-Letnikov formula with $0 < \alpha < 1$ and then the errors are corrected by the medians of remainder parts of signals, which has some very impressive natures in signal processing. That is, it has very high impulses in singularities, which can detect and locate singularities easily; the values of the new definition are equal to zeros in smooth segments, which can be used efficiently in signal smoothing and filtering. Moreover, it also has good performance in weak singularity detection and location.

Conflict of Interests

The author declares that there is no conflict of interests regarding the publication of this paper.

Acknowledgments

This paper is supported by the National Natural Science Foundation of China (nos. 60873102 and 60873264), Major State Basic Research Development Program (no. 2010CB732501), and Open Foundation of Visual Computing and Virtual Reality Key Laboratory of Sichuan Province (no. J2010N03). This work was supported by a grant from the National High Technology Research and Development Program of China (no. 2009AA12Z140).

References

- [1] S. Hu, Z. Liao, D. Sun, and W. Chen, "A numerical method for preserving curve edges in nonlinear anisotropic smoothing," *Mathematical Problems in Engineering*, vol. 2011, Article ID 186507, 14 pages, 2011.
- [2] Y. Chen, Y. Li, W. Yu, L. Luo, W. Chen, and C. Toumoulin, "Joint-map tomographic reconstruction with patch similarity based mixture prior model," *Multiscale Modeling & Simulation*, vol. 9, no. 4, pp. 1399–1419, 2011.
- [3] Y. Chen, X. Yin, L. Shi et al., "Improving abdomen tumor low-dose CT images using a fast dictionary learning based processing," *Physics in Medicine and Biology*, vol. 58, pp. 5803–5820, 2013.
- [4] Z. Bian, J. Ma, J. Huang et al., "SR-NLM: a sinogram restoration induced non-local means image filtering for low-dose computed tomography," *Computerized Medical Imaging and Graphics*, vol. 37, no. 4, pp. 293–303, 2013.
- [5] J. Ma, H. Zhang, Y. Gao et al., "Iterative image reconstruction for cerebral perfusion CT using a pre-contrast scan induced edge-preserving prior," *Physics and Medical Biology*, vol. 57, pp. 7519–7542, 2012.
- [6] Z. Liao, "Low-dosed x-ray computed tomography imaging by regularized fully spatial fractional-order Perona-Malik diffusion," *Advances in Mathematical Physics*, vol. 2013, Article ID 371868, 9 pages, 2013.
- [7] S. Hu, Z. Liao, and W. Chen, "Sinogram restoration for low-dosed X-ray computed tomography using fractional-order Perona-Malik diffusion," *Mathematical Problems in Engineering*, vol. 2012, Article ID 391050, 13 pages, 2012.
- [8] Z. Jun and W. Zhihui, "A class of fractional-order multi-scale variational models and alternating projection algorithm for image denoising," *Applied Mathematical Modelling. Simulation and Computation for Engineering and Environmental Systems*, vol. 35, no. 5, pp. 2516–2528, 2011.
- [9] J. Bai and X.-C. Feng, "Fractional-order anisotropic diffusion for image denoising," *IEEE Transactions on Image Processing*, vol. 16, no. 10, pp. 2492–2502, 2007.
- [10] M. Janev, S. Pilipović, T. Atanacković, R. Obradović, and N. Ralević, "Fully fractional anisotropic diffusion for image denoising," *Mathematical and Computer Modelling*, vol. 54, no. 1-2, pp. 729–741, 2011.
- [11] C. Wang, L. Lan, and S. Zhou, "Grunwald-Letnikov based adaptive fractional differential algorithm on image texture enhancing," *Journal of Computational Information Systems*, vol. 9, no. 2, pp. 445–454, 2013.
- [12] H. A. Jalab and R. W. Ibrahim, "Texture enhancement based on the Savitzky-Golay fractional differential operator," *Mathematical Problems in Engineering*, vol. 2013, Article ID 149289, 8 pages, 2013.
- [13] S. Hu, "External fractional-order gradient vector Perona-Malik diffusion for sinogram restoration of low-dosed x-ray computed tomography," *Advances in Mathematical Physics*, vol. 2013, Article ID 516919, 10 pages, 2013.
- [14] R. Hilfer, *Applications of Fractional Calculus in Physics*, World Scientific Publishing, River Edge, NJ, USA, 2000.
- [15] S. Hu and P. Liang, "Theory analysis of left-handed Grunwald-Letnikov formula with $0 < \alpha < 1$ to detect and locatesingularities," *Abstract and Applied Analysis*. In press.
- [16] W.-S. Chen, C. Zhang, and S. Y. Chen, "Geometric distribution weight information modeled using radial basis function with fractional order for linear discriminant analysis method," *Advances in Mathematical Physics*, vol. 2013, Article ID 825861, 9 pages, 2013.
- [17] W.-S. Chen, P. C. Yuen, and X. Xie, "Kernel machine-based rank-lifting regularized discriminant analysis method for face recognition," *Neurocomputing*, vol. 74, no. 17, pp. 2953–2960, 2011.
- [18] M. Li, "A class of negatively fractal dimensional Gaussian random functions," *Mathematical Problems in Engineering*, vol. 2011, Article ID 291028, 18 pages, 2011.
- [19] M. Li and W. Zhao, "On bandlimitedness and lag-limitedness of fractional Gaussian noise," *Physica A: Statistical Mechanics and its Applications*, vol. 392, no. 9, pp. 1955–1961, 2013.
- [20] M. Li, S. C. Lim, C. Cattani, and M. Scalia, "Characteristic roots of a class of fractional oscillators," *Advances in High Energy Physics*, vol. 2013, Article ID 853925, 7 pages, 2013.
- [21] I. Podlubny, *Fractional Differential Equations*, vol. 198 of *Mathematics in Science and Engineering*, Academic Press, San Diego, Calif, USA, 1999.
- [22] S. G. Samko, A. A. Kilbas, and O. I. Marichev, *Fractional Integrals and Derivatives: Theory and Applications*, Gordon and Breach Science Publishers, London, UK, 1993.
- [23] E. Sousa, "How to approximate the fractional derivative of order $1 < \alpha \leq 2$," *International Journal of Bifurcation and Chaos in Applied Sciences and Engineering*, vol. 22, no. 4, 13 pages, 2012.

Research Article

Theory Analysis of Left-Handed Grünwald-Letnikov Formula with $0 < \alpha < 1$ to Detect and Locate Singularities

Shaoxiang Hu¹ and Ping Liang²

¹ School of Automation Engineering, University of Electronic Science and Technology of China, Chengdu, Sichuan 611731, China

² Ningbo Xingaoyi Co., Ltd., No. 555 Yeshan Road, Yuyao City, Zhejiang 315400, China

Correspondence should be addressed to Ping Liang; clarke.liang@gmail.com

Received 21 January 2014; Accepted 9 March 2014; Published 3 April 2014

Academic Editor: Zhiwu Liao

Copyright © 2014 S. Hu and P. Liang. This is an open access article distributed under the Creative Commons Attribution License, which permits unrestricted use, distribution, and reproduction in any medium, provided the original work is properly cited.

We study fractional-order derivatives of left-handed Grünwald-Letnikov formula with $0 < \alpha < 1$ to detect and locate singularities in theory. The widely used four types of ideal singularities are analyzed by deducing their fractional derivative formula. The local extrema of fractional derivatives are used to locate the singularities. Theory analysis indicates that fractional-order derivatives of left-handed Grünwald-Letnikov formula with $0 < \alpha < 1$ can detect and locate four types of ideal singularities correctly, which shows better performance than classical 1-order derivatives in theory.

1. Introduction

How to preserve singularities in image and signal processing is a very important problem [1–5]. Recently, fractional derivatives become very important tools in the field [6–17]. All of the methods based on fractional derivatives reported good processing results by modifying some classical partial differential equations (PDEs) to fully or partial fractional-order derivative PDEs. Just as the recent theory analysis efforts in fractional derivatives by mathematicians [18–20], all theory analyses focus on how to approach the PDEs and how to find their exact solutions.

However, we think fractional derivatives should be studied differently. It is well known that one powerful method to preserve singularities in signal processing is to detect and locate singularities correctly and then to protect them in signal processing. Thus, we think the most important problem in theory analysis should be if the fractional derivatives can detect and locate singularities well.

In this paper, we study fractional-order derivatives of left-handed Grünwald-Letnikov formula with $0 < \alpha < 1$ to detect and locate the widely used four types of ideal singularities in theory. Theory analysis is from deducing the fractional derivatives of four types of ideal singularities

with an indicated singularity in each case. The differences of these fractional derivative values are studied to find the local extrema. The extrema are considered as the singularities.

The rest of this paper is as follows. Section 2 introduces some basic theory backgrounds in fractional derivatives; we also deduce some useful results based on these theory backgrounds. In Section 3, we introduce the 1-order differential method used in singularity detection and location, and the detected and located results of four types of ideal singularities are also presented. Section 4 discusses the steps in singularities detection and location using fractional derivatives, and then they are used to detect and locate the four types of ideal singularities. We also give conclusions and acknowledgments finally.

2. Fractional Derivatives

In contrast to integer-order differentials d^n/dt^n , fractional-order derivatives are defined as operators whose orders have been extended to noninteger numbers. There are a number of definitions of fractional derivatives. The usual way of representing the fractional derivatives is by the left-handed Riemann-Liouville formula (R-L formula).

The left-handed R-L formula of order α , for $x \in [a, b]$, is defined by [21, 22]

$$D_{RL}^\alpha u(x) = \frac{1}{\Gamma(n-\alpha)} \frac{d^n}{dx^n} \int_a^x u(\tau) (x-\tau)^{n-\alpha-1} d\tau, \quad (1)$$

where $n-1 < \alpha < n$ and $n = [\alpha] + 1$, with $[\alpha]$ denoting the integer part of α , and $\Gamma(\cdot)$ is the Gamma function defined as

$$\Gamma(z) = \int_0^\infty t^{z-1} e^{-t} dt. \quad (2)$$

Another way to represent the fractional derivatives is by the Grünwald-Letnikov (G-L) formula, which is a generalization of the ordinary discretization formulas for integer-order derivatives. For $\alpha > 0$, the left-handed G-L formula is

$$D_{GL}^\alpha u(x) = \lim_{\Delta x \rightarrow 0} \frac{1}{\Delta x^\alpha} \sum_{k=0}^{[(x-a)/\Delta x]} \omega_k^{(\alpha)} u(x-k\Delta x), \quad (3)$$

where Δx denotes the uniform space step and $\omega_k^{(\alpha)} = (-1)^k \binom{\alpha}{k}$ represents the normalized G-L weights that are given by

$$\begin{aligned} \omega_0^{(\alpha)} &= 1, \\ \omega_k^{(\alpha)} &= (-1)^k \frac{\alpha(\alpha-1)\cdots(\alpha-k+1)}{k!} \\ &= \frac{\Gamma(k-\alpha)}{\Gamma(-\alpha)\Gamma(k+1)}, \quad \text{for } k = 1, 2, 3, \dots \end{aligned} \quad (4)$$

The above two definitions have different forms. However, by requiring a reasonable behavior of the function $u(x)$ and their derivatives, we can relate the two definitions with the following proposition [21, 23].

Proposition 1. *Let us assume that the function $u(x)$ is $(n-1)$ times differential in $[a, b]$ and that the n th derivative of $u(x)$ is integrable in $[a, b]$. Then, for every $n-1 < \alpha < n$, one has*

$$D_{GL}^\alpha u(x) = D_{RL}^\alpha u(x), \quad a \leq x \leq b. \quad (5)$$

Generally, the analytic definition given by (1) is used in the formulation of the fractional partial differential equations (PDEs), while G-L definitions in (3) are maybe used to discretize the fractional PDEs to obtain a numerical solution. Since the problem in this paper has discrete form, G-L formula defined in (3) will be adopted in our following discussion.

Remark 2. For $\alpha = 1$, (1) and (3) become the classical first derivative, and, for any $\alpha = n$, $n \in \mathbb{N}$ is a positive integer; they are classical n th derivatives of $u(x)$ if the function $u(x)$ is $(n-1)$ times differentiable. Note that, for α is a positive integer, the equations are with limit support whose support length is $\alpha + 1$. However, for α is not an integer, fractional derivatives defined above are nonlocal operators. That is, the value of the fractional derivative at a point x depends on the function values at all the points to the left of the point x .

Therefore, in order to handle fractional derivative numerically, it is necessary to compute the coefficients $\omega_k^{(\alpha)}$, where α is the order of the fractional derivative. For that, we can use the recurrence relationships presented in Lemma 3.

Lemma 3. *The recurrence relationship of the coefficients of G-L formula $\omega_k^{(\alpha)}$ defined in (3) is*

$$\omega_0^{(\alpha)} = 1; \quad \omega_k^{(\alpha)} = \left(1 - \frac{\alpha+1}{k}\right) \omega_{k-1}^{(\alpha)}, \quad k = 1, 2, 3, \dots \quad (6)$$

Proof. For $k = 0$, $\omega_0^{(\alpha)} = 1$.

Assume that when $n = k - 1$, we have

$$\omega_{k-1}^{(\alpha)} = \left(1 - \frac{\alpha+1}{k-1}\right) \omega_{k-2}^{(\alpha)}. \quad (7)$$

For $n = k$,

$$\begin{aligned} \omega_k^{(\alpha)} &= \frac{\Gamma(k-\alpha)}{\Gamma(-\alpha)\Gamma(k+1)} = \frac{(k-1-\alpha)\Gamma(k-1-\alpha)}{k\Gamma(-\alpha)\Gamma(k)} \\ &= \left(1 - \frac{\alpha+1}{k}\right) \omega_{k-1}^{(\alpha)}. \end{aligned} \quad (8)$$

Therefore, for all $k = 1, 2, 3, \dots$, we have

$$\omega_k^{(\alpha)} = \left(1 - \frac{\alpha+1}{k}\right) \omega_{k-1}^{(\alpha)}. \quad (9)$$

□

Lemma 4. *The nonlocal operator defined in (3) is a linear operator.*

Proof. $u(x)$ and $v(x)$ are two functions, and $x \in [a, b]$, λ , is a real number, since

(1)

$$\begin{aligned} D_{GL}^\alpha [u(x) + v(x)] &= \lim_{\Delta x \rightarrow 0} \frac{1}{\Delta x^\alpha} \sum_{k=0}^{[(x-a)/\Delta x]} \omega_k^{(\alpha)} \\ &\quad \times [u(x-k\Delta x) + v(x-k\Delta x)] \\ &= \lim_{\Delta x \rightarrow 0} \frac{1}{\Delta x^\alpha} \sum_{k=0}^{[(x-a)/\Delta x]} \omega_k^{(\alpha)} u(x-k\Delta x) \\ &\quad + \lim_{\Delta x \rightarrow 0} \frac{1}{\Delta x^\alpha} \sum_{k=0}^{[(x-a)/\Delta x]} \omega_k^{(\alpha)} v(x-k\Delta x) \\ &= D_{GL}^\alpha u(x) + D_{GL}^\alpha v(x), \end{aligned} \quad (10)$$

(2)

$$\begin{aligned} D_{GL}^\alpha [\lambda u(x)] &= \lim_{\Delta x \rightarrow 0} \frac{1}{\Delta x^\alpha} \sum_{k=0}^{[(x-a)/\Delta x]} \omega_k^{(\alpha)} [\lambda u(x)] \\ &= \lambda \lim_{\Delta x \rightarrow 0} \frac{1}{\Delta x^\alpha} \sum_{k=0}^{[(x-a)/\Delta x]} \omega_k^{(\alpha)} u(x) \\ &= \lambda D_{GL}^\alpha u(x). \end{aligned} \quad (11)$$

□

Lemma 5. Consider $\sum_{k=0}^{\infty} \omega_k^{(\alpha)} = 0$.

Proof. Since $(1 - z)^\alpha = \sum_{k=0}^{\infty} \omega_k^{(\alpha)} z^k$, let $k = 1$, and we have

$$\sum_{k=0}^{\infty} \omega_k^{(\alpha)} = (1 - 1)^\alpha = 0. \tag{12}$$

□

Lemma 6. For $0 < \alpha < 1$, t is a positive integer, $m \geq t$, and one has

$$\omega_k^{(\alpha)} < 0, \quad k = 1, 2, 3, \dots, \tag{13}$$

and $\sum_{k=t}^{\infty} \omega_k^{(\alpha)} < 0$, $\sum_{k=t}^m \omega_k^{(\alpha)} < 0$.

Proof. For $k = 1$, $\omega_1^{(\alpha)} = -\alpha < 0$.

Assume that $\omega_k^{(\alpha)} < 0$.

According to Lemma 3, we have $\omega_{k+1}^{(\alpha)} = (1 - ((\alpha + 1)/(k + 1)))\omega_k^{(\alpha)}$. Since $0 < \alpha < 1$ and $k + 1 \geq 2$, $(1 - ((\alpha + 1)/(k + 1))) > 0$. Thus, $\text{sgn}(\omega_{k+1}^{(\alpha)}) = \text{sgn}(\omega_k^{(\alpha)}) < 0$. Here,

$$\text{sgn}(x) = \begin{cases} 1, & x \geq 0, \\ -1, & x < 0. \end{cases} \tag{14}$$

Then we have $\omega_{k+1}^{(\alpha)} < 0$. Thus $\sum_{k=t}^{\infty} \omega_k^{(\alpha)} < 0$, $\sum_{k=t}^m \omega_k^{(\alpha)} < 0$. □

Lemma 7. For $0 < \alpha < 1$, $t \geq 0$ is an integer,

$$\sum_{k=0}^t \omega_k^{(\alpha)} > 0. \tag{15}$$

Proof. According to Lemma 5, we have

$$0 = \sum_{k=0}^{\infty} \omega_k^{(\alpha)} = \sum_{k=0}^t \omega_k^{(\alpha)} + \sum_{k=t+1}^{\infty} \omega_k^{(\alpha)}. \tag{16}$$

According to Lemma 6, $\sum_{k=t+1}^{\infty} \omega_k^{(\alpha)} < 0$. Therefore, $\sum_{k=0}^t \omega_k^{(\alpha)} > 0$. □

Lemma 8. For $0 < \alpha < 1$, $m \geq 0$ is an integer and t is a positive integer

$$\begin{aligned} \sum_{k=m}^t \omega_k^{(\alpha)}(-k) &> 0, \\ \sum_{k=m}^{\infty} \omega_k^{(\alpha)}(-k) &> 0. \end{aligned} \tag{17}$$

Proof. From Lemma 6, for $0 < \alpha < 1$, $\omega_k^{(\alpha)} < 0$, $k = 1, 2, 3, \dots$.

Thus, $\omega_k^{(\alpha)}(-k) > 0$ for $k = 1, 2, 3, \dots$, and $t > 0$. We have $\sum_{k=m}^{\infty} \omega_k^{(\alpha)}(-k) > 0$, $m \geq 1$, and $\sum_{k=m}^t \omega_k^{(\alpha)}(-k) > 0$, $m \geq 1$, $t \geq 1$. □

3. Classical Singularity Detection and Location

Singularity detection is the name for a set of mathematical methods which aim at identifying points in a digital signal at which the signal value changes sharply or, more formally, has discontinuities.

3.1. Singularity Types. We can categorize singularities as step, roof, jump, and ramp. They can be represented as

(1) ideal step

$$s(x) = \begin{cases} 1, & x \geq x_0, \\ 0, & x < x_0, \end{cases} \tag{18}$$

(2) ideal roof

$$s(x) = \begin{cases} m(x - x_0) + c_0, & x_0 - h_1 < x \leq x_0, \\ n(x - x_0) + c_0, & x_0 < x < x_0 + h_2, \end{cases} \tag{19}$$

(3) ideal impulse

$$s(x) = \begin{cases} b, & x = x_0, \\ 0, & x \neq x_0, \end{cases} \tag{20}$$

(4) ideal ramp

$$s(x) = \begin{cases} m(x - x_0) + c_0, & x_0 - h_1 < x \leq x_0, \\ c_0, & x > x_0. \end{cases} \tag{21}$$

4. Singularity Detection by 1-Order Derivatives

Singularity detection is the name for a set of mathematical methods which aim at identifying points in a digital signal at which the signal value changes sharply or, more formally, has discontinuities.

4.1. The First-Order Derivatives for Singularities. The singularity detection by 1-order derivatives detects singularities by first computing a measure of singularity strength, usually a first-order derivative expression, and then searching for local absolute maxima as the locations of singularities. The simplest approach to compute first-order derivatives is to use left-handed differences

$$Du(x) = u(x) - u(x - 1). \tag{22}$$

Therefore, first-order derivatives of the four types of singularities are

(1) ideal step

$$Ds(x) = \begin{cases} 0, & x < x_0, \\ 1, & x = x_0, \\ 0, & x > x_0, \end{cases} \tag{23}$$

(2) ideal roof

$$Ds(x) = \begin{cases} m, & x_0 - h_1 < x \leq x_0, \\ n, & x_0 < x < x_0 + h_2, \end{cases} \tag{24}$$

(3) ideal impulse

$$Ds(x) = \begin{cases} b, & x = x_0 \\ -b, & x = x_0 + 1 \\ 0, & \text{otherwise,} \end{cases} \quad (25)$$

(4) ideal ramp

$$Ds(x) = \begin{cases} m, & x_0 - h_1 < x \leq x_0 \\ 0, & x > x_0. \end{cases} \quad (26)$$

Then, find absolute maxima of $Ds(x)$ to locate the positions of singularities. Here, absolute maxima are the maxima of absolute values of $Ds(x)$.

4.2. Detect and Locate Singularities. The main steps to locate singularities are as follows: (1) find all points with $Ds(x) \neq 0$; (2) compute absolute values of $Ds(x)$; (3) if $Ds(x) > 0$, compare absolute values of $Ds([x])$ and $Ds([x + 1])$, and if $abs(Ds(x)) > abs(Ds(x + 1))$, x is the singularity; if $Ds(x) < 0$, compare absolute values of $Ds([x])$ and $Ds([x - 1])$, and if $abs(Ds(x)) > abs(Ds(x - 1))$, x is the singularity. Four types of ideal singularities are discussed as follows. Each one has a corresponding singularity on x_0 .

Ideal Step. The absolute values of $D(s(x))$ are the same as $D(s(x))$. Therefore, the absolute maxima are 1 on the position x_0 , and then compare absolute values of $Ds(x_0)$ and $Ds([x_0 + 1])$, and we have $Ds(x_0) = 1 > Ds([x_0 + 1]) = 0$. Therefore, the singularity is detected by 1-order derivative and is located on x_0 , which means 1-order derivatives can detect and locate ideal step singularities correctly.

Ideal Roof. The absolute value of $D(s)$ is

$$abs(Ds(x)) = \begin{cases} abs(m), & x_0 - h_1 < x \leq x_0, \\ abs(n), & x_0 < x < x_0 + h_2. \end{cases} \quad (27)$$

Here, $abs(\cdot)$ is

$$abs(x) = \begin{cases} x, & x \geq 0, \\ -x, & x < 0. \end{cases} \quad (28)$$

For $D(s(x)) = m > 0$, $x_0 - h_1 < x < x_0$, we should compare the absolute values of $D(s(x))$ and $D(s(x + 1))$. Since $abs(D(s(x))) = abs(D(s(x + 1))) = m$, all $x \in (x_0 - h_1, x_0)$ are not singularities.

For $D(s(x)) = m < 0$, $x_0 - h_1 < x \leq x_0$, we should compare the absolute values of $D(s(x))$ and $D(s(x - 1))$. Since $abs(D(s(x))) = abs(D(s(x - 1))) = m$, all $x \in (x_0 - h_1, x_0]$ are not singularities.

$D(s(x_0)) = m > 0$, and we should compare the absolute values of $D(s(x_0))$ and $D(s(x_0 + 1))$. Since $abs(D(s(x_0))) = abs(m)$ and $abs(D(s(x_0 + 1))) = abs(n)$, if $abs(m) > abs(n)$, x_0 is the singularity; otherwise, x_0 is not a singularity.

$D(s(x_0 + 1)) = n < 0$, and we should compare the absolute values of $D(s(x_0 + 1))$ and $D(s(x_0))$. Since $abs(D(s(x_0))) = abs(m)$ and $abs(D(s(x_0 + 1))) = abs(n)$, if

$abs(m) < abs(n)$, $x_0 + 1$ is the singularity; otherwise, $x_0 + 1$ is not a singularity.

For $D(s(x)) = n < 0$, $x_0 + 1 < x < x_0 + h_2$, we should compare the absolute values of $D(s(x))$ and $D(s(x - 1))$. Since $abs(D(s(x - 1))) = abs(D(s(x))) = abs(n)$, $x \in (x_0 + 1, x_0 + h_2)$ are not the singularities.

For $D(s(x)) = n > 0$, $x_0 + 1 \leq x < x_0 + h_2$, we should compare the absolute values of $D(s(x))$ and $D(s(x + 1))$. Since $abs(D(s(x + 1))) = abs(D(s(x))) = abs(n)$, $x \in [x_0 + 1, x_0 + h_2)$ are not the singularities.

Ideal Impulse. $(D(s))$ has two nonzeros, that is, $x = x_0$ and $x = x_0 + 1$. For $D(s(x_0)) = b > 0$, comparing the absolute values of $D(s(x_0))$ and $D(s(x_0 + 1))$, we have $abs(D(s(x_0))) = abs(D(s(x_0 + 1))) = abs(b)$. Thus, x_0 is not the singularity. For $D(s(x_0)) = b < 0$, comparing the absolute values of $D(s(x_0))$ and $D(s(x_0 - 1))$, we have $abs(D(s(x_0))) = abs(b) > abs(D(s(x_0 - 1))) = 0$. Thus, x_0 is the singularity.

For $D(s(x_0 + 1)) = -b < 0$, comparing the absolute values of $D(s(x_0 + 1))$ and $D(s(x_0))$, we have $abs(D(s(x_0 + 1))) = abs(D(s(x_0))) = abs(b)$. Thus, $x_0 + 1$ is not the singularity. For $D(s(x_0 + 1)) = -b > 0$, comparing the absolute values of $D(s(x_0 + 1))$ and $D(s(x_0 + 2))$, we have $abs(D(s(x_0 + 1))) = abs(b) > abs(D(s(x_0 + 2))) = 0$. Thus, $x_0 + 1$ is the singularity.

In summary, for $b > 0$, no singularity is detected; for $b < 0$, both x_0 and $x_0 + 1$ are located as singularities.

Ideal Ramp. The absolute value of $D(s)$ is

$$abs(Ds(x)) = \begin{cases} m, & x_0 - h_1 < x \leq x_0 \\ 0, & x > x_0. \end{cases} \quad (29)$$

For $D(s(x)) = m > 0$, $x_0 - h_1 < x < x_0$, we should compare the absolute values of $D(s(x))$ and $D(s(x + 1))$. Since $abs(D(s(x))) = abs(D(s(x + 1))) = abs(m)$, all $x_0 - h_1 < x < x_0$ are not singularities.

For $D(s(x)) = m < 0$, $x_0 - h_1 < x \leq x_0$, we should compare the absolute values of $D(s(x))$ and $D(s(x - 1))$. Since $abs(D(s(x))) = abs(D(s(x - 1))) = abs(m)$, all $x_0 - h_1 < x \leq x_0$ are not singularities.

$D(s(x_0)) = m > 0$, and we should compare the absolute values of $D(s(x_0))$ and $D(s(x_0 + 1))$. Since $abs(D(s(x_0))) = m$ and $abs(D(s(x_0 + 1))) = 0$, x_0 is the singularity. Thus, when $m > 0$, ideal ramp singularity can be detected and located correctly by 1-order derivatives.

Summarizing the above conclusion, we have the following.

Theorem 9. *The detection and location of four types of ideal singularities using 1-order derivatives are*

- (1) *ideal step: 1-order derivative can detect and locate ideal step singularities correctly;*
- (2) *ideal roof: 1-order derivative can detect ideal roof singularities when $abs(m) \neq abs(n)$. But, for $abs(m) < abs(n)$, a false singularity $x_0 + 1$ is located;*
- (3) *ideal impulse: the singularity can not be detected;*

(4) *ideal ramp*: 1-order derivative can detect and locate ideal ramp singularities correctly when $m > 0$, for $m < 0$, and the singularity can not be detected.

5. Singularity Detection by Fractional-Order Derivatives

The singularity detection by fractional-order derivatives detects singularities by computing fractional-order derivative expression firstly and then searching for local extrema as the locations of singularities.

5.1. *Fractional Derivatives of Four Types of Singularities.* Fractional-order derivatives of the four types of singularities are as follows.

Ideal Step. The fractional-order derivatives of ideal step singularities are

$$D_{GL}^\alpha s(x) = \begin{cases} \sum_0^{[x-x_0]} \omega_k^{(\alpha)}, & x \geq x_0 \\ 0, & x < x_0. \end{cases} \quad (30)$$

Ideal Roof. The fractional-order derivatives of ideal roof singularities are

$$D_{GL}^\alpha s(x) = \begin{cases} m \sum_{k=0}^{[x-x_0+h_1]} \omega_k^{(\alpha)} (-k + [x - x_0]) \\ + c_0 \sum_{k=0}^{[x-x_0+h_1]} \omega_k^{(\alpha)}, & x_0 - h_1 < x \leq x_0 \\ n \sum_{k=0}^{[x-x_0]-1} \omega_k^{(\alpha)} (-k + [x - x_0]) \\ + m \sum_{k=[x-x_0]}^{[x-x_0+h_1]} \omega_k^{(\alpha)} (-k + [x - x_0]) \\ + c_0 \sum_{k=0}^{[x-x_0+h_1]} \omega_k^{(\alpha)}, & x_0 < x < x_0 + h_2. \end{cases} \quad (31)$$

Ideal Impulse. Since there are only $s(x_0) \neq 0$, we have

$$D_{GL}^\alpha s(x) = \begin{cases} \omega_{[x-x_0]}^{(\alpha)} b, & x - x_0 \leq t \\ 0, & \text{otherwise.} \end{cases} \quad (32)$$

Ideal Ramp. The fractional-order derivatives of ideal ramp singularities are

$$D_{GL}^\alpha s(x) = \begin{cases} m \sum_{k=0}^{[x-x_0+h_1]} \omega_k^{(\alpha)} (-k + [x - x_0]) \\ + c_0 \sum_{k=0}^{[x-x_0+h_1]} \omega_k^{(\alpha)}, & x_0 - h_1 < x \leq x_0 \\ m \sum_{k=[x-x_0+1]}^{[x-x_0+h_1]} \omega_k^{(\alpha)} (-k + [x - x_0]) \\ + c_0 \sum_{k=0}^{[h_1]} \omega_k^{(\alpha)}, & x > x_0. \end{cases} \quad (33)$$

5.2. *Find Extremum.* The main steps to find extrema of fractional-order derivatives $D_{GL}^\alpha s(x)$ with $0 < \alpha < 1$ are as follows: for all $D_{GL}^\alpha s(x) \neq 0$, compare values of $D_{GL}^\alpha s(x - 1)$, $D_{GL}^\alpha s(x)$, and $D_{GL}^\alpha s(x + 1)$. If $D_{GL}^\alpha s(x) - D_{GL}^\alpha s(x - 1) > t_0$ and $D_{GL}^\alpha s(x) - D_{GL}^\alpha s(x + 1) > t_0$ or $D_{GL}^\alpha s(x - 1) - D_{GL}^\alpha s(x) > t_0$ and $D_{GL}^\alpha s(x + 1) - D_{GL}^\alpha s(x) > t_0$, where t_0 is predefined threshold, x is the singularity. Four types of ideal singularities are discussed as follows. Each one has a corresponding singularity on x_0 .

Based on the above discussion, we can detect and locate four types of singularities as follows.

Ideal Step. Since $D(s(x_0)) = \omega_0^{(\alpha)} = 1$, $D(s(x_0 - 1)) = 0$ and $D(s(x_0 + 1)) = 1 + \omega_1^{(\alpha)}$. According to Lemma 6, $\omega_1^{(\alpha)} < 0$ for $0 < \alpha < 1$. Thus, $D(s(x_0)) = 1 > D(s(x_0 + 1))$ and $D(s(x_0)) = 1 > D(s(x_0 - 1)) = 0$. So, x_0 is the singularity. When $x > x_0$, $D(s(x - 1)) \geq D(s(x))$ and $D(s(x + 1)) \leq D(s(x))$, so all $x > x_0$ are not singularities.

From the summary above, there is only one singularity on x_0 .

Ideal Roof. Since

$$D_{GL}^{(\alpha)} s(x_0) = m \sum_{k=1}^{[h_1]} \omega_k^{(\alpha)} (-k) + c_0 \sum_{k=0}^{[h_1]} \omega_k^{(\alpha)},$$

$$D_{GL}^{(\alpha)} s(x_0 - 1) = m \sum_{k=0}^{[h_1]-1} \omega_k^{(\alpha)} (-k - 1) + c_0 \sum_{k=0}^{[h_1]-1} \omega_k^{(\alpha)},$$

$$D_{GL}^{(\alpha)} s(x_0 + 1) = n + m \sum_{k=2}^{[h_1+1]} \omega_k^{(\alpha)} (-k + 1) + c_0 \sum_{k=0}^{[h_1+1]} \omega_k^{(\alpha)}, \quad (34)$$

thus,

$$D_{GL}^{(\alpha)} s(x_0) - D_{GL}^{(\alpha)} s(x_0 - 1) = m \sum_{k=0}^{[h_1]-1} \omega_k^{(\alpha)} + m \omega_{[h_1]}^{(\alpha)} (-[h_1]) + c_0 \omega_{[h_1]}^{(\alpha)}, \quad (35)$$

$$\begin{aligned}
 D_{GL}^{(\alpha)}s(x_0) - D_{GL}^{(\alpha)}s(x_0 + 1) &= -n - m \sum_{k=1}^{[h_1]} \omega_k^{(\alpha)} \\
 &\quad + m\omega_{[h_1+1]}^{(\alpha)} [h_1] - c_0\omega_{[h_1]+1}^{(\alpha)}.
 \end{aligned}
 \tag{36}$$

The ideal roof implies that when $m > 0$, we have $c_0 > 0, n < 0$, and when $m < 0$, we have $c_0 < 0, n > 0$.

According to Lemma 6, $\sum_{k=0}^{[h_1-1]} \omega_k^{(\alpha)} > 0$ and, according to Lemma 7, $\omega_{[h_1]}^{(\alpha)}(-[h_1]) > 0$. Moreover, $-mh_1 + c_0 = 0$. Thus, the right hand of (35) is $m \sum_{k=0}^{[h_1-1]} \omega_k^{(\alpha)}$ and it has the same sign as m . That is, when $m > 0$, it is a positive number while when $m < 0$, it is a negative number. The right hand of (36) can be written as $-n - m \sum_{k=1}^{[h_1]} \omega_k^{(\alpha)}$, which also has the same sign as m . Therefore, when $m > 0$, $D_{GL}^{(\alpha)}s(x_0)$ is a maximum while when $m < 0$, $D_{GL}^{(\alpha)}s(x_0)$ is a minimum. In summary, x_0 is a singularity.

Ideal Impulse. For $x = x_0$, $D_{GL}^{(\alpha)}s(x_0) = b, D_{GL}^{(\alpha)}s(x_0 - 1) = 0$, and $D_{GL}^{(\alpha)}s(x_0 + 1) = \omega_1^{(\alpha)}b$. According to Lemma 5, $\omega_1^{(\alpha)} < 0$ and $abs(\omega_1^{(\alpha)}) < 1$ for $0 < \alpha < 1$. Thus, when $b > 0$, we have $D_{GL}^{(\alpha)}s(x_0) - D_{GL}^{(\alpha)}s(x_0 - 1) = b > 0$ and $D_{GL}^{(\alpha)}s(x_0) - D_{GL}^{(\alpha)}s(x_0 + 1) = b(1 - \omega_1^{(\alpha)}) > 0$, while when $b < 0$, we have $D_{GL}^{(\alpha)}s(x_0) - D_{GL}^{(\alpha)}s(x_0 - 1) = b < 0$ and $D_{GL}^{(\alpha)}s(x_0) - D_{GL}^{(\alpha)}s(x_0 + 1) = b(1 - \omega_1^{(\alpha)}) < 0$. Therefore, x_0 is the singularity.

Ideal Ramp. Since

$$\begin{aligned}
 D_{GL}^{(\alpha)}s(x_0) &= m \sum_{k=1}^{[h_1]} \omega_k^{(\alpha)}(-k) + c_0 \sum_{k=0}^{[h_1]} \omega_k^{(\alpha)}, \\
 D_{GL}^{(\alpha)}s(x_0 - 1) &= m \sum_{k=0}^{[h_1-1]} \omega_k^{(\alpha)}(-k - 1) + c_0 \sum_{k=0}^{[h_1-1]} \omega_k^{(\alpha)}, \tag{37} \\
 D_{GL}^{(\alpha)}s(x_0 + 1) &= m \sum_{k=1}^{[h_1+1]} \omega_k^{(\alpha)}(-k + 1) + c_0 \sum_{k=0}^{[h_1]} \omega_k^{(\alpha)},
 \end{aligned}$$

according to the above discussion of ideal roof, we know that $D_{GL}^{(\alpha)}s(x_0) - D_{GL}^{(\alpha)}s(x_0 - 1)$ has the same sign as m . Thus, we only discuss $D_{GL}^{(\alpha)}s(x_0) - D_{GL}^{(\alpha)}s(x_0 + 1)$ as follows:

$$\begin{aligned}
 D_{GL}^{(\alpha)}s(x_0) - D_{GL}^{(\alpha)}s(x_0 + 1) &= m \sum_{k=1}^{[h_1]} (-\omega_k^{(\alpha)}) + m\omega_{[h_1]+1}^{(\alpha)} [h_1] \\
 &= m \sum_{k=1}^{[h_1]} \left(\omega_{[h_1+1]}^{(\alpha)} - \omega_k^{(\alpha)} \right).
 \end{aligned}
 \tag{38}$$

According to Lemma 4, $\omega_{[h_1]+1}^{(\alpha)} < 0$, and $abs(\omega_{[h_1]+1}^{(\alpha)}) < abs(\omega_k^{(\alpha)})$, we have $\sum_{k=1}^{[h_1]} (\omega_{[h_1+1]}^{(\alpha)} - \omega_k^{(\alpha)}) > 0$. Therefore, $D_{GL}^{(\alpha)}s(x_0) - D_{GL}^{(\alpha)}s(x_0 + 1)$ has the same sign as m . That is, when $m > 0$, we have $D_{GL}^{(\alpha)}s(x_0) - D_{GL}^{(\alpha)}s(x_0 - 1) > 0$ and

$D_{GL}^{(\alpha)}s(x_0) - D_{GL}^{(\alpha)}s(x_0 + 1) > 0$, and when $m < 0$, we have $D_{GL}^{(\alpha)}s(x_0) - D_{GL}^{(\alpha)}s(x_0 - 1) < 0$ and $D_{GL}^{(\alpha)}s(x_0) - D_{GL}^{(\alpha)}s(x_0 + 1) < 0$. Thus, x_0 is the singularity.

Summarizing the above conclusion, we have the following.

Theorem 10. *The fractional derivatives can detect and locate four types of ideal singularities correctly.*

6. Conclusions

In this paper, we study fractional-order derivatives of left-handed Grünwald-Letnikov formula with $0 < \alpha < 1$ to detect and locate singularities in theory. Theory analysis indicates that fractional-order derivatives of left-handed Grünwald-Letnikov formula with $0 < \alpha < 1$ can detect and locate the ideal four types of singularities correctly, which shows better performance than classical 1-order derivatives in theory.

Conflict of Interests

The authors declare that there is no conflict of interests regarding the publication of this paper.

Acknowledgments

This paper is supported by the National Natural Science Foundation of China (nos. 60873102 and 60873264), Major State Basic Research Development Program (no. 2010CB732501), and Open Foundation of Visual Computing and Virtual Reality Key Laboratory of Sichuan Province (no. J2010N03). This work was supported by a Grant from the National High Technology Research and Development Program of China (no. 2009AA12Z140).

References

- [1] Y. Chen, Y. Li, W. Yu, L. Luo, W. Chen, and C. Toumoulin, "Joint-map tomographic reconstruction with patch similarity based mixture prior model," *Multiscale Modeling and Simulation*, vol. 9, no. 4, pp. 1399–1419, 2011.
- [2] S. Hu, Z. Liao, D. Sun, and W. Chen, "A numerical method for preserving curve edges in nonlinear anisotropic smoothing," *Mathematical Problems in Engineering*, vol. 2011, Article ID 186507, 14 pages, 2011.
- [3] Y. Chen, X. Yin, L. Shi et al., "Improving abdomen tumor low-dose CT images using a fast dictionary learning based processing," *Physics in Medicine and Biology*, vol. 58, no. 16, pp. 5803–5820, 2013.
- [4] Z. Bian, J. Ma, J. Huang et al., "SR-NLM: a sinogram restoration induced non-local means image filtering for low-dose computed tomography," *Computerized Medical Imaging and Graphics*, vol. 37, no. 4, pp. 293–303, 2013.
- [5] J. Ma, H. Zhang, Y. Gao et al., "Iterative image reconstruction for cerebral perfusion CT using a pre-contrast scan induced edge-preserving prior," *Physics and Medical Biology*, vol. 57, no. 22, pp. 7519–7542, 2012.
- [6] Z. Jun and W. Zhihui, "A class of fractional-order multi-scale variational models and alternating projection algorithm for

- image denoising,” *Applied Mathematical Modelling*, vol. 35, no. 5, pp. 2516–2528, 2011.
- [7] J. Bai and X.-C. Feng, “Fractional-order anisotropic diffusion for image denoising,” *IEEE Transactions on Image Processing*, vol. 16, no. 10, pp. 2492–2502, 2007.
- [8] M. Janev, S. Pilipović, T. Atanacković, R. Obradović, and N. Ralević, “Fully fractional anisotropic diffusion for image denoising,” *Mathematical and Computer Modelling*, vol. 54, no. 1-2, pp. 729–741, 2011.
- [9] C. Wang, L. Lan, and S. Zhou, “Grünwald-Letnikov based adaptive fractional differential algorithm on image texture enhancing,” *Journal of Computational Information Systems*, vol. 9, no. 2, pp. 445–454, 2013.
- [10] H. A. Jalab and R. W. Ibrahim, “Texture enhancement based on the Savitzky-Golay fractional differential operator,” *Mathematical Problems in Engineering*, vol. 2013, Article ID 149289, 8 pages, 2013.
- [11] S. Hu, Z. Liao, and W. Chen, “Sinogram restoration for low-dosed X-ray computed tomography using fractional-order Perona-Malik diffusion,” *Mathematical Problems in Engineering*, vol. 2012, Article ID 391050, 13 pages, 2012.
- [12] Z. Liao, “Low-dosed x-ray computed tomography imaging by regularized fully spatial fractional-order Perona-Malik diffusion,” *Advances in Mathematical Physics*, vol. 2013, Article ID 371868, 9 pages, 2013.
- [13] Z. Liao, “A new definition of fractional derivatives based on truncated left-handed Grünwald-Letnikov formula with $0 < \alpha < 1$ and median correction,” *Abstract and Applied Analysis*. In press.
- [14] M. Li, “A class of negatively fractal dimensional Gaussian random functions,” *Mathematical Problems in Engineering*, vol. 2011, Article ID 291028, 18 pages, 2011.
- [15] M. Li and W. Zhao, “On bandlimitedness and lag-limitedness of fractional Gaussian noise,” *Physica A: Statistical Mechanics and Its Applications*, vol. 392, no. 9, pp. 1955–1961, 2013.
- [16] M. Li, S. C. Lim, C. Cattani, and M. Scalia, “Characteristic roots of a class of fractional oscillators,” *Advances in High Energy Physics*, vol. 2013, Article ID 853925, 7 pages, 2013.
- [17] S. Hu, “External fractional-order gradient vector Perona-Malik diffusion for sinogram restoration of low-dosed x-ray computed tomography,” *Advances in Mathematical Physics*, vol. 2013, Article ID 516919, 10 pages, 2013.
- [18] D. A. Benson, S. W. Wheatcraft, and M. M. Meerschaert, “Application of a fractional advection-dispersion equation,” *Water Resources Research*, vol. 36, no. 6, pp. 1403–1412, 2000.
- [19] R. Hilfer, *Applications of Fractional Calculus in Physics*, vol. 463, World Scientific, Singapore, 2000.
- [20] E. Sousa, “How to approximate the fractional derivative of order $1 < \alpha \leq 2$,” *International Journal of Bifurcation and Chaos in Applied Sciences and Engineering*, vol. 22, no. 4, Article ID 1250075, 13 pages, 2012.
- [21] I. Podlubny, *Fractional Differential Equations*, Academic Press, San Diego, Calif, USA, 1999.
- [22] S. G. Samko, A. A. Kilbas, and O. I. Marichev, *Fractional Integrals and Derivatives: Theory and Applications*, Gordon and Breach, London, UK, 1993.
- [23] A. A. Kilbas, H. M. Srivastava, and J. J. Trujillo, *Theory and Applications of Fractional Differential Equations*, Elsevier, Amsterdam, The Netherlands, 2006.

Research Article

Mathematical Models Arising in the Fractal Forest Gap via Local Fractional Calculus

Chun-Ying Long,¹ Yang Zhao,² and Hossein Jafari^{3,4}

¹ School of Civil Engineering and Architecture, Nanchang University, Nanchang 330031, China

² Electronic and Information Technology Department, Jiangmen Polytechnic, Jiangmen 529090, China

³ Department of Mathematics, Faculty of Mathematical Sciences, University of Mazandaran, Babolsar 47415-416, Iran

⁴ African Institute for Mathematical Sciences, Muizenberg 7945, South Africa

Correspondence should be addressed to Yang Zhao; zhaoyang19781023@gmail.com

Received 8 January 2014; Accepted 10 February 2014; Published 18 March 2014

Academic Editor: Carlo Cattani

Copyright © 2014 Chun-Ying Long et al. This is an open access article distributed under the Creative Commons Attribution License, which permits unrestricted use, distribution, and reproduction in any medium, provided the original work is properly cited.

The forest new gap models via local fractional calculus are investigated. The JABOWA and FORSKA models are extended to deal with the growth of individual trees defined on Cantor sets. The local fractional growth equations with local fractional derivative and difference are discussed. Our results are first attempted to show the key roles for the nondifferentiable growth of individual trees.

1. Introduction

Fractals had been used to describe special problems in biology and ecology [1–4] because of the measure of nature objects underlying the geometry, replacing the complex real-world objects by describing the Euclidean ideas. Fractal dimension was applied to describe the measure of the complexity in biology and ecology. In forestry, the fractal geometry had been applied to estimate stand density, predict forest succession, and describe the form of trees [5–7]. The scaling of dynamics in hierarchical structure was investigated in [8–12]. The ecological resilience example from boreal forest was presented in the context [8]. The quantitative theory of forest structure was discussed [9]. The allometric scaling laws in biology were proposed in the works [10, 11]. Based upon the cross-scale analysis, the geometry and dynamics of ecosystems were considered and the structure ecosystems across scales in time and space were discussed in [12, 13]. Fractal forestry was modeled by using the scaling of the testing parameters for ecological complexity.

Forest gap model (JABOWA) developed by Botkin et al. [14–16] was the first simulation model for gap-phase replacement. It was applied to describe a forest as a mosaic of closed canopies and simulate forest dynamics based upon

the establishment, growth, and death of individual trees [17–20]. The JABOWA model in the form of the FORET model (called JABOWA-FORET) was further developed in [21–24]. The JABOWA model of the simulation of stand structure in a forest gap model was improved in [24] and the FORSKA [25] was proposed by Botkin et al. In [14–16], the ecological functions are continuous. In [10–13], the ecological functions were expressed across scales in time and space. However, as it is shown in Figure 1 the ecological functions distinguishing hierarchical size scales in nature, such as the measures of tree size and measure of soil fertility, are defined on Cantor sets. The above approaches do not deal with them.

Local fractional calculus theory [26–38] was applied to handle the nondifferentiable functions defined on Cantor sets. The heat-conduction, transport, Maxwell, diffusion, wave, Fokker-Planck, and the mechanical structure equations were usefully shown (see for more details [28–36] and the cited references therein). In order to simulate forest dynamics on the basis of the establishment, growth, and death of individual trees defined on Cantor sets, the aim of this paper is to present the forest new gap models for simulating the gap-phase replacement by employing the local fractional calculus.

The paper has been organized as follows. In Section 2, we review the JABOWA and FORSKA models for the forest

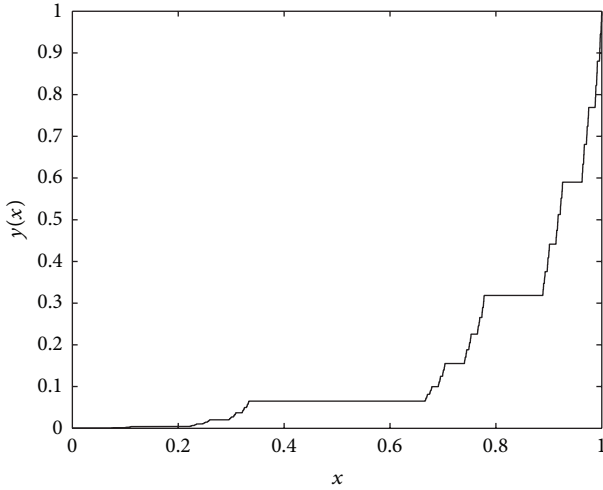


FIGURE 1: The ecological function $f(x)$ defined on Cantor set.

succession. In Section 3, we propose JABOWA and FORSKA models for the fractal forest succession. Finally, Section 4 is conclusions.

2. Growth Models for Forest Gap

In this section we will revise the JABOWA and FORSKA models.

2.1. The JABOWA Model. The growth equation with difference form is given by [15, 16, 24, 39]

$$\frac{\Delta D}{\Delta t} = G \cdot D \cdot \phi(D) \cdot \frac{1}{b(D)} \cdot f(e), \quad (1)$$

where the function D is diameter at breast height of the trees, the parameter H is tree height, G is a growth rate, the function $b(D)$ is a quantity encapsulating this allometric relationship, $f(e)$ is a quantity influencing the abiotic and biotic environment on tree growth, $\phi(D) = (1 - D \cdot H / (D_{\max} \cdot H_{\max}))$, and D_{\max} and H_{\max} are the maximum measures of the tree dimensions.

The parameter $f(e)$ is simulated as follows [24]:

$$f(e) = g_1(\text{AL}) \cdot g_2(\text{SBAR}) \cdot g_3(\text{DD}), \quad (2)$$

where $g_1(\text{AL})$ is a quantity of available light, $g_2(\text{SBAR})$ is a quantity of stand basal area, and $g_3(\text{DD})$ is a quantity of the annual degree-day sum. It was referred to as Liebig's law of the minimum [24].

The allometric relationship with a parabolic form is written as follows [24, 40]:

$$b(D) = b_1 + b_2 D + b_3 D^2, \quad (3)$$

where b_1 , b_2 , and b_3 are parameters.

Leaf area index reads as follows [24]:

$$\text{LAI} = \mu D^2, \quad (4)$$

where $\mu = c/k$ with a species-specific parameter c and the scale leaf weight per tree to the projected leaf area k .

In order to implement a new height-diameter relationship [40], the differential form of growth equation in the JABOWA model was suggested as follows [41]:

$$\frac{dD}{dt} = G \cdot D \cdot \varphi(D), \quad (5)$$

where the function has the following form:

$$\varphi(D) = \frac{1 - H/H_{\max}}{2H_{\max} - b(-sD/b + 2)e^{-Ds/b}} \quad (6)$$

with the parameter $b = H_{\max} - 137$ and the initial slope value of the height diameter relationship s .

2.2. The FORSKA Model. The FORSKA model was developed for unmanaged natural forests and tree height had H - D relationship with the FORSKA model given by [24, 25, 39, 41]

$$H = 1.3 + (H_{\max} - 1.3) \cdot (1 - e^{-sD/(H_{\max}-1.3)}), \quad (7)$$

where the parameter s is the initial slope value of the height diameter relationship at $D = 0$, H_{\max} is the maximum measure of the tree dimension, D is diameter at breast height of the trees, and H is tree height.

As it is known, the trees in the real forest do not follow the H - D relationship. The growth equation with differential form can be written as follows [24, 25]:

$$\frac{dH}{dD} = s \cdot f(H), \quad (8)$$

where

$$f(H) = \frac{H - 1.3}{H_{\max} - 1.3}. \quad (9)$$

3. The JABOWA and FORSKA Models for the Fractal Forest Succession

In this section, based upon the local fractional calculus theory, we show the JABOWA and FORSKA models for the fractal forest succession. At first, we start with the local fractional derivative.

3.1. Local Fractional Derivative. We now give the local fractional calculus and the recent results.

If

$$|f(x) - f(x_0)| < \varepsilon^\alpha \quad (10)$$

with $|x - x_0| < \delta$, for $\varepsilon, \delta > 0$ and $\varepsilon, \delta \in \mathbb{R}$, then we denote [26-28]

$$f(x) \in C_\alpha(a, b). \quad (11)$$

If $f(x) \in C_\alpha(a, b)$, then we have [26]

$$\dim_H(F \cap (a, b)) = \dim_H(C_\alpha(a, b)) = \alpha, \quad (12)$$

where $C_\alpha(a, b) = \{f : f(x) \text{ is local fractional continuous, } x \in F \cap (a, b)\}$.

Let $f(x) \in C_\alpha(a, b)$. The local fractional derivative of $f(x)$ of order α at $x = x_0$ is defined as [26–34]

$$f^{(\alpha)}(x_0) = \left. \frac{d^\alpha f(x)}{dx^\alpha} \right|_{x=x_0} = \lim_{x \rightarrow x_0} \frac{\Delta^\alpha (f(x) - f(x_0))}{(x - x_0)^\alpha}, \quad (13)$$

where $\Delta^\alpha (f(x) - f(x_0)) \cong \Gamma(1 + \alpha)\Delta(f(x) - f(x_0))$.

For $0 < \alpha \leq 1$, the increment of $f(x)$ can be written as follows [26, 27]:

$$\Delta^\alpha f(x) = f^{(\alpha)}(x) (\Delta x)^\alpha + \lambda (\Delta x)^\alpha, \quad (14)$$

where Δx is an increment of x and $\lambda \rightarrow 0$ as $\Delta x \rightarrow 0$.

For $0 < \alpha \leq 1$, the α -local fractional differential of $f(x)$ reads as [26, 27]

$$d^\alpha f = f^{(\alpha)}(x) (dx)^\alpha. \quad (15)$$

From (14), we have approximate formula in the form

$$\Delta^\alpha f(x) \cong \Gamma(1 + \alpha) \Delta(f(x) - f(x_0)). \quad (16)$$

Let $f(x) \in C_\alpha(a, b)$. The local fractional integral of $f(x)$ of order α is given by [26–31]

$$\begin{aligned} {}_a I_b^{(\alpha)} f(x) &= \frac{1}{\Gamma(1 + \alpha)} \int_a^b f(t) (dt)^\alpha \\ &= \frac{1}{\Gamma(1 + \alpha)} \lim_{\Delta t \rightarrow 0} \sum_{j=0}^{j=N-1} f(t_j) (\Delta t_j)^\alpha, \end{aligned} \quad (17)$$

where $\Delta t_j = t_{j+1} - t_j$, $\Delta t = \max\{\Delta t_1, \Delta t_2, \Delta t_j, \dots\}$, and $[t_j, t_{j+1}]$, $j = 0, \dots, N - 1$, $t_0 = a$, $t_N = b$, is a partition of the interval $[a, b]$.

The α -dimensional Hausdorff measure H_α is calculated by [26]

$$H_\alpha(F \cap (0, x)) = {}_0 I_x^{(\alpha)} 1 = \frac{x^\alpha}{\Gamma(1 + \alpha)}. \quad (18)$$

3.2. The Local Fractional JABOWA Models (LFJABOWA). Here, we structure the LFJABOWA models via local fractional derivative and difference.

From (5), when

$$G \cdot \varphi(D) = \lambda_0 D^{\beta-1}, \quad (19)$$

the Enquist growth model in JABOWA model reads as [11, 42]

$$\frac{dD}{dt} = \lambda_0 D^\beta, \quad (20)$$

where D is the diameter at breast height, λ_0 is the scaling coefficient, and β is the fractal dimension.

Making use of the fractional complex transform [29] and (20), the growth equation in the JABOWA model with local fractional derivative (LFJABOWA) is suggested by

$$\frac{d^\alpha D}{dt^\alpha} = \lambda_0 D^\beta, \quad (21)$$

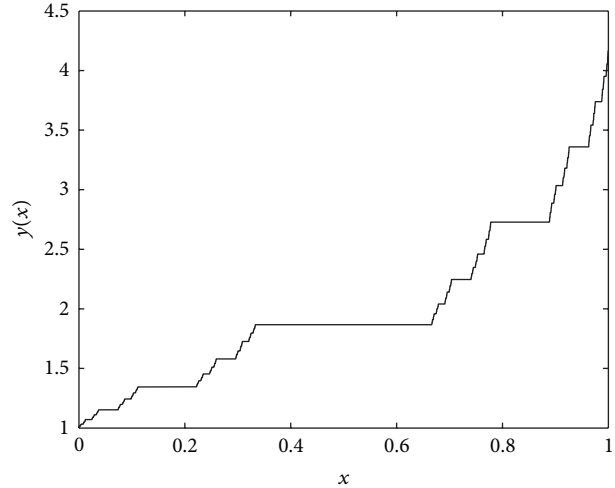


FIGURE 2: The graph of (22) with parameters $\beta = 1$, $\lambda_0 = 1$, and $t_0 = 0$.

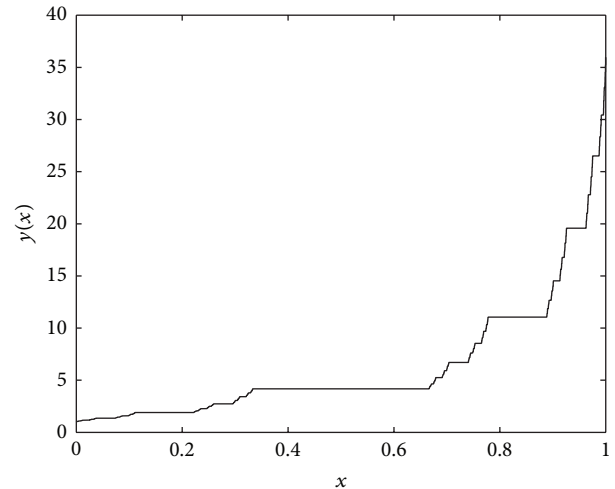


FIGURE 3: The graph of (22) with parameters $\beta = 1$, $\lambda_0 = 2$, and $t_0 = 0$.

where D is the diameter at breast height, λ_0 is the scaling coefficient, and α and β are the fractal dimensions. In order to illustrate the difference from the works presented in [42], we consider the following case: when $\beta = 1$, (21) can be integrated to give

$$D(t) = E_\alpha(\lambda_0 t^\alpha) - E_\alpha(\lambda_0 t_0^\alpha). \quad (22)$$

For the parameters $\beta = 1$, $t = 0$, the solutions of (21) with different values $\lambda_0 = 1$, $\lambda_0 = 2$, $\lambda_0 = 3$, and $\lambda_0 = 4$ are, respectively, shown in Figures 2, 3, 4, and 5.

Using the fractional complex transform, (5) becomes into

$$\frac{d^\alpha D}{dt^\alpha} = G \cdot D \cdot \varphi(D). \quad (23)$$

Comparing (22) and (23), we have

$$\frac{d^\alpha D}{dt^\alpha} = \psi(t, D), \quad (24)$$

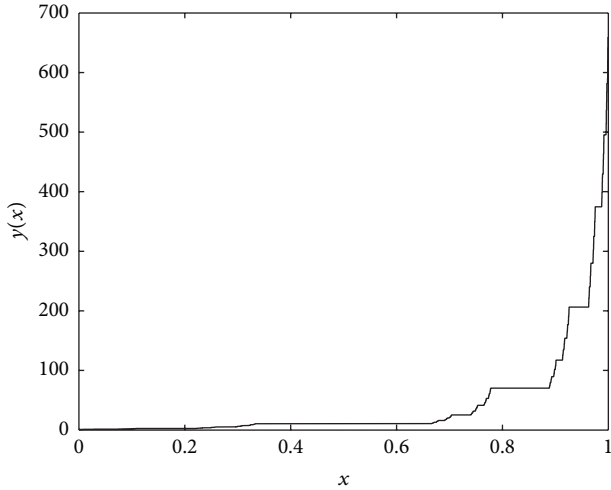


FIGURE 4: The graph of (22) with parameters $\beta = 1$, $\lambda_0 = 3$, and $t_0 = 0$.

where

$$\psi(t, D) = G \cdot D \cdot \varphi(D) \tag{25}$$

or

$$\psi(t, D) = \lambda_0 D^\beta. \tag{26}$$

From (25) and (26), we could get

$$\varphi(D) = D^{\beta-1}, \tag{27}$$

$$\lambda_0 = G. \tag{28}$$

Hence, the local fractional JABOWA model (LFJABOWA) reads as follows:

$$\frac{d^\alpha D}{dt^\alpha} = \psi(t, D), \tag{29}$$

where $\psi(t, D)$ is a nondifferentiable function and D is the diameter at breast height.

In view of (16), from (29) we give the difference form of local fractional JABOWA model (LFJABOWA) in the following form:

$$\frac{\Delta^\alpha D}{(\Delta t)^\alpha} = \psi(t, D), \tag{30}$$

where D is the diameter at breast height and $\Delta^\alpha D(t) \cong \Gamma(1 + \alpha)\Delta(D(t) - D(t_0))$.

When the fractal dimension α is equal to 1, we get the generalized form of (1); namely,

$$\frac{\Delta D}{\Delta t} = \psi(t, D), \tag{31}$$

where

$$\psi(t, D) = G \cdot D \cdot \phi(D) \cdot \frac{1}{b(D)} \cdot f(e). \tag{32}$$

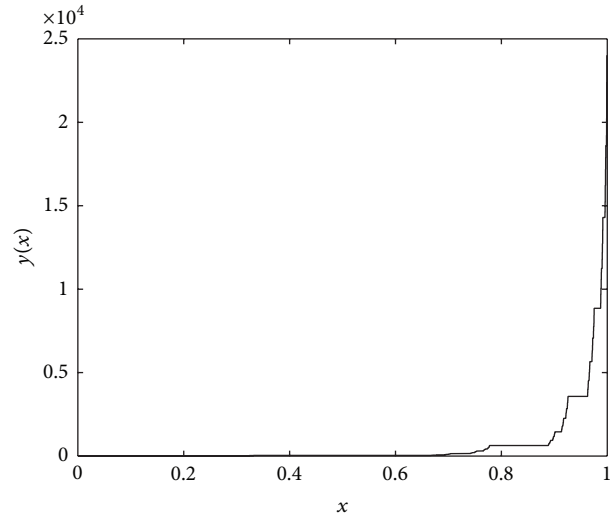


FIGURE 5: The graph of (22) with parameters $\beta = 1$, $\lambda_0 = 4$, and $t_0 = 0$.

3.3. *The Local Fractional FORSKA Models (LFFORSKA).* Here, we present the LFFORSKA models via local fractional derivative and difference.

The tree height H is the nondifferentiable function; namely,

$$|H(D) - H(D_0)| < \varsigma^\alpha, \tag{33}$$

where for $\varsigma, \vartheta > 0$, $\varsigma, \vartheta \in R$, and $|D - D_0| < \vartheta$.

Following the fractional complex transform [29], from (8) we have the local fractional growth equation in the following form:

$$\frac{d^\alpha H}{dD^\alpha} = s \cdot f(H), \tag{34}$$

where $f(H)$ is a local fractional continuous function, H is the tree height, and s is a parameter.

Therefore, the generalized form of (34) is suggested as follows:

$$\frac{d^\alpha H}{dD^\alpha} = \chi(D, H), \tag{35}$$

where D is the diameter at breast height and H is the tree height. In view of (16), (35) can be rewritten as follows:

$$\frac{\Delta^\alpha H}{(\Delta D)^\alpha} = \chi(D, H), \tag{36}$$

where

$$|D - D_0| < \vartheta, \tag{37}$$

$$|H(D) - H(D_0)| < \varsigma^\alpha.$$

The expression (36) is the difference form of local fractional FORSKA model (LFFORSKA).

4. Conclusions

In this work we investigated the local fractional models for the fractal forest succession. Based on the local fractional operators, we suggested the differential and difference forms of the local fractional JABOWA and FORSKA models. The nondifferentiable growths of individual trees were discussed. It is a good start for solving the rhetorical models for the fractal forest succession in the mathematical analysis.

Conflict of Interests

The authors declare that they have no conflict of interests regarding the publication of this paper.

Acknowledgment

This work is supported by the Science and Technology Commission Planning Project of Jiangxi Province (no. 20122BBG70078).

References

- [1] A. Fielding, "Applications of fractal geometry to biology," *Computer Applications in the Biosciences*, vol. 8, no. 4, pp. 359–366, 1992.
- [2] B. L. Li, "Fractal geometry applications in description and analysis of patch patterns and patch dynamics," *Ecological Modelling*, vol. 132, no. 1, pp. 33–50, 2000.
- [3] G. Sugihara and R. M. May, "Applications of fractals in ecology," *Trends in Ecology & Evolution*, vol. 5, no. 3, pp. 79–86, 1990.
- [4] J. H. Brown, V. K. Gupta, B. L. Li, B. T. Milne, C. Restrepo, and G. B. West, "The fractal nature of nature: power laws, ecological complexity and biodiversity," *Philosophical Transactions of the Royal Society of London B*, vol. 357, no. 1421, pp. 619–626, 2002.
- [5] N. D. Lorimer, R. G. Haight, and R. A. Leary, *The Fractal Forest: Fractal Geometry and Applications in Forest Science*, North Central Forest Experiment Station, Berkeley, Calif, USA, 1994.
- [6] B. Zeide, "Fractal geometry in forestry applications," *Forest Ecology and Management*, vol. 46, no. 3, pp. 179–188, 1991.
- [7] B. Zeide, "Analysis of the $3/2$ power law of self-thinning," *Forest Science*, vol. 33, no. 2, pp. 517–537, 1987.
- [8] G. D. Peterson, "Scaling ecological dynamics: self-organization, hierarchical structure, and ecological resilience," *Climatic Change*, vol. 44, no. 3, pp. 291–309, 2000.
- [9] G. B. West, B. J. Enquist, and J. H. Brown, "A general quantitative theory of forest structure and dynamics," *Proceedings of the National Academy of Sciences*, vol. 106, no. 17, pp. 7040–7045, 2009.
- [10] G. B. West, J. H. Brown, and B. J. Enquist, "A general model for the origin of allometric scaling laws in biology," *Science*, vol. 276, no. 5309, pp. 122–126, 1997.
- [11] B. J. Enquist, G. B. West, E. L. Charnov, and J. H. Brown, "Allometric scaling of production and life-history variation in vascular plants," *Nature*, vol. 401, no. 6756, pp. 907–911, 1999.
- [12] C. S. Holling, "Cross-scale morphology, geometry, and dynamics of ecosystems," *Ecological Monographs*, vol. 62, no. 4, pp. 447–502, 1992.
- [13] G. Peterson, C. R. Allen, and C. S. Holling, "Ecological resilience, biodiversity, and scale," *Ecosystems*, vol. 1, no. 1, pp. 6–18, 1998.
- [14] D. B. Botkin, J. F. Janak, and J. R. Wallis, "Rationale, limitations, and assumptions of a northeastern forest growth simulator," *IBM Journal of Research and Development*, vol. 16, no. 2, pp. 101–116, 1972.
- [15] D. B. Botkin, J. F. Janak, and J. R. Wallis, "Some ecological consequences of a computer model of forest growth," *The Journal of Ecology*, vol. 60, no. 3, pp. 849–872, 1972.
- [16] D. B. Botkin, *Forest Dynamics: An Ecological Model*, Oxford University Press, New York, NY, USA, 1993.
- [17] G. L. Perry and N. J. Enright, "Spatial modelling of vegetation change in dynamic landscapes: a review of methods and applications," *Progress in Physical Geography*, vol. 30, no. 1, pp. 47–72, 2006.
- [18] R. Chen and R. R. Twilley, "A gap dynamic model of mangrove forest development along gradients of soil salinity and nutrient resources," *Journal of Ecology*, vol. 86, no. 1, pp. 37–51, 1998.
- [19] R. W. Hall, "JABOWA revealed-finally," *Ecology*, vol. 75, no. 3, p. 859, 1994.
- [20] M. I. Ashraf, C. P. A. Bourque, D. A. MacLean, T. Erdle, and F. R. Meng, "Using JABOWA-3 for forest growth and yield predictions under diverse forest conditions of Nova Scotia, Canada," *The Forestry Chronicle*, vol. 88, no. 6, pp. 708–721, 2012.
- [21] H. H. Shugart and I. R. Noble, "A computer model of succession and fire response of the high-altitude *Eucalyptus* forest of the Brindabella Range, Australian Capital Territory," *Australian Journal of Ecology*, vol. 6, no. 2, pp. 149–164, 1981.
- [22] H. H. Shugart and D. C. West, "Development of an Appalachian deciduous forest succession model and its application to assessment of the impact of the chestnut blight," *Journal of Environmental Management*, vol. 5, pp. 161–179, 1977.
- [23] H. H. Shugart, *A Theory of Forest Dynamics. The Ecological Implications of Forest Succession Models*, Springer, New York, NY, USA, 1984.
- [24] H. Bugmann, "A review of forest gap models," *Climatic Change*, vol. 51, no. 3-4, pp. 259–305, 2001.
- [25] M. Lindner, R. Sievänen, and H. Pretzsch, "Improving the simulation of stand structure in a forest gap model," *Forest Ecology and Management*, vol. 95, no. 2, pp. 183–195, 1997.
- [26] X.-J. Yang, *Advanced Local Fractional Calculus and Its Applications*, World Science, New York, NY, USA, 2012.
- [27] X. J. Yang, *Local Fractional Functional Analysis and Its Applications*, Asian Academic, Hong Kong, China, 2011.
- [28] X. J. Yang and D. Baleanu, "Fractal heat conduction problem solved by local fractional variation iteration method," *Thermal Science*, vol. 17, no. 2, pp. 625–628, 2013.
- [29] X. J. Yang, D. Baleanu, and J. H. He, "Transport equations in fractal porous media within fractional complex transform method," *Proceedings of the Romanian Academy A*, vol. 14, no. 4, pp. 287–292, 2013.
- [30] C. F. Liu, S. S. Kong, and S. J. Yuan, "Reconstructive schemes for variational iteration method within Yang-Laplace transform with application to fractal heat conduction problem," *Thermal Science*, vol. 17, no. 3, pp. 715–721, 2013.
- [31] A. M. Yang, Y. Z. Zhang, and Y. Long, "The Yang-Fourier transforms to heat-conduction in a semi-infinite fractal bar," *Thermal Science*, vol. 17, no. 3, pp. 707–713, 2013.
- [32] Y. Zhao, D. Baleanu, C. Cattani, D. F. Cheng, and X.-J. Yang, "Maxwell's equations on Cantor Sets: a local fractional

- approach,” *Advances in High Energy Physics*, vol. 2013, Article ID 686371, 6 pages, 2013.
- [33] X. J. Yang, D. Baleanu, and W. P. Zhong, “Approximate solutions for diffusion equations on Cantor space-time,” *Proceedings of the Romanian Academy A*, vol. 14, no. 2, pp. 127–133, 2013.
- [34] X.-J. Yang, H. M. Srivastava, J. H. He, and D. Baleanu, “Cantor-type cylindrical-coordinate method for differential equations with local fractional derivatives,” *Physics Letters A*, vol. 377, no. 28–30, pp. 1696–1700, 2013.
- [35] K. M. Kolwankar and A. D. Gangal, “Local fractional Fokker-Planck equation,” *Physical Review Letters*, vol. 80, no. 2, pp. 214–217, 1998.
- [36] A. Carpinteri, B. Chiaia, and P. Cornetti, “Static-kinematic duality and the principle of virtual work in the mechanics of fractal media,” *Computer Methods in Applied Mechanics and Engineering*, vol. 191, no. 1-2, pp. 3–19, 2001.
- [37] F. Ben Adda and J. Cresson, “About non-differentiable functions,” *Journal of Mathematical Analysis and Applications*, vol. 263, no. 2, pp. 721–737, 2001.
- [38] A. Babakhani and V. Daftardar-Gejji, “On calculus of local fractional derivatives,” *Journal of Mathematical Analysis and Applications*, vol. 270, no. 1, pp. 66–79, 2002.
- [39] H. K. Bugmann, X. Yan, M. T. Sykes et al., “A comparison of forest gap models: model structure and behaviour,” *Climatic Change*, vol. 34, no. 2, pp. 289–313, 1996.
- [40] A. D. Moore, “On the maximum growth equation used in forest gap simulation models,” *Ecological Modelling*, vol. 45, no. 1, pp. 63–67, 1989.
- [41] A. C. Risch, C. Heiri, and H. Bugmann, “Simulating structural forest patterns with a forest gap model: a model evaluation,” *Ecological Modelling*, vol. 181, no. 2-3, pp. 161–172, 2005.
- [42] D. A. Coomes and R. B. Allen, “Effects of size, competition and altitude on tree growth,” *Journal of Ecology*, vol. 95, no. 5, pp. 1084–1097, 2007.

Research Article

A Discretized Tikhonov Regularization Method for a Fractional Backward Heat Conduction Problem

Zhi-Liang Deng¹ and Xiao-Mei Yang²

¹ School of Mathematical Sciences, University of Electronic Science and Technology of China, Chengdu 610054, China

² School of Mathematics, Southwest Jiaotong University, Chengdu 610031, China

Correspondence should be addressed to Zhi-Liang Deng; dengzhl@uestc.edu.cn

Received 30 December 2013; Accepted 7 February 2014; Published 18 March 2014

Academic Editor: Ming Li

Copyright © 2014 Z.-L. Deng and X.-M. Yang. This is an open access article distributed under the Creative Commons Attribution License, which permits unrestricted use, distribution, and reproduction in any medium, provided the original work is properly cited.

We propose a numerical reconstruction method for solving a time-fractional backward heat conduction problem. Based on the idea of reproducing kernel approximation, we reconstruct the unknown initial heat distribution from a finite set of scattered measurements of transient temperature at a fixed final time. The standard Tikhonov regularization technique using the norm of reproducing the kernel Hilbert space as the penalty term is adopted to provide a stable solution when the measurement data contains noise. Numerical results indicate that the proposed method is efficient.

1. Introduction

Let $\Omega \subset \mathbb{R}^d$, $d \in \mathbb{N}$, be a bounded domain with sufficiently smooth boundary $\partial\Omega$. Consider the following initial boundary value problem for time-fractional diffusion equation (TFDE):

$$\begin{aligned} {}_0D_t^\gamma u(x, t) &= \mathcal{L}u, \quad x \in \Omega, t \in [0, T], \\ u(x, 0) &= f(x), \quad x \in \bar{\Omega}, \end{aligned} \quad (1)$$

$$\mathcal{B}u(x, t) := \mu u(x, t) + \beta \frac{\partial u}{\partial \nu} = 0, \quad x \in \partial\Omega, t \in [0, T].$$

Here ${}_0D_t^\gamma$ denotes the Caputo fractional derivative with respect to t and is defined by

$${}_0D_t^\gamma \psi(t) = \begin{cases} \frac{1}{\Gamma(1-\gamma)} \int_0^t \frac{\psi'(\tau)}{(t-\tau)^\gamma} d\tau, & 0 < \gamma < 1, \\ \psi'(t), & \gamma = 1. \end{cases} \quad (2)$$

$\Gamma(\cdot)$ is the Gamma function and \mathcal{L} is a symmetric uniformly elliptic operator and $T > 0$ is a fixed final time, μ and β

are constants, and ν is the outward unit normal vector of the domain Ω . In what follows, let $0 < \gamma < 1$ and \mathcal{L} be given by

$$\begin{aligned} \mathcal{L}u(x) &:= \sum_{i=1}^d \frac{\partial}{\partial x_i} \left(\sum_{j=1}^d D_{ij}(x) \frac{\partial}{\partial x_j} u(x) \right) \\ &+ Q(x) u(x), \quad x \in \Omega, \end{aligned} \quad (3)$$

where $Q \in C(\bar{\Omega})$, $Q(x) \leq 0$ for $x \in \bar{\Omega}$ and $D_{ij} = D_{ji} \in C^1(\bar{\Omega})$, $1 \leq i, j \leq d$. Moreover, we assume that there exists a positive constant $D > 0$ such that

$$D \sum_{i=1}^d \eta_i^2 \leq \sum_{i,j=1}^d D_{ij}(x) \eta_i \eta_j, \quad x \in \bar{\Omega}, \eta \in \mathbb{R}^d. \quad (4)$$

Recently, people are shifting their partial focus to fractional-order differential equations (FDEs) with the realization that the use of fractional-order derivatives and integrals leads to formulas of certain physical processes (for instance, some anomalous diffusion processes) which is more economical and useful than the classical approach in terms of Fick's laws of diffusion. In this paper, we consider the fractional-order partial differential equation (FPDE) in (1), which is obtained from the standard diffusion equation by replacing the first-order time derivative with a fractional

derivative of order γ , with $0 < \gamma < 1$. Different models using this kind of FDEs have been proposed [1–3], and there has been significant interest in developing numerical schemes for their solution. Physically, the time-fractional partial differential equations describe the continuous time random walk problems (the non-Markovian process). The physical interpretation of the fractional derivative is that it represents a degree of memory in the diffusing material [4]. Actually, the convolution integral in the definition of the Caputo fractional-order derivatives for $\gamma \in (0, 1)$ at time t requires all the knowledge of classical derivative $\psi'(\tau)$ for $\tau \in (0, t)$, which reflects the “memory effect” of fractional derivatives. The utilization of the memory effect of fractional derivatives comes with a high cost regarding numerical solvability. Any algorithm using a discretization of a noninteger derivative has to take into account its nonlocal structure which means in general a high storage requirement and great overall complexity of the algorithm. Similar convolution model can be used to depict the tumor-immune system [5]. Fractional dimensional model is also used to characterize the binary images of DNA [6] and oscillators [7, 8]. In [9], a general approach is proposed to approximate ideal filters based on fractional calculus from the point of view of systems of fractional order. Recently, numerous attempts to solve TFDE can be found in the literature [4, 10–14]. We can refer to [15–18] for more specified knowledge about fractional calculus.

The backward problem governed by time-fractional partial differential equation in (1) is to recover the heat distribution at any earlier time $0 \leq t < T$ from the measurement $u_\epsilon(x, T)$, written as u_T^ϵ , which is noise-contaminated data for the exact temperature $u(x, T)$:

$$\|u_\epsilon(\cdot, T) - u(\cdot, T)\|_{L^2(\Omega)} \leq \epsilon \quad (5)$$

for some known noise level $\epsilon > 0$. Such inverse problems have been considered by several authors. Based on the eigenfunction expansions, Sakamoto and Yamamoto [19] establish the unique existence of the weak solution and the asymptotic behavior as the time t goes to ∞ for the forward problem and prove the stability and uniqueness in the backward problem in time. For the one-dimensional case, Liu and Yamamoto [20] propose a regularizing scheme by the quasi-reversibility to restore the stability of the backward problem. In [21], a regularization by projection is applied to the same problem as in [20] and the corresponding convergence rates are obtained under *a priori* and *a posteriori* parameter choice strategies, respectively. Here, we pay our attention to the situation of stable reconstruction of the initial heat distribution $f(x)$ from some scattered noisy data of $u_\epsilon(\cdot, T)$. More specifically, the data $u_\epsilon(\cdot, T)$ are collected only at a finite set of points $\{z_1, z_2, \dots, z_m\} \in \Omega$. We then reconstruct the initial temperature distribution $u(x, 0)$ from the scattered noisy data at $t = T$. For solving the backward diffusion problem, we employ a discretized Tikhonov regularization by the Ritz approach coupled with the reproducing kernel Hilbert space (RKHS), which is proposed in [22].

The Tikhonov regularization method has been widely studied and applied to all varieties of ill-posed problems [23, 24]. The discretized Tikhonov regularization method

and its relative theories are also explored in detail [24]. We adopt the Tikhonov regularization method by a reproducing kernel Hilbert space into the backward problem (1). As we know, the theory and practice of reproducing kernel are a fast growing research area. The numerical methods by RKHS have been also rapidly developed in recent years [25, 26]. These developments are due to the increasing interest in the use of reproducing kernel for the solution of mathematical and engineering problems, for instance, machine learning [27], signal processing [28], stochastic processes [29], wavelet transforms [30], and so forth. For the details of RKHS, we are able to refer to [31]. However, to the authors' knowledge, there are few applications of RKHS to inverse problems. We provide the partial list of the recent works. Takeuchi and Yamamoto [22] prove the convergence of the discretized Tikhonov regularization method by RKHS. Hon and Takeuchi [32] apply this method into a backward heat conduction problem for parabolic-type partial differential equations. In reproducing the kernel Hilbert space settings, an inverse source identification problem for parabolic equations is considered in [33]. In [34], Saitoh discusses comprehensively the corresponding applications of RKHS in inverse problems.

The remainder of this paper is composed of five sections. In Section 2, we discuss Green's function for problem (1) and use it to construct the reproducing kernel. In Section 3, we state the reconstruction method of the fractional backward diffusion problem by using the reproducing kernel. In Section 4, some numerical examples are given to illustrate the effectiveness of our method. A summary is made in the Section 5. Finally, we list some existing knowledge about the reproducing kernel Hilbert space in the Appendix.

2. Green's Function and the Reproducing Kernel

In this section, we explore Green's function of system (1) and use it to construct the reproducing kernel. Firstly, let function $G(x, t; \xi)$ be Green's function of the system (1); that is, G satisfies the following equations in distribution's sense:

$$\begin{aligned} {}_0D_t^\gamma G(x, t; \xi) &= \mathcal{L}G(x, t; \xi), \quad x, \xi \in \Omega, t \in [0, T], \\ G(x, 0; \xi) &= \delta(x - \xi), \quad x, \xi \in \Omega, \end{aligned}$$

$$\mathcal{B}G(x, t; \xi) := \mu G(x, t; \xi) + \beta \frac{\partial G}{\partial \nu} = 0, \quad x \in \partial\Omega, t \in [0, T]. \quad (6)$$

It is easy to know that problem (6) is equivalent to the following problem:

$$\begin{aligned} {}_0D_t^\gamma G(x, t; \xi) - \mathcal{L}G(x, t; \xi) &= \delta(x - \xi) \delta(t), \\ & x, \xi \in \Omega, t \in [0, T], \\ G(x, 0; \xi) &= 0, \quad x, \xi \in \Omega, \end{aligned} \quad (7)$$

$$\mathcal{B}G(x, t; \xi)$$

$$:= \mu G(x, t; \xi) + \beta \frac{\partial G}{\partial \nu} = 0, \quad x \in \partial\Omega, t \in [0, T].$$

Let us employ the Laplace transform to solve the system (6). The Laplace transform of a function φ on \mathbb{R}^+ is defined by

$$\phi(s) := \int_0^\infty e^{-st} \varphi(t) dt, \quad \text{Re}(s) > 0. \quad (8)$$

The Laplace transform of the Caputo fractional derivative is given by [10]

$$\int_0^\infty e^{-st} {}_0D_t^\gamma \varphi(t) dt = s^\gamma \phi(s) - \sum_{k=0}^{J-1} s^{\gamma-k-1} {}_0D_t^k \varphi(0), \quad (9)$$

where $J-1 < \gamma \leq J$. The Caputo fractional derivative appears more suitable to be treated by the Laplace transforming in that it requires the knowledge of initial values of the function and of its integer derivatives of order $k = 1, 2, \dots, J-1$. By the Laplace transforming about the time variable t , the system (6) becomes

$$\begin{aligned} & s^\gamma g(x, s; \xi) - s^{\gamma-1} \delta(x - \xi) \\ &= \mathcal{L}g(x, s; \xi), \quad x, \xi \in \Omega, \text{Re}(s) > 0, \quad (10) \\ & \mu g(x, s; \xi) + \beta \frac{\partial g}{\partial \nu}(x, s; \xi) = 0, \end{aligned}$$

where g denotes the Laplace transform of Green's function G . It should be noted here that the system in (1) is only defined on $t \in [0, T]$, not on $[0, +\infty)$. When we make the Laplace transform, some necessary preprocess, for example, the function continuation technique, needs to be done on the solution of (1) to satisfy the condition of the Laplace transform. Because we do not use the value of u for $t > T$, the condition can be satisfied easily.

Applying this technique of eigenfunction expansions to problems (10), we have that

$$g(x, s; \xi) = \sum_{n=1}^\infty \frac{s^{\gamma-1}}{s^\gamma + \lambda_n^2} \varphi_n(\xi) \varphi_n(x), \quad (11)$$

where $\varphi_n(x)$ is the n th orthonormal eigenfunction and λ_n is the corresponding eigenvalue to the Sturm-Liouville problem

$$\mathcal{L}\varphi(x) + k^2 \varphi(x) = 0, \quad (12)$$

subject to the boundary conditions

$$\mu \varphi(x) + \beta \frac{\partial \varphi}{\partial \nu} = 0. \quad (13)$$

Taking the Laplace inverse of (11), we have that

$$G(x, t; \xi) = \sum_{n=1}^\infty E_\gamma(-\lambda_n^2 t^\gamma) \varphi_n(\xi) \varphi_n(x), \quad (14)$$

where $E_\gamma(z)$ is the Mittag-Leffler function defined by

$$E_\gamma(z) = \sum_{k=0}^\infty \frac{z^k}{\Gamma(\gamma k + 1)}. \quad (15)$$

For the details of the Mittag-Leffler function, one can refer to [3]. Subsequently, one can easily verify that the unique solution of system (1) with initial value $u(x, 0) = f \in H$ can be written as

$$u(x, t) = \int_\Omega G(x, t; \xi) f(\xi) d\xi, \quad (16)$$

where $G(x, t; \xi)$ is Green's function defined by (14). With the aid of (16), for each $f \in L^2(\Omega)$, introducing the operator $K : L^2(\Omega) \rightarrow L^2(\Omega)$ by

$$Kf(x) := \int_\Omega G(x, T; \xi) f(\xi) d\xi, \quad (17)$$

we may formulate the inverse problem as an integral equation of the first kind

$$Kf(x) = u(x, T). \quad (18)$$

The symmetry of Green's function indicates that the operator K is self-adjoint. We proceed by giving a brief account on the close connections of the ill posedness of operator equation (18) with the singular value system of operator K . According to the symmetry of operator K , we only need to discuss its eigensystem. It is easy to know that the eigensystem of K is given by

$$\{E_\gamma(-T^\gamma \lambda_n^2), \varphi_n\}_{n=1}^\infty, \quad (19)$$

where $E_\gamma(-T^\gamma \lambda_n^2)$ is the eigenvalue and φ_n is the corresponding eigenfunction. We can see the decay of the eigenvalues $\{E_\gamma(-T^\gamma \lambda_n^2)\}_{n=1}^\infty$ with the increase of λ_n from the following asymptotic behavior of the Mittag-Leffler function $E_\gamma(\cdot)$ which can be found in [20, 21] or by the results in [3].

Lemma 1 (see [20]). *Let $0 < \gamma_0 < \gamma_1 < 1$. Then there exist constants $C_{1,\pm}, C_{2,\pm} > 0$ depending only on γ_0 and γ_1 such that*

$$\frac{C_{1,-}}{\gamma} e^{x^{1/\gamma}} \leq E_\gamma(x) \leq \frac{C_{1,+}}{\gamma} e^{x^{1/\gamma}}, \quad \forall x \geq 0, \quad (20)$$

$$\frac{C_{2,-}}{\Gamma(1-\gamma)} \frac{1}{1-x} \leq E_\gamma(x) \leq \frac{C_{2,+}}{\Gamma(1-\gamma)} \frac{1}{1-x}, \quad \forall x \leq 0. \quad (21)$$

These estimates are uniform for all $\gamma \in [\gamma_0, \gamma_1]$.

Next, we consider the construction of reproducing kernel using Green's function $G(x, t; \xi)$. Define $\Phi(x, \xi) := G(x, t_0; \xi)$ for some $t_0 \in (0, T)$. The symmetry about the space variable x, ξ of Green's function indicates that $\Phi(\cdot, \cdot) : \Omega \times \Omega \rightarrow \mathbb{R}$ is symmetric. Now that Φ is a symmetric positive definite kernel, a unique RKHS in which the given kernel acts as the reproducing kernel can be constructed (see [26] for details). Henceforth we denote by H_{t_0} the RHKS generated by the kernel $\Phi(x, \xi) = G(x, t_0; \xi)$. Actually, according to [26, Chapter 10], the inner product and norm on H_{t_0} are defined by

$$\begin{aligned} (f, g)_{H_{t_0}} &:= \sum_{n=1}^\infty \frac{1}{E_\gamma(-\lambda_n^2 t_0^\gamma)} (f, \varphi_n)_{L^2(\Omega)} (g, \varphi_n)_{L^2(\Omega)}, \\ \|f\|_{H_{t_0}}^2 &:= \sum_{n=1}^\infty \frac{1}{E_\gamma(-\lambda_n^2 t_0^\gamma)} |(f, \varphi_n)_{L^2(\Omega)}|^2, \end{aligned} \quad (22)$$

respectively. The space H_{t_0} is actually given by

$$H_{t_0} = \left\{ f \in L^2(\Omega) : \sum_{n=1}^{\infty} \frac{1}{E_\gamma(-\lambda_n^2 t_0^\gamma)} |(f, \varphi_n)_{L^2(\Omega)}|^2 < \infty \right\}. \quad (23)$$

The second inequalities in Lemma 1 show that, as the function of $\lambda_n, 1/E_\gamma(-\lambda_n^2 t_0^\gamma) \in \mathcal{S}\mathcal{F}$, where $\mathcal{S}\mathcal{F}$ denotes the collection of slowly increasing functions [26] defined by

$$\mathcal{S}\mathcal{F} := \left\{ f : \mathbb{R}^d \rightarrow \mathbb{R} \mid f(x) = O(\|x\|_2^m) \text{ as } \|x\|_2 \rightarrow \infty \text{ for some } m \in \mathbb{N}_0 \right\}. \quad (24)$$

Hence, according to the theoretical results of [26, Chapter 10], we assert that the space H_{t_0} is consistent with some Sobolev space $H^k(\Omega)$ for $k > d/2$ and the norm on H_{t_0} is equivalent to the norm $\|f\|_{H^k(\Omega)} = [\sum_{|\alpha| \leq k} \|D^\alpha f\|_{L^2(\Omega)}^2]^{1/2}$.

3. Formulation of the Inverse Problem and the Reconstruction Method

In order to find the initial temperature distribution $f(x)$, we would like to determine the solution of minimization problem

$$\inf_{f \in L^2(\Omega)} \|Kf - u_\epsilon(\cdot, T)\|_{L^2(\Omega)}. \quad (25)$$

However, the minimization element of (25) generally is a poor approximation of the desired initial function f due to the error ϵ in $u(x, T)$ and the ill posedness of operator equation (18). The Tikhonov regularization replaces the minimization problem (25) by the solution of a penalized least-squares problem

$$\inf_{f \in H_{t_0}(\Omega)} J_\alpha(f) := \inf_{f \in H_{t_0}(\Omega)} \|Kf - u_\epsilon(\cdot, T)\|_{L^2(\Omega)}^2 + \alpha \|f\|_{H_{t_0}}^2 \quad (26)$$

with regularization parameter $\alpha > 0$. We can see from [23, Proposition 3.11] that the convergence of any regularization method can be arbitrarily slow in general. Actually, convergence rates can be given only on some subset of H_{t_0} , that is, under *a priori* assumptions on the exact data. Here, we assume the exact solution f belongs to the set of source conditions

$$\mathcal{M}_\mu := \{f \in H_{t_0}(\Omega) : f = (K^* K)^\mu \omega, \|\omega\|_{L^2(\Omega)} \leq E\}, \quad (27)$$

where E is the *a priori* bound and $\mu > 0$ is a constant. As in [23], we know that there exists a constant μ_0 , named the “qualification” of the regularization method, such that $0 < \mu \leq \mu_0$. For the Tikhonov regularization method, the qualification $\mu_0 = 1$. However, according to (21), it is easy to know that $\mathcal{M}_{\mu_2} \subset \mathcal{M}_{\mu_1}$ as $\mu_1 > \mu_2$ and $\mathcal{M}_{1/4} = H_{t_0}$. Therefore, here we only need consider the case of $0 < \mu \leq 1/4$ for the Tikhonov method (26).

In order to solve the minimization problem (26), some discretization scheme needs to be given. A natural way to obtain such discretization is to generate a finite dimensional approximation to the minimal element of the Tikhonov functional J_α . For this, we define a subspace $V_N := \text{span}\{\Phi(\cdot, \xi) : \xi \in X_N\} \subset H_{t_0}$, where $X_N := \{\xi_1, \xi_2, \dots, \xi_N\} \subset \Omega$. This approximation by discretization is equivalent to finding the minimal norm least-squares solution of the equation

$$K_N f := K P_N f = u_T, \quad (28)$$

where $P_N : H_{t_0} \rightarrow V_N$ is the projection operator. Moreover, we produce a finite dimensional approximation $f_{\alpha, N}$ to $K^\dagger u_T$ by minimizing the Tikhonov functional (26) over the finite dimensional space V_N . Denote by $f_{\alpha, N, \epsilon}$ the minimizer of J_α for noise input data u_T^ϵ . It is well known that $f_{\alpha, N, \epsilon}$ satisfy [23, 24]

$$f_{\alpha, N, \epsilon} = (K_N^* K_N + \alpha I)^{-1} K_N^* u_T^\epsilon. \quad (29)$$

Provided $\{V_N\}$ is an expanding sequence, the convergence of the Tikhonov regularized solutions is proved [24]. Takeuchi and Yamamoto [22] show that the discretized Tikhonov regularized solutions converge to the exact solution without the monotonicity of V_N under an *a priori* choice strategy for N and α . However, one can see that, from the existing results, in both cases, the regularized solutions $f_{\alpha, N}$ converging to the exact solution depends on whether $r_N := \|K(I - P_N)\| \rightarrow 0$, ($N \rightarrow \infty$). Moreover, the convergence of r_N requires the knowledge of the fill distance $h_{X_N, \Omega}$, which is defined by [26]

$$h_{X_N, \Omega} := \sup_{x \in \Omega} \min_{\xi_k \in X_N} \|x - \xi_k\|. \quad (30)$$

The fill distance can be interpreted in various geometrical ways. For example, we can consider it as the radius of the largest ball which is completely contained in Ω and which does not contain a data site. In this sense $h_{X_N, \Omega}$ describes the largest data-site-free hole in Ω .

Here, we utilize the same proof as in [32] to give the following lemma.

Lemma 2. Consider $r_N = \|K(I - P_N)\| \rightarrow 0$ as $N \rightarrow \infty$.

Proof. Consider

$$\|K(I - P_N)\| = \sup_{\substack{f \in H_{t_0} \\ f \neq 0}} \frac{\|K(I - P_N)f\|_{L^2(\Omega)}}{\|f\|_{H_{t_0}}}. \quad (31)$$

It is obvious that the kernel function $\Phi(x, y)$ is sufficiently smooth. Therefore, according to the error estimate in the Appendix, we can find a positive constant k such that the estimate

$$\|f - P_N f\|_{L^\infty(\Omega)} \leq h_{X_N, \Omega}^k \|f\|_{H_{t_0}} \quad (32)$$

holds for all $f \in H_{t_0}$. Meanwhile, it is easy to know

$$\begin{aligned} \|Kf\|_{L^2(\Omega)} &= \left[\int_{\Omega} |Kf|^2 dx \right]^{1/2} \\ &= \left[\int_{\Omega} \left| \int_{\Omega} G(x, T; \xi) f(\xi) d\xi \right|^2 dx \right]^{1/2} \quad (33) \\ &\leq C \|f\|_{L^\infty(\Omega)}, \quad \forall f \in H_{t_0}, \end{aligned}$$

where $C := \{ \int_{\Omega} [\int_{\Omega} |G(x, T; \xi)| d\xi]^2 dx \}^{1/2}$ is a constant. Moreover, the property of RKHS, $f(x) = (f(\cdot), \Phi(x, \cdot))$, leads to

$$\|f\|_{L^\infty(\Omega)} \leq \sup_{x \in \Omega} \sqrt{\Phi(x, x)} \|f\|_{H_{t_0}}. \quad (34)$$

Combining (32)–(34), we get

$$\|K(I - P_N)f\|_{L^2(\Omega)} \leq M \|f - P_N f\|_{L^\infty(\Omega)} \leq M h_{X_N, \Omega}^k \|f\|_{H_{t_0}}, \quad (35)$$

where M is a constant. Consequently, substituting the estimate (35) into (31) and letting $N \rightarrow \infty$, we complete the proof. \square

According to the classical results on the Tikhonov regularization for linear ill-posed problem (see, e.g., [23, 24]) and in view of (1), it holds that

$$\begin{aligned} \|f - f_{\alpha, N, \epsilon}\| &\leq \|f - (K_N^* K_N + \alpha I)^{-1} K_N^* u\| \\ &\quad + \|(K_N^* K_N + \alpha I)^{-1} K_N^* (u - u_T^\epsilon)\| \quad (36) \\ &\leq \|f - (K_N^* K_N + \alpha I)^{-1} K_N^* u\| + \frac{\epsilon}{2\sqrt{\alpha}}. \end{aligned}$$

As in [35], we can estimate the noise-free term as follows:

$$\begin{aligned} &\|f - (K_N^* K_N + \alpha I)^{-1} K_N^* u\| \\ &= \|f - (K_N^* K_N + \alpha I)^{-1} K_N^* Kf\| \\ &\leq \| [I - (K_N^* K_N + \alpha I)^{-1} K_N^* K_N] f \| \\ &\quad + \| (K_N^* K_N + \alpha I)^{-1} K_N^* (K_N - K) f \| \\ &= \| [I - (K_N^* K_N + \alpha I)^{-1} K_N^* K_N] (K^* K)^\mu w \| \\ &\quad + \| (K_N^* K_N + \alpha I)^{-1} K_N^* (K_N - K) f \| \\ &\leq \| [I - (K_N^* K_N + \alpha I)^{-1} K_N^* K_N] \\ &\quad \times [(K^* K)^\mu - (K_N^* K_N)^\mu] w \| \\ &\quad + \| [I - (K_N^* K_N + \alpha I)^{-1} K_N^* K_N] (K_N^* K_N)^\mu w \| \\ &\quad + \frac{1}{\sqrt{\alpha}} \|K(I - P_N)f\| \\ &\leq \| [(K^* K)^\mu - (K_N^* K_N)^\mu] w \| \\ &\quad + \alpha^\mu E + \frac{1}{\sqrt{\alpha}} \|K(I - P_N)f\| \end{aligned}$$

$$\begin{aligned} &\leq \|K^* K - K_N^* K_N\|^\mu E + \alpha^\mu E \\ &\quad + \frac{1}{\sqrt{\alpha}} \|K(I - P_N)f\| \\ &\leq C \|K(I - P_N)\|^{2\mu} E + \alpha^\mu E \\ &\quad + \frac{1}{\sqrt{\alpha}} \|K(I - P_N)f\| \\ &\leq C \|K(I - P_N)\|^{2\mu} E + \alpha^\mu E \\ &\quad + \frac{1}{\sqrt{\alpha}} \|K(I - P_N)\|^{2\mu+1}, \quad (37) \end{aligned}$$

where C is a constant. In view of the best possible error bound being $\epsilon^{2\mu/(2\mu+1)}$, the term $\|K(I - P_N)\|$ has to be chosen such that

$$\|K(I - P_N)\| \leq \epsilon^{1/(2\mu+1)}. \quad (38)$$

From the above discussions, we have the following theorem.

Theorem 3. Under assumptions (5) and (38), there holds that

$$\|f - f_{\alpha, N, \epsilon}\| \leq C \epsilon^{2\mu/(2\mu+1)} + \alpha^\mu E + \frac{\epsilon}{\sqrt{\alpha}}. \quad (39)$$

Moreover, if the regularization parameter α is chosen by $\alpha = O(\epsilon^{2/(2\mu+1)})$, one then obtains the following estimate:

$$\|f - f_{\alpha, N, \epsilon}\| \leq \bar{C} \epsilon^{2\mu/(2\mu+1)}, \quad (40)$$

where the constant \bar{C} does not depend on ϵ .

4. Numerical Tests

In this section, we present numerical results to illustrate the feasibility of the reconstruction method as described in the previous section.

In practical situation, we only can get the scattered noisy data of $u(\cdot, T)$, that is, $\{u_\epsilon(z_1, T), u_\epsilon(z_2, T), \dots, u_\epsilon(z_m, T)\}$. As a result, instead of solving (25) we intend to deal with the following problem:

$$\inf_{f \in V_N} \|Kf - u_\epsilon(\cdot, T)\|_{\mathbb{R}^m}^2 + \alpha \|f\|_{H_{t_0}(\Omega)}^2, \quad (41)$$

where

$$\|Kf - u_\epsilon(\cdot, T)\|_{\mathbb{R}^m} = \left\{ \sum_{j=1}^m |Kf(z_j) - u_\epsilon(z_j, T)|^2 \right\}^{1/2}. \quad (42)$$

Since $V_N = \text{span}\{\Phi(\cdot, \xi) \mid \xi \in \{\xi_1, \xi_2, \dots, \xi_N\}\}$, the minimizer $f_{\alpha, N, \epsilon}$ can be written as

$$f_{\alpha, N, \epsilon}(\cdot) = \sum_{k=1}^N \tilde{\lambda}_k \Phi(\cdot, \xi_k) = \sum_{k=1}^N \tilde{\lambda}_k G(\cdot, t_0; \xi_k), \quad \xi_k \in X_N. \quad (43)$$

From the definition of RKHS, it follows that

$$\|f_{\alpha, N, \epsilon}\|_{H_{t_0}}^2 = \sum_{j,k=1}^N \tilde{\lambda}_k \tilde{\lambda}_j G(\xi_k, t_0; \xi_j). \quad (44)$$

In addition, we know that

$$\begin{aligned} KG(z_j, t_0; \xi_k) \\ = \int_{\Omega} G(z_j, T; \xi) G(\xi, t_0; \xi_k) d\xi = G(z_j, t_0 + T; \xi_k) \end{aligned} \quad (45)$$

for $j = 1, 2, \dots, m$ and $k = 1, 2, \dots, N$. Now, it is easy to see that the coefficient vector $\tilde{\lambda} = (\tilde{\lambda}_k)_{k=1}^N$ satisfies the following linear system:

$$(A^*A + \alpha B)\tilde{\lambda} = A^*u_T^\epsilon, \quad (46)$$

where A is an $m \times N$ matrix, A^* is the transpose of A , and B is an $N \times N$ matrix defined by

$$\begin{aligned} A_{j,k} &= G(z_j, t_0 + T; \xi_k), \quad j = 1, \dots, m, \quad k = 1, \dots, N, \\ B_{j,k} &= G(\xi_j, t_0; \xi_k), \quad j, k = 1, \dots, N. \end{aligned} \quad (47)$$

If we truncate Green's function to the former J terms, matrix B can be decomposed to the following product:

$$B = L^*L, \quad (48)$$

where L^* denotes the conjugate transpose of L and L is given by

$$\begin{aligned} L = (L_{j,k}) &= \left([E_\gamma(-\lambda_j^2 t_0^\gamma)]^{1/2} \varphi_j(\xi_k) \right), \\ j &= 1, 2, \dots, J, \quad k = 1, 2, \dots, N. \end{aligned} \quad (49)$$

Moreover, we turn to search for the minimizer $\tilde{\lambda}$ of the following functional:

$$F_\alpha(\lambda) := \|A\lambda - u_T^\epsilon\|_{\mathbb{R}^m}^2 + \|L\lambda\|_{\mathbb{R}^J}^2. \quad (50)$$

After obtaining the vector $\tilde{\lambda}$, we substitute it into (43) and then get the regularized approximation $f_{\alpha, N, \epsilon}$.

In our tests, the measurement points $\{z_j\}_{j=1}^m$, which are randomly generated by using the Matlab function $\text{rand}(\cdot)$, are scattered in the domain Ω . Now we generate the final measurement data at T with noise by

$$u_T^\epsilon = u(z, T) + \sqrt{\frac{2}{\pi}} \frac{\epsilon}{100} \times \text{rand}(z) \times \text{norm}(u(z, T)), \quad (51)$$

where $z = \{z_j\}_{j=1}^m$ are the measurement points and $\text{rand}(z)$ generates a standard m -dimensional random vector. To

evaluate the proposed method, we compute the relative error of the reconstructed solutions denoted by $R(f)$:

$$\begin{aligned} R(f) &= \frac{\|f_{\alpha, N, \epsilon}(\cdot) - f(\cdot)\|_{l^2}}{\|f(\cdot)\|_{l^2}}, \quad \text{for 1-dimensional case,} \\ R(f) &= \frac{\|f_{\alpha, N, \epsilon}(\cdot) - f(\cdot)\|_{\infty}}{\|f(\cdot)\|_{\infty}}, \quad \text{for 2-dimensional case,} \end{aligned} \quad (52)$$

where $\|\cdot\|_{l^2}$ denotes the l^2 norm and $\|\cdot\|_{\infty}$ denotes the ∞ norm. Before we proceed, it is natural that we have to determine t_0 , X_N , measurement points $\{z_j\}_{j=1}^m$, and observation time T to define A, B . According to the convergence theorem, smaller $h_{X_N, \Omega}$ yields better numerical solution, which implies that we need to choose as large N as possible. However, the ill posedness of the backward diffusion problem results in the ill condition of the matrix A^*A , which causes us not to implement the numerical computation of the inverse of $A^*A + \alpha B$ when the regularizing term B is also ill conditioned. We use the following one-dimensional example to depict the change trend of the condition number of B , $\text{cond}(B)$, with respect to N .

Example 1. Consider the following Dirichlet boundary value problem:

$$\begin{aligned} {}_0D_t^\gamma u(x, t) &= \frac{\partial^2 u(x, t)}{\partial x^2}, \quad x \in (0, 1), \quad t \in [0, T], \\ u(x, 0) &= x(1-x), \quad x \in [0, 1], \\ u(0, t) &= u(1, t) = 0, \quad t \in [0, 1]. \end{aligned} \quad (53)$$

The forward problem has a unique solution

$$u(x, t) = \sum_{n=1}^{\infty} d_n E_\gamma(-n^2 \pi^2 t^\gamma) \sin n\pi x, \quad (54)$$

where the coefficient

$$\begin{aligned} d_n &= 2 \int_0^1 u(x, 0) \sin n\pi x dx \\ &= \frac{4}{n^3 \pi^3} [1 - (-1)^n], \quad n = 1, 2, \dots \end{aligned} \quad (55)$$

To clarify the numerical influence of some relative parameters but γ , we fix parameter $\gamma = 1/2$ firstly.

In this test, we fix $m = 59$ firstly. In Figure 1, for the cases of $t_0 \in \{1e-8, 1e-9, 1e-10\}$, we plot $\text{cond}(B)$ versus the number of N running from 10 to 100, respectively. The displayed results in Figure 1 show that the condition number $\text{cond}(B)$ increases exponentially as N increases. Nevertheless, we can remove such influence of the ill condition of B on numerical computation through modifying its small singular value as a fixed small constant $\tilde{\epsilon}$. And in doing so, the numerical precision does not change significantly. Therefore, we can implement the proposed method without worrying so much about the size limitation of N . For the

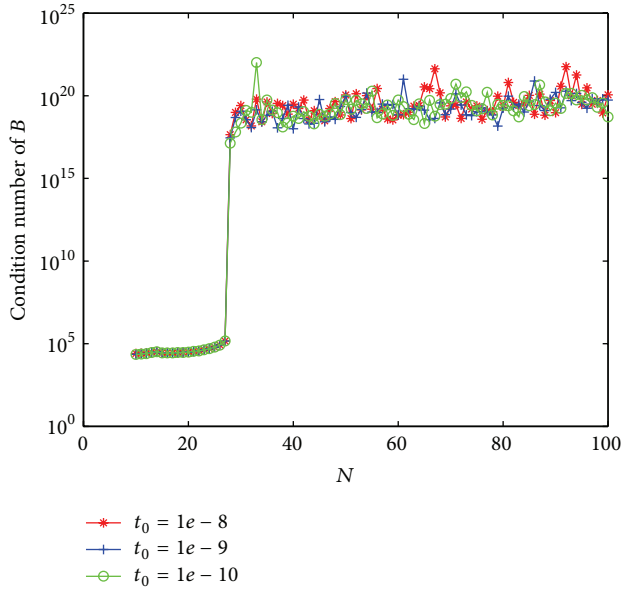


FIGURE 1: The effect of an increasing number of N on the condition number of B for the cases when $t_0 \in \{1e-8, 1e-9, 1e-10\}$.

TABLE 1: Example 1: the relative errors with $t_0 = 1e-10$, $N = 59$, and $m = 59$.

ϵ	T		
	1	5	10
0.1%	0.0143	0.0156	0.0177
1%	0.0295	0.0239	0.0332
2%	0.0388	0.0390	0.0387
5%	0.0483	0.0441	0.0505
10%	0.0528	0.0601	0.0703

choice of t_0 , we compare the computational results for some different t_0 's and T 's using exact final data $u(x, T)$ for Example 1. For this, a preset value for the regularization parameter α needs to be provided. Here, we simply choose $\alpha = 10^{-5}(\max(A^*A)/\max(B))$ as in [32], where $\max(C) = \max_{i,j} c_{ij}$ for matrix $C = (c_{ij})$. In the following computation, the Matlab code developed by Hansen [36, 37] is used to obtain the approximation solution for solving the discrete system (46). In addition, note that the Mittag-Leffler function is numerically realized by implementing the Matlab toolbox by Podlubny [38]. In Figure 2, we plot the relative errors for different t_0 , $t_0 = 1e-5, 1e-7, 1e-10$, versus the number of N running from 10 to 100 for $\epsilon = 0$ and $T = 25$. The computational results show that, using smaller t_0 , we have less relative error. In addition, we also see from Figure 2 that, with the increase of the number of N , the relative error becomes smaller firstly and then it remains steady after arriving to a certain extent.

We also need to consider the effect of the number J of truncation term of Green's function and the number of measurement points m on the numerical precision. With $T = 3$, we display the numerical results for several m and J as the

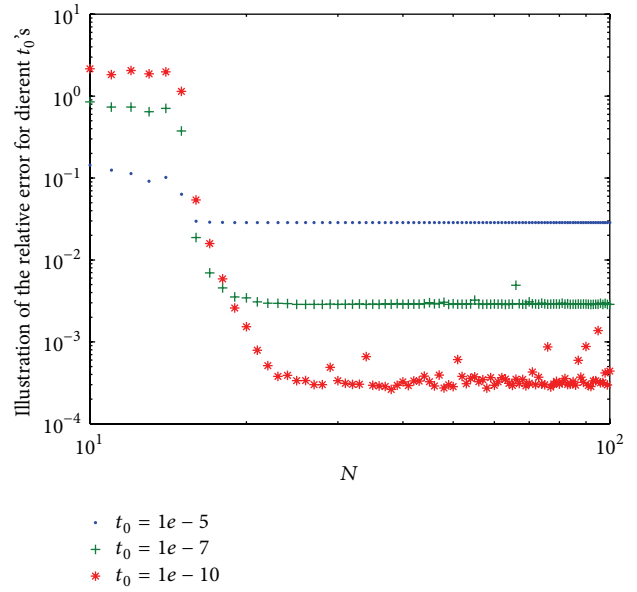


FIGURE 2: The effect of an increasing number of N on the relative error for the cases when $t_0 \in \{1e-5, 1e-7, 1e-10\}$ with noise-free data.

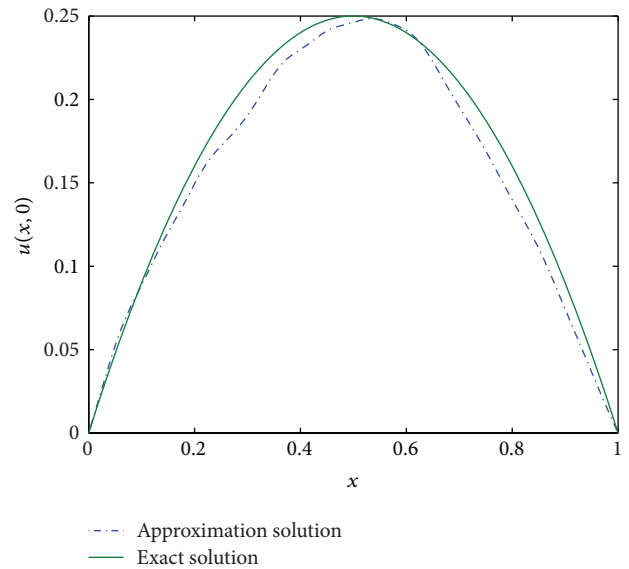


FIGURE 3: Exact solution $u(x, 0)$ and numerical solution for $\epsilon = 20\%$ with the final time $T = 25$ and $m = 59$, $N = 59$, and $t_0 = 1e-10$.

noise level $\epsilon = 0$ in Table 2. It can be seen that when J and m become sufficiently large, the relative errors almost remain at the level 10^{-4} .

Next, in the absence of the *a priori* information, we only evaluate the proposed algorithm in (46) for noisy data by using L-curve parameter choice method instead of that in Theorem 3. In Example 1, we fix $N = 59$, $m = 59$, and $t_0 = 1e-10$. Table 1 reports the relative errors of $f_{\alpha, N, \epsilon}$ for different noise levels ϵ and final measurement times T . These numerical results for all noisy cases are satisfactory. In

TABLE 2: Example 1: the relative errors with $t_0 = 1e - 10$, $N = 59$, and $\epsilon = 0\%$.

J	m					
	19	29	39	49	59	69
5	$3.3721e - 3$	$3.4356e - 3$	$3.3769e - 3$	$3.3737e - 3$	$3.4008e - 3$	$3.3724e - 3$
10	$1.0725e - 3$	$1.5791e - 3$	$9.9642e - 4$	$9.9488e - 4$	$9.9616e - 4$	$9.9901e - 4$
15	$6.1811e - 4$	$3.4322e - 4$	$5.7376e - 4$	$3.2938e - 4$	$3.2952e - 4$	$3.3259e - 4$
20	$5.0304e - 3$	$3.5813e - 4$	$8.9305e - 4$	$4.7205e - 4$	$9.8808e - 4$	$5.4753e - 4$
25	$3.7310e - 3$	$4.3286e - 4$	$2.1742e - 4$	$1.5605e - 4$	$1.5743e - 4$	$1.5375e - 4$
30	$5.9706e - 3$	$2.6680e - 3$	$1.6015e - 4$	$1.5884e - 4$	$2.0451e - 4$	$1.3825e - 4$

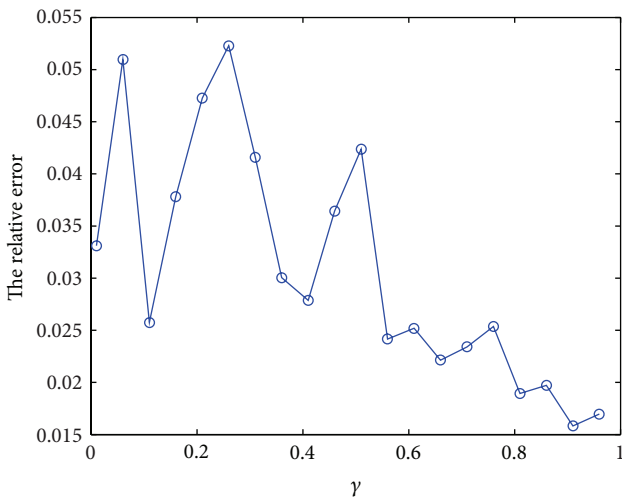


FIGURE 4: The relative error versus order γ for Example 1 with $T = 0.5$, $m = 59$, $N = 59$, and $t_0 = 1e - 10$ for noise $\epsilon = 1\%$.

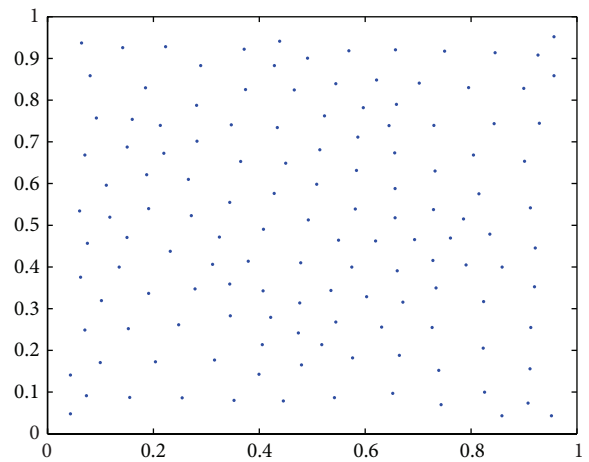


FIGURE 6: The illustration of the set X_N .

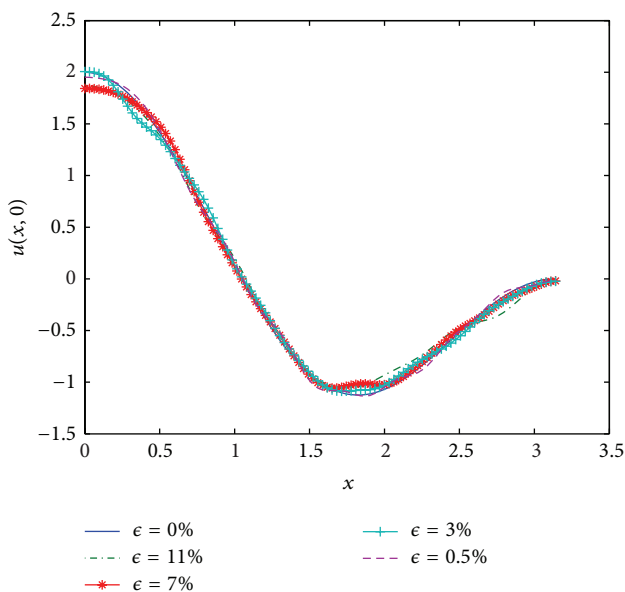


FIGURE 5: Exact solution $u(x,0)$ and numerical solution for $\epsilon \in \{11\%, 7\%, 3\%, 0.5\%$ with the final time $T = 0.1$ and $m = 59$, $N = 55$, and $t_0 = 1e - 10$.

TABLE 3: Example 3: the relative errors with $t_0 = 1e - 10$ and $m = 100$ for $\gamma = 1/2$.

ϵ	T			
	1	2	5	10
1%	0.0131	0.0117	0.0138	0.0199
2%	0.0118	0.0141	0.0229	0.0201
5%	0.0272	0.0192	0.0304	0.0535

general, it can be seen from Table 1 that, at the smaller T and ϵ , the numerical effects are better. In addition, when the measurement time $T = 25$, the exact solution $u(x, 0)$ and the numerical solution $f_{\alpha, N, \epsilon}$ with the relative noise level $\epsilon = 20\%$ are displayed in Figure 3. It can be observed that the method works even for the case of $T = 25$ with noise level $\epsilon = 20\%$ as well.

Finally, we hope to use Example 1 to show that the proposed algorithm is robust for order γ . For varying γ , we plot the relative error versus γ in Figure 4. The displayed results show that the numerical method is robust when γ is varying.

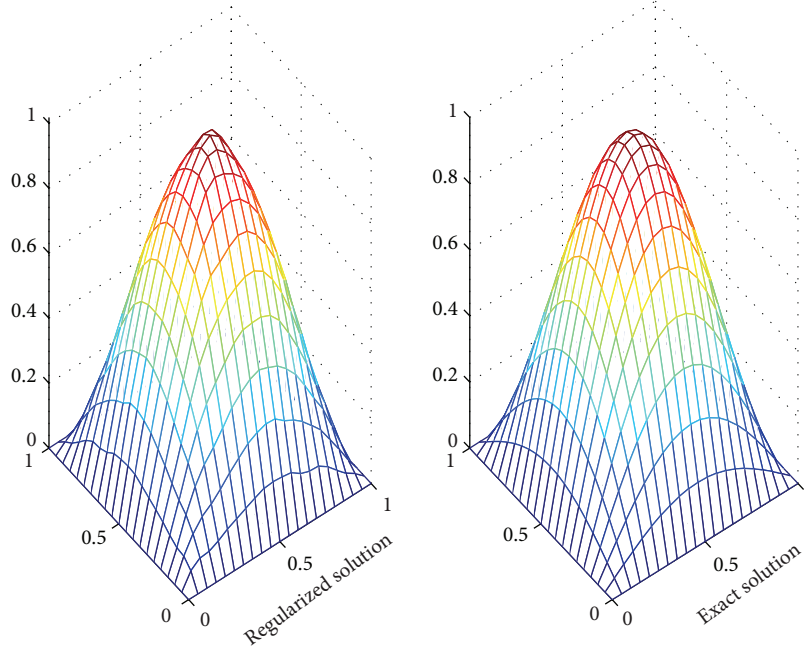


FIGURE 7: The comparison between the exact solution and regularized solution for Example 3.

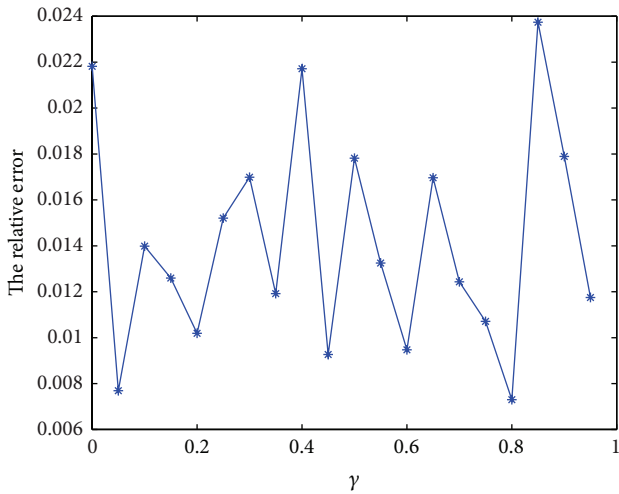


FIGURE 8: The relative error versus order γ for Example 3 with $T = 1$, $m = 100$, and $t_0 = 1e - 10$ for noise $\epsilon = 1\%$.

Example 2. Consider the following Neumann boundary value problem:

$$\begin{aligned}
 {}_0D_t^{1/2}u(x, t) &= \frac{\partial^2 u(x, t)}{\partial x^2}, \quad x \in (0, \pi), t \in (0, T), \\
 u(x, 0) &= \cos x + \cos 2x, \quad x \in [0, \pi], \\
 u_x(0, t) &= u_x(\pi, t) = 0, \quad t \in [0, T].
 \end{aligned}
 \tag{56}$$

The unique solution to (56) is given by

$$u(x, t) = E_{1/2}(-t^{1/2}) \cos x + E_{1/2}(-4t^{1/2}) \cos 2x. \tag{57}$$

In this example, we show the numerical results for $T = 0.1$ under the setting $m = 59$, $t_0 = 1e - 10$, and $N = 55$. Figure 5 shows that the proposed method is capable of giving satisfactory results for the case of the Neumann boundary condition.

Example 3. We consider a two-dimensional fractional diffusion problem with the Dirichlet boundary value in $\Omega = (0, 1) \times (0, 1)$:

$$\begin{aligned}
 {}_0D_t^\gamma u(x, y, t) &= \Delta u, \quad x \in \Omega, t \in (0, T), \\
 u(x, y, 0) &= \sin \pi x \sin \pi y, \quad x \in \bar{\Omega}, \\
 u(x, y, t) &= 0, \quad x \in \partial\Omega, t \in [0, T].
 \end{aligned}
 \tag{58}$$

The initial distribution $u(x, y, 0)$ is to be recovered by using the exact solution

$$u(x, y, t) = E_\gamma(-\pi^2 t^\gamma) \sin \pi x \sin \pi y. \tag{59}$$

We firstly display the choice of the set X_N in Figure 6. According to the analysis for 1-dimensional case about the number of J and m , we only deal with the case of $t_0 = 1e - 10$ and $m = 100$. The measurement points $\{x_1, x_2, \dots, x_m\}$ are scattered in Ω , which are generated using the Matlab command rand. We report the relative error of $f_{\alpha, N, \epsilon}$ for different final times T and noise levels ϵ in Table 3 for $\gamma = 1/2$. The numerical comparison between exact solution and regularized solution is shown in Figure 7. The numerical results show that the proposed method is acceptable for the 2-dimensional example. We also consider the influence of varying γ on the numerical stability. The relative error versus γ is plotted in Figure 8, from which we can see that the proposed method is robust about parameter γ .

5. Conclusion

In this paper, in a reproducing kernel Hilbert space setting, we propose a numerical reconstruction method, namely, the discretized Tikhonov regularization method, to recover the initial temperature distribution of the backward fractional diffusion problem. The implementation of the proposed method is simple and easy. Numerical tests show that the method is efficient.

Appendix

Reproducing the Kernel Hilbert Spaces and Positive Definite Kernels

Most of the material in this appendix can be found in the excellent monograph [26]. For the readers' convenience we would like to repeat the theoretical results of RKHS. We are interested in linear vector spaces consisting of functions $f : \Omega \rightarrow \mathbb{R}$ defined on a connected domain Ω of \mathbb{R}^d .

Definition A.1. Let H be a Hilbert space consisting of functions $f : \Omega \rightarrow \mathbb{R}$. H is called a reproducing kernel Hilbert space and a kernel $\Phi : \Omega \times \Omega \rightarrow \mathbb{R}$ is called a reproducing kernel for H if

- (i) $\Phi(\cdot, y) \in H$ for all $y \in \mathbb{R}^d$,
- (ii) $f(y) = (f, \Phi(\cdot, y))_H$ for all $f \in H$ and all $y \in \mathbb{R}^d$,

where $(\cdot, \cdot)_H$ is the inner product of H .

The reproducing kernel of a RKHS is uniquely determined. According to [26], H is a RKHS if and only if the point evaluation functionals are continuous, that is, $\delta_y \in H^*$ for all $y \in \Omega$. Also [26] discloses the connection between RKHS and positive definite kernels. Here, we call Φ symmetric if $\Phi(x, y) = \Phi(y, x)$ for all $x, y \in \Omega$.

Definition A.2. A continuous symmetric $\Phi : \Omega \times \Omega \rightarrow \mathbb{R}$ is called positive definite on $\Omega \subset \mathbb{R}^d$ if, for all $N \in \mathbb{N}$, all sets of pairwise distinct centers $X_N = \{\xi_1, \xi_2, \dots, \xi_N\} \subset \Omega$; the quadratic form

$$\sum_{j=1}^N \sum_{k=1}^N \lambda_j \lambda_k \Phi(\xi_j, \xi_k) > 0, \tag{A.1}$$

$$\forall \lambda := (\lambda_1, \lambda_2, \dots, \lambda_N)^T \in \mathbb{R}^N \setminus \{0\}.$$

If Φ is a symmetric positive definite kernel, then a unique RKHS in which the given kernel acts as the reproducing kernel can be constructed. Now, it follows from the definition of RKHS that

- (i) $\Phi(x, y) = (\Phi(\cdot, x), \Phi(\cdot, y))_H$ for all $x, y \in \Omega$,
- (ii) $\|f\|_H^2 = \sum_{j=1}^N \sum_{k=1}^N \lambda_j \lambda_k \Phi(\xi_j, \xi_k)$ for all $f \in H$ in the form of $f = \sum_{k=1}^N \lambda_k \Phi(\cdot, \xi_k)$ with $\xi_k \in \Omega$.

For a symmetric positive definite kernel, introduce integral operator $T : L^2(\Omega) \rightarrow L^2(\Omega)$ by

$$Tv(x) := \int_{\Omega} \Phi(x, y) v(y) dy, \quad v \in L^2(\Omega), x \in \Omega. \tag{A.2}$$

By [26, Proposition 10.28], T maps $L^2(\Omega)$ continuously into the RKHS H and is the adjoint of the embedding operator of the RKHS H into $L^2(\Omega)$. For such an operator, Mercer's theorem [39] shows that Φ can be represented as

$$\Phi(x, y) = \sum_{j=1}^{\infty} \rho_j \varphi_j(x) \varphi_j(y), \quad x, y \in \Omega, \tag{A.3}$$

where $\{\rho_j\}$ are the nonnegative eigenvalues and φ_j are the eigenfunctions of T . This allows us to derive the final characterization for RKHS H .

Theorem A.3. *Suppose Φ is a symmetric positive definite kernel on a compact set $\Omega \subset \mathbb{R}^d$. Then the RKHS is given by*

$$H = \left\{ f \in L^2(\Omega) : \sum_{j=1}^{\infty} \frac{1}{\rho_j} \left| (f, \varphi_j)_{L^2(\Omega)} \right|^2 < \infty \right\} \tag{A.4}$$

and the inner product has the representation

$$(f, g)_H = \sum_{n=1}^{\infty} \frac{1}{\rho_j} (f, \varphi_j)_{L^2(\Omega)} (g, \varphi_j)_{L^2(\Omega)}, \quad f, g \in H. \tag{A.5}$$

For a finite set of points $X_N := \{\xi_1, \xi_2, \dots, \xi_N\} \subset \Omega$ and $f \in \mathcal{H}$, consider the finite sum

$$S_{f, X_N}(x) = \sum_{j=1}^N \lambda_j \Phi(x, \xi_j), \quad x \in \Omega, \tag{A.6}$$

as an approximation of $f(x)$, which is actually the interpolant function of f . We also can consider S_{f, X_N} in the following way: define a subspace $\mathcal{H}_N := \text{span}\{\Phi(\cdot, \xi) \mid \xi \in X_N\} \subset H$. We define the projection operator $P_N : \mathcal{H} \rightarrow \mathcal{H}_N \subset \mathcal{H}$ by

$$P_N(f)(x) = S_{f, X_N}(x), \quad x \in \Omega, \tag{A.7}$$

where P_N is an orthogonal projection operator [26]. If the unknown function f belongs to the related RKHS H , the error bound for the interpolant S_{f, X_N} setup by the reproducing kernel Φ can be obtained by the following theorem.

Theorem A.4. *Let domain Ω be open and bounded, satisfying an interior cone condition. Suppose that the $\Phi \in C^{2k}(\Omega \times \Omega)$ is positive definite. If $f \in H$ and $h_{X_N, \Omega}$ is small enough, then*

$$\left| D^\alpha f(x) - D^\alpha S_{f, X_N} \right| \leq Ch_{X_N, \Omega}^{k-|\alpha|} \|f\|_H, \quad x \in \Omega, \tag{A.8}$$

where C is a positive constant independent of x and f and $\alpha \in \mathbb{N}_0^d$ with $|\alpha| \leq k$. Here D^α denotes a derivative of order $\alpha = (\alpha_1, \alpha_2, \dots, \alpha_d)^T$; that is,

$$D^\alpha := \prod_{k=1}^d \frac{\partial^{\alpha_k}}{\partial x_k^{\alpha_k}}. \tag{A.9}$$

Conflict of Interests

The authors declare that there is no conflict of interests regarding the publication of this paper.

Acknowledgments

This work was supported by the Fundamental Research Funds for the Central Universities (ZYGX2011J104, SWJTU11BR078), the NSF of China (no. 11226040), and China Scholarship Council (no. 201208510083).

References

- [1] K. Diethelm and N. J. Ford, "Numerical solution of the Bagley-Torvik equation," *BIT Numerical Mathematics*, vol. 42, no. 3, pp. 490–507, 2002.
- [2] F. Mainardi, "Some basic problems in continuum and statistical mechanics," in *Fractals and Fractional Calculus in Continuum Mechanics*, A. Carpinteri and F. Mainardi, Eds., pp. 291–348, Springer, Wien, Austria, 1997.
- [3] I. Podlubny, *Fractional Differential Equations*, vol. 198, Academic Press, San Diego, Calif, USA, 1999.
- [4] R. Gorenflo, F. Mainardi, D. Moretti, and P. Paradisi, "Time fractional diffusion: a discrete random walk approach," *Nonlinear Dynamics*, vol. 29, no. 1–4, pp. 129–143, 2002.
- [5] C. Cattani and A. Ciancio, "Separable transition density in the hybrid model for tumor-immune system competition," *Computational and Mathematical Methods in Medicine*, vol. 2012, Article ID 610124, 6 pages, 2012.
- [6] C. Cattani and G. Pierro, "On the fractal geometry of DNA by the binary image analysis," *Bulletin of Mathematical Biology*, vol. 75, no. 9, pp. 1544–1570, 2013.
- [7] M. Li, S. C. Lim, C. Cattani, and M. Scalia, "Characteristic roots of a class of fractional oscillators," *Advances in High Energy Physics*, vol. 2013, Article ID 853925, 7 pages, 2013.
- [8] M. Li, S. C. Lim, and S. Chen, "Exact solution of impulse response to a class of fractional oscillators and its stability," *Mathematical Problems in Engineering*, vol. 2011, Article ID 657839, 9 pages, 2011.
- [9] M. Li, "Approximating ideal filters by systems of fractional order," *Computational and Mathematical Methods in Medicine*, vol. 2012, Article ID 365054, 6 pages, 2012.
- [10] R. Gorenflo and F. Mainardi, *Fractional Calculus: Integral and Differential Equations of Fractional Order: From, Fractals and Fractional Calculus*, Carpinteri & Mainardi, New York, NY, USA, 1997.
- [11] Y. M. Lin and C. J. Xu, "Finite difference/spectral approximations for the time-fractional diffusion equation," *Journal of Computational Physics*, vol. 225, no. 2, pp. 1533–1552, 2007.
- [12] F. Liu, V. V. Anh, I. Turner, and P. Zhuang, "Time fractional advection-dispersion equation," *Journal of Applied Mathematics & Computing*, vol. 13, no. 1-2, pp. 233–245, 2003.
- [13] W. R. Schneider and W. Wyss, "Fractional diffusion and wave equations," *Journal of Mathematical Physics*, vol. 30, no. 1, pp. 134–144, 1989.
- [14] W. Wyss, "The fractional diffusion equation," *Journal of Mathematical Physics*, vol. 27, no. 11, pp. 2782–2785, 1986.
- [15] V. V. Kulish and J. L. Lage, "Fractional-diffusion solution for transient local temperature and heat flux," *Transactions of the ASME*, vol. 122, pp. 372–376, 2000.
- [16] K. B. Oldham and J. Spanier, *The Fractional Calculus: Theory and Application of Differential and Integration to Arbitrary Order*, Academic Press, 1974.
- [17] K. B. Oldham and J. Spanier, "A general solution of the diffusion equation for semiinfinite geometries," *Journal of Mathematical Analysis and Applications*, vol. 39, pp. 655–669, 1972.
- [18] K. B. Oldham and J. Spanier, "The replacement of Fick's law by a formulation involving semidifferentiation," *Journal of Electroanalytical Chemistry*, vol. 26, pp. 331–341, 1970.
- [19] K. Sakamoto and M. Yamamoto, "Initial value/boundary value problems for fractional diffusion-wave equations and applications to some inverse problems," *Journal of Mathematical Analysis and Applications*, vol. 382, no. 1, pp. 426–447, 2011.
- [20] J. J. Liu and M. Yamamoto, "A backward problem for the time-fractional diffusion equation," *Applicable Analysis*, vol. 89, no. 11, pp. 1769–1788, 2010.
- [21] C. X. Ren, X. Xu, and S. Lu, "Regularization by projection for a backward problem of the time-fractional diffusion equation," *Journal of Inverse and Ill-Posed Problems*, vol. 22, no. 1, pp. 121–139, 2012.
- [22] T. Takeuchi and M. Yamamoto, "Tikhonov regularization by a reproducing kernel Hilbert space for the Cauchy problem for an elliptic equation," *SIAM Journal on Scientific Computing*, vol. 31, no. 1, pp. 112–142, 2008.
- [23] H. W. Engl, M. Hanke, and A. Neubauer, *Regularization of Inverse Problems*, vol. 375, Kluwer Academic Publishers Group, Dordrecht, The Netherlands, 1996.
- [24] C. W. Groetsch, *The Theory of Tikhonov Regularization for Fredholm Equations of the First Kind*, vol. 105, Pitman, Boston, Mass, USA, 1984.
- [25] I. Steinwart and A. Christmann, *Support Vector Machines*, Springer, New York, NY, USA, 2008.
- [26] H. Wendland, *Scattered Data Approximation*, vol. 17 of *Cambridge Monographs on Applied and Computational Mathematics*, Cambridge University Press, Cambridge, UK, 2005.
- [27] M. Pontil, "A note on different covering numbers in learning theory," *Journal of Complexity*, vol. 19, no. 5, pp. 665–671, 2003.
- [28] J. Xian, S. P. Luo, and W. Lin, "Weighted sampling and signal reconstruction in spline subspaces," *Signal Process*, vol. 86, pp. 331–340, 2006.
- [29] H. Hult, "Approximating some Volterra type stochastic integrals with applications to parameter estimation," *Stochastic Processes and Their Applications*, vol. 105, no. 1, pp. 1–32, 2003.
- [30] I. Antoniou and K. Gustafson, "Wavelets and stochastic processes," *Mathematics and Computers in Simulation*, vol. 49, no. 1-2, pp. 81–104, 1999.
- [31] N. Aronszajn, "Theory of reproducing kernels," *Transactions of the American Mathematical Society*, vol. 68, pp. 337–404, 1950.
- [32] Y. C. Hon and T. Takeuchi, "Discretized Tikhonov regularization by reproducing kernel Hilbert space for backward heat conduction problem," *Advances in Computational Mathematics*, vol. 34, no. 2, pp. 167–183, 2011.
- [33] W. Y. Wang, B. Han, and M. Yamamoto, "Inverse heat problem of determining time-dependent source parameter in reproducing kernel space," *UTMS 2011-11*, University of Tokyo, 2011.
- [34] S. Saitoh, "Applications of Tikhonov regularization to inverse problems using reproducing kernels," *Inverse Problems*, vol. 73, Article ID 012019, 2007.
- [35] P. Mathé and S. V. Pereverzev, "Discretization strategy for linear ill-posed problems in variable Hilbert scales," *Inverse Problems*, vol. 19, no. 6, pp. 1263–1277, 2003.

- [36] P. C. Hansen, *Rank-Deficient and Discrete Ill-Posed Problems*, SIAM, Philadelphia, Pa, USA, 1998.
- [37] P. C. Hansen, "Regularization tools: a Matlab package for analysis and solution of discrete ill-posed problems," *Numerical Algorithms*, vol. 6, no. 1-2, pp. 1-35, 1994.
- [38] I. Podlubny, "Mittag-Leffler function, The MATLAB routine," <http://www.mathworks.com/matlabcentral/fileexchange>.
- [39] W. Pogorzelski, *Integral Equations and Their Applications*, vol. 1, Pergamon Press, Oxford, UK, 1966.

Research Article

Construction of Fusion Frame Systems in Finite Dimensional Hilbert Spaces

Jinsong Leng and Tingzhu Huang

School of Mathematical Sciences, University of Electronic Science and Technology of China, Chengdu 610054, China

Correspondence should be addressed to Jinsong Leng; jslengjs@gmail.com

Received 26 November 2013; Accepted 25 January 2014; Published 12 March 2014

Academic Editor: Carlo Cattani

Copyright © 2014 J. Leng and T. Huang. This is an open access article distributed under the Creative Commons Attribution License, which permits unrestricted use, distribution, and reproduction in any medium, provided the original work is properly cited.

We first investigate the construction of a fusion frame system in a finite-dimensional Hilbert space \mathbb{F}^n when its fusion frame operator matrix is given and provides a corresponding algorithm. The matrix representations of its local frame operators and inverse frame operators are naturally obtained. We then study the related properties of the constructed fusion frame systems. Finally, we implement the construction of fusion frame systems which behave optimally for erasures in some special sense in signal transmission.

1. Introduction

The theory of frames has gradually become an attractive research area in the past twenty years. A prominent feature of frames is redundancy which has two advantages: it makes the construction of various frames more flexible and it provides stability and robustness of signal in transmission. This leads to the rapid development of theory and applications of frames in past twenty years. We refer to [1–3] and the references therein for more details about the frame theory and its new achievements. In applications, we only mention some areas here such as signal and image processing [4], quantization [5], capacity of transmission channel [1, 2, 6], coding theory [7–12], and data transmission technology [13].

But in some modern applications, the data which need to be handled are so large that the processing procedures cannot be implemented effectively by using a single frame. Fusion frames are naturally suitable tools for dealing with this problem. One can see the systemic introduction of theory of fusion frames in [14, 15]. In recent years, many excellent results about the theory and applications of fusion frames have been achieved at an amazing speed [15–20]. In fact, fusion frames are generalization of conventional frames and go beyond them. The procedure of using fusion frame systems to handle information can be described as follows. A large number of data can be assigned to a set of

small spaces and processed in these subsystems, finally all the information are fused together at a center. Fusion frames have been applied to various fields where distributed or parallel processing is required. For instance, in a coding transmission process, the encoded and quantized data must be put in numbers of packets. When one or more packets are scrambled, lost, or delayed, fusion frames can enhance the robustness to the packet erasures. Furthermore, we can see the successful applications of fusion frames in sensors network [21], transmission coding [22–25], and so forth.

However, some problems about fusion frame systems are open. Many excellent results about conventional frames have been obtained and applied successfully, but how to generalize them to fusion frames? Even in mathematics application, the relation between the theory of fusion frames and the interesting fields studied in [26–28] is worth further researching. It is an appealing subject due to the complexity of the structure of fusion frames compared with conventional frames. In this paper, we focus on the matrix representations of fusion frame operators of fusion frame systems and the construction of fusion frame systems if their fusion frame operator matrices are provided. To this end, we first study the correspondence between frames of a subspace W with dimension l of an n -dimensional Hilbert space \mathcal{H} with frames of Hilbert space \mathbb{F}^l , where $l \leq n$. We obtain the matrix representations of the local inverse frame operators and the

fusion frame operator of a given fusion frame system by using the correspondence. Based on these matrix representations, the concrete algorithm for constructing a dual fusion frame system is provided. Then we investigate the construction of fusion frame systems, which fusion frame operators are given. It is essential for constructing fusion frame systems to get their local frames. We show that the constructed local frame of a subspace with dimension l can inherit some properties from the corresponding frame of Hilbert space \mathbb{F}^l such as Parseval and harmony. Finally, we give a method for construction of the optimal fusion frame systems for one local frame vector erasure.

We organize the structure of this paper as follows. In Section 2, we introduce and recall some notations, conceptions, and some basic theory about frames and fusion frame systems. Then we recall the method to obtain the matrix representation of the fusion frame operator of a given fusion frame system in a finite-dimensional Hilbert space \mathbb{F}^n . In Section 3, we study the construction of frames of an l -dimensional subspace W of \mathbb{F}^n by using the corresponding frames of \mathbb{F}^l , where $l \leq n$. We then present an algorithm for constructing a fusion frame system when its fusion frame operator is given. Moreover, we get the matrix representations of its local frame operators and inverse frame operators and research the related characteristics of the constructed fusion frame systems. The optimal fusion frame systems under erasures in some particular sense can be obtained by using our method. An example is given to show the effectiveness of our construction in image coding.

2. Preliminaries

We refer to [1–3, 15, 25] for the details of the basic notations, concepts, and results about frames and fusion frame systems. We will adopt the same notations as [25] throughout this paper. We recall the main concepts and results about the construction of the matrix representation of the fusion frame operator of a given fusion frame system in this section.

Let $\mathcal{W} = \{(W_i, v_i)\}_{i \in I}$ be a fusion frame for \mathcal{H} . The analysis operator $\Theta_{\mathcal{W}}$ is defined by

$$\Theta_{\mathcal{W}} : \mathcal{H} \longrightarrow \left(\sum_{i \in I} \oplus W_i \right)_{\ell_2} \quad \text{with } \Theta_{\mathcal{W}}(f) = \{v_i P_{W_i}(f)\}_{i \in I}, \quad (1)$$

where

$$\left(\sum_{i \in I} \oplus W_i \right)_{\ell_2} = \left\{ \{f_i\}_{i \in I} \mid f_i \in W_i, \{\|f_i\|\}_{i \in I} \in \ell^2(I) \right\} \quad (2)$$

is called the *representation space*. The synthesis operator $\Theta_{\mathcal{W}}^*$ (the adjoint operator of $\Theta_{\mathcal{W}}$) can be defined by

$$\Theta_{\mathcal{W}}^* : \left(\sum_{i \in I} \oplus W_i \right)_{\ell_2} \longrightarrow \mathcal{H} \quad \text{with } \Theta_{\mathcal{W}}^*(f) = \sum_{i \in I} v_i f_i, \quad (3)$$

$$f = \{f_i\}_{i \in I} \in \left(\sum_{i \in I} \oplus W_i \right)_{\ell_2}.$$

The fusion frame operator $S_{\mathcal{W}}$ for \mathcal{W} is defined by

$$S_{\mathcal{W}}(f) = \Theta_{\mathcal{W}}^* \Theta_{\mathcal{W}}(f) = \sum_{i \in I} v_i^2 P_{W_i}(f). \quad (4)$$

The following result shows how to obtain the global dual frame from the local dual frames.

Proposition 1 (c.f. [15], Proposition 4.3). *Let $\{(W_i, v_i, \{f_{ij}\}_{j \in J_i})\}_{i \in I}$ be a fusion frame system for \mathcal{H} with associated fusion frame operator $S_{\mathcal{W}}$, common local frame bounds, and local dual frames $\{\tilde{f}_{ij}\}_{j \in J_i}$, $i \in I$. Then $\{v_i S_{\mathcal{W}}^{-1}(\tilde{f}_{ij})\}_{j \in J_i, i \in I}$ is a dual frame for the frame $\{v_i f_{ij}\}_{j \in J_i, i \in I}$.*

Because we only consider finite-dimensional Hilbert spaces, I will denote the identity operator (matrix) exclusively in the rest of the paper.

Let $\{(W_i, v_i, \{f_{ij}\}_{j=1}^{k_i})\}_{i=1}^m$ be a fusion frame system for \mathbb{F}^n ; then the analysis operator of the local frame of W_i is a $k_i \times n$ matrix Θ_{F_i} with f_{ij}^* as its j th row and the $n \times k_i$ matrix $\Theta_{F_i}^*$ is its synthesis operator. Furthermore, the i th local frame operator is an $n \times n$ matrix $S_{F_i} = \Theta_{F_i}^* \Theta_{F_i}$.

Notation. For the purpose of coding of any $f \in \mathbb{F}^n$, Θ_{F_i} always denote the analysis operator of the system $\{f_{ij}\}_{j=1}^{k_i}$ in \mathbb{F}^n throughout this paper. Hence it is a $k_i \times n$ matrix, not a $k_i \times (\dim W_i)$ matrix.

The following definition is given by [25].

Definition 2. Let W be an l -dimensional subspace of \mathbb{F}^n with a local frame $F = \{f_i\}_{i=1}^k$, where $l \leq n$. S_F is the local frame operator of F . If there exists an operator A such that $f = S_F A(f) = A S_F(f)$ holds for all $f \in W$, we call A the *inverse of S_F in W* and denote it by S_F^{-1} .

For any $f \in \mathbb{F}^n$, $\Theta_{F_i} f$ is its encoding version in subspace W_i . For obtaining $P_{W_i}(f) = \sum_{j=1}^{k_i} \langle f, f_{ij} \rangle \tilde{f}_{ij} = \sum_{j=1}^{k_i} \langle f, f_{ij} \rangle S_{F_i}^{-1} f_{ij} = \Theta_{F_i}^* \Theta_{F_i}(f)$, the following lemma is given to calculate the matrix representation of $S_{F_i}^{-1}$ and the i th local dual frame $\{\tilde{f}_{ij}\}_{j=1}^{k_i}$.

Lemma 3 (c.f. [25], Lemma 11). *Let W be an l -dimensional subspace of \mathbb{F}^n with an orthonormal basis $\{e_i\}_{i=1}^l$ and a frame $F = \{f_i\}_{i=1}^k$ with frame bounds A, B , where $l \leq n$. Define L to be an $l \times n$ matrix with the vector e_i^* as its i th row for $i = 1, 2, \dots, l$, where e_i^* is the conjugate-transpose of e_i . The sequence $G = \{g_i\}_{i=1}^k$ is given by $g_i = L f_i$ for $i = 1, 2, \dots, k$. Then $\{g_i\}_{i=1}^k$ is a frame of \mathbb{F}^l with the same frame bounds as F . In particular, if F is a tight (or Parseval) frame, also is G .*

By applying this lemma, we can obtain a method to compute the matrix representation of the inverse frame operator of a subspace endowed with an orthonormal basis in the following theorem.

Theorem 4 (c.f. [25], Theorem 12). *Let W be an l -dimensional subspace of \mathbb{F}^n with an orthonormal basis $\{e_i\}_{i=1}^l$ and a frame*

$F = \{f_i\}_{i=1}^k$, where $l \leq n$. L is defined as the above lemma. S_F is the frame operator of F . Then

$$S_F^{-1} = L^*(LS_FL^*)^{-1}L \quad (5)$$

is the inverse of S_F in W . Moreover, the orthogonal projection P_W from F^n onto W is $P_W = S_F^{-1}S_F = S_F S_F^{-1} = L^*L$.

For a given fusion frame system $\{(W_i, v_i, F_i = \{f_{ij}\}_{j=1}^{k_i})_{i=1}^m$, we can calculate the orthonormal basis of its each subspace by finding the maximally linear independent subset of F_i and taking the Gram-Schmidt process on it. Then by using the above theorem, we derive the matrix representations of all local inverse frame operators and orthogonal projections onto the subspaces $\{W_i\}_{i=1}^m$. Furthermore, we can compute the matrix representation of the fusion frame operator by applying the formula provided by the following proposition.

Proposition 5 (c.f. [25], Proposition 13). *Let $\{(W_i, v_i, F_i = \{f_{ij}\}_{j=1}^{k_i})_{i=1}^m$ be a fusion frame system for \mathbb{F}^n , and let $\tilde{F}_i = \{\tilde{f}_{ij}\}_{j \in J_i}$, $i \in I$, be the local dual frames given by $\tilde{f}_{ij} = S_{F_i}^{-1}f_{ij}$ for all $j = 1, 2, \dots, k_i$, $i = 1, 2, \dots, m$. Then the matrix representation of the fusion frame operator is given by*

$$\begin{aligned} S_{\mathcal{W}} &= \sum_{i=1}^m v_i^2 \Theta_{\tilde{F}_i}^* \Theta_{F_i} = \sum_{i=1}^m v_i^2 \Theta_{F_i}^* \Theta_{\tilde{F}_i} \\ &= \sum_{i=1}^m v_i^2 S_{F_i}^{-1} S_{F_i} = \sum_{i=1}^m v_i^2 S_{F_i} S_{F_i}^{-1}, \end{aligned} \quad (6)$$

where Θ_{F_i} and $\Theta_{\tilde{F}_i}$ are the analysis operators of F_i and \tilde{F}_i , respectively, and S_{F_i} is the frame operator of F_i for each $i \in I$.

Given a fusion frame system of a finite-dimensional Hilbert space \mathbb{F}^n , the matrix representation of its fusion frame operator as well as its one dual fusion frame system can be obtained by using the above two results. The concrete algorithm is presented in [25].

3. Construction of Fusion Frame Systems

In this section, we research the construction of a fusion frame system with a given positive invertible matrix S as its fusion frame operator. The constructing approach should include two stages. First, construct the orthogonal projections of all subspaces as well as their weights if the fusion frame operator is given. Secondly, construct the local frames of all subspaces with the desired properties. By using this method, we can derive the optimal fusion frame systems for erasures in some special sense.

3.1. Construction of Fusion Frame Systems. We first recall our previous work in [19] on the construction of fusion frames which fusion frame operators are provided. In practise, the local frames of a fusion frame system are served as coder in their respective subspaces. The main distribution of this subsection is the derivation of the local frames with the expected characteristics which can be implemented by constructing

frames of \mathbb{F}^{l_i} with the same dimension as subspace W_i for each $i \in \{1, 2, \dots, m\}$. And then, we get the construction of fusion frame systems combined with the previous work.

Notations and Assumptions. We set up some notations that will be used throughout this subsection. Let S be a positive $n \times n$ matrix with eigenvalues $\{\lambda_i\}_{i=1}^n$ where $\lambda_i > 0$ for all $1 \leq i \leq n$ and let $e_i, i = 1, 2, \dots, n$ be the orthonormal eigenvectors of S corresponding to the eigenvalues λ_i , respectively, which form an orthonormal basis of \mathbb{F}^n . Let m be a positive integer, and $L_i = (e_{i1}, e_{i2}, \dots, e_{il_i})^*$; that is, the matrix L_i is constituted by $e_{ij}^*, j = 1, 2, \dots, l_i$ as its rows for $i = 1, 2, \dots, m$, where $e_{ij} \in \{e_i\}_{i=1}^n$ and $e_{ij_1} \neq e_{ij_2}$ when $j_1 \neq j_2$. Assume that the matrix $[L_1^*, L_2^*, \dots, L_m^*]$ has rank n ; that is, the rows of all $L_i, i = 1, 2, \dots, m$ can span the space \mathbb{F}^n . Set $\Lambda_i = \{j \mid e_i^* \text{ is one of the rows of } L_j\}$ for $i = 1, 2, \dots, n$.

The following theorem provides the method of orthogonal projection decomposition of a given positive matrix.

Theorem 6 (c.f. [19], Theorem 3.2). *Let the notations and assumptions be as described in the previous setup. Let the positive numbers $\{v_i\}_{i=1}^m$ satisfy the following condition:*

$$\sum_{j \in \Lambda_i} v_j^2 = \lambda_i \quad (7)$$

for all $i = 1, 2, \dots, m$; then the positive matrix S has the following decomposition:

$$S = \sum_{i=1}^m v_i^2 P_i, \quad (8)$$

where $P_i = L_i^* L_i, i = 1, 2, \dots, m$ are orthogonal projection matrices on $W_i = \text{span}\{e_{ij}\}_{j=1}^{l_i}$.

The following proposition provides a method for the construction of a fusion frame as well as orthonormal projections on its subspaces with a given fusion frame operator.

Proposition 7 (c.f. [19], Proposition 3.4). *Let the notations and assumptions be as described in the previous setup, and the positive numbers $\{v_i\}_{i=1}^m$ satisfy equation (7). Then $\{(W_i, v_i)\}_{i=1}^m$ is a fusion frame for \mathbb{F}^n with frame operator $S_{\mathcal{W}} = S$, where $W_i = \text{span}\{e_{ij}\}_{j=1}^{l_i}$. In the case that $S = AI$, we have that if $\{v_i\}_{i=1}^m$ satisfies the following condition:*

$$\sum_{j \in \Lambda_i} v_j^2 = A, \quad (9)$$

for all $i = 1, 2, \dots, m$, where $A > 0$ is a positive real number; then $\{(W_i, v_i)\}_{i=1}^m$ is an A -tight fusion frame for \mathbb{F}^n . In particular, if $A = 1$, then it is a Parseval fusion frame.

Then we will focus on the construction of local frames of the fusion frames derived by the above proposition. It is an important step for constructing fusion frame systems. We first show the following theorem which is the converse of Lemma 3.

Theorem 8. Let W be an l -dimensional subspace of \mathbb{F}^n with an orthonormal basis $\{e_i\}_{i=1}^l$, and let $G = \{g_i\}_{i=1}^k$ be a frame of \mathbb{F}^l with frame bounds A, B , where $l \leq n$. L is defined as Lemma 3. The sequence $F = \{f_i\}_{i=1}^k$ is given by $f_i = L^*g_i$, for $i = 1, 2, \dots, k$. Then F is a frame of W with the same frame bounds as G . In particular, if G is a tight (or Parseval) frame, also is F .

Proof. For any $f \in W$, we have $Lf = (\langle f, e_1 \rangle, \langle f, e_2 \rangle, \dots, \langle f, e_l \rangle)^T \in \mathbb{F}^l$ and $\|Lf\|^2 = \sum_{i=1}^l |\langle f, e_i \rangle|^2 = \|f\|^2$. Therefore,

$$\begin{aligned} A\|f\|^2 &= A\|Lf\|^2 \leq \sum_{i=1}^k |\langle Lf, g_i \rangle|^2 = \sum_{i=1}^k |\langle f, L^*g_i \rangle|^2 \\ &= \sum_{i=1}^k |\langle f, f_i \rangle|^2 \leq B\|Lf\|^2 = B\|f\|^2, \end{aligned} \quad (10)$$

as required. The particular assertion is obvious. \square

The following proposition gives the matrix representations of the local frame operator and inverse frame operator of a subspace W of \mathbb{F}^n derived by the above theorem.

Proposition 9. Let W be an l -dimensional subspace of \mathbb{F}^n with an orthonormal basis $\{e_i\}_{i=1}^l$, and let $G = \{g_i\}_{i=1}^k$ be a frame of \mathbb{F}^l with frame bounds A, B , where $l \leq n$. L and $F = \{f_i\}_{i=1}^k$ are defined as the above theorem. S_G is the frame operator of G . Then the frame operator of F and its inverse are given by

$$\begin{aligned} S_F &= L^*S_GL, \\ S_F^{-1} &= L^*S_G^{-1}L. \end{aligned} \quad (11)$$

Moreover, the orthogonal projection P_W from \mathbb{F}^n onto W is $P_W = S_F^{-1}S_F = S_F S_F^{-1} = L^*L$.

Proof. Let Θ_G and Θ_G^* be the analysis operator and synthesis operator of G , respectively; then $\Theta_F^* = (L^*g_1, L^*g_2, \dots, L^*g_k) = L^*\Theta_G^*$ is the synthesis operator of F . Hence, the frame operator of F is $S_F = \Theta_F^*\Theta_F = L^*\Theta_G^*\Theta_GL = L^*S_GL$.

Since S_G is invertible, we will show that $S_F^{-1} = L^*S_G^{-1}L$ is inverse of S_F . Note that $LL^* = I$ and $L^*Lf = f$ for any $f \in W$. Hence, we have

$$\begin{aligned} S_F^{-1}S_F f &= L^*S_G^{-1}LL^*S_GL f = L^*Lf = f, \\ S_F S_F^{-1} f &= L^*S_GL L^*S_G^{-1}L f = L^*Lf = f, \end{aligned} \quad (12)$$

as claimed. The proof of the moreover part is the same as that of Theorem 12 of [25]. \square

The following two propositions show that the constructed frame of W inherits some features of the corresponding frame of \mathbb{F}^l .

Proposition 10. Let W be an l -dimensional subspace of \mathbb{F}^n with an orthonormal basis $\{e_i\}_{i=1}^l$, and let $G = \{g_i\}_{i=1}^k$ be

a frame of \mathbb{F}^l with frame bounds A, B , where $l \leq n$. L and $F = \{f_i\}_{i=1}^k$ are defined as Theorem 8. If $\tilde{G} = \{\tilde{g}_i\}_{i=1}^k$ is a dual frame of G , then $\tilde{F} = \{L^*\tilde{g}_i\}_{i=1}^k$ is a dual frame of F . Furthermore, if \tilde{G} is the canonical one, so is \tilde{F} .

Proof. For any $f \in W$, we have

$$\begin{aligned} \sum_{i=1}^k \langle f, L^*g_i \rangle L^*\tilde{g}_i &= L^* \sum_{i=1}^k \langle Lf, g_i \rangle \tilde{g}_i = \sum_{i=1}^k \langle f, L^*\tilde{g}_i \rangle L^*g_i \\ &= L^* \sum_{i=1}^k \langle Lf, \tilde{g}_i \rangle g_i = L^*Lf = f. \end{aligned} \quad (13)$$

Hence, \tilde{F} is a dual frame of F . If $\tilde{g}_i = S_G^{-1}g_i$, then $\tilde{f}_i = L^*\tilde{g}_i = L^*S_G^{-1}LL^*g_i = S_F^{-1}f_i$ for $i = 1, 2, \dots, k$, which implies that \tilde{F} is the canonical dual frame of F . \square

Proposition 11. Let W be an l -dimensional subspace of \mathbb{F}^n with an orthonormal basis $\{e_i\}_{i=1}^l$, and let $G = \{g_i\}_{i=0}^{k-1}$ be a harmonic frame of \mathbb{F}^l , where $l \leq n$. L and $F = \{f_i\}_{i=0}^{k-1}$ are defined as Theorem 8. Then F is a harmonic frame of W .

Proof. Since G is a harmonic frame of \mathbb{F}^l , there exists a unitary U on \mathbb{F}^l such that $U^k = I, U^i \neq I$ for $1 \leq i \leq k-1$, and $g_i = U^i g_0$ for $0 \leq i \leq k-1$. Let $L^*UL = V$. For any $f \in W$, we have

$$\begin{aligned} VV^*f &= L^*ULL^*U^*Lf = V^*Vf = L^*U^*LL^*ULf \\ &= L^*Lf = f. \end{aligned} \quad (14)$$

Therefore, V is a unitary on W . It is obvious that $V^i = L^*U^iL$. So we have $V^k = L^*L, V^i \neq L^*L$ for $1 \leq i \leq k-1$, and $f_i = L^*g_i = L^*U^i g_0 = L^*U^i LL^*g_0 = V^i f_0$, which implies that F is a harmonic frame. \square

Summarizing the related results of this subsection, we can obtain the algorithm for constructing a required fusion frame system with a given fusion frame operator S as follows.

Step 1. Compute the eigenvalues $\{\lambda_i\}_{i=1}^n$ and their corresponding independent eigenvectors $\{h_i\}_{i=1}^n$ of S .

Step 2. Take the Gram-Schmidt process on $\{h_i\}_{i=1}^n$ to get an orthonormal basis $\{e_i\}_{i=1}^n$ for \mathbb{F}^n .

Step 3. According to the requirement, construct the matrix L_i constituted by this basis as follows:

$$L_i = \begin{bmatrix} \leftarrow e_{i1}^* \rightarrow \\ \leftarrow e_{i2}^* \rightarrow \\ \vdots \\ \leftarrow e_{il}^* \rightarrow \end{bmatrix}, \quad (15)$$

for $i = 1, 2, \dots, m$, where $e_{ij} \in \{e_i\}_{i=1}^n$, and $e_{ij_1} \neq e_{ij_2}$, when $j_1 \neq j_2$.

Step 4. Resolve (7) to derive the sequence of weights $\{v_i\}_{i=1}^n$. Set $W_i = \text{span}\{e_i\}_{j=1}^{l_i}$. Use formula (8) to decompose S and get the orthogonal projections P_{W_i} , for $i = 1, 2, \dots, m$. Then we obtain a required fusion frame $\{(W_i, v_i)\}_{i=1}^m$.

Step 5. Construct the frames $G_i = \{g_{ij}\}_{j=1}^{k_i}$ in \mathbb{F}^{l_i} with requirement properties for $i = 1, 2, \dots, m$.

Step 6. Apply Theorem 8 to compute the local frames $F_i = \{f_{ij}\}_{j=1}^{k_i}$ for $i = 1, 2, \dots, m$. Then we derive a required fusion frame system $\{(W_i, v_i, \{f_{ij}\}_{j=1}^{k_i})\}_{i=1}^m$.

3.2. Construction of Optimal Fusion Frame Systems for Erasures. We apply our construction method to obtain optimal Parseval fusion frame systems for the packet erasure problem in some special sense in this subsection. Bodmann initiated in [22] the investigation about the optimality of (m, k, n) -protocols that are used to the packet erasure problem. Let $\{B_j\}_{j=1}^m$ be a family of coordinate operators $B_j : \mathcal{H} \rightarrow \mathcal{K}$ into a finite-dimensional Hilbert space \mathcal{K} of maximal rank k that provide a resolution of the identity $I = \sum_{j=1}^m B_j^* B_j$ for the Hilbert space $\mathcal{H} = \mathbb{F}^n$, where m, k, n are positive integers satisfying $n < mk$; then the analysis operator Θ of such a family $\{B_j\}$ is called a (m, k, n) -protocol. The optimality of (m, k, n) -protocols requires to get weighted projective resolutions of the identity operator: $I = \sum_{j=1}^m B_j^* B_j = \sum_{j=1}^m v_j P_j$, where $v_j > 0$, and P_j is a projection on some Hilbert space with rank- k for $j = 1, 2, \dots, m$. This can be also phrased by Parseval fusion frames (Theorem 3.6 of [18]). Furthermore, optimal Parseval fusion frame systems for one local frame vector erasure have been depicted in Theorem 4.3 of [18]). We point out that a special type of Parseval fusion frames that are optimal for the one packet erasure problem can be easily constructed by using Proposition 7. Moreover, Parseval fusion frame systems that are optimal for the one local frame vector erasure problem described by [18] can be easily constructed by using Theorem 8. Let us recall the description of the optimal Parseval fusion frames for the one packet erasure problem.

Definition 12. Let $\mathcal{W} = \{(W_i, v_i)\}_{i=1}^m$ be a Parseval fusion frame for an n -dimension Hilbert space \mathbb{F}^n with analysis operator $\Theta_{\mathcal{W}}$. Define the operator $D_j : (\sum_{i=1}^m \oplus W_i)_{\ell_2} \rightarrow (\sum_{i=1}^m \oplus W_i)_{\ell_2}$ by $\{D_j(g)\}_i = \delta_{ji} g_i$ for all $i = 1, 2, \dots, m$, where $g = \{g_i\}_{i=1}^m \in (\sum_{i=1}^m \oplus W_i)_{\ell_2}$. For any $f \in \mathcal{H}$, we call $D_j \Theta_{\mathcal{W}} f$ the j th coding packet for $j = 1, 2, \dots, m$. The one packet erasure reconstruction error $e_1(\mathcal{W})$ of \mathcal{W} is defined by

$$e_1(\mathcal{W}) = \max \{ \|\Theta_{\mathcal{W}}^* D_i \Theta_{\mathcal{W}}\| : 1 \leq i \leq m \}. \quad (16)$$

In practise, a signal (vector) $f \in \mathcal{H}$ is encoded as $\Theta_{\mathcal{W}} f$ including m coding packets and decoded (reconstructed) as $\Theta_{\mathcal{W}}^* \Theta_{\mathcal{W}} f$ by using a Parseval fusion frame \mathcal{W} . If one packet is lost in the transmission process, then $e_1(\mathcal{W})$ depict the reconstruction error in the worst case. The optimal Parseval fusion frame can be used to implement the optimal coding in this special sense in applications [18, 22]. The following

theorem describe the optimal Parseval fusion frames with a prescribed number of subspaces and prescribed dimensions of the subspaces under one subspace (packet) erasure.

Theorem 13 (c.f. [18], Theorem 3.6). *Let $\mathcal{W} = \{(W_i, v_i)\}_{i=1}^m$ be a Parseval fusion frame for an n -dimension Hilbert space \mathbb{F}^n . Then the following are equivalent.*

(i) *The Parseval fusion frame \mathcal{W} satisfies*

$$e_1(\mathcal{W}) = \min \left\{ e_1 \left(\left\{ (\widetilde{W}_i, \widetilde{v}_i) \right\}_{i=1}^m \right) : \begin{aligned} & \left\{ (\widetilde{W}_i, \widetilde{v}_i) \right\}_{i=1}^m \text{ is a Parseval fusion} \\ & \text{frame with } \dim \widetilde{W}_i \\ & = \dim W_i, \forall 1 \leq i \leq m \end{aligned} \right\}. \quad (17)$$

(ii) *We have*

$$v_i^2 = \frac{\dim \mathcal{H}}{m \cdot \dim W_i}, \quad \forall 1 \leq i \leq m. \quad (18)$$

Moreover, let $f \in \mathcal{H}$ and \tilde{f} be the reconstructed vector. Then we have the following error bound

$$\|f - \tilde{f}\| \leq \frac{\dim \mathcal{H}}{m \cdot \min \{ \dim W_i : 1 \leq i \leq m \}}. \quad (19)$$

The following proposition which follows from Proposition 7 and Theorem 13 describe the construction of one kind of optimal Parseval fusion frames for one packet erasure.

Proposition 14 (c.f. [19], Proposition 3.8). *Let $\{e_i\}_{i=1}^n$ be an orthonormal basis for a Hilbert space \mathbb{F}^n , and let k be a positive integer. Assume that W_j is a subspace spanned by some elements in $\{e_i\}_{i=1}^n$ for $j = 1, 2, \dots, m$, and $\text{span}\{W_j\}_{j=1}^m = \mathcal{H}$. Let h_i be number of subspaces W_j that contain e_i ($1 \leq i \leq n$). If all $\dim W_j$ are equal to l and all h_i are equal to h , then $\{(W_j, \sqrt{v_j})\}_{j=1}^m$ is an optimal Parseval fusion frame for one packet erasure described in Theorem 13, where $v_j = n/ml$ for all $1 \leq j \leq m$.*

The optimal Parseval fusion frame systems with local Parseval frames of prescribed numbers of frame vectors and prescribed dimensions of subspaces under the erasure of one local frame vector is presented in [18]. We find that constructing this kind of fusion frame systems can be reduced to constructing the conventional optimal Parseval frames with respect to one frame vector erasure under our method. Now let us first recall the related knowledge.

Let $(D_1, D_2, \dots, D_m) \in \prod_{i=1}^m M(k_i \times k_i, \mathbb{F})$ be a vector of matrices, where $D_{i_0} = (d_{ij})_{k_{i_0} \times k_{i_0}}$, $d_{ij} = \delta_{i,j_0} \delta_{j,j_0}$ for some $i_0 \in \{1, 2, \dots, m\}$, $j_0 \in \{1, 2, \dots, k_{i_0}\}$, and other matrices are all zero-matrices, which simulate the erasure of vector $f_{i_0 j_0}$. Denote the set of all these matrix vectors by \mathcal{D} .

Definition 15. Let $\mathcal{W} = \{(W_i, v_i, \{f_{ij}\}_{j=1}^{k_i})\}_{i=1}^m$ be a Parseval fusion frame system with local Parseval frames. Let $\Theta_{\mathcal{W}}$ denote the analysis operator of the associated fusion frame, and Θ_{F_i} the analysis operator of the local frames for $1 \leq i \leq m$. Then the associated 1-erasure of local frame vector reconstruction error is defined to be

$$e_1^*(\mathcal{W}) = \max \left\{ \left\| \sum_{i=1}^m v_i^2 \Theta_{F_i}^* D_i \Theta_{F_i} \right\| : (D_1, D_2, \dots, D_m) \in \mathcal{D} \right\}. \tag{20}$$

The following theorem characterizes the optimal Parseval fusion frame systems with subspaces of fixed dimensions and local Parseval frames having fixed numbers of frame vectors under one local frame vector erasure.

Theorem 16 (c.f. [18], Theorem 4.3). *Let $\mathcal{W} = \{(W_i, v_i, \{f_{ij}\}_{j=1}^{k_i})\}_{i=1}^m$ be a Parseval fusion frame system with local Parseval frames for an n -dimension Hilbert space \mathbb{F}^n . Then the following are equivalent:*

- (i) *The Parseval fusion frame system satisfies $e_1^*(\mathcal{W}) = \min \{e_1^*(\{(\widetilde{W}_i, \widetilde{v}_i, \{\widetilde{f}_{ij}\}_{j=1}^{k_i})\}_{i=1}^m) : \{(\widetilde{W}_i, \widetilde{v}_i, \{\widetilde{f}_{ij}\}_{j=1}^{k_i})\}_{i=1}^m$ is a Parseval fusion frame system with local Parseval frames satisfying $\dim \widetilde{W}_i = \dim W_i$, for all $1 \leq i \leq m\}$.*
- (ii) *We have*

$$\|f_{ij}\|^2 = \frac{\dim W_i}{k_i}, \quad \forall 1 \leq i \leq m, 1 \leq j \leq k_i. \tag{21}$$

Moreover, let $f \in \mathcal{H}$ and \widetilde{f} be the reconstructed vector. Then we have the following error bound

$$\|f - \widetilde{f}\| \leq \frac{\max \{\dim W_i : 1 \leq i \leq m\}}{\min \{k_i : 1 \leq i \leq m\}} \|f\|. \tag{22}$$

The following proposition can be easily obtained by using the above theorem together with Proposition 2.1 of [9] and Theorem 8. We omit its proof.

Proposition 17. *Let $G_i = \{g_{ij}\}_{j=1}^{k_i}$ be the optimal Parseval frames with 1-erasure of \mathbb{F}^{l_i} for $i = 1, 2, \dots, m$, let $\{(W_i, v_i)\}_{i=1}^m$ be a Parseval fusion frame of \mathbb{F}^n endowed with an orthonormal basis $\{e_{ij}\}_{j=1}^{l_i}$ for each subspace W_i . Set $L_i = (e_{i1}, e_{i2}, \dots, e_{il_i})^*$, and $F_i = \{f_{ij} = L_i^* g_{ij}\}_{j=1}^{k_i}$ for all $1 \leq i \leq m$. Then $\mathcal{W} = \{(W_i, v_i, \{f_{ij}\}_{j=1}^{k_i})\}_{i=1}^m$ is an optimal Parseval fusion frame system with local Parseval frames for one local frame vector erasure described in Theorem 16.*

The above proposition provide a method for constructing the optimal Parseval fusion frame systems for one local frame vector erasure described in Theorem 16. First, we construct the optimal Parseval frames for 1-erasure in Hilbert space \mathbb{F}^{l_i} for $i = 1, 2, \dots, m$. Then, by using the algorithm presented by the above subsection we can derive the required optimal Parseval fusion frame system $\mathcal{W} = \{(W_i, v_i, \{f_{ij}\}_{j=1}^{k_i})\}_{i=1}^m$. Finally, we give a concrete example.

Example 18. Consider Hilbert space $\mathcal{H} = \mathbb{R}^4$, and let

$$S = \begin{bmatrix} \frac{22}{3} & -\frac{2}{3} & -\frac{2}{3} & 0 \\ -\frac{2}{3} & \frac{22}{3} & -\frac{2}{3} & 0 \\ -\frac{2}{3} & -\frac{2}{3} & \frac{22}{3} & 0 \\ 0 & 0 & 0 & 6 \end{bmatrix}. \tag{23}$$

The eigenvalues of S are $\lambda_1 = \lambda_2 = 8, \lambda_3 = \lambda_4 = 6$, and the corresponding orthonormal eigenvectors are given by

$$e_1 = \begin{bmatrix} -\frac{\sqrt{2}}{2} \\ \frac{\sqrt{2}}{2} \\ 0 \\ 0 \end{bmatrix}, \quad e_2 = \begin{bmatrix} -\frac{\sqrt{6}}{6} \\ \frac{\sqrt{6}}{6} \\ \frac{2\sqrt{6}}{6} \\ 0 \end{bmatrix}, \tag{24}$$

$$e_3 = \begin{bmatrix} -\frac{\sqrt{3}}{6} \\ -\frac{\sqrt{3}}{6} \\ -\frac{\sqrt{3}}{6} \\ \frac{\sqrt{3}}{2} \end{bmatrix}, \quad e_4 = \begin{bmatrix} \frac{1}{2} \\ \frac{1}{2} \\ \frac{1}{2} \\ \frac{1}{2} \end{bmatrix}.$$

Let $W_1 = \text{span}\{e_1, e_2\}, W_2 = \text{span}\{e_1, e_3\}, W_3 = \text{span}\{e_1, e_4\}, W_4 = \text{span}\{e_2, e_3\}, W_5 = \text{span}\{e_2, e_4\}$, and $W_6 = \text{span}\{e_3, e_4\}$. According to the condition (7), we need positive solutions for the following equations:

$$\begin{aligned} v_1 + v_2 + v_3 &= 8, & v_1 + v_4 + v_5 &= 8, \\ v_2 + v_4 + v_6 &= 6, & v_3 + v_5 + v_6 &= 6. \end{aligned} \tag{25}$$

These equations have infinite many positive solutions which can be expressed as

$$\begin{aligned} v_1 &= b + 2, & v_2 &= a, \\ v_3 &= v_4 = -a - b + 6, \\ v_5 &= a, & v_6 &= b, \end{aligned} \tag{26}$$

where $a + b < 2, a > 0, b > 0$. For example, we can take $a = b = 2$, then we have $v_1 = 4, v_2 = v_3 = v_4 = v_5 = v_6 = 2$. Then we get a fusion frame $\{(W_i, v_i)\}_{i=1}^4$.

We can obtain a harmonic Parseval frame $G = \{g_1, g_2, g_3\}$ for \mathbb{F}^2 by using Example 4.1 in [8], where $g_1 = (\sqrt{6}/3, 0)^T, g_2 = (-\sqrt{6}/6, \sqrt{2}/2)^T$, and $g_3 = (-\sqrt{6}/6, -\sqrt{2}/2)^T$. Since all vectors in G have the same norm $\sqrt{6}/3$, it is an

optimal Parseval frame for 1-erasure by Proposition 2.1 of [9].
Set

$$\begin{aligned}
 L_1 &= \begin{bmatrix} -\frac{\sqrt{2}}{2} & \frac{\sqrt{2}}{2} & 0 & 0 \\ -\frac{\sqrt{6}}{6} & -\frac{\sqrt{6}}{6} & \frac{2\sqrt{6}}{6} & 0 \end{bmatrix}, \\
 L_2 &= \begin{bmatrix} -\frac{\sqrt{2}}{2} & \frac{\sqrt{2}}{2} & 0 & 0 \\ -\frac{\sqrt{3}}{6} & -\frac{\sqrt{3}}{6} & -\frac{\sqrt{3}}{6} & \frac{\sqrt{3}}{2} \end{bmatrix}, \\
 L_3 &= \begin{bmatrix} -\frac{\sqrt{2}}{2} & \frac{\sqrt{2}}{2} & 0 & 0 \\ \frac{1}{2} & \frac{1}{2} & \frac{1}{2} & \frac{1}{2} \end{bmatrix}, \\
 L_4 &= \begin{bmatrix} -\frac{\sqrt{6}}{6} & -\frac{\sqrt{6}}{6} & \frac{2\sqrt{6}}{6} & 0 \\ -\frac{\sqrt{3}}{6} & -\frac{\sqrt{3}}{6} & -\frac{\sqrt{3}}{6} & \frac{\sqrt{3}}{2} \end{bmatrix}, \\
 L_5 &= \begin{bmatrix} -\frac{\sqrt{6}}{6} & -\frac{\sqrt{6}}{6} & \frac{2\sqrt{6}}{6} & 0 \\ \frac{1}{2} & \frac{1}{2} & \frac{1}{2} & \frac{1}{2} \end{bmatrix}, \\
 L_6 &= \begin{bmatrix} -\frac{\sqrt{3}}{6} & -\frac{\sqrt{3}}{6} & -\frac{\sqrt{3}}{6} & \frac{\sqrt{3}}{2} \\ \frac{1}{2} & \frac{1}{2} & \frac{1}{2} & \frac{1}{2} \end{bmatrix}.
 \end{aligned}
 \tag{27}$$

We compute $\{f_{ij}\}_{i=1, j=1}^{6,3}$ as follows:

$$\begin{aligned}
 f_{11} &= L_1^*g_1 = \left(-\frac{\sqrt{3}}{3}, \frac{\sqrt{3}}{3}, 0, 0\right)^T, \\
 f_{12} &= L_1^*g_2 = \left(0, -\frac{\sqrt{3}}{3}, \frac{\sqrt{3}}{3}, 0\right)^T, \\
 f_{13} &= L_1^*g_3 = \left(\frac{\sqrt{3}}{3}, 0, -\frac{\sqrt{3}}{3}, 0\right)^T, \\
 f_{21} &= L_2^*g_1 = \left(-\frac{\sqrt{3}}{3}, \frac{\sqrt{3}}{3}, 0, 0\right)^T, \\
 f_{22} &= L_2^*g_2 = \left(\frac{2\sqrt{3}-\sqrt{6}}{12}, -\frac{2\sqrt{3}+\sqrt{6}}{12}, -\frac{\sqrt{6}}{12}, \frac{\sqrt{6}}{4}\right)^T, \\
 f_{23} &= L_2^*g_3 = \left(\frac{2\sqrt{3}+\sqrt{6}}{12}, -\frac{2\sqrt{3}-\sqrt{6}}{12}, \frac{\sqrt{6}}{12}, -\frac{\sqrt{6}}{4}\right)^T,
 \end{aligned}$$

$$\begin{aligned}
 f_{31} &= L_3^*g_1 = \left(-\frac{\sqrt{3}}{3}, \frac{\sqrt{3}}{3}, 0, 0\right)^T, \\
 f_{32} &= L_3^*g_2 = \left(\frac{2\sqrt{3}+3\sqrt{2}}{12}, -\frac{2\sqrt{3}-3\sqrt{2}}{12}, \frac{\sqrt{2}}{4}, \frac{\sqrt{2}}{4}\right)^T, \\
 f_{33} &= L_3^*g_3 = \left(\frac{2\sqrt{3}-3\sqrt{2}}{12}, -\frac{2\sqrt{3}+3\sqrt{2}}{12}, -\frac{\sqrt{2}}{4}, -\frac{\sqrt{2}}{4}\right)^T, \\
 f_{41} &= L_4^*g_1 = \left(-\frac{1}{3}, -\frac{1}{3}, \frac{2}{3}, 0\right)^T, \\
 f_{42} &= L_4^*g_2 = \left(\frac{2-\sqrt{6}}{12}, \frac{2-\sqrt{6}}{12}, -\frac{4+\sqrt{6}}{12}, \frac{\sqrt{6}}{4}\right)^T, \\
 f_{43} &= L_4^*g_3 = \left(\frac{2+\sqrt{6}}{12}, \frac{2+\sqrt{6}}{12}, -\frac{4-\sqrt{6}}{12}, -\frac{\sqrt{6}}{4}\right)^T, \\
 f_{51} &= L_5^*g_1 = \left(-\frac{1}{3}, -\frac{1}{3}, \frac{2}{3}, 0\right)^T, \\
 f_{52} &= L_5^*g_2 = \left(\frac{2+3\sqrt{2}}{12}, \frac{2+3\sqrt{2}}{12}, -\frac{4-3\sqrt{2}}{12}, \frac{\sqrt{2}}{4}\right)^T, \\
 f_{53} &= L_5^*g_3 = \left(\frac{2-3\sqrt{2}}{12}, \frac{2-3\sqrt{2}}{12}, -\frac{4+3\sqrt{2}}{12}, -\frac{\sqrt{2}}{4}\right)^T, \\
 f_{61} &= L_6^*g_1 = \left(-\frac{\sqrt{2}}{6}, -\frac{\sqrt{2}}{6}, -\frac{\sqrt{2}}{6}, \frac{\sqrt{2}}{2}\right)^T, \\
 f_{62} &= L_6^*g_2 = \left(\frac{\sqrt{2}}{3}, \frac{\sqrt{2}}{2}, \frac{\sqrt{2}}{3}, 0\right)^T, \\
 f_{63} &= L_6^*g_3 = \left(-\frac{\sqrt{2}}{6}, -\frac{\sqrt{2}}{6}, -\frac{\sqrt{2}}{6}, -\frac{\sqrt{2}}{2}\right)^T.
 \end{aligned}
 \tag{28}$$

Then $\mathcal{W} = \{(W_j, v_j, \{f_{ij}\}_{j=1}^3)\}_{j=1}^6$ is an optimal Parseval fusion frame system with local Parseval frames under one local frame vector erasure in the sense of Theorem 16 by Proposition 17.

The original gray image of windmill is shown in Figure 1. We encode the data of the image by using the local frames of the Parseval fusion frame system given by this example. Then we decode the coded data, where first element of every local vector is deleted by using the Parseval fusion frame of this example. The reconstructed image is shown in Figure 2. One can observe the reconstruction effect by comparing the two figures.

4. Conclusion

We studied the method for constructing a fusion frame system in a finite-dimensional Hilbert space \mathbb{F}^n according to its fusion frame operator matrix in this paper. The corresponding algorithm was given. Then we obtained the



FIGURE 1: The original gray image of windmill.



FIGURE 2: The reconstructed gray image of windmill. The data of the original image is encoded by the local frames of the Parseval fusion frame system computed by Example 18. The first coefficient of every local vector is deleted. The remained data is decoded by the Parseval fusion frame of Example 18.

matrix representations of its local frame operators and inverse frame operators and researched the related characteristics of these fusion frame systems. We provided methods to get the optimal fusion frame systems for erasures in some special sense in signal transmission. Finally, we constructed a fusion frame system as an example by our method and successfully applied it in image coding.

Conflict of Interests

The authors declare that there is no conflict of interests regarding the publication of this paper.

Acknowledgments

The authors wish to thank the anonymous reviewers for their valuable comments and suggestions that have improved

the presentation of this paper. This work was supported by the National Natural Science Foundation of China (11271001 and 61370147), 973 Program (2013CB329404), and Sichuan Province Science and Technology Research Project (12ZC1802).

References

- [1] I. Cidon, H. Kodesh, and M. Sidi, "Erasure, capture, and random power level selection in multiple-access systems," *IEEE Transactions on Communications*, vol. 36, no. 3, pp. 263–271, 1988.
- [2] A. F. Dana, R. Gowaikar, R. Palanki, B. Hassibi, and M. Effros, "Capacity of wireless erasure networks," *IEEE Transactions on Information Theory*, vol. 52, no. 3, pp. 789–804, 2006.
- [3] D. Han, K. Kornelson, D. Larson, and E. Weber, *Frames for Undergraduates*, vol. 40 of *Mathematical Library Book Series*, American Mathematical Society, Providence, RI, USA, 2007.
- [4] E. J. Candès and D. L. Donoho, "New tight frames of curvelets and optimal representations of objects with piecewise C^2 singularities," *Communications on Pure and Applied Mathematics*, vol. 57, no. 2, pp. 219–266, 2004.
- [5] B. G. Bodmann and V. I. Paulsen, "Frame paths and error bounds for sigma-delta quantization," *Applied and Computational Harmonic Analysis*, vol. 22, no. 2, pp. 176–197, 2007.
- [6] C. H. Bennett, D. P. DiVincenzo, and J. A. Smolin, "Capacities of quantum erasure channels," *Physical Review Letters*, vol. 78, no. 16, pp. 3217–3220, 1997.
- [7] B. G. Bodmann and V. I. Paulsen, "Frames, graphs and erasures," *Linear Algebra and its Applications*, vol. 404, pp. 118–146, 2005.
- [8] V. K. Goyal, J. Kovačević, and J. A. Kelner, "Quantized frame expansions with erasures," *Applied and Computational Harmonic Analysis*, vol. 10, no. 3, pp. 203–233, 2001.
- [9] R. B. Holmes and V. I. Paulsen, "Optimal frames for erasures," *Linear Algebra and its Applications*, vol. 377, pp. 31–51, 2004.
- [10] J. Leng and D. Han, "Optimal dual frames for erasures II," *Linear Algebra and its Applications*, vol. 435, no. 6, pp. 1464–1472, 2011.
- [11] J. S. Leng, D. Han, and T. Huang, "Optimal dual frames for communication coding with probabilistic erasures," *IEEE Transactions on Signal Processing*, vol. 59, no. 11, pp. 5380–5389, 2011.
- [12] J. S. Leng, D. Han, and T. Huang, "Probability modelled optimal frames for erasures," *Linear Algebra and its Applications*, vol. 438, no. 11, pp. 4222–4236, 2013.
- [13] A. Albanese, J. Blömer, J. Edmonds, M. Luby, and M. Sudan, "Priority encoding transmission," *IEEE Transactions on Information Theory*, vol. 42, no. 6, part 1, pp. 1737–1744, 1996.
- [14] P. G. Casazza and G. Kutyniok, "Frames of subspaces," in *Wavelets, Frames, and Operator Theory*, vol. 345 of *Contemporary Mathematics Series*, pp. 87–113, American Mathematical Society, Providence, RI, USA, 2004.
- [15] P. G. Casazza, G. Kutyniok, and S. Li, "Fusion frames and distributed processing," *Applied and Computational Harmonic Analysis*, vol. 25, no. 1, pp. 114–132, 2008.
- [16] P. G. Casazza and M. Fickus, "Minimizing fusion frame potential," *Acta Applicandae Mathematicae*, vol. 107, no. 1–3, pp. 7–24, 2009.
- [17] P. G. Casazza, M. Fickus, D. G. Mixon, Y. Wang, and Z. Zhou, "Constructing tight fusion frames," *Applied and Computational Harmonic Analysis*, vol. 30, no. 2, pp. 175–187, 2011.

- [18] P. G. Casazza and G. Kutyniok, "Robustness of fusion frames under erasures of subspaces and of local frame vectors," in *Radon Transforms, Geometry, and Wavelets*, vol. 464 of *Contemporary Mathematics Series*, pp. 149–160, American Mathematical Society, Providence, RI, 2008.
- [19] J. S. Leng and D. Han, "Orthogonal projection decomposition of matrices and construction of fusion frames," *Advances in Computational Mathematics*, vol. 38, no. 2, pp. 369–381, 2013.
- [20] P. G. Massey, M. A. Ruiz, and D. Stojanoff, "The structure of minimizers of the frame potential on fusion frames," *The Journal of Fourier Analysis and Applications*, vol. 16, no. 4, pp. 514–543, 2010.
- [21] P. G. Casazza, G. Kutyniok, S. Li, and C. J. Rozell, "Modeling sensor networks with fusion frames," in *Wavelets XII*, vol. 6701 of *Proceedings of SPIE*, San Diego, Calif, USA, August 2007.
- [22] B. G. Bodmann, "Optimal linear transmission by loss-insensitive packet encoding," *Applied and Computational Harmonic Analysis*, vol. 22, no. 3, pp. 274–285, 2007.
- [23] B. G. Bodmann and G. Kutyniok, "Erasure-proof transmissions: fusion frames meet coding theory," in *Wavelets XIII*, vol. 7446 of *Proceedings of SPIE*, San Diego, Calif, USA, August 2009.
- [24] B. G. Bodmann, D. W. Kribs, and V. I. Paulsen, "Decoherence-insensitive quantum communication by optimal C^{ast} -encoding," *IEEE Transactions on Information Theory*, vol. 53, no. 12, pp. 4738–4749, 2007.
- [25] J. S. Leng, Q. X. Guo, and T. Z. Huang, "The duals of fusion frames for experimental data transmission coding of high energy physics," *Advances in High Energy Physics*, vol. 2013, Article ID 837129, 9 pages, 2013.
- [26] C. Cattani and A. Ciancio, "Separable transition density in the hybrid model for tumor-immune system competition," *Computational and Mathematical Methods in Medicine*, vol. 2012, Article ID 610124, 6 pages, 2012.
- [27] C. Cattani, A. Ciancio, and B. Lods, "On a mathematical model of immune competition," *Applied Mathematics Letters*, vol. 19, no. 7, pp. 678–683, 2006.
- [28] C. Cattani and L. M. S. Ruiz, "Discrete differential operators in multidimensional Haar wavelet spaces," *International Journal of Mathematics and Mathematical Sciences*, no. 41–44, pp. 2347–2355, 2004.

Research Article

Similarity Solution for Fractional Diffusion Equation

Jun-Sheng Duan,¹ Ai-Ping Guo,² and Wen-Zai Yun²

¹ School of Sciences, Shanghai Institute of Technology, Shanghai 201418, China

² School of Mathematics, Baotou Teachers College, Baotou, Inner Mongolia 014030, China

Correspondence should be addressed to Jun-Sheng Duan; duanjs@sit.edu.cn

Received 4 January 2014; Accepted 11 February 2014; Published 12 March 2014

Academic Editor: Ming Li

Copyright © 2014 Jun-Sheng Duan et al. This is an open access article distributed under the Creative Commons Attribution License, which permits unrestricted use, distribution, and reproduction in any medium, provided the original work is properly cited.

Fractional diffusion equation in fractal media is an integropartial differential equation parametrized by fractal Hausdorff dimension and anomalous diffusion exponent. In this paper, the similarity solution of the fractional diffusion equation was considered. Through the invariants of the group of scaling transformations we derived the integro-ordinary differential equation for the similarity variable. Then by virtue of Mellin transform, the probability density function $p(r, t)$, which is just the fundamental solution of the fractional diffusion equation, was expressed in terms of Fox functions.

1. Introduction

Standard diffusion in d -dimensional space, where d is a positive integer, is a process described by Gaussian distribution. A main feature of the process is the linear relation between the mean square displacement and time; namely, $\langle r^2(t) \rangle \propto t$. Some anomalous diffusion phenomena that take place in impure media, biological tissues, and porous media can be simulated by the diffusion model in fractals [1–6]. In recent years, the fractal theory has been developed rapidly, and it was found to be closely related to the anomalous diffusion phenomena [3–12].

In fractal media, the geometric obstacles existing on all length scales slow down the particle motion in a random walk. The mean square displacement behaves as [2]

$$R^2 \equiv \langle r^2(t) \rangle \propto t^{2/d_w}, \quad (1)$$

where $d_w (> 2)$ is the anomalous diffusion exponent. The numerical simulation found that on a large class of fractal structures the general form of the probability density function $p(r, t)$ that the walker is at distance r at time t from its starting point at time $t = 0$ obeys asymptotically a non-Gaussian shape of the form [2, 3]

$$p(r, t) \sim t^{-d_f/d_w} \exp \left[-\text{const.} \times \left(\frac{r}{R} \right)^u \right], \quad \frac{r}{R} \gg 1, \quad (2)$$

where $u = d_w/(d_w - 1)$ and d_f is the fractal Hausdorff dimension.

In order to simulate the diffusion phenomena in fractal media, some scholars have introduced fractional diffusion equations [4, 5, 11–13]. In this paper, we consider the fractional diffusion equation [5, 13]:

$$\frac{\partial^\gamma p(r, t)}{\partial t^\gamma} = \frac{1}{r^{d_s-1}} \frac{\partial}{\partial r} \left(r^{d_s-1} \frac{\partial p}{\partial r} \right), \quad r > 0, t > 0, \quad (3)$$

where $\gamma = 2/d_w$, $d_s = 2d_f/d_w$ is the spectral dimension of the fractal, and the fractional time derivative on the left hand side of (3) is defined as the convolution integral [14–20]:

$$\frac{\partial^\gamma p(r, t)}{\partial t^\gamma} = \frac{\partial}{\partial t} \int_0^t \frac{(t-\tau)^{-\gamma}}{\Gamma(1-\gamma)} p(r, \tau) d\tau, \quad 0 < \gamma < 1, \quad (4)$$

where $\Gamma(\cdot)$ is Euler's gamma function. In the limit case, $d_w \rightarrow 2$ and $d_f \rightarrow d$, (3) reduces to the standard d -dimensional diffusion equation.

The fractional calculus has been applied to many fields in science and engineering, such as viscoelasticity, anomalous diffusion, biology, chemistry, and control theory [5, 11–13, 15, 19–22]. Researches on the fractional differential equations attract much attention [15, 23–28]. For linear fractional differential equations, the integral transforms, including the

Laplace, Fourier, and Mellin transforms, are usually used to obtain analytic solutions.

In this paper using the similarity method [29] we solve (3) with the following initial and boundary conditions and the conservation condition:

$$\begin{aligned} p(r, 0) &= 0, \quad r > 0, \\ p(\infty, t) &= 0, \quad t > 0, \\ \omega(d_f) \int_0^\infty p(r, t) r^{d_f-1} dr &= 1, \end{aligned} \tag{5}$$

where $\omega(d_f)$ is a constant, which is defined as

$$\omega(d_f) = \frac{2\pi^{d_f/2}}{\Gamma(d_f/2)}. \tag{6}$$

We note that the probability density function $p(r, t)$ is just the fundamental solution of the fractional diffusion equation. The similarity method was used by Gorenflo et al. [30], Wyss [31], and Buckwar and Luchko [32] for solving problems of time fractional partial differential equations in one-dimensional case.

2. Derivation of Similarity Solution

First we determine a symmetric group of scaling transformations

$$T_\alpha : r = \alpha \bar{r}, \quad t = \alpha^h \bar{t}, \quad p = \alpha^l \bar{p}, \tag{7}$$

where $\alpha > 0$ is a parameter and h, l are constants to be determined. Applying the group of scaling transformations (7), the fractional derivative is converted as follows:

$$\begin{aligned} \frac{\partial^\gamma p(r, t)}{\partial t^\gamma} &= \alpha^l \frac{\partial}{\partial t} \int_0^t \frac{(t-\tau)^{-\gamma}}{\Gamma(1-\gamma)} \bar{p}(\bar{r}, \alpha^{-h}\tau) d\tau \\ &= \alpha^{l-h\gamma} \frac{\partial}{\partial \bar{t}} \int_0^{\bar{t}} \frac{(\bar{t}-\tau')^{-\gamma}}{\Gamma(1-\gamma)} \bar{p}(\bar{r}, \tau') d\tau' \\ &= \alpha^{l-h\gamma} \frac{\partial^\gamma \bar{p}(\bar{r}, \bar{t})}{\partial \bar{t}^\gamma}, \end{aligned} \tag{8}$$

where $\tau' = \alpha^{-h}\tau$. Hence the problem (3)–(5) is invariant under the group (7) if and only if

$$h = \frac{2}{\gamma}, \quad l = -d_f. \tag{9}$$

So the symmetric group of scaling transformations is determined:

$$T_\alpha : r = \alpha \bar{r}, \quad t = \alpha^{2/\gamma} \bar{t}, \quad p = \alpha^{-d_f} \bar{p}. \tag{10}$$

Eliminating the parameter α leads to two invariants:

$$r t^{-\gamma/2} = \bar{r} \bar{t}^{-\gamma/2}, \quad r^{d_f} p = \bar{r}^{d_f} \bar{p}. \tag{11}$$

We denote the two invariants of the group of the scaling transformation T_α as

$$\eta = r t^{-\gamma/2}, \quad F = r^{d_f} p. \tag{12}$$

Next we use the transformation

$$p(r, t) = r^{-d_f} F(\eta), \quad \eta = r t^{-\gamma/2} \tag{13}$$

to determine the equations for the similarity solution of the problem (3)–(5). Calculating derivative we have

$$\begin{aligned} \frac{\partial p}{\partial r} &= -d_f r^{-d_f-1} F(\eta) + r^{-d_f} t^{-\gamma/2} F'(\eta), \\ \frac{1}{r^{d_s-1}} \frac{\partial}{\partial r} \left(r^{d_s-1} \frac{\partial p}{\partial r} \right) &= r^{-d_f} t^{-\gamma} F''(\eta) + \Delta_1 r^{-d_f-1} t^{-\gamma/2} F'(\eta) \\ &\quad + \Delta_2 r^{-d_f-2} F(\eta), \end{aligned} \tag{14}$$

where

$$\Delta_1 = d_s - 1 - 2d_f, \quad \Delta_2 = d_f(d_f - d_s + 2). \tag{16}$$

For the left hand side of (3), we introduce the new integral variable

$$\xi = r \tau^{-\gamma/2}, \tag{17}$$

we obtain $p(r, \tau) = r^{-d_f} F(\xi)$, and

$$\begin{aligned} \frac{\partial^\gamma p(r, t)}{\partial t^\gamma} &= \frac{\partial}{\partial t} \int_0^t \frac{(t-\tau)^{-\gamma}}{\Gamma(1-\gamma)} p(r, \tau) d\tau \\ &= -r^{2/\gamma-d_f-1} t^{-\gamma/2-1} \frac{d}{d\eta} \int_\eta^{+\infty} \frac{[(\eta/\xi)^{-2/\gamma} - 1]^{-\gamma}}{\Gamma(1-\gamma)} \\ &\quad \times F(\xi) \xi^{1-2/\gamma} d\xi. \end{aligned} \tag{18}$$

Letting

$$g(w) = \begin{cases} \frac{(w^{-2/\gamma} - 1)^{-\gamma}}{\Gamma(1-\gamma)}, & 0 < w < 1, \\ 0, & w > 1, \end{cases} \tag{19}$$

we rewrite (18) as

$$\frac{\partial^\gamma p(r, t)}{\partial t^\gamma} = -r^{2/\gamma-d_f-1} t^{-2/\gamma-1} \frac{d}{d\eta} \int_0^{+\infty} g\left(\frac{\eta}{\xi}\right) F(\xi) \xi^{1-2/\gamma} d\xi. \tag{20}$$

From (15) and (20), we obtain the integro-ordinary differential equation for the similarity variables:

$$\begin{aligned} -\frac{d}{d\eta} \int_0^{+\infty} g\left(\frac{\eta}{\xi}\right) F(\xi) \xi^{-2/\gamma+1} d\xi \\ = \eta^{-2/\gamma+1} F''(\eta) + \Delta_1 \eta^{-2/\gamma} F'(\eta) + \Delta_2 \eta^{-2/\gamma-1} F(\eta). \end{aligned} \tag{21}$$

The conditions (5) are converted to

$$F(+\infty) = 0, \quad \omega(d_f) \int_0^{+\infty} F(\eta) \eta^{-1} d\eta = 1. \tag{22}$$

Considering the integration in (21), we use Mellin transforms for the new problem (21) and (22). The Mellin transform of function $f(x)$ is defined as [33]

$$\hat{f}(s) = \mathcal{M}[f(x), s] = \int_0^{+\infty} f(x) x^{s-1} dx. \tag{23}$$

Applying Mellin transform with respect to η to both sides of (21), we get

$$(s-1) \hat{g}(s-1) \hat{F}\left(s - \frac{2}{\gamma} + 1\right)$$

$$\begin{aligned}
 &= \left(\left(s - \frac{2}{\gamma} \right) \left(s - \frac{2}{\gamma} - 1 \right) - \Delta_1 \left(s - \frac{2}{\gamma} - 1 \right) + \Delta_2 \right) \\
 &\quad \times \widehat{F} \left(s - \frac{2}{\gamma} - 1 \right).
 \end{aligned} \tag{24}$$

Calculating integrations we obtain Mellin transform of the function $g(w)$:

$$\widehat{g}(s) = \frac{\Gamma(\gamma + \gamma s/2)}{s\Gamma(\gamma s/2)}. \tag{25}$$

Inserting (25) into (24) and then replacing s by $s + 2/\gamma + 1$ we obtain the difference equation for the function $\widehat{F}(s)$:

$$\frac{\Gamma(\gamma(s/2 + 1/\gamma + 1))}{\Gamma(\gamma(s/2 + 1/\gamma))} \widehat{F}(s + 2) = (s^2 + s - \Delta_1 s + \Delta_2) \widehat{F}(s). \tag{26}$$

In order to solve the difference equation, we introduce $s = 2q$ and $\widehat{F}(2q) = T(q)$, and rewrite (26) into

$$\frac{T(q + 1)}{T(q)} = 4 \left(q + \frac{d_f}{2} \right) \left(q + 1 + \frac{d_f - d_s}{2} \right) \frac{\Gamma(\gamma q + 1)}{\Gamma(\gamma q + \gamma + 1)}. \tag{27}$$

A particular solution of (27) is

$$T(q) = C \frac{4^q \Gamma(q + d_f/2) \Gamma(q + 1 + (d_f - d_s)/2)}{\Gamma(\gamma q + 1)}, \tag{28}$$

where C is an arbitrary constant. For the solution of (27), we can multiply $T(q)$ by any function $Y(q)$ which satisfies $Y(q + 1)/Y(q) = 1$.

We notice that $\widehat{F}(s)$ is a Mellin transform defined only in some strip $0 \leq \sigma_1 < \text{Re}(s) < \sigma_2$ from the conditions (22). So (26) is valid only in the overlap of the two strips $\sigma_1 < \text{Re}(s) < \sigma_2$ and $\sigma_1 < \text{Re}(s + 2) < \sigma_2$, and there is no such overlap unless $\sigma_1 + 2 < \sigma_2$. Thus $Y(q)$ cannot have poles; otherwise, it would have a row of poles separated exactly by one unit. In addition, $Y(q)$ cannot grow faster than $|q|$ as $\text{Im}(q) \rightarrow \infty$ in the inversion strip; otherwise the inversion integral would diverge. Thus $Y(q)$ is a bounded entire function and equals a constant by Liouville's theorem.

Therefore, $T(q)$ has only the form of (28) and we have

$$\begin{aligned}
 \widehat{F}(s) &= T \left(\frac{s}{2} \right) \\
 &= C \frac{2^s \Gamma(d_f/2 + s/2) \Gamma(1 + (d_f - d_s)/2 + s/2)}{\Gamma(1 + \gamma s/2)}.
 \end{aligned} \tag{29}$$

It follows from (22) that $\widehat{F}(0) = 1/\omega(d_f)$. Thus we have

$$C = \frac{1}{\omega(d_f) \Gamma(d_f/2) \Gamma(1 + (d_f - d_s)/2)}. \tag{30}$$

The inverse Mellin transform of (29) is

$$\begin{aligned}
 F(\eta) &= \frac{C}{2\pi i} \int_{c-i\infty}^{c+i\infty} \frac{2^s \Gamma(d_f/2 + s/2) \Gamma(1 + (d_f - d_s)/2 + s/2)}{\Gamma(1 + \gamma s/2)} \\
 &\quad \times \eta^{-s} ds.
 \end{aligned} \tag{31}$$

Replacing s by $-s$ and using the definition of Fox functions we obtain [34, 35]

$$F(\eta) = CH_{1,2}^{2,0} \left(\frac{\eta^{(1,\gamma/2)}}{2 \Gamma(d_f/2, 1/2)_{(1+(d_f-d_s)/2, 1/2)}} \right). \tag{32}$$

Inserting the expressions into (13) and using properties of Fox functions, we obtain the probability density function in terms of the Fox function:

$$\begin{aligned}
 p(r, t) &= \frac{d_w 2^{-d_f} t^{-d_f/d_w}}{\omega(d_f) \Gamma(d_f/2) \Gamma(1 + d_f/2 - d_f/d_w)} \\
 &\quad \times H_{1,2}^{2,0} \left(\frac{r^{d_w}}{2^{d_w} t} \middle|_{(0, d_w/2), (1-d_f/d_w, d_w/2)} \right).
 \end{aligned} \tag{33}$$

For a large class of fractal structures, the spectral dimension [2] satisfies $d_s < 2$; that is, $d_f < d_w$. So the Fox function in (33) can be expanded into a series by using residue theorem on the simple poles:

$$P_a = \left\{ \frac{2k}{d_w} \mid k=0, 1, \dots \right\} \cup \left\{ \frac{2}{d_w} \left(1 - \frac{d_f}{d_w} + k \right) \mid k=0, 1, \dots \right\}. \tag{34}$$

The series representation for the probability density is calculated to be

$$\begin{aligned}
 p(r, t) &= \frac{2^{1-d_f} t^{-d_f/d_w}}{\omega(d_f) \Gamma(d_f/2) \Gamma(1 + d_f/2 - d_f/d_w)} \\
 &\quad \times \sum_{k=0}^{\infty} \frac{(-1)^k}{k!} \times \left[\frac{\Gamma(1 - d_f/d_w - k)}{\Gamma(1 - d_f/d_w - 2k/d_w)} \left(\frac{r^{d_w}}{2^{d_w} t} \right)^{2k/d_w} \right. \\
 &\quad \left. + \frac{\Gamma(d_f/d_w - 1 - k)}{\Gamma(1 - d_f/d_w - 2/d_w (1 - d_f/d_w + k))} \right. \\
 &\quad \left. \times \left(\frac{r^{d_w}}{2^{d_w} t} \right)^{2/d_w (1 - d_f/d_w + k)} \right].
 \end{aligned} \tag{35}$$

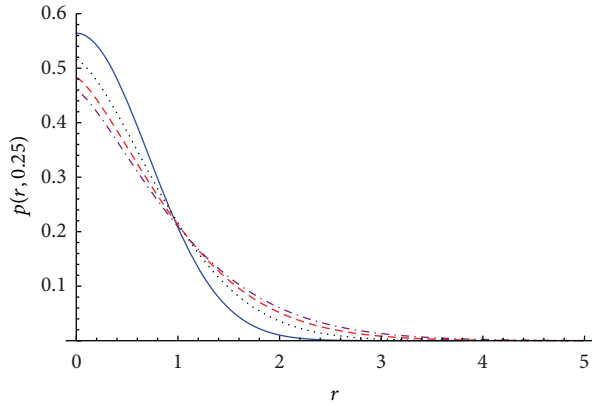


FIGURE 1: Curves of $p(r, 0.25)$ versus r for $d_f = 1$ and for $d_w = 2$ (solid line), $d_w = 2.5$ (dot line), $d_w = 3$ (dash line), and $d_w = 3.5$ (dot-dash line).

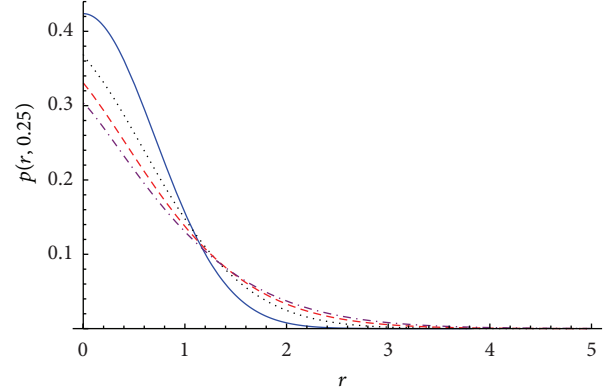


FIGURE 3: Curves of $p(r, 0.25)$ versus r for $d_f = 1.5$ and for $d_w = 2$ (solid line), $d_w = 2.5$ (dot line), $d_w = 3$ (dash line), and $d_w = 3.5$ (dot-dash line).

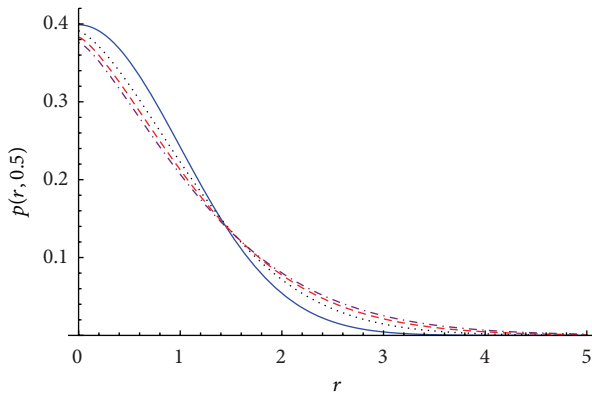


FIGURE 2: Curves of $p(r, 0.5)$ versus r for $d_f = 1$ and for $d_w = 2$ (solid line), $d_w = 2.5$ (dot line), $d_w = 3$ (dash line), and $d_w = 3.5$ (dot-dash line).

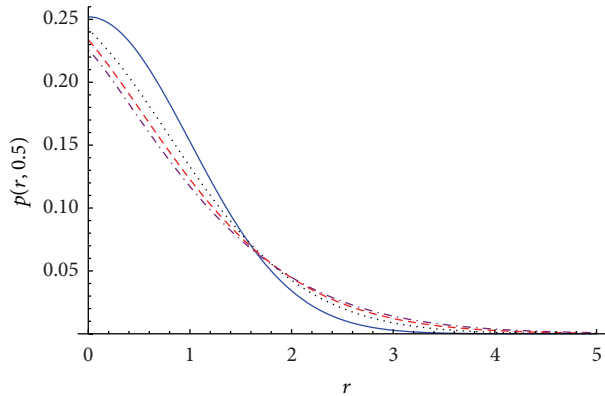


FIGURE 4: Curves of $p(r, 0.5)$ versus r for $d_f = 1.5$ and for $d_w = 2$ (solid line), $d_w = 2.5$ (dot line), $d_w = 3$ (dash line), and $d_w = 3.5$ (dot-dash line).

3. Discussions and Conclusions

In the limit case, $d_w \rightarrow 2$ and $d_f \rightarrow d$, (3) reduces to the d -dimensional standard diffusion equation, and the probability density (35) is simplified to the Gaussian distribution:

$$p(r, t) = \frac{1}{(4\pi t)^{d/2}} \exp\left(-\frac{r^2}{4t}\right). \quad (36)$$

In Figures 1 and 2, we plot the curves of $p(r, 0.25)$ versus r and $p(r, 0.5)$ versus r , respectively, for $d_f = 1$ and different values of d_w . In Figures 3 and 4, we plot the curves of $p(r, 0.25)$ versus r and $p(r, 0.5)$ versus r , respectively, for $d_f = 1.5$ and different values of d_w . The figures display that, as the anomalous diffusion exponent d_w increases, the peak value of the probability density function $p(r, t)$ at $r = 0$ decreases. In addition, as the fractal Hausdorff dimension d_f increases from 1 to 1.5, the peak value of $p(r, t)$ at $r = 0$ decreases.

Compared with the similarity method for classic partial differential equations, the similarity method for fractional diffusion equation involves the similarity integral variable $\xi = r\tau^{-\gamma/2}$, and the reduction equation is an integro-ordinary differential equation for the similarity solution. The obtained

probability density $p(r, t)$ is just the fundamental solution of the fractional diffusion equation.

Conflict of Interests

The authors declare that there is no conflict of interests regarding the publication of this paper.

Acknowledgments

This work was supported by the National Natural Science Foundation of China (11201308) and the Innovation Program of Shanghai Municipal Education Commission (14ZZ161).

References

- [1] B. B. Mandelbrot, *The Fractal Geometry of Nature*, W. H. Freeman, New York, NY, USA, 1982.
- [2] S. Havlin and D. Ben-Avraham, "Diffusion in disordered media," *Advances in Physics*, vol. 51, no. 1, pp. 187–292, 2002.
- [3] D. Liu, H. Li, F. Chang, and L. Lin, "Anomalous diffusion on the percolating networks," *Fractals*, vol. 6, no. 2, pp. 139–144, 1998.

- [4] F.-Y. Ren, J.-R. Liang, and X.-T. Wang, "The determination of the diffusion kernel on fractals and fractional diffusion equation for transport phenomena in random media," *Physics Letters A*, vol. 252, no. 3-4, pp. 141-150, 1999.
- [5] Q. Zeng and H. Li, "Diffusion equation for disordered fractal media," *Fractals*, vol. 8, no. 1, pp. 117-121, 2000.
- [6] C. Cattani, "Fractals and hidden symmetries in DNA," *Mathematical Problems in Engineering*, vol. 2010, Article ID 507056, 31 pages, 2010.
- [7] M. Li and W. Zhao, "On bandlimitedness and lag-limitedness of fractional Gaussian noise," *Physica A*, vol. 392, no. 9, pp. 1955-1961, 2013.
- [8] M. Li, "A class of negatively fractal dimensional Gaussian random functions," *Mathematical Problems in Engineering*, vol. 2011, Article ID 291028, 18 pages, 2011.
- [9] M. Li, C. Cattani, and S.-Y. Chen, "Viewing sea level by a one-dimensional random function with long memory," *Mathematical Problems in Engineering*, vol. 2011, Article ID 654284, 13 pages, 2011.
- [10] C. Cattani and G. Pierro, "On the fractal geometry of DNA by the binary image analysis," *Bulletin of Mathematical Biology*, vol. 75, no. 9, pp. 1544-1570, 2013.
- [11] R. Metzler and J. Klafter, "The random walk's guide to anomalous diffusion: a fractional dynamics approach," *Physics Reports*, vol. 339, no. 1, pp. 1-77, 2000.
- [12] M. Giona and H. E. Roman, "Fractional diffusion equation for transport phenomena in random media," *Physica A*, vol. 185, no. 1-4, pp. 87-97, 1992.
- [13] R. Metzler, W. G. Glöckle, and T. F. Nonnenmacher, "Fractional model equation for anomalous diffusion," *Physica A*, vol. 211, no. 1, pp. 13-24, 1994.
- [14] S. G. Samko, A. A. Kilbas, and O. I. Marichev, *Fractional Integrals and Derivatives*, Gordon and Breach, Amsterdam, The Netherlands, 1993.
- [15] I. Podlubny, *Fractional Differential Equations*, Academic Press, San Diego, Calif, USA, 1999.
- [16] K. B. Oldham and J. Spanier, *The Fractional Calculus*, Academic Press, New York, NY, USA, 1974.
- [17] D. Baleanu, K. Diethelm, E. Scalas, and J. J. Trujillo, *Fractional Calculus: Models and Numerical Methods*, Series on Complexity, Nonlinearity and Chaos, World Scientific, Boston, Mass, USA, 2012.
- [18] K. S. Miller and B. Ross, *An Introduction to the Fractional Calculus and Fractional Differential Equations*, John Wiley & Sons, New York, NY, USA, 1993.
- [19] A. A. Kilbas, H. M. Srivastava, and J. J. Trujillo, *Theory and Applications of Fractional Differential Equations*, Elsevier, Amsterdam, The Netherlands, 2006.
- [20] F. Mainardi, *Fractional Calculus and Waves in Linear Viscoelasticity*, Imperial College Press, London, UK, 2010.
- [21] M. Y. Xu and W. C. Tan, "Theoretical analysis of the velocity field, stress field and vortex sheet of generalized second order fluid with fractional anomalous diffusion," *Science in China A*, vol. 44, no. 11, pp. 1387-1399, 2001.
- [22] C. P. Li, W. H. Deng, and D. Xu, "Chaos synchronization of the Chua system with a fractional order," *Physica A*, vol. 360, no. 2, pp. 171-185, 2006.
- [23] J.-S. Duan, "Time- and space-fractional partial differential equations," *Journal of Mathematical Physics*, vol. 46, no. 1, Article ID 013504, pp. 13504-13511, 2005.
- [24] J.-S. Duan, "The periodic solution of fractional oscillation equation with periodic input," *Advances in Mathematical Physics*, vol. 2013, Article ID 869484, 6 pages, 2013.
- [25] J. S. Duan, R. Rach, D. Baleanu, and A. M. Wazwaz, "A review of the Adomian decomposition method and its applications to fractional differential equations," *Communications in Fractional Calculus*, vol. 3, no. 2, pp. 73-99, 2012.
- [26] F. Liu, P. Zhuang, V. Anh, I. Turner, and K. Burrage, "Stability and convergence of the difference methods for the space-time fractional advection-diffusion equation," *Applied Mathematics and Computation*, vol. 191, no. 1, pp. 12-20, 2007.
- [27] Z. H. Wang and X. Wang, "General solution of the Bagley-Torvik equation with fractional-order derivative," *Communications in Nonlinear Science and Numerical Simulation*, vol. 15, no. 5, pp. 1279-1285, 2010.
- [28] A. M. Yang, C. Cattani, H. Jafari, and X. J. Yang, "Analytical solutions of the onedimensional heat equations arising in fractal transient conduction with local fractional derivative," *Abstract and Applied Analysis*, vol. 2013, Article ID 462535, 5 pages, 2013.
- [29] G. W. Bluman and S. C. Anco, *Symmetry and Integration Methods for Differential Equations*, Springer, New York, NY, USA, 2002.
- [30] R. Gorenflo, Y. Luchko, and F. Mainardi, "Wright functions as scale-invariant solutions of the diffusion-wave equation," *Journal of Computational and Applied Mathematics*, vol. 118, no. 1-2, pp. 175-191, 2000.
- [31] W. Wyss, "The fractional diffusion equation," *Journal of Mathematical Physics*, vol. 27, no. 11, pp. 2782-2785, 1986.
- [32] E. Buckwar and Y. Luchko, "Invariance of a partial differential equation of fractional order under the Lie group of scaling transformations," *Journal of Mathematical Analysis and Applications*, vol. 227, no. 1, pp. 81-97, 1998.
- [33] B. Davies, *Integral Transforms and Their Applications*, Springer, New York, NY, USA, 3rd edition, 2002.
- [34] A. M. Mathai and R. K. Saxena, *The H-Function with Applications in Statistics and Other Disciplines*, John Wiley & Sons, New Delhi, India, 1978.
- [35] H. M. Srivastava, K. C. Gupta, and S. P. Goyal, *The H-Functions of One and Two Variables with Applications*, South Asian, New Delhi, India, 1982.

Research Article

On the (p, q) th Relative Order Oriented Growth Properties of Entire Functions

Luis Manuel Sánchez Ruiz,¹ Sanjib Kumar Datta,²
Tanmay Biswas,³ and Golok Kumar Mondal⁴

¹ ETSID, Departamento de Matemática Aplicada & CITG, Universitat Politècnica de València, 46022 Valencia, Spain

² Department of Mathematics, University of Kalyani, Kalyani, District Nadia, West Bengal 741235, India

³ Rajbari, Rabindrapalli, R. N. Tagore Road, P.O.-Krishnagar, District Nadia, West Bengal 741101, India

⁴ Dhulauri Rabindra Vidyaniketan (H.S.), Vill +P.O. Dhulauri, P.S. Domkal, District Murshidabad, West Bengal 742308, India

Correspondence should be addressed to Luis Manuel Sánchez Ruiz; lmsr@mat.upv.es

Received 24 November 2013; Accepted 25 January 2014; Published 11 March 2014

Academic Editor: Carlo Cattani

Copyright © 2014 Luis Manuel Sánchez Ruiz et al. This is an open access article distributed under the Creative Commons Attribution License, which permits unrestricted use, distribution, and reproduction in any medium, provided the original work is properly cited.

The relative order of growth gives a quantitative assessment of how different functions scale each other and to what extent they are self-similar in growth. In this paper for any two positive integers p and q , we wish to introduce an alternative definition of relative (p, q) th order which improves the earlier definition of relative (p, q) th order as introduced by Lahiri and Banerjee (2005). Also in this paper we discuss some growth rates of entire functions on the basis of the improved definition of relative (p, q) th order with respect to another entire function and extend some earlier concepts as given by Lahiri and Banerjee (2005), providing some examples of entire functions whose growth rate can accordingly be studied.

1. Introduction

A single valued function of one complex variable which is analytic in the finite complex plane is called an integral (entire) function. For example, \exp , \sin , \cos , and so forth are all entire functions. In 1926 Rolf Nevanlinna initiated the value distribution theory of entire functions which is a prominent branch of Complex Analysis and is the prime concern of this paper. Perhaps the Fundamental Theorem of Classical Algebra which states that “If f is a polynomial of degree n with real or complex coefficients, then the equation $f(z) = 0$ has at least one root” is the most well known value distribution theorem, and consequently any such given polynomial can take any given, real or complex, value. In the value distribution theory one studies how an entire function assumes some values and, conversely, what is the influence in some specific manner of taking certain values on a function. It also deals with various aspects of the behavior of entire functions, one of which is the study of their comparative growth.

For any entire function f , the so-called maximum modulus function, denoted by M_f , is defined on each nonnegative real value r as

$$M_f(r) = \max_{|z|=r} |f(z)|. \quad (1)$$

And given two entire functions f and g the ratio $M_f(r)/M_g(r)$ as $r \rightarrow \infty$ is called the growth of f with respect to g in terms of their maximum moduli.

The *order* of an entire function f which is generally used in computational purpose is defined in terms of the growth of f with respect to the exponential function as

$$\rho_f = \limsup_{r \rightarrow \infty} \frac{\log \log M_f(r)}{\log \log M_{\exp z}(r)} = \limsup_{r \rightarrow \infty} \frac{\log \log M_f(r)}{\log(r)}. \quad (2)$$

Bernal [1, 2] introduced the relative order between two entire functions to avoid comparing growth just with $\exp z$. Extending the notion of relative order as cited in the

reference, in this paper we extend some results related to the growth rates of entire functions on the basis of avoiding some restriction, introducing a new type of relative order (p, q) , and revisiting ideas developed by a number of authors including Lahiri and Banerjee [3].

2. Notation and Preliminary Remarks

Our notation is standard within the theory of Nevanlinna's value distribution of entire functions. For short, given a real function h and whenever the corresponding domain and range allow it, we will use the notation

$$h^{[0]}(x) = x, \tag{3}$$

$$h^{[k]}(x) = h(h^{[k-1]}(x)) \quad \text{for } k = 1, 2, 3, \dots$$

omitting the parenthesis when h happens to be the log or exp function. Taking this into account the *order* (resp., *lower order*) of an entire function f is given by

$$\rho_f = \limsup_{r \rightarrow \infty} \frac{\log^{[2]} M_f(r)}{\log r}, \tag{4}$$

$$\left(\text{resp. } \lambda_f = \liminf_{r \rightarrow \infty} \frac{\log^{[2]} M_f(r)}{\log r} \right).$$

Let us recall that Juneja et al. [4] defined the order (p, q) and lower order (p, q) of an entire function f , respectively, as follows:

$$\rho_f(p, q) = \limsup_{r \rightarrow \infty} \frac{\log^{[p]} M_f(r)}{\log^{[q]} r}, \tag{5}$$

$$\lambda_f(p, q) = \liminf_{r \rightarrow \infty} \frac{\log^{[p]} M_f(r)}{\log^{[q]} r},$$

where p, q are any two positive integers with $p \geq q$. These definitions extended the generalized order $\rho_f^{[l]}$ and generalized lower order $\lambda_f^{[l]}$ of an entire function f considered in [5] for each integer $l \geq 2$ since these correspond to the particular case $\rho_f^{[l]} = \rho_f(l, 1)$ and $\lambda_f^{[l]} = \lambda_f(l, 1)$. Clearly $\rho_f(2, 1) = \rho_f$ and $\lambda_f(2, 1) = \lambda_f$.

In this connection let us recall that if $0 < \rho_f(p, q) < \infty$, then the following properties hold:

$$\begin{aligned} \rho_f(p - n, q) &= \infty, & \text{for } n < p, \\ \rho_f(p, q - n) &= 0, & \text{for } n < q, \\ \rho_f(p + n, q + n) &= 1, & \text{for } n = 1, 2, \dots \end{aligned} \tag{6}$$

Similarly for $0 < \lambda_f(p, q) < \infty$, one can easily verify that

$$\begin{aligned} \lambda_f(p - n, q) &= \infty, & \text{for } n < p, \\ \lambda_f(p, q - n) &= 0, & \text{for } n < q, \\ \lambda_f(p + n, q + n) &= 1, & \text{for } n = 1, 2, \dots \end{aligned} \tag{7}$$

Recalling that for any pair of integer numbers m, n the Kronecker function is defined by $\delta_{m,n} = 1$ for $m = n$ and $\delta_{m,n} = 0$ for $m \neq n$, the aforementioned properties provide the following definition.

Definition 1 (see [4]). An entire function f is said to have index-pair $(1, 1)$ if $0 < \rho_f(1, 1) < \infty$. Otherwise, f is said to have index-pair $(p, q) \neq (1, 1)$, $p \geq q \geq 1$, if $\delta_{p-q,0} < \rho_f(p, q) < \infty$ and $\rho_f(p - 1, q - 1) \notin \mathbb{R}^+$.

Definition 2 (see [4]). An entire function f is said to have lower index-pair $(1, 1)$ if $0 < \lambda_f(1, 1) < \infty$. Otherwise, f is said to have lower index-pair $(p, q) \neq (1, 1)$, $p \geq q \geq 1$, if $\delta_{p-q,0} < \lambda_f(p, q) < \infty$ and $\lambda_f(p - 1, q - 1) \notin \mathbb{R}^+$.

An entire function f of index-pair (p, q) is said to be of regular (p, q) -growth if its (p, q) th order coincides with its (p, q) th lower order; otherwise f is said to be of irregular (p, q) -growth.

Given a nonconstant entire function f defined in the open complex plane \mathbb{C} its maximum modulus function M_f is strictly increasing and continuous. Hence there exists its inverse function $M_f^{-1} : (|f(0)|, \infty) \rightarrow (0, \infty)$ with $\lim_{s \rightarrow \infty} M_f^{-1}(s) = \infty$.

Then Bernal [1, 2] introduced the definition of relative order of f with respect to g , denoted by $\rho_g(f)$ as follows:

$$\begin{aligned} \rho_g(f) &= \inf \{ \mu > 0 : M_f(r) < M_g(r^\mu), \forall r > r_0(\mu) > 0 \} \\ &= \limsup_{r \rightarrow \infty} \frac{\log M_g^{-1} M_f(r)}{\log r}. \end{aligned} \tag{8}$$

This definition coincides with the classical one [6] if $g = \exp z$. Similarly one can define the relative lower order of f with respect to g denoted by $\lambda_g(f)$ as

$$\lambda_g(f) = \liminf_{r \rightarrow \infty} \frac{\log M_g^{-1} M_f(r)}{\log r}. \tag{9}$$

Lahiri and Banerjee [7] gave a more generalized concept of relative order in the following way.

Definition 3 (see [7]). If $k \geq 1$ is a positive integer, then the k th generalized relative order of f with respect to g , denoted by $\rho_g^k(f)$, is defined by

$$\begin{aligned} \rho_g^k(f) &= \inf \{ \mu > 0 : M_f(r) < M_g(\exp^{[k-1]} r^\mu), \\ &\quad \forall r > r_0(\mu) > 0 \} \\ &= \limsup_{r \rightarrow \infty} \frac{\log^{[k]} M_g^{-1} M_f(r)}{\log r}. \end{aligned} \tag{10}$$

Clearly, $\rho_g^1(f) = \rho_g(f)$ and $\rho_{\exp z}^1(f) = \rho_f$.

In the case of relative order, it was then natural for Lahiri and Banerjee [3] to define the relative (p, q) th order of entire functions as follows.

Definition 4 (see [3]). Let p and q be any two positive integers with $p > q$. The relative (p, q) th order of f with respect to g is defined by

$$\begin{aligned} \rho_g^{(p,q)}(f) &= \inf \{ \mu > 0 : M_f(r) < M_g(\exp^{[p-1]}(\mu \log^{[q]} r)) \}, \\ &\quad \forall r > r_0(\mu) > 0 \} \\ &= \limsup_{r \rightarrow \infty} \frac{\log^{[p-1]} M_g^{-1} M_f(r)}{\log^{[q]} r}. \end{aligned} \tag{11}$$

Then $\rho_{\exp z}^{(p,q)}(f) = \rho_f(p, q)$ and $\rho_g^{(k+1,1)}(f) = \rho_g^k(f)$ for any $k \geq 1$.

In this paper we give an alternative definition of (p, q) th relative order $\rho_g^{(p,q)}(f)$ of an entire function f with respect to another entire function g , in the light of index-pair. Our next definition avoids the restriction $p > q$ and gives the more natural particular case $\rho_g^{(k,1)}(f) = \rho_g^k(f)$.

Definition 5. Let f and g be any two entire functions with index-pair (m, q) and (m, p) , respectively, where p, q, m are positive integers such that $m \geq \max(p, q)$. Then the (p, q) th relative order of f with respect to g is defined as

$$\rho_g^{(p,q)}(f) = \limsup_{r \rightarrow \infty} \frac{\log^{[p]} M_g^{-1} M_f(r)}{\log^{[q]} r}. \tag{12}$$

The (p, q) th relative lower order of f with respect to g is defined by

$$\lambda_g^{(p,q)}(f) = \liminf_{r \rightarrow \infty} \frac{\log^{[p]} M_g^{-1} M_f(r)}{\log^{[q]} r}. \tag{13}$$

The previous definitions are easily generated as particular cases; for example, if f and g have got index-pair $(m, 1)$ and (m, k) , respectively, then Definition 5 reduces to Definition 3. If the entire functions f and g have the same index-pair $(p, 1)$, where p is any positive integer, we get the definition of relative order introduced by Bernal [1] and if $g = \exp^{[m-1]} z$, then $\rho_g(f) = \rho_f^{[m]}$ and $\rho_g^{(p,q)}(f) = \rho_f(m, q)$. And if f is an entire function with index-pair $(2, 1)$ and $g = \exp z$, then Definition 5 becomes the classical one given in [6].

3. Some Examples

In this section we present some examples of entire functions in connection with definitions given in the previous section.

Example 6 (order of exp). Given any natural number n , the exponential function $f(z) = \exp z^n$ has got $M_f(r) = \exp r^n$, and therefore $\log^{[2]} M_f(r) / \log r$ is constantly equal to n and, consequently,

$$\rho_f = \lambda_f = n. \tag{14}$$

Example 7 (generalized order). Given any natural numbers k, n , the function $f(z) = \exp^{[k]} z^n$ has got $M_f(r) = \exp^{[k]} r^n$. Therefore $\log^{[k]} M_f(r) / \log r$ is constantly equal to n for each natural $k \geq 2$, following that

$$\rho_f^{[k+1]} = \lambda_f^{[k+1]} = n. \tag{15}$$

Note that $\rho_f^{[l]} = \lambda_f^{[l]} = +\infty$ for $2 \leq l \leq k$ and $\rho_f^{[l]} = \lambda_f^{[l]} = 0$ for $l > k + 1$.

Example 8 (index-pair). Given any four positive integers k, n, p, q with $p \geq q$, then function $f(z) = \exp^{[k]} z^n$ generates a constant quotient $\log^{[p]} M_f(r) / \log^{[q]} r$, and clearly

$$\rho_f(p, q) = \lambda_f(p, q) = n, \quad \text{for } (p, q) = (k + 1, 1) \tag{16}$$

but

$$\begin{aligned} \rho_f(p, q) &= \lambda_f(p, q) \\ &= \begin{cases} 1, & \forall (p, q) \text{ such that } p = q + k, q > 1, \\ \infty, & \forall (p, q) \text{ such that } p < q + k, \\ 0, & \forall (p, q) \text{ such that } p > q + k. \end{cases} \end{aligned} \tag{17}$$

Thus f is a regular function with growth $(k + 1, 1)$.

Example 9 (regular function of growth (1,1)). Given any positive integer n , and nonnull real number a , the power function $f(z) = az^n$ generates a constant quotient $\log^{[p]} M_f(r) / \log^{[q]} r$, and clearly

$$\rho_f(p, q) = \lambda_f(p, q) = n, \quad \text{for } (p, q) = (1, 1) \tag{18}$$

but

$$\begin{aligned} \rho_f(p, q) &= \lambda_f(p, q) \\ &= \begin{cases} 1, & \forall (p, q) \text{ such that } p = q, q > 1, \\ \infty, & \forall (p, q) \text{ such that } p < q, \\ 0, & \forall (p, q) \text{ such that } p > q. \end{cases} \end{aligned} \tag{19}$$

Thus f is a regular function with growth $(1, 1)$.

Example 10 (relative order between functions). From the above examples it follows that given the natural numbers m, n the functions

$$f(z) = \exp z^m, \quad g(z) = \exp z^n \tag{20}$$

are of regular growth $(2, 1)$. In order to find their relative order of growth we evaluate

$$\frac{\log M_g^{-1} M_f(r)}{\log r} = \frac{\log [\log [\exp r^m]]^{1/n}}{\log r}, \tag{21}$$

which happens to be constant. Its upper and lower limits provide

$$\rho_g(f) = \lambda_g(f) = \frac{m}{n}. \tag{22}$$

Example 11 (relative order (p, q) between functions). Let k, m, n be any three positive integers and let $f(z) = \exp^{[k]}z^m$ and $g = \exp^{[k]}z^n$. Then f and g are regular functions with $(k + 1, 1)$ -growth for which

$$\rho_f(k + 1, 1) = m, \quad \rho_g(k + 1, 1) = n. \quad (23)$$

In order to find out their $(1, 1)$ relative order we evaluate

$$\frac{\log M_g^{-1} M_f(r)}{\log r} = \frac{\log(1/n) \{ \log^{[k]}(\exp^{[k]}r^m) \}^{1/n}}{\log r}, \quad (24)$$

which happens to be constant. By taking limits, we easily get that

$$\rho_g^{(1,1)}(f) = \lambda_g^{(1,1)}(f) = \frac{m}{n}. \quad (25)$$

The orders obtained in the last two examples will be easy consequences of the results given in Section 4.

4. Results

In this section we state the main results of the paper. We include the proof of the first main theorem for the sake of completeness. The others are basically omitted since they are easily proven with the same techniques or with some easy reasoning.

Theorem 12. *Let f and g be any two entire functions with index-pair (m, q) and (m, p) , respectively, where p, q, m are all positive integers such that $m \geq p$ and $m \geq q$. Then*

$$\begin{aligned} \frac{\lambda_f(m, q)}{\rho_g(m, p)} &\leq \lambda_g^{(p,q)}(f) \leq \min \left\{ \frac{\lambda_f(m, q)}{\lambda_g(m, p)}, \frac{\rho_f(m, q)}{\rho_g(m, p)} \right\} \\ &\leq \max \left\{ \frac{\lambda_f(m, q)}{\lambda_g(m, p)}, \frac{\rho_f(m, q)}{\rho_g(m, p)} \right\} \leq \rho_g^{(p,q)}(f) \quad (26) \\ &\leq \frac{\rho_f(m, q)}{\lambda_g(m, p)}. \end{aligned}$$

Proof. From the definitions of $\rho_f(m, q)$ and $\lambda_f(m, q)$ we have for all sufficiently large values of r that

$$M_f(r) \leq \exp^{[m]} \{ (\rho_f(m, q) + \varepsilon) \log^{[q]} r \}, \quad (27)$$

$$M_f(r) \geq \exp^{[m]} \{ (\lambda_f(m, q) - \varepsilon) \log^{[q]} r \} \quad (28)$$

and also for a sequence of values of r tending to infinity we get that

$$M_f(r) \geq \exp^{[m]} \{ (\rho_f(m, q) - \varepsilon) \log^{[q]} r \}, \quad (29)$$

$$M_f(r) \leq \exp^{[m]} \{ (\lambda_f(m, q) + \varepsilon) \log^{[q]} r \}. \quad (30)$$

Similarly from the definitions of $\rho_g(m, p)$ and $\lambda_f(m, q)$ it follows for all sufficiently large values of r that

$$M_g(r) \leq \exp^{[m]} \{ (\rho_g(m, p) + \varepsilon) \log^{[p]} r \}$$

$$\text{i.e., } r \leq M_g^{-1} \left[\exp^{[m]} \{ (\rho_g(m, p) + \varepsilon) \log^{[p]} r \} \right] \quad (31)$$

$$\text{i.e., } M_g^{-1}(r) \geq \exp^{[p]} \left[\frac{\log^{[m]} r}{(\rho_g(m, p) + \varepsilon)} \right],$$

$$M_g(r) \geq \exp^{[m]} \{ (\lambda_g(m, p) - \varepsilon) \log^{[p]} r \}$$

$$\text{i.e., } M_g^{-1}(r) \leq \exp^{[p]} \left[\frac{\log^{[m]} r}{(\lambda_g(m, p) - \varepsilon)} \right] \quad (32)$$

and for a sequence of values of r tending to infinity we obtain that

$$M_g(r) \geq \exp^{[m]} \{ (\rho_g(m, p) - \varepsilon) \log^{[p]} r \}$$

$$\text{i.e., } M_g^{-1}(r) \leq \exp^{[p]} \left[\frac{\log^{[m]} r}{(\rho_g(m, p) - \varepsilon)} \right], \quad (33)$$

$$M_g(r) \leq \exp^{[m]} \{ (\lambda_g(m, p) + \varepsilon) \log^{[p]} r \}$$

$$\text{i.e., } M_g^{-1}(r) \geq \exp^{[p]} \left[\frac{\log^{[m]} r}{(\lambda_g(m, p) + \varepsilon)} \right]. \quad (34)$$

Now from (29) and in view of (31), for a sequence of values of r tending to infinity we get that

$$\log^{[p]} M_g^{-1} M_f(r)$$

$$\geq \log^{[p]} M_g^{-1} \left[\exp^{[m]} \{ (\rho_f(m, q) - \varepsilon) \log^{[q]} r \} \right]$$

$$\text{i.e., } \log^{[p]} M_g^{-1} M_f(r)$$

$$\geq \log^{[p]} \exp^{[p]} \left[\frac{\log^{[m]} \exp^{[m]} \{ (\rho_f(m, q) - \varepsilon) \log^{[q]} r \}}{(\rho_g(m, p) + \varepsilon)} \right]$$

$$= \frac{(\rho_f(m, q) - \varepsilon)}{(\rho_g(m, p) + \varepsilon)} \log^{[q]} r$$

$$\text{i.e., } \frac{\log^{[p]} M_g^{-1} M_f(r)}{\log^{[q]} r} \geq \frac{(\rho_f(m, q) - \varepsilon)}{(\rho_g(m, p) + \varepsilon)}.$$

$$(35)$$

As $\varepsilon(> 0)$ is arbitrary, it follows that

$$\rho_g^{(p,q)}(f) \geq \frac{\rho_f(m, q)}{\rho_g(m, p)}. \quad (36)$$

Analogously from (28) and in view of (34) it follows for a sequence of values of r tending to infinity that

$$\begin{aligned} & \log^{[p]} M_g^{-1} M_f(r) \\ & \geq \log^{[p]} M_g^{-1} \left[\exp^{[m]} \{ (\lambda_f(m, q) - \varepsilon) \log^{[q]} r \} \right] \\ \text{i.e., } & \log^{[p]} M_g^{-1} M_f(r) \\ & \geq \log^{[p]} \exp^{[p]} \left[\frac{\log^{[m]} \exp^{[m]} \{ (\lambda_f(m, q) - \varepsilon) \log^{[q]} r \}}{(\lambda_g(m, p) + \varepsilon)} \right] \\ & = \frac{(\lambda_f(m, q) - \varepsilon)}{(\lambda_g(m, p) + \varepsilon)} \log^{[q]} r \\ \text{i.e., } & \frac{\log^{[p]} M_g^{-1} M_f(r)}{\log^{[q]} r} \geq \frac{(\lambda_f(m, q) - \varepsilon)}{(\lambda_g(m, p) + \varepsilon)}. \end{aligned} \tag{37}$$

Since $\varepsilon(> 0)$ is arbitrary, we get from above that

$$\rho_g^{(p,q)}(f) \geq \frac{\lambda_f(m, q)}{\lambda_g(m, p)}. \tag{38}$$

Again in view of (32) we have from (27) for all sufficiently large values of r that

$$\begin{aligned} & \log^{[p]} M_g^{-1} M_f(r) \\ & \leq \log^{[p]} M_g^{-1} \left[\exp^{[m]} \{ (\rho_f(m, q) + \varepsilon) \log^{[q]} r \} \right] \\ \text{i.e., } & \log^{[p]} M_g^{-1} M_f(r) \\ & \leq \log^{[p]} \exp^{[p]} \left[\frac{\log^{[m]} \exp^{[m]} \{ (\rho_f(m, q) + \varepsilon) \log^{[q]} r \}}{(\lambda_g(m, p) - \varepsilon)} \right] \\ & = \frac{(\rho_f(m, q) + \varepsilon)}{(\lambda_g(m, p) - \varepsilon)} \log^{[q]} r \\ \text{i.e., } & \frac{\log^{[p]} M_g^{-1} M_f(r)}{\log^{[q]} r} \leq \frac{(\rho_f(m, q) + \varepsilon)}{(\lambda_g(m, p) - \varepsilon)}. \end{aligned} \tag{39}$$

Since $\varepsilon(> 0)$ is arbitrary, we obtain that

$$\rho_g^{(p,q)}(f) \leq \frac{\rho_f(m, q)}{\lambda_g(m, p)}. \tag{40}$$

Again from (28) and in view of (31) with the same reasoning we get that

$$\lambda_g^{(p,q)}(f) \geq \frac{\lambda_f(m, q)}{\rho_g(m, p)}. \tag{41}$$

Also in view of (33), we get from (27) for a sequence of values of r tending to infinity that

$$\begin{aligned} & \log^{[p]} M_g^{-1} M_f(r) \\ & \leq \log^{[p]} M_g^{-1} \left[\exp^{[m]} \{ (\rho_f(m, q) + \varepsilon) \log^{[q]} r \} \right] \\ \text{i.e., } & \log^{[p]} M_g^{-1} M_f(r) \\ & \leq \log^{[p]} \exp^{[p]} \left[\frac{\log^{[m]} \exp^{[m]} \{ (\rho_f(m, q) + \varepsilon) \log^{[q]} r \}}{(\rho_g(m, p) - \varepsilon)} \right] \\ & = \frac{(\rho_f(m, q) + \varepsilon)}{(\rho_g(m, p) - \varepsilon)} \log^{[q]} r \\ \text{i.e., } & \frac{\log^{[p]} M_g^{-1} M_f(r)}{\log^{[q]} r} \leq \frac{(\rho_f(m, q) + \varepsilon)}{(\rho_g(m, p) - \varepsilon)}. \end{aligned} \tag{42}$$

Since $\varepsilon(> 0)$ is arbitrary, we get from above that

$$\lambda_g^{(p,q)}(f) \leq \frac{\rho_f(m, q)}{\rho_g(m, p)}. \tag{43}$$

Similarly from (30) and in view of (32) it follows for a sequence of values of r tending to infinity that

$$\begin{aligned} & \log^{[p]} M_g^{-1} M_f(r) \\ & \leq \log^{[p]} M_g^{-1} \left[\exp^{[m]} \{ (\lambda_f(m, q) + \varepsilon) \log^{[q]} r \} \right] \\ \text{i.e., } & \log^{[p]} M_g^{-1} M_f(r) \\ & \leq \log^{[p]} \exp^{[p]} \left[\frac{\log^{[m]} \exp^{[m]} \{ (\lambda_f(m, q) + \varepsilon) \log^{[q]} r \}}{(\lambda_g(m, p) - \varepsilon)} \right] \\ & = \frac{(\lambda_f(m, q) + \varepsilon)}{(\lambda_g(m, p) - \varepsilon)} \log^{[q]} r \\ \text{i.e., } & \frac{\log^{[p]} M_g^{-1} M_f(r)}{\log^{[q]} r} \leq \frac{(\lambda_f(m, q) + \varepsilon)}{(\lambda_g(m, p) - \varepsilon)}. \end{aligned} \tag{44}$$

As $\varepsilon(> 0)$ is arbitrary, from above we obtain that

$$\lambda_g^{(p,q)}(f) \leq \frac{\lambda_f(m, q)}{\lambda_g(m, p)}. \tag{45}$$

The theorem follows from (36), (38), (40), (41), (43), and (45). \square

Corollary 13. Let f be an entire function with index-pair (m, q) and let g be an entire of regular (m, p) -growth, where p, q, m are all positive integers such that $m \geq p$ and $m \geq q$. Then

$$\lambda_g^{(p,q)}(f) = \frac{\lambda_f(m, q)}{\rho_g(m, p)}, \quad \rho_g^{(p,q)}(f) = \frac{\rho_f(m, q)}{\rho_g(m, p)}. \tag{46}$$

In addition, if $\rho_f(m, q) = \rho_g(m, p)$, then

$$\rho_g^{(p,q)}(f) = \lambda_f^{(q,p)}(g) = 1. \quad (47)$$

Remark 14. The first part of Corollary 13 improves [8, Theorem 2.1 and Theorem 2.2].

Corollary 15. Let f and g be any two entire functions with regular (m, q) -growth and regular (m, p) -growth, respectively, where p, q, m are all positive integers with $m \geq \max\{p, q\}$. Then

$$\lambda_g^{(p,q)}(f) = \rho_g^{(p,q)}(f) = \frac{\rho_f(m, q)}{\rho_g(m, p)}. \quad (48)$$

Corollary 16. Let f and g be any two entire functions with regular (m, q) th growth and regular (m, p) th growth, respectively, where p, q, m are all positive integers with $m \geq p$ and $m \geq q$. Also suppose that $\rho_f(m, q) = \rho_g(m, p)$. Then

$$\lambda_g^{(p,q)}(f) = \rho_g^{(p,q)}(f) = \lambda_f^{(q,p)}(g) = \rho_f^{(q,p)}(g) = 1. \quad (49)$$

Corollary 17. Let f and g be any two entire functions with regular growth (m, q) and (m, p) , respectively, where p, q, m are all positive integers such that $m \geq \max\{p, q\}$. Then

$$\rho_g^{(p,q)}(f) \cdot \rho_f^{(q,p)}(g) = \lambda_g^{(p,q)}(f) \cdot \lambda_f^{(q,p)}(g) = 1. \quad (50)$$

Corollary 18. Let f and g be any two entire functions with index-pair (m, q) and (m, p) , respectively, where p, q, m are all positive integers such that $m \geq p$ and $m \geq q$. If either f is not of regular (m, q) th growth or g is not of regular (m, p) th growth, then

$$\lambda_g^{(p,q)}(f) \cdot \lambda_f^{(q,p)}(g) < 1 < \rho_g^{(p,q)}(f) \cdot \rho_f^{(q,p)}(g). \quad (51)$$

Remark 19. Corollaries 17 and 18 can be regarded as an extension of the Corollaries of [8, Theorems 2.1 and 2.2].

Corollary 20. Let f be an entire function with index-pair (m, q) , where m, q are positive integers with $m \geq q$. Then for any entire function g ,

- (i) $\lambda_g^{(p,q)}(f) = \infty$ when $\rho_g(m, p) = 0$,
- (ii) $\rho_g^{(p,q)}(f) = \infty$ when $\lambda_g(m, p) = 0$,
- (iii) $\lambda_g^{(p,q)}(f) = 0$ when $\rho_g(m, p) = \infty$,
- (iv) $\rho_g^{(p,q)}(f) = 0$ when $\lambda_g(m, p) = \infty$,

where p is any positive integer with $m \geq p$.

Remark 21. The first part of Corollary 20 improves [8, Theorem 2.3].

Corollary 22. Let g be an entire function with index-pair (m, p) , where m, p are positive integers with $m \geq p$. Then for any entire function f ,

- (i) $\rho_g^{(p,q)}(f) = 0$ when $\rho_f(m, q) = 0$,

$$(ii) \lambda_g^{(p,q)}(f) = 0 \text{ when } \lambda_f(m, q) = 0,$$

$$(iii) \rho_g^{(p,q)}(f) = \infty \text{ when } \rho_f(m, q) = \infty,$$

$$(iv) \lambda_g^{(p,q)}(f) = \infty \text{ when } \lambda_f(m, q) = \infty,$$

where q is any positive integer such that $m \geq q$.

Example 23 (relative order between polynomials). To simplify let us consider any two given natural numbers m and n and $a \in \mathbb{R}, a \neq 0$, so that

$$f(z) = z^m, \quad g(z) = az^n. \quad (52)$$

Then

$$\rho_f(1, 1) = \lambda_f(1, 1) = m, \quad \rho_g(1, 1) = \lambda_g(1, 1) = n. \quad (53)$$

Now

$$\rho_g^{(1,1)}(f) = \lambda_g^{(1,1)}(f) = \frac{\rho_f(1, 1)}{\rho_g(1, 1)} = \frac{m}{n}. \quad (54)$$

Example 24 (relative order between exponentials of the same order). Let n be any natural number and a any positive real number and consider

$$f(z) = \exp z^n, \quad g(z) = \exp(az)^n. \quad (55)$$

In this case f and g are two entire functions with regular $(2, 1)$ growth; thus

$$\lambda_g^{(1,1)}(f) = \rho_g^{(1,1)}(f) = \frac{\rho_f(2, 1)}{\rho_g(2, 1)} = \frac{n}{n} = 1. \quad (56)$$

Clearly

$$\rho_f^{(1,1)}(g) = \lambda_f^{(1,1)}(g) = 1. \quad (57)$$

Example 25 (relative order between exponential and power function). Let m, n be any two natural numbers and consider

$$f = \exp z^m, \quad g = z^n. \quad (58)$$

Then

$$\rho_f = \lambda_f = m, \quad \rho_g = \lambda_g = 0. \quad (59)$$

Now

$$\begin{aligned} \rho_g^{(1,1)}(f) &= \lambda_g^{(1,1)}(f) = \infty, \\ \rho_f^{(1,1)}(g) &= \lambda_f^{(1,1)}(g) = 0. \end{aligned} \quad (60)$$

When f and g are any two entire functions with index-pair (m, q) and (n, p) , respectively, where p, q, m, n are all positive integers such that $m \geq q$ and $n \geq p$, but $m \neq n$, the next definition enables studying their relative order.

Definition 26. Let f and g be any two entire functions with index-pair (m, q) and (n, p) , respectively, where p, q, m, n are all positive integers such that $m \geq q$ and $n \geq p$. If $m > n$, then the relative $(p+m-n, q)$ th order (resp., relative $(p+m-n, q)$ th lower) of f with respect to g is defined as

(i)

$$\rho_g^{(p+m-n, q)}(f) = \limsup_{r \rightarrow \infty} \frac{\log^{[p+m-n]} M_g^{-1} M_f(r)}{\log^{[q]} r},$$

$$\left(\text{resp. } \lambda_g^{(p+m-n, q)}(f) = \liminf_{r \rightarrow \infty} \frac{\log^{[p+m-n]} M_g^{-1} M_f(r)}{\log^{[q]} r} \right).$$
(61)

If $m < n$, then the relative $(p, q+n-m)$ th order (resp., relative $(p, q+n-m)$ th lower) of f with respect to g is defined as

(ii)

$$\rho_g^{(p, q+n-m)}(f) = \limsup_{r \rightarrow \infty} \frac{\log^{[p]} M_g^{-1} M_f(r)}{\log^{[q+n-m]} r},$$

$$\left(\text{resp. } \lambda_g^{(p, q+n-m)}(f) = \liminf_{r \rightarrow \infty} \frac{\log^{[p]} M_g^{-1} M_f(r)}{\log^{[q+n-m]} r} \right).$$
(62)

The following result is easy to check.

Theorem 27. Under the hypothesis of Definition 26, for $m > n$:

(i)

$$\rho_g^{(p+m-n, q)}(f) = \limsup_{r \rightarrow \infty} \frac{\log^{[m]} M_f(r)}{\log^{[q]} r},$$

$$\lambda_g^{(p+m-n, q)}(f) = \liminf_{r \rightarrow \infty} \frac{\log^{[m]} M_f(r)}{\log^{[q]} r},$$
(63)

and for $m < n$:

(ii)

$$\rho_g^{(p, q+n-m)}(f) = \limsup_{r \rightarrow \infty} \frac{\log^{[p]} r}{\log^{[n]} M_g(r)},$$

$$\lambda_g^{(p, q+n-m)}(f) = \liminf_{r \rightarrow \infty} \frac{\log^{[p]} r}{\log^{[n]} M_g(r)}.$$
(64)

The next example will make an alternative use of Theorem 27.

Example 28 (relative order between exponentials of different order). Let

$$f(z) = \exp^{[27]} z^5, \quad g(z) = \exp^{[50]} z^{17}. \quad (65)$$

In this case f and g are entire functions of regular growth $(m, p) = (28, 1)$ and $(n, q) = (51, 1)$, respectively, with

$$\rho_f(28, 1) = \lambda_f(28, 1) = 5, \quad \rho_g(51, 1) = \lambda_g(51, 1) = 17. \quad (66)$$

Now

$$\frac{\log^{[p]} M_g^{-1} M_f(r)}{\log^{[q+n-m]} r} = \frac{\log [\log^{[50]} (\exp^{[27]} r^5)]^{1/17}}{\log^{[24]} r} \quad (67)$$

and by taking lim sup and lim inf, we get

$$\rho_g^{(p, q+n-m)}(f) = \frac{1}{17} = \lambda_g^{(p, q+n-m)}(f). \quad (68)$$

Obviously, the same limit is achieved if, by using Theorem 27, we consider the quotient

$$\frac{\log^{[p]} r}{\log^{[n]} M_g(r)} = \frac{\log r}{\log^{[51]} M_g(r)}. \quad (69)$$

Reciprocally, in order to evaluate $\rho_f^{(p+m-n, q)}(g)$ and $\lambda_f^{(p+m-n, q)}(g)$, we would take limits in either

$$\frac{\log^{[24]} M_f^{-1} M_g(r)}{\log r}$$

$$= \frac{\log^{[24]} [\log^{[27]} (\exp^{[50]} r^{17})]^{1/5}}{\log r} \quad \text{or} \quad \frac{\log^{[51]} M_g(r)}{\log r}, \quad (70)$$

obtaining that

$$\rho_f^{(p+m-n, q)}(g) = 17 = \lambda_f^{(p+m-n, q)}(g). \quad (71)$$

5. Conclusion

The main aim of the paper is to extend and modify the notion of order to relative order of higher dimensions in case of entire functions as the relative order of growth gives a quantitative assessment of how different functions scale each other and to what extent they are self-similar in growth, and in this connection we have established some theorems. In fact, some works on relative order of entire functions and the growth estimates of composite entire functions on the basis of it have been explored in [8–15]. Actually we are trying to generalize the growth properties of composite entire functions on the basis of relative (p, q) th order and relative (p, q) th lower order and, analogously, we may also define relative (p, q) th order of meromorphic functions in order to establish related growth properties, improving the results of [16–18]. For any two positive integers p and q , we are trying to establish the concepts of relative (p, q) th type and relative (p, q) th weak type of entire and meromorphic functions, too, in order to determine the relative growth of two entire or meromorphic functions having the same nonzero finite relative (p, q) th order or relative (p, q) th lower order with respect to another entire function, respectively. Moreover, the notion of relative order, relative type, and relative weak type of higher dimensions may also be applied in the field of slowly changing functions and also in case of entire or meromorphic functions of several complex variables.

The results of this paper in connection with Nevanlinna's value distribution theory of entire functions on the basis of relative (p, q) th order and relative (p, q) th lower order may have a wide range of applications in complex dynamics, factorization theory of entire functions of single complex variable, the solution of complex differential equations, and so forth. In fact complex dynamics is a thrust area in modern function theory and it is solely based on the study of fixed points of entire functions as well as the normality of them. For further details in the progress of research in complex dynamics via Nevanlinna's value distribution theory one may see [19–24]. Factorization theory of entire functions is another branch of applications of Nevanlinna's theory which actually deals with how a given entire function can be factorized into other simpler entire functions in the sense of composition. Also Nevanlinna's value distribution theory has immense applications into the study of the properties of the solutions of complex differential equations and is still an active area of research.

Conflict of Interests

The authors declare that there is no conflict of interests regarding the publication of this paper.

References

- [1] L. Bernal, "Orden relativo de crecimiento de funciones enteras," *Collectanea Mathematica*, vol. 39, no. 3, pp. 209–229, 1988.
- [2] L. Bernal, *Crecimiento relativo de funciones enteras. Contribución al estudio de las funciones enteras con índice exponencial finito [Doctoral Dissertation]*, University of Seville, Seville, Spain, 1984.
- [3] B. K. Lahiri and D. Banerjee, "Entire functions of relative order (p, q) ," *Soochow Journal of Mathematics*, vol. 31, no. 4, pp. 497–513, 2005.
- [4] O. P. Juneja, G. P. Kapoor, and S. K. Bajpai, "On the (p, q) -order and lower (p, q) -order of an entire function," *Journal für die Reine und Angewandte Mathematik*, vol. 282, pp. 53–67, 1976.
- [5] D. Sato, "On the rate of growth of entire functions of fast growth," *Bulletin of the American Mathematical Society*, vol. 69, pp. 411–414, 1963.
- [6] E. C. Titchmarsh, *The Theory of Functions*, Oxford University Press, Oxford, UK, 2nd edition, 1968.
- [7] B. K. Lahiri and D. Banerjee, "Generalised relative order of entire functions," *Proceedings of the National Academy of Sciences A*, vol. 72, no. 4, pp. 351–371, 2002.
- [8] C. Roy, "On the relative order and lower relative order of an entire function," *Bulletin of the Calcutta Mathematical Society*, vol. 102, no. 1, pp. 17–26, 2010.
- [9] B. C. Chakraborty and C. Roy, "Relative order of an entire function," *Journal of Pure Mathematics*, vol. 23, pp. 151–158, 2006.
- [10] S. K. Datta and T. Biswas, "Growth of entire functions based on relative order," *International Journal of Pure and Applied Mathematics*, vol. 51, no. 1, pp. 49–58, 2009.
- [11] S. K. Datta and T. Biswas, "Relative order of composite entire functions and some related growth properties," *Bulletin of the Calcutta Mathematical Society*, vol. 102, no. 3, pp. 259–266, 2010.
- [12] S. K. Datta, T. Biswas, and R. Biswas, "On relative order based growth estimates of entire functions," *International Journal of Mathematical Sciences and Applications*, vol. 7, no. 2, pp. 59–67, 2013.
- [13] S. K. Datta, T. Biswas, and R. Biswas, "Comparative growth properties of composite entire functions in the light of their relative order," *The Mathematics Student*, vol. 82, no. 1–4, pp. 1–8, 2013.
- [14] S. K. Datta, T. Biswas, and D. C. Pramanick, "On relative order and maximum term-related comparative growth rates of entire functions," *Journal of Tripura Mathematical Society*, vol. 14, pp. 60–68, 2012.
- [15] B. K. Lahiri and D. Banerjee, "A note on relative order of entire functions," *Bulletin of the Calcutta Mathematical Society*, vol. 97, no. 3, pp. 201–206, 2005.
- [16] D. Banerjee, "A note on relative order of meromorphic functions," *Bulletin of the Calcutta Mathematical Society*, vol. 98, no. 1, pp. 25–30, 2006.
- [17] D. Banerjee and S. Jana, "Meromorphic functions of relative order (p, q) ," *Soochow Journal of Mathematics*, vol. 33, no. 3, pp. 343–357, 2007.
- [18] B. K. Lahiri and D. Banerjee, "Relative order of meromorphic functions," *Proceedings of the National Academy of Sciences A*, vol. 75, no. 2, pp. 129–135, 2005.
- [19] A. F. Beardon, *Iteration of Rational Functions*, vol. 132, Springer, Berlin, Germany, 1991.
- [20] W. Bergweiler, "Periodic points of entire functions: proof of a conjecture of Baker," *Complex Variables*, vol. 17, no. 1–2, pp. 57–72, 1991.
- [21] L. Carleson and T. W. Gamelin, *Complex Dynamics*, Springer, New York, NY, USA, 1993.
- [22] P. C. Hua and C. C. Yang, *Dynamics of Transcendental Functions*, Gordon and Breach Science Publisher, 1998.
- [23] J. Milnor, *Dynamics in One Complex Variable: Introductory Lectures*, Vieweg, Braunschweig, Germany, 2000.
- [24] S. Morosawa, Y. Nishimura, M. Taniguchi, and T. Ueda, *Holomorphic Dynamics*, vol. 66, Cambridge University Press, Cambridge, UK, 2000.

Research Article

Local Fractional Z -Transforms with Applications to Signals on Cantor Sets

Kai Liu,¹ Ren-Jie Hu,¹ Carlo Cattani,² Gong-Nan Xie,³ Xiao-Jun Yang,⁴ and Yang Zhao⁵

¹ School of Electrical Engineering, Southeast University, Nanjing 210096, China

² Department of Mathematics, University of Salerno, Via Ponte don Melillo, Fisciano, 84084 Salerno, Italy

³ School of Mechanical Engineering, Northwestern Polytechnical University, Xi'an, Shaanxi 710048, China

⁴ Department of Mathematics and Mechanics, China University of Mining and Technology, Xuzhou, Jiangsu 221008, China

⁵ Department of Electronic and Information Technology, Jiangmen Polytechnic, Jiangmen 529090, China

Correspondence should be addressed to Yang Zhao; zhaoyang19781023@gmail.com

Received 28 January 2014; Accepted 3 February 2014; Published 10 March 2014

Academic Editor: Ming Li

Copyright © 2014 Kai Liu et al. This is an open access article distributed under the Creative Commons Attribution License, which permits unrestricted use, distribution, and reproduction in any medium, provided the original work is properly cited.

The Z -transform has played an important role in signal processing. In this paper the Z -transform has been generalized by the coupling of both the Z -transform and the local fractional complex calculus. In the literature the local fractional Z -transform is applied to analyze signals, in the following it will be used to analyze signals on Cantor sets. Some examples are also given to show the efficiency and accuracy for handling the signals on Cantor sets.

1. Introduction

Integral transforms [1, 2], such as Fourier, Laplace, Mellin, Hilbert, and Hankel transforms, play important roles in solving the mathematical problems arising in applied mathematics, mathematical physics, and engineering science. In recent years, fractional calculus [3–11] was developed and used to model also some anomalous behaviors of diffusion [12–21] and transport [22–27]. Fractional integral transforms are suitable generalizations of the classical ones and were recently proposed by some researchers. For example, the fractional Fourier transforms were considered in [28, 29]. In [30], the fractional Hilbert transform was presented. The fractional Mellin transform [31, 32] was proposed to be used in image encryption. The fractional wavelet transform was presented and some applications were investigated in [33–35]. In [36], the fractional Hankel transform was reported in order to research the charge-amplitude state representations.

The Z -transform method [1, 2, 37] was applied to handle the linear time-invariant discrete-time systems (LTI discrete-time systems) and difference equations in Z -domain. However, the fractional derivative and integrals (the fractional PDIs) were used to transfer the fractional LTI discrete-time systems to Z -domain [38]. There appear signals defined on

Cantor sets, which are the most striking properties of non-differentiable functions. The classical Z -transform method and PDIs did not deal with them. In order to overcome them, local fractional calculus [39–43] may be applied to handle the function defined on Cantor sets shown in Figure 1. The local fractional integral transforms via local fractional calculus theory were proposed in [44–51]. For example, local fractional Fourier transforms reported in [40, 44] were used to find nondifferentiable solutions for local fractional ODEs and PDEs [45–47]. Laplace transforms via local fractional calculus [40] were generalized and reported in order to solve the local fractional ODEs and PDEs [48–50].

Fractal signal processing [51–59] is a hot topic for scientists and engineers. Very recently, the concept of the Z -transform method via local fractional calculus was considered only in [60]. However, there is no report on signal processing by using the local fractional Z -transforms. The main aim of this paper is to investigate the properties of local fractional Z -transforms and to present some examples for processing signals defined on Cantor sets.

The paper is organized as follows. In Section 2, the concepts of local fractional complex derivatives and integrals are given. In Section 3, the notions and properties of local

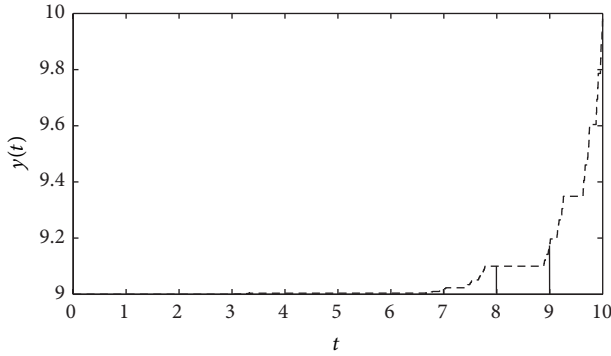


FIGURE 1: The chart of the signal $y(t)$ defined on Cantor sets.

fractional Z-transform method are presented. In Section 4, some examples and applications of this method are shown. Finally, Section 5 is the conclusions.

2. Local Fractional Derivatives and Integrals of Complex Functions and Recent Results

In this section, we introduce the concepts of local fractional derivative and integrals of complex functions. Let us first give the local fractional continuity of complex functions.

Definition 1 (see [40, 60]). The function $f(z)$ is said to be local fractional continuous at z_0 if there exists

$$\lim_{z \rightarrow z_0} f(z) = f(z_0). \quad (1)$$

There is the local fractional continuous relation in the following form:

$$f(z) \in C_\alpha(\mathfrak{R}), \quad (2)$$

where

$$\lim_{z \rightarrow z_0} f(z) = f(z_0), \quad z, z_0 \in \mathfrak{R}. \quad (3)$$

Definition 2 (see [40, 60]). The local fractional derivative of complex function $f(z)$ of order α is defined as

$$f^{(\alpha)}(z) = \frac{d^\alpha f(z)}{dz^\alpha} = \lim_{z \rightarrow z_0} \frac{\Delta^\alpha f(z)}{(z - z_0)^\alpha}, \quad \alpha \in (0, 1], \quad (4)$$

where

$$\Delta^\alpha f(z) \cong \Gamma(1 + \alpha)(f(z) - f(z_0)). \quad (5)$$

If the limit of (4) exists for all z_0 in a region \mathfrak{R} , then the complex function $f(z)$ is said to be local fractional analytic in a region \mathfrak{R} .

The properties of the local fractional derivatives of some complex functions are presented as follows [40]:

$$\begin{aligned} \frac{d^\alpha z^{k\alpha}}{dz^\alpha} &= \frac{\Gamma(1 + k\alpha)}{\Gamma(1 + (k-1)\alpha)} z^{(k-1)\alpha}, \\ \frac{d^\alpha E_\alpha(z^\alpha)}{dz^\alpha} &= E_\alpha(z^\alpha), \\ \frac{d^\alpha \sin_\alpha z^\alpha}{dz^\alpha} &= \cos_\alpha z^\alpha, \\ \frac{d^\alpha \cos_\alpha z^\alpha}{dz^\alpha} &= -\sin_\alpha z^\alpha, \end{aligned} \quad (6)$$

where

$$\begin{aligned} E_\alpha(z^\alpha) &= \sum_{k=0}^{\infty} \frac{z^{k\alpha}}{\Gamma(1 + k\alpha)}, \\ \sin_\alpha z^\alpha &= \sum_{k=0}^{\infty} \frac{(-1)^k z^{\alpha(2k+1)}}{\Gamma(1 + \alpha(2k+1))}, \\ \cos_\alpha z^\alpha &= \sum_{k=0}^{\infty} \frac{(-1)^k z^{2\alpha k}}{\Gamma(1 + 2\alpha k)}. \end{aligned} \quad (7)$$

Definition 3 (see [40, 46–50, 60]). The local fractional integral of complex function $f(z)$ of order α along the closed contour C is defined as

$$I_C^\alpha f(z) = \frac{1}{\Gamma(1 + \alpha)} \oint_C f(z) (dz)^\alpha, \quad \alpha \in (0, 1]. \quad (8)$$

The properties of the local fractional integrals of some complex functions are suggested as follows [40]:

$$\begin{aligned} \frac{1}{\Gamma(1 + \alpha)} \int_C (f(z) + g(z)) (dz)^\alpha &= \frac{1}{\Gamma(1 + \alpha)} \int_C f(z) (dz)^\alpha + \frac{1}{\Gamma(1 + \alpha)} \int_C g(z) (dz)^\alpha, \\ \frac{1}{\Gamma(1 + \alpha)} \int_{C_1 + C_2} f(z) (dz)^\alpha &= \frac{1}{\Gamma(1 + \alpha)} \int_{C_1} f(z) (dz)^\alpha + \frac{1}{\Gamma(1 + \alpha)} \int_{C_2} f(z) (dz)^\alpha, \\ \frac{1}{\Gamma(1 + \alpha)} \int_{C_1} f(z) (dz)^\alpha &= -\frac{1}{\Gamma(1 + \alpha)} \int_{-C_1} f(z) (dz)^\alpha. \end{aligned} \quad (9)$$

Theorem 4 (see [40]). *If $f(z)$ is local fractional analytic within and on a simple closed contour C and a is any point interior to C , then we have*

$$\frac{1}{(2\pi)^\alpha i^\alpha} \cdot \left\{ \frac{1}{\Gamma(1 + \alpha)} \oint_C \frac{f(z)}{(z - z_0)^\alpha} (dz)^\alpha \right\} = \frac{f(z_0)}{\Gamma(1 + \alpha)}. \quad (10)$$

Proof. See [40]. \square

Definition 5 (see [40, 60]). If z_0 is an isolated singular point of $f(z)$, then we have a local fractional Laurent series of $f(z)$ at $C : |z - z_0| < r$ given by

$$f(z) = \sum_{i=-\infty}^{\infty} a_k(z - z_0)^{k\alpha}. \tag{11}$$

The coefficient a_{-1} of $(z - z_0)^{-\alpha}$ is called the local fractional residue of $f(z)$ at $z = z_0$ and is frequently written as

$$\text{Re}_{z=z_0} s \{f(z)\} = a_{-1}. \tag{12}$$

Theorem 6 (see [40]). *If $f(z)$ is local fractional analytic within and on the boundary C of a region \mathfrak{R} except at a number of poles a within \mathfrak{R} , having a residue a_{-1} , then*

$$\frac{1}{(2\pi)^\alpha i^\alpha} \cdot \left\{ \frac{1}{\Gamma(1 + \alpha)} \oint_C f(z) (dz)^\alpha \right\} = \text{Re}_{z=z_0} s \{f(z)\}. \tag{13}$$

Proof. See [40]. □

Theorem 7 (see [40]). *If $f(z)$ is local fractional analytic within and on the boundary C of a region \mathfrak{R} except at a number of poles a within \mathfrak{R} , having numbers of residues, then*

$$\frac{1}{(2\pi)^\alpha i^\alpha} \cdot \left\{ \frac{1}{\Gamma(1 + \alpha)} \oint_C f(z) (dz)^\alpha \right\} = \sum_{i=1}^n \text{Re}_{z=z_k} s \{f(z)\}. \tag{14}$$

Proof. See [40]. □

3. Local Fractional Z-Transforms and Their Properties

In this section, we give the local fractional Z-transforms and their properties.

Definition 8 (see [60]). Local fractional Z-transform of $f(n)$ of order α is defined as

$$Z_\alpha \{f(n)\} = F_\alpha(z) = \sum_{n=0}^{\infty} f(n) z^{-n\alpha}, \tag{15}$$

where the above formula is convergent.

For a given sequence, the set \mathfrak{R} of values of z for which its local fractional Z-transform converges is called the region of convergence (ROC), namely,

$$\sum_{n=0}^{\infty} |f(n) z^{-n\alpha}| < \infty. \tag{16}$$

The inverse formula of local fractional Z-transform of $f(n)$ of order α reads as follows (see [60]):

$$\begin{aligned} Z_\alpha^{-1} \{F_\alpha(z)\} &= f(n) \\ &= \frac{1}{(2\pi i)^\alpha \Gamma(1 + \alpha)} \oint_C F_\alpha(z) z^{(n-1)\alpha} (dz)^\alpha, \end{aligned} \tag{17}$$

where C is a counterclockwise closed fractal path encircling the origin and entirely in the region of convergence.

Let $Z_\alpha \{f(n)\} = F_\alpha(z)$ within the region of convergence \mathfrak{R}_1 and let $Z_\alpha \{g(n)\} = G_\alpha(z)$ within the region of convergence \mathfrak{R}_2 .

Property 1 (linearity). We have

$$Z_\alpha \{f(n) + g(n)\} = F_\alpha(z) + G_\alpha(z) \tag{18}$$

within the region of convergence $\mathfrak{R}_1 \cap \mathfrak{R}_2$.

Proof. From (15) we have

$$\begin{aligned} Z_\alpha \{f(n) + g(n)\} &= \sum_{n=0}^{\infty} (f(n) + g(n)) z^{-n\alpha} \\ &= Z_\alpha \{f(n)\} + Z_\alpha \{g(n)\} \end{aligned} \tag{19}$$

within the region of convergence $\mathfrak{R}_1 \cap \mathfrak{R}_2$. □

Property 2 (time shifting). If the variable z has a useful interpretation in terms of time delay, then we have

$$Z_\alpha \{f(n - k)\} = z^{-k\alpha} F_\alpha(z). \tag{20}$$

Proof. From (15), we have

$$\begin{aligned} Z_\alpha \{f(n - k)\} &= \sum_{n=0}^{\infty} f(n - k) z^{-n\alpha} = \sum_{n=0}^{\infty} f(n) z^{-(n+k)\alpha} \\ &= z^{-k\alpha} \sum_{n=0}^{\infty} f(n) z^{-n\alpha} = z^{-k\alpha} Z_\alpha \{f(n)\}. \end{aligned} \tag{21}$$

□

Property 3 (frequency modulation). We have

$$Z_\alpha \{z_0^{n\alpha} f(n)\} = F_\alpha\left(\frac{z}{z_0}\right). \tag{22}$$

Proof. From (15), we have

$$\begin{aligned} Z_\alpha \{z_0^{n\alpha} f(n)\} &= \sum_{n=0}^{\infty} f(n) z_0^{n\alpha} z^{-n\alpha} \\ &= \sum_{n=0}^{\infty} f(n) \left(\frac{z}{z_0}\right)^{-n\alpha} = F_\alpha\left(\frac{z}{z_0}\right). \end{aligned} \tag{23}$$

□

4. Some Illustrative Examples

In this section, we give some samples for nondifferentiable signals defined on Cantor sets.

Example 1. Let us consider the following signal in the form:

$$f(n) = \delta_\alpha(n) = \begin{cases} 1, & n = 0, \\ 0, & n \neq 0. \end{cases} \tag{24}$$

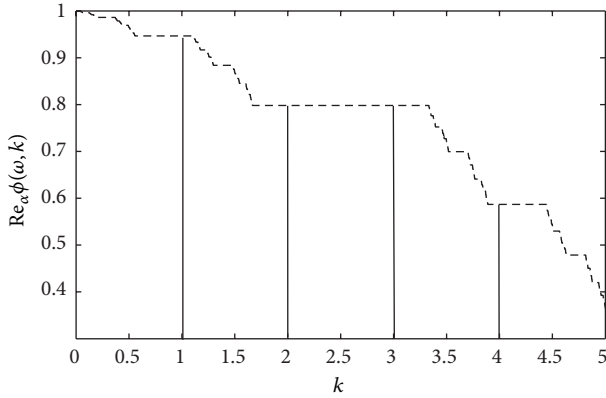


FIGURE 2: The graph of $\text{Re}_\alpha \phi(\omega, k)$ with premasters $\omega = 1$ and $\alpha = \ln 2 / \ln 3$.

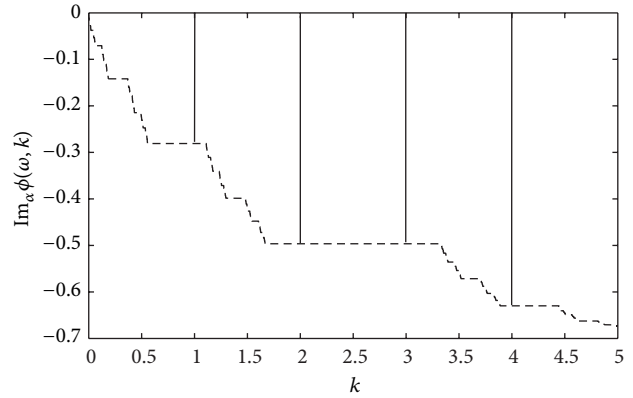


FIGURE 3: The plot of $\text{Im}_\alpha \phi(\omega, k)$ with premasters $\omega = 1$ and $\alpha = \ln 2 / \ln 3$.

Taking local fractional Z-transform, we have

$$Z_\alpha \{f(n)\} = Z_\alpha \{\delta_\alpha(n)\} = \sum_{n=-\infty}^{\infty} \delta_\alpha(n) z^{-n\alpha} = 1. \quad (25)$$

Example 2. We now suggest the following signal in the form:

$$f(n) = \delta_\alpha(n - k) = \begin{cases} 1, & n = k, \\ 0, & n \neq k. \end{cases} \quad (26)$$

Taking local fractional Z-transform, we obtain

$$Z_\alpha \{f(n)\} = Z_\alpha \{\delta_\alpha(n - k)\} = \sum_{n=-\infty}^{\infty} \delta_\alpha(n - k) z^{-n\alpha} = z^{-k\alpha}. \quad (27)$$

When $z^\alpha = E_\alpha(j^\alpha \omega^\alpha)$ with the imaginary unit j^α [40, 44–50], we get

$$\begin{aligned} \phi(\omega, k) &= Z_\alpha \{f(n)\} = E_\alpha(-j^\alpha \omega^\alpha k^\alpha) \\ &= \cos_\alpha(\omega^\alpha k^\alpha) - j^\alpha \sin_\alpha(\omega^\alpha k^\alpha). \end{aligned} \quad (28)$$

Hence, from (28), we get

$$\begin{aligned} \text{Re}_\alpha \phi(\omega, k) &= \cos_\alpha(\omega^\alpha k^\alpha), \\ \text{Im}_\alpha \phi(\omega, k) &= -\sin_\alpha(\omega^\alpha k^\alpha) \end{aligned} \quad (29)$$

with the real part graph in Figure 2 and imaginary part graph in Figure 3.

Example 3. There is the signal in the following form:

$$f(n) = \delta_\alpha(n - k) + \delta_\alpha(n + k) = \begin{cases} 1, & n = \pm k, \\ 0, & n \neq \pm k. \end{cases} \quad (30)$$

Taking local fractional Z-transform, we have

$$\begin{aligned} Z_\alpha \{f(n)\} &= Z_\alpha \{\delta_\alpha(n - k) + \delta_\alpha(n + k)\} \\ &= \sum_{n=-\infty}^{\infty} (\delta_\alpha(n - k) + \delta_\alpha(n + k)) z^{-n\alpha} = z^{-k\alpha} + z^{k\alpha}. \end{aligned} \quad (31)$$

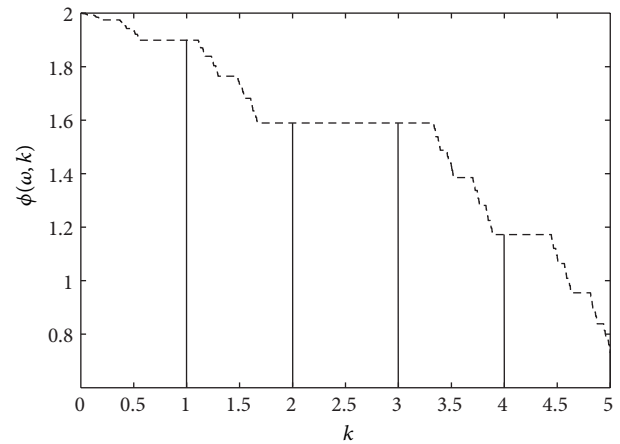


FIGURE 4: The map of $\phi(\omega, k)$ with premasters $\omega = 1$ and $\alpha = \ln 2 / \ln 3$.

When $z^\alpha = E_\alpha(j^\alpha \omega^\alpha)$, we get

$$\phi(\omega, k) = Z_\alpha \{f(n)\} = E_\alpha(j^\alpha \omega^\alpha k^\alpha) = 2\cos_\alpha(\omega^\alpha k^\alpha) \quad (32)$$

with the graph of $\phi(\omega, k)$ shown in Figure 4.

Example 4. We have the following signal in the form:

$$f(n) = \begin{cases} a^{n\alpha}, & a \geq 0, \\ 0, & a < 0. \end{cases} \quad (33)$$

Local fractional Z-transform gives the following form:

$$Z_\alpha \{f(n)\} = Z_\alpha \{a^{n\alpha}\} = \sum_{n=0}^{\infty} a^{n\alpha} z^{-n\alpha} = \sum_{n=0}^{\infty} \left(\frac{z}{a}\right)^{-n\alpha} \quad (34)$$

with the region of convergence $|z| > |a|$.

Example 5. We consider the following signal in the form:

$$f(n) = \begin{cases} 0, & a \geq 0, \\ a^{n\alpha}, & a < 0. \end{cases} \quad (35)$$

Taking local fractional Z-transform, we arrive at the following form:

$$Z_{\alpha} \{f(n)\} = Z_{\alpha} \{a^{n\alpha}\} = \sum_{n=-\infty}^0 a^{n\alpha} z^{-n\alpha} = \sum_{n=-\infty}^0 \left(\frac{z}{a}\right)^{-n\alpha} \tag{36}$$

with the region of convergence $|z| < |a|$.

Example 6. We present the following signal in the form:

$$f(n) = \begin{cases} b^{n\alpha}, & a \geq 0, \\ a^{n\alpha}, & a < 0. \end{cases} \tag{37}$$

Local fractional Z-transform gives the following form:

$$\begin{aligned} Z_{\alpha} \{f(n)\} &= Z_{\alpha} \{a^{n\alpha} + b^{n\alpha}\} = \sum_{n=0}^{\infty} b^{n\alpha} z^{-n\alpha} + \sum_{n=-\infty}^0 a^{n\alpha} z^{-n\alpha} \\ &= \sum_{n=0}^{\infty} \left(\frac{z}{b}\right)^{-n\alpha} + \sum_{n=-\infty}^0 \left(\frac{z}{a}\right)^{-n\alpha} \end{aligned} \tag{38}$$

with the region of convergence $|b| < |z| < |a|$.

5. Conclusions

In this work, we investigated the local fractional Z-transforms based on the local fractional complex calculus and some properties are also obtained. Some illustrative examples were also given. The obtained results show the accuracy and efficiency of the presented method.

Conflict of Interests

The authors declare that they have no competing interests in this paper.

Acknowledgment

This work was supported by Science and Technology Commission Planning Project of Jiangsu Province (no. BE2013737).

References

[1] B. Davies, *Integral Transforms and Their Applications*, Texts in Applied Mathematics, Springer, New York, NY, USA, 2002.
 [2] L. Debnath and D. Bhatta, *Integral Transforms and Their Applications*, CRC Press, New York, NY, USA, 2010.
 [3] V. E. Tarasov, *Fractional Dynamics*, Nonlinear Physical Science, Springer, New York, NY, USA, 2010.
 [4] R. Herrmann, *Fractional Calculus: An Introduction for Physicists*, World Scientific, Singapore, 2011.
 [5] A. B. Malinowska and D. F. M. Torres, *Introduction to the Fractional Calculus of Variations*, Imperial College Press, London, UK, 2012.

[6] M. D. Ortigueira, *Fractional Calculus for Scientists and Engineers*, Lecture Notes in Electrical Engineering, Springer, New York, NY, USA, 2011.
 [7] F. Mainardi, *Fractional Calculus and Waves in Linear Viscoelasticity*, Imperial College Press, London, UK, 2010.
 [8] J. Sabatier, O. P. Agrawal, and J. A. T. Machado, *Advances in Fractional Calculus: Theoretical Developments and Applications in Physics and Engineering*, Springer, New York, NY, USA, 2007.
 [9] A. A. Kilbas, H. M. Srivastava, and J. J. Trujillo, *Theory and Applications of Fractional Differential Equations*, vol. 204 of *North-Holland Mathematics Studies*, Elsevier Science B.V., Amsterdam, The Netherlands, 2006.
 [10] I. Podlubny, *Fractional Differential Equations*, vol. 198 of *Mathematics in Science and Engineering*, Academic Press, San Diego, Calif, USA, 1999.
 [11] B. J. West, M. Bologna, and P. Grigolini, *Physics of Fractal Operators*, Institute for Nonlinear Science, Springer, New York, NY, USA, 2003.
 [12] R. Metzler and J. Klafter, "The random walk's guide to anomalous diffusion: a fractional dynamics approach," *Physics Reports*, vol. 339, no. 1, pp. 1-77, 2000.
 [13] L. Miller, "On the controllability of anomalous diffusions generated by the fractional Laplacian," *Mathematics of Control, Signals, and Systems*, vol. 18, no. 3, pp. 260-271, 2006.
 [14] B. J. West, P. Grigolini, R. Metzler, and T. F. Nonnenmacher, "Fractional diffusion and Lévy stable processes," *Physical Review E*, vol. 55, no. 1, pp. 99-106, 1997.
 [15] V. V. Uchaikin, "Anomalous diffusion and fractional stable distributions," *Journal of Experimental and Theoretical Physics*, vol. 97, no. 4, pp. 810-825, 2003.
 [16] Y. Zhang, D. A. Benson, M. M. Meerschaert, E. M. LaBolle, and H. P. Scheffler, "Random walk approximation of fractional-order multiscaling anomalous diffusion," *Physical Review E*, vol. 74, no. 2, Article ID 026706, 2006.
 [17] Q. Yang, I. Turner, F. Liu, and M. Ilic, "Novel numerical methods for solving the time-space fractional diffusion equation in two dimensions," *SIAM Journal on Scientific Computing*, vol. 33, pp. 1159-1180, 2011.
 [18] R. L. Magin, O. Abdullah, D. Baleanu, and X. J. Zhou, "Anomalous diffusion expressed through fractional order differential operators in the Bloch-Torrey equation," *Journal of Magnetic Resonance*, vol. 190, no. 2, pp. 255-270, 2008.
 [19] H. Sun, W. Chen, C. Li, and Y. Chen, "Fractional differential models for anomalous diffusion," *Physica A*, vol. 389, no. 14, pp. 2719-2724, 2010.
 [20] M. Xu and W. Tan, "Theoretical analysis of the velocity field, stress field and vortex sheet of generalized second order fluid with fractional anomalous diffusion," *Science in China A*, vol. 44, no. 11, pp. 1387-1399, 2001.
 [21] A. V. Chechkin, R. Gorenflo, and I. M. Sokolov, "Fractional diffusion in inhomogeneous media," *Journal of Physics A*, vol. 38, no. 42, pp. L679-L684, 2005.
 [22] G. M. Zaslavsky, "Chaos, fractional kinetics, and anomalous transport," *Physics Reports*, vol. 371, no. 6, pp. 461-580, 2002.
 [23] B. Berkowitz, J. Klafter, R. Metzler, and H. Scher, "Physical pictures of transport in heterogeneous media: advection-dispersion, random-walk, and fractional derivative formulations," *Water Resources Research*, vol. 38, no. 10, pp. 9-1-9-12, 2002.
 [24] J. D. Seymour, J. P. Gage, S. L. Codd, and R. Gerlach, "Anomalous fluid transport in porous media induced by biofilm

- growth," *Physical Review Letters*, vol. 93, no. 19, Article ID 198103, 4 pages, 2004.
- [25] Y. Luchko and A. Punzi, "Modeling anomalous heat transport in geothermal reservoirs via fractional diffusion equations," *GEM—International Journal on Geomathematics*, vol. 1, no. 2, pp. 257–276, 2011.
- [26] J. Klafter, S. C. Lim, and R. Metzler, *Fractional Dynamics, Recent Advances*, World Scientific, Singapore, 2012.
- [27] P. Chun and J. Inoue, "Yet another possible mechanism for anomalous transport: theory, numerical method, and experiments," *KSCE Journal of Civil Engineering*, vol. 16, no. 1, pp. 45–53, 2012.
- [28] A. C. McBride and F. H. Kerr, "On Namias's fractional Fourier transforms," *IMA Journal of Applied Mathematics*, vol. 39, no. 2, pp. 159–175, 1987.
- [29] H. M. Ozaktas and O. Aytür, "Fractional Fourier domains," *Signal Processing*, vol. 46, no. 1, pp. 119–124, 1995.
- [30] A. W. Lohmann, D. Mendlovic, and Z. Zalevsky, "Fractional Hilbert transform," *Optics Letters*, vol. 21, no. 4, pp. 281–283, 1996.
- [31] N. Zhou, Y. Wang, and L. Gong, "Novel optical image encryption scheme based on fractional Mellin transform," *Optics Communications*, vol. 284, no. 13, pp. 3234–3242, 2011.
- [32] Y. Luchko and V. Kiryakova, "The Mellin integral transform in fractional calculus," *Fractional Calculus and Applied Analysis*, vol. 16, no. 2, pp. 405–430, 2013.
- [33] D. Mendlovic, Z. Zalevsky, D. Mas, J. García, and C. Ferreira, "Fractional wavelet transform," *Applied Optics*, vol. 36, no. 20, pp. 4801–4806, 1997.
- [34] J. Shi, N. Zhang, and X. Liu, "A novel fractional wavelet transform and its applications," *Science China: Information Sciences*, vol. 55, no. 6, pp. 1270–1279, 2012.
- [35] E. Dinç and D. Baleanu, "Fractional wavelet transform for the quantitative spectral resolution of the composite signals of the active compounds in a two-component mixture," *Computers & Mathematics with Applications*, vol. 59, no. 5, pp. 1701–1708, 2010.
- [36] H. Y. Fan, "Fractional Hankel transform studied by charge-amplitude state representations and complex fractional Fourier transformation," *Optics Letters*, vol. 28, no. 22, pp. 2177–2179, 2003.
- [37] E. I. Jury, *Theory and Applications of the Z-Transform Method*, John Wiley & Sons, New York, NY, USA, 1964.
- [38] J. A. T. Machado, "Analysis and design of fractional-order digital control systems," *Systems Analysis Modelling Simulation*, vol. 27, no. 2-3, pp. 107–122, 1997.
- [39] X. J. Yang, *Advanced Local Fractional Calculus and Its Applications*, World Science, New York, NY, USA, 2012.
- [40] X. J. Yang, *Local Fractional Functional Analysis and Its Applications*, Asian Academic Publisher, Hong Kong, China, 2011.
- [41] X. J. Yang and D. Baleanu, "Fractal heat conduction problem solved by local fractional variation iteration method," *Thermal Science*, vol. 17, no. 2, pp. 625–628, 2013.
- [42] X. J. Yang, D. Baleanu, and W. P. Zhong, "Approximation solutions for diffusion equation on Cantor time-space," *Proceeding of the Romanian Academy A*, vol. 14, no. 2, pp. 127–133, 2013.
- [43] Y. Zhao, D. Baleanu, C. Cattani, D. F. Cheng, and X. J. Yang, "Maxwell's equations on Cantor sets: a local fractional approach," *Advances in High Energy Physics*, vol. 2013, Article ID 686371, 6 pages, 2013.
- [44] X. J. Yang, D. Baleanu, and J. A. T. Machado, "Mathematical aspects of the Heisenberg uncertainty principle within local fractional Fourier analysis," *Boundary Value Problems*, no. 1, article 131, 20132013.
- [45] F. Gao, W. P. Zhong, and X. M. Shen, "Applications of Yang-Fourier transform to local fractional equations with local fractional derivative and local fractional integral," *Advanced Materials Research*, vol. 461, pp. 306–310, 2012.
- [46] Y. Zhao, D. Baleanu, M. C. Baleanu, D. F. Cheng, and X. J. Yang, "Mappings for special functions on Cantor sets and special integral transforms via local fractional operators," *Abstract and Applied Analysis*, vol. 2013, Article ID 316978, 6 pages, 2013.
- [47] J.-H. He, "Asymptotic methods for solitary solutions and compactons," *Abstract and Applied Analysis*, vol. 2012, Article ID 916793, 130 pages, 2012.
- [48] C. F. Liu, S. S. Kong, and S. J. Yuan, "Reconstructive schemes for variational iteration method within Yang-Laplace transform with application to fractal heat conduction problem," *Thermal Science*, vol. 17, no. 3, pp. 715–721, 2013.
- [49] C. G. Zhao, A. M. Yang, H. Jafari, and A. Haghbin, "The Yang-Laplace transform for solving the IVPs with local fractional derivative," *Abstract and Applied Analysis*, vol. 2014, Article ID 386459, 5 pages, 2014.
- [50] S. Q. Wang, Y. J. Yang, and H. K. Jassim, "Local fractional function decomposition method for solving inhomogeneous wave equations with local fractional derivative," *Abstract and Applied Analysis*, vol. 2014, Article ID 176395, 7 pages, 2014.
- [51] M. Li and W. Zhao, "On bandlimitedness and lag-limitedness of fractional Gaussian noise," *Physica A*, vol. 392, no. 9, pp. 1955–1961, 2013.
- [52] C. Cattani, "Harmonic wavelet approximation of random, fractal and high frequency signals," *Telecommunication Systems*, vol. 43, no. 3-4, pp. 207–217, 2010.
- [53] J. Nagler and J. C. Claussen, " $1/f^\alpha$ spectra in elementary cellular automata and fractal signals," *Physical Review E*, vol. 71, no. 6, Article ID 067103, 4 pages, 2005.
- [54] A. Gupta and S. Joshi, "Variable step-size LMS algorithm for fractal signals," *IEEE Transactions on Signal Processing*, vol. 56, no. 4, pp. 1411–1420, 2008.
- [55] B. J. West, *Fractal Physiology and Chaos in Medicine*, World Scientific, Singapore, 2013.
- [56] M. Li, "Power spectrum of generalized fractional Gaussian noise," *Advances in Mathematical Physics*, vol. 2013, Article ID 315979, 3 pages, 2013.
- [57] M. Li, "Modeling autocorrelation functions of long-range dependent teletraffic series based on optimal approximation in Hilbert space—a further study," *Applied Mathematical Modelling*, vol. 31, no. 3, pp. 625–631, 2007.
- [58] M. Li and S. C. Lim, "Power spectrum of generalized Cauchy process," *Telecommunication Systems*, vol. 43, no. 3-4, pp. 219–222, 2010.
- [59] M. Li, "A class of negatively fractal dimensional Gaussian random functions," *Mathematical Problems in Engineering*, vol. 2011, Article ID 291028, 18 pages, 2011.
- [60] G. Yi, "Local fractional Z transform in fractal space," *Advances in Digital Multimedia*, vol. 1, no. 2, pp. 96–102, 2012.

Research Article

Nonlinear Methodologies for Identifying Seismic Event and Nuclear Explosion Using Random Forest, Support Vector Machine, and Naive Bayes Classification

Longjun Dong,¹ Xibing Li,¹ and Gongnan Xie²

¹ School of Resources and Safety Engineering, Central South University, Changsha 410083, China

² School of Mechanical Engineering, Northwestern Polytechnical University, Xi'an 710129, China

Correspondence should be addressed to Longjun Dong; rydong001@csu.edu.cn

Received 26 December 2013; Accepted 16 January 2014; Published 26 February 2014

Academic Editor: Carlo Cattani

Copyright © 2014 Longjun Dong et al. This is an open access article distributed under the Creative Commons Attribution License, which permits unrestricted use, distribution, and reproduction in any medium, provided the original work is properly cited.

The discrimination of seismic event and nuclear explosion is a complex and nonlinear system. The nonlinear methodologies including Random Forests (RF), Support Vector Machines (SVM), and Naïve Bayes Classifier (NBC) were applied to discriminant seismic events. Twenty earthquakes and twenty-seven explosions with nine ratios of the energies contained within predetermined “velocity windows” and calculated distance are used in discriminators. Based on the one out cross-validation, ROC curve, calculated accuracy of training and test samples, and discriminating performances of RF, SVM, and NBC were discussed and compared. The result of RF method clearly shows the best predictive power with a maximum area of 0.975 under the ROC among RF, SVM, and NBC. The discriminant accuracies of RF, SVM, and NBC for test samples are 92.86%, 85.71%, and 92.86%, respectively. It has been demonstrated that the presented RF model can not only identify seismic event automatically with high accuracy, but also can sort the discriminant indicators according to calculated values of weights.

1. Introduction

The problems of seismic source locations and identifications are two of the most important and fundamental issues in earthquake monitoring, microseismic monitoring, analyses of active tectonics, and assessment of seismic hazards [1–4].

Seismic analysts identify seismic signals from those of explosions or blasts by visual inspection and by calculating some characteristics of seismogram. As recorded quarry blasts or nuclear explosions can mislead scientists interpreting the active tectonics and lead to erroneous results in the analysis of seismic hazards in the area; an event classification task is an important step in seismic signal processing. Such task analyses data in order to find to which class each recorded event belongs.

Such work supposes a great deal of workload for seismic analysts. Therefore, an automatic classification tool is necessary to be developed for reducing dramatically this arduous

task, turning classification as reliable, as well as removing errors associated with tedious evaluations and change of personnel.

Most discrimination methods are designed for a particular source region and a particular distance of the recording station from the epicenter [5]. Some of them heavily depend on the heterogeneity of the uppermost crust in the sense that they might be effective only for a given region.

The widely used methods for discriminators include simulating explosion spectra in order to predict spectral details indicative of explosions and not of earthquakes or single-event explosions [6, 7]; examining compressional and shear-wave ratios (amplitude and spectral) between all types of explosions and earthquakes, in an attempt to apply the basic physical conclusion that explosions excite more compressional waves than earthquakes relative to shear waves [8–11]; differences in high frequency S-to-P ratios between all types of explosions and earthquakes [12–14];

analyzing observed spectra of ripple-fired explosions, instantaneous explosions, and earthquakes and contrasting time-independent modulations, path-independent modulations, spectral ratios, spectral slopes, and spectral maxima and minima [15–17]; and examining differences in energy ratios of various wave in velocity windows [18, 19].

However, most of developed methods above are based on single index or liner discriminant methods. And the methods seem to fail to capture the discontinuities, the nonlinearities, and the high complexity of wave series.

Random Forests (RFs), Support Vector Machines (SVMs), and Naive Bayes Classifier (NBC) provide enough learning capacity and are more likely to capture the complex nonlinear models, which are widely used in natural and science areas, including medicine, agriculture, and geotechnics.

So far, as to our knowledge, the RFs and SVMs were not used for seismic classification. The performance of RFs, SVMs, and NBC in this type of application has not been thoroughly compared.

In present work, RF, SVM, and NBC were applied to discriminate between earthquakes and nuclear explosions. And based on the one out cross-validation, ROC curve, and test accuracy, their discriminating performances were discussed and compared.

2. Materials and Methods

2.1. Materials. The measurements or parameters consist of ratios of the “high energies” contained within predetermined “velocity windows” on the seismograms [18]. The choice of velocity windows is guided by the assumption that earthquake source mechanism is extended both in time and space and generates a larger fraction of energy in shear waves as compared to explosion source mechanism.

The different waves of “velocity windows” are listed as follows:

- (i) P_1 : first arrival to 4.6 km/s;
- (ii) S_1 : arrival to 4.6 to 2.5 km/s;
- (iii) S_2 : first arrival to 4.9 km/s;
- (iv) S_2 : arrival to 4.9 to 2.0 km/s;
- (v) P_g : arrival to 6.2 to 4.9 km/s;
- (vi) B : arrival to 4.9 to 3.6 km/s;
- (vii) L_{g1} : arrival to 3.6 to 3.2 km/s;
- (viii) R_{g1} : arrival to 3.2 to 2.8 km/s; and
- (ix) R : arrival to 2.8 to 2.5 km/s.

The factors, including ratios P_1/S_1 , P_2/S_2 , P_g/B , P_g/L_{g1} , $P_g/(R_{g1} + R)$, $P_g/(L_{g1} + R_{g1})$, R/R_{g1} , R_{g1}/L_{g1} , and R_{g2}/L_{g2} , as well as Average Distance, were expressed as $Ratio_1$, $Ratio_2$, $Ratio_3$, $Ratio_4$, $Ratio_5$, $Ratio_6$, $Ratio_7$, $Ratio_8$, $Ratio_9$, $Ratio_{10}$, and AD , respectively.

Nine ratios of energies included within certain velocity windows have been computed for 20 earthquakes and 27 nuclear explosions by Booker and Mitronovas [18]. All seismograms were recorded by the VELA UNIFORM LRSM Network on short-period Benioff instruments [18]. $Ratio_1$,

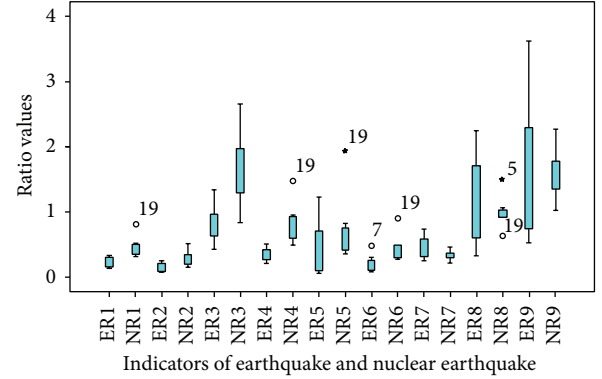


FIGURE 1: Box plot graph showing the distribution of values of ratios of energies (ER1, ER2, ER3, ER4, ER5, ER6, ER7, ER8, and ER9 represented $Ratio_1$, $Ratio_2$, $Ratio_3$, $Ratio_4$, $Ratio_5$, $Ratio_6$, $Ratio_7$, $Ratio_8$, and $Ratio_9$ for earthquake, respectively; NR1, NR2, NR3, NR4, NR5, NR6, NR7, NR8, and NR9 represented $Ratio_1$, $Ratio_2$, $Ratio_3$, $Ratio_4$, $Ratio_5$, $Ratio_6$, $Ratio_7$, $Ratio_8$, and $Ratio_9$ for nuclear earthquake, resp.).

$Ratio_2$, $Ratio_3$, $Ratio_4$, $Ratio_5$, $Ratio_6$, $Ratio_7$, $Ratio_8$, $Ratio_9$, and AD were selected as discriminant indicators. z -score is used to standardize variables in this work. First, the mean is subtracted from the value for each case, resulting in a mean of zero. Then, the difference between the individual’s score and the mean is divided by the standard deviation, which results in a standard deviation of one. If we start with a variable x and generate a variable x^* , the process is

$$x^* = \frac{(x - m)}{sd}, \quad (1)$$

where m is the mean of x and sd is the standard deviation of x . z -score of each ratio and distance for seismic event and nuclear earthquake were listed in Tables 1 and 2, respectively.

Box plot graphs of energy ratios and distance were plotted in Figures 1 and 2, respectively. Each group is represented as a box whose top and bottom are drawn at the lower and upper quartiles, with a small square at the median. Thus, the box contains the middle half of the scores in the distribution. Vertical lines outside the box extend to the largest and the smallest observations within 1.5 interquartile ranges. We conclude that $Ratio_1$, $Ratio_2$, $Ratio_3$, $Ratio_4$, $Ratio_5$, $Ratio_6$, $Ratio_7$, $Ratio_8$, $Ratio_9$, $Ratio_{10}$, and AD for earthquake and nuclear earthquake are obviously different. Such it is reasonable to select the ten factors as discriminating indicator.

2.2. Methodologies. The first 70% dataset of earthquake and nuclear earthquake were used to establish discriminating models and the other 30% dataset were used to test the model.

2.2.1. Overview of Random Forest. Random Forest (RF), a metalearner comprising many individual trees, was first developed by Tin Kam Ho in 1995 and later improved by Breiman in 2001. It was developed to operate quickly over large datasets and to be diverse by using random samples to build each tree in the forest. Each tree depends on the values

TABLE 1: Earthquakes dataset.

No.	Earthquakes	X_1 <i>Ratio</i> ₁	X_2 <i>Ratio</i> ₂	X_3 <i>Ratio</i> ₃	X_4 <i>Ratio</i> ₄	X_5 <i>Ratio</i> ₅	X_6 <i>Ratio</i> ₆	X_7 <i>Ratio</i> ₇	X_8 <i>Ratio</i> ₈	X_9 <i>Ratio</i> ₉	X_{10} <i>AD</i>
1	Baja Calif	0.123	0.495	-0.570	-0.145		-0.498		1.023	0.547	1.023
2	Baja Calif	-0.274	0.130	-0.207	-0.291		-0.824		2.904	1.407	2.031
3	Boxelder Creek	0.515	0.741	0.624	0.471		0.531		-0.652	0.057	0.576
4	Bridgeport	-0.371	-0.101	-0.681	-0.994	0.040	-0.686	-0.531	-1.543	-0.833	-0.614
5	Cache Creek	-0.803	-1.188	-1.082	-1.038	-0.860	-1.001	-0.750	-0.393	-0.875	2.114
6	Cache Creek AS	-0.349	-0.157	-0.866	-0.771	-0.426	-0.578	-0.876	-0.910	-0.356	0.259
7	Colona	-0.309	0.011	-0.430	-0.420	0.710	0.416	0.308	-1.453	-1.047	0.108
8	Mont.-Wyo Border	-0.446	0.243	-0.873	-0.462		-0.007		-0.661	-0.368	0.825
9	Pierre, S.Dakota	-1.354	-1.300	-1.574	-1.284		-1.131		-1.075	-0.719	2.498
10	Red Rock River	0.383	0.628	-0.231	0.120		0.315		-0.720	-0.579	0.945
11	Sierra De Juarez	-1.090	-0.992	0.624	-0.931		-1.004		1.102	4.306	1.002
12	Teton County	0.343	0.502	0.541	-0.164		0.044		-0.700	-0.442	-0.001
13	Western Mary land	-1.575	-1.546	-0.828	-1.365		-1.228		0.867	-0.459	-0.963
14	Western Vermont	-1.672	-1.602	-2.047	-1.438		-1.282		-1.472	-1.048	2.956
15	Western Vermont	-1.138	-1.034	-1.323	-0.779	-1.246	-0.896	2.417	1.004	0.238	1.184
16	Western Vermont	-1.010	-0.929	-1.538	-0.727	-1.204	-0.932	2.919	2.277	0.719	0.612
17	Western Vermont	-0.975	-0.844	-0.779	-1.023	-0.036	-0.751	0.018	-0.810	-0.842	-0.765
18	Western Vermont	0.013	0.046	0.116	-0.416	0.955	0.018	-0.758	-1.298	-0.902	-0.329
19	Western Vermont	-1.164	-1.202	-0.823	-0.754	-1.164	-0.925	1.084	1.480	1.614	0.950
20	Western Vermont	-0.494	-0.290	0.027	-0.462	-0.312	-0.245	0.567	-0.894	-0.476	1.023

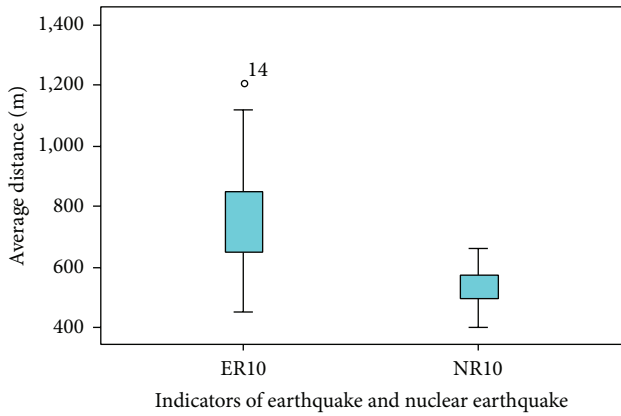


FIGURE 2: Box plot graph showing the distribution of values of the distance between hypocenter and sensors (ER10 and NR10 represented distance between hypocenter and sensors for earthquake and nuclear earthquake, resp.).

of a random vector sampled independently and with the same distribution for all trees in the forest. The generalization error of a forest of tree classifiers depends on the strength of the individual trees in the forest and the correlation between them [20]. Comprehensive review of applications of Random Forest have been provided by Rodriguez-Galiano et al., [21], Granitto et al. [22], and by Genuer et al. [23]. Also, a number of researches have compared the performance of other data mining technique and Random Forest in different kinds of problems [23–26]. The theory of RF is summarized as follows [20].

A Random Forest is a classifier consisting of a collection of tree-structured classifiers $\{h(x, \Theta_k), k = 1, \dots\}$, where the $\{\Theta_k\}$ are independent identically distributed random vectors and each tree casts a unit vote for the most popular class at input x [18].

Given an ensemble of classifiers $h_1(X), h_2(X), \dots, h_K(X)$ and with the training set drawn at random from the distribution of the random vector Y, X , define the margin function as

$$mg(X, Y) = av_K I(h_K(X) = Y) - \max_{j \neq Y} av_K I(h_K(X) = j), \tag{2}$$

where $I(\cdot)$ is the indicator function. The margin measures the extent to which the average number of votes at X, Y for the right class exceeds the average vote for any other class. The larger the margin, the more confidence in the classification. The generalization error is given by

$$PE^* = P_{X,Y} (mg(X, Y) < 0), \tag{3}$$

where the subscripts X, Y indicate that the probability is over the X, Y space. In Random Forests, $h_K(X) = h(X, k)$. For a large number of trees, it follows from the Strong Law of Large Numbers and the tree structure the following.

As the number of trees increases, for almost surely all sequences Θ_1, \dots, PE^* converges to

$$P_{X,Y} \left(P_{\Theta} (h(X, \Theta) = Y) - \max_{j \neq Y} P_{\Theta} (h(X, \Theta) = j) < 0 \right). \tag{4}$$

TABLE 2: Nuclear explosion dataset.

No.	Nuclear explosion	X_1 <i>Ratio</i> ₁	X_2 <i>Ratio</i> ₂	X_3 <i>Ratio</i> ₃	X_4 <i>Ratio</i> ₄	X_5 <i>Ratio</i> ₅	X_6 <i>Ratio</i> ₆	X_7 <i>Ratio</i> ₇	X_8 <i>Ratio</i> ₈	X_9 <i>Ratio</i> ₉	X_{10} <i>AD</i>
1	Aardvark	1.027	1.575	2.096	1.015	0.342	0.903	-0.523	-0.334	-0.321	-0.313
2	Agouti	-0.067	-0.101	0.984	-0.124		-0.047		-0.054	-0.192	-0.547
3	Armadillo	1.164	1.042	0.761	2.079	0.202	1.315	0.535	1.102	0.324	-0.516
4	Chinchilla II	0.317	0.194	0.197	1.222		0.575		0.338	0.384	-0.562
5	Cimarron	0.335	0.095	-0.009	0.185	-0.579	-0.065	-0.515	0.827	0.093	-0.329
6	Codsaw	-0.402	-0.676	-0.830	-0.378	-0.731	-0.372	0.755	-0.152	0.453	-0.859
7	Danny Boy	-0.388	-0.480	-0.096	-0.458	-0.736	-0.426	0.120	-0.207	-0.209	-1.202
8	Des Moines	1.133	0.874	0.590	0.954		0.759		-0.074	-0.149	-0.646
9	Dormouse II	0.171	-0.290	0.094	-0.182		-0.278		1.160	-0.252	-0.640
10	Fisher	-0.314	-0.417	0.077	-0.136	-0.565	-0.332	-0.782	0.886	0.117	-0.802
11	Gnome	2.178	2.452	1.087	2.319	1.431	2.688	-1.393	-0.914	0.100	-0.656
12	Hardhat	3.293	3.321	2.319	3.245	2.420	3.505	-0.625	-0.740	-0.562	-0.396
13	Haymaker	2.495	0.965	2.235	2.208	1.889	2.276	-0.782	-0.399	-0.583	-0.074
14	Mad	-0.675	-0.746	-0.282	-0.527	-0.906	-0.545	0.206	-0.362	-0.934	-0.833
15	Madison	0.361	0.635	1.172	0.414	0.023	0.470	-0.452	-0.319	-0.020	-0.370
16	Marshmallow	-0.031	-0.150	0.094	-0.099	-0.530	-0.144	-0.170	-0.015	-0.356	-0.375
17	Mississippi	0.546	0.762	1.052	0.508	-0.178	0.427	-0.225	-0.221	-0.307	-0.084
18	Packrat	-0.177	-0.683	-0.657	-0.339	-1.351	-0.361		-0.230	-0.313	-1.041
19	Pampas	1.768	1.898	2.267	1.597	1.900	1.915	-1.119	-0.879	-0.614	0.134
20	Passaic	0.352	0.586	0.659	0.131	-0.257	0.156	0.002	-0.283	-0.227	-0.090
21	Platte	-0.181	-0.311	0.008	-0.197		-0.206		-0.211	0.014	-1.171
22	Scaramento	-0.221	-0.431	-0.436	0.145	-0.183	-0.202		0.063	-0.023	-0.599
23	Small Boy	-0.018	0.264	0.111	0.370		0.231	0.567	0.181	-0.356	-0.765
24	Stillwater	-0.622	-0.929	-0.916	-0.420		-0.643		1.170	0.926	-0.931
25	Stoat	-0.014	-0.627	-0.334	-0.199		-0.408		1.944	3.308	-1.311
26	Witchita	-0.468	-0.571	-0.300	-0.443		-0.441		-0.279	-0.330	-0.583
27	York	0.083	0.137	-0.026	-0.018		-0.086		-0.074	0.083	0.129

The margin function for a Random Forest is

$$\text{mr}(X, Y) = P_{\Theta}(h(X, \Theta) = Y) - \max_{j \neq Y} P_{\Theta}(h_K(X, \Theta) = j), \tag{5}$$

and the strength of the set of classifiers $\{(h(X, \Theta))\}$ is

$$s = E_{X,Y} \text{mr}(X, Y). \tag{6}$$

Assume that $s \geq 0$, Chebychev's inequality gives

$$PE^* \leq \frac{\text{var}(\text{mr})}{s^2}. \tag{7}$$

A more revealing expression for the variance of mr is derived in the following. Let

$$\hat{j}(X, Y) = \arg \max_{j \neq Y} P_{\Theta}(h(X, \Theta) = j) \tag{8}$$

so

$$\begin{aligned} \text{mr}(X, Y) &= P_{\Theta}(h(X, \Theta) = Y) - P_{\Theta}(h(X, \Theta) = \hat{j}(X, Y)) \\ &= E_{\Theta} \left[(I(X, \Theta) = Y) \right. \\ &\quad \left. - I(h(X, \Theta) = \hat{j}(X, Y)) \right]. \end{aligned} \tag{9}$$

The raw margin function is

$$\text{rmg}(\Theta, X, Y) = I(h(X, \Theta) = Y) - I(h(X, \Theta) = \hat{j}(X, Y)). \tag{10}$$

Thus, $\text{mr}(X, Y)$ is the expectation of $\text{rmg}(\Theta, X, Y)$ with respect to Θ . For any function f the identity

$$[E_{\Theta} f(\Theta)]^2 = E_{\Theta, \Theta'} f(\Theta) f(\Theta') \tag{11}$$

holds where Θ, Θ' are independent with the same distribution, implying that

$$\text{mr}(X, Y)^2 = E_{\Theta, \Theta'} \text{rmg}(\Theta, X, Y) \text{rmg}(\Theta', X, Y). \tag{12}$$

Using (12) gives

$$\begin{aligned} \text{var}(\text{mr}) &= E_{\Theta, \Theta'} \left(\text{cov}_{X,Y} \text{rmg}(\Theta, X, Y) \text{rmg}(\Theta', X, Y) \right) \\ &= E_{\Theta, \Theta'} \left(\rho(\Theta, \Theta') \text{sd}(\Theta) \text{sd}(\Theta') \right), \end{aligned} \tag{13}$$

where $\rho(\Theta, \Theta')$ is the correlation between $\text{rmg}(\Theta, X, Y)$ and $\text{rmg}(\Theta', X, Y)$ holding Θ, Θ' fixed and $\text{sd}(\Theta)$ is the standard deviation of $\text{rmg}(\Theta, X, Y)$ holding Θ fixed. Then,

$$\begin{aligned} \text{var}(\text{mr}) &= \bar{\rho}(E_{\Theta} \text{sd}(\Theta))^2 \\ &\leq \bar{\rho}E_{\Theta}v(\Theta), \end{aligned} \tag{14}$$

where $\bar{\rho}$ is the mean value of the correlation; that is,

$$\bar{\rho} = \frac{E_{\Theta, \Theta'}(\rho(\Theta, \Theta') \text{sd}(\Theta) \text{sd}(\Theta'))}{E_{\Theta, \Theta'}(\text{sd}(\Theta) \text{sd}(\Theta'))}. \tag{15}$$

Write

$$E_{\Theta} \text{var}(\Theta) \leq E_{\Theta}(E_{X, Y} \text{rmg}(\Theta, X, Y))^2 - S^2 \leq 1 - S^2. \tag{16}$$

In this work, A RF model of discriminating between natural earthquake and nuclear earthquake is established with optimal 5000 NT trees and 8 variables in rode. In the developed RF model, the calculated weighted values of the *Ratio*₁, *Ratio*₂, *Ratio*₃, *Ratio*₄, *Ratio*₅, *Ratio*₆, *Ratio*₇, *Ratio*₈, *Ratio*₉, and *AD* are 1.2713, 0.1034, 0.0759, 0.3093, 0.3432, 0.1782, 0.2536, 0.0943, 0.2463, and 0.1512, respectively.

2.2.2. SVM Algorithm. The original SVM algorithm was invented by Vladimir N. Vapnik and the current standard incarnation (soft margin) was proposed by Cortes and Vapnik in 1995 [27].

SVM models were originally defined for the classification of linearly separable classes of objects. For any original separable set of two-class objects SVM are able to find the optimal hyperplanes that separates them providing the bigger margin area between the two hyperplanes. Furthermore they can also be used to separate classes that cannot be separated with a linear classifier.

The feature space in which every object is projected is a high dimensional space in which the two classes can be separated with the linear classifier. The effectiveness of SVM depends on the selection of kernel, the kernel's parameters, and soft margin parameter *C*.

In the present work we used the Radial Basis Function (RBF) as Kernel functions for the SVM models because of its efficiency in providing very high performance classification results. The optimal RBF parameters *C* and gamma were found to be 9 and 0.6, respectively, reassuring that the model does not over fit.

2.2.3. Naive Bayes Classier. The Naive Bayes Classier produces a very efficient probability estimation based on a simply structure, requiring a small amount of training data to estimate the parameters necessary for the classification. Its construction relies on two main assumptions: independency of features and absence of hidden or latent attributes.

An advantage of Naive Bayes is that it only requires a small amount of training data to estimate the parameters (means and variances of the variables) necessary for classification. Because independent variables are assumed, only the variances of the variables for each class need to be determined and not the entire covariance matrix.

The aim of the NBC, as with other classifiers, is to assign an object *I* to one of a discrete set of categories *C*₁, *C*₂, . . . , *C*_{*m*} based on its observable attributes *X*₁, *X*₂, . . . , *X*_{*n*}. The NBC calculates the probability that *I* belongs to each category, conditioning on the observed attributes; *I* is typically assigned to the category with the greatest probability. This classifier is naive in the sense that it makes the strong assumption that the attributes are mutually conditionally independent; that is, the conditional probability that *I* belongs to a particular class given the value of some attribute is independent of the values of all other attributes. Despite this unrealistic assumption, empirical studies demonstrate that this assumption does not need to significantly compromise the accuracy of the prediction, and NBCs are used in a variety of applications, including document classification [28], medical diagnosis [29, 30], systems performance management [31], probability classification of rockburst [32], and other fields. Domingos and Pazzani [33] prove optimality of the NBC under certain conditions even when the conditional independence assumption is violated.

In this paper, the prior probability of natural earthquake and nuclear earthquake is calculated according to the size of data. The prior probabilities of earthquake and nuclear earthquake are 0.424 and 0.576, respectively.

The discriminate functions for the earthquake and nuclear are

$$\begin{aligned} Y_1 &= 0.45X_1 + 2.72X_2 - 1.28X_3 - 4.6X_4 + 1.61X_5 + 0.34X_6 \\ &\quad + 0.03X_7 - 0.17X_8 + 0.68X_9 + 1.65X_{10} - 1.92, \\ Y_2 &= -0.87X_1 - 2.28X_2 + 1.44X_3 + 4.34X_4 - 2.69X_5 \\ &\quad + 0.31X_6 - 2.04X_7 + 0.11X_8 + 0.68X_9 - 0.76X_{10} \\ &\quad - 1.73. \end{aligned} \tag{17}$$

If $Y_1 > Y_2$, the record is an earthquake, otherwise a nuclear event.

2.2.4. Classification Performance. ROC is a graphical plot which illustrates the performance of a binary classifier system as its discrimination threshold is varied [34]. It is created by plotting the fraction of true positives out of the positives (TPR = true positive rate) versus the fraction of false positives out of the negatives (FPR = false positive rate), at various threshold settings.

ROC analysis provides tools to select possibly optimal models and to discard suboptimal ones independently from (and prior to specifying) the cost context or the class distribution. ROC analysis is related in a direct and natural way to cost/benefit analysis of diagnostic decision making.

In this study, seismic event and nuclear explosion were considered as a two-class prediction problem (binary classification), in which the outcomes were labeled either as positive (*p*, events) or negative (*n*, blasts). There are four possible outcomes from a binary classifier. If the outcome from a prediction is *p'* and the actual value is also *p*, then it is called a true positive (TP); however, if the actual value is *n* then it is said to be a false positive (FP). Conversely, a true negative

TABLE 3: Contingency matrix for two class prediction problem.

Prediction outcome	Actual value		Total
	P	N	
p'	True Positive (TP)	False Positive (FP)	P
n'	False Negative (FN)	True Negative (TN)	N
Total	P	N	

(TN) has occurred when both the prediction outcome and the actual value is n and false negative (FN) is when the prediction outcome is n' , while the actual value is p .

An experiment from P positive and N negative was defined, for instance. The four outcomes can be formulated in a 2×2 contingency table or confusion matrix, as follows in Table 3.

The specificity or true negative rate (TNR) is defined as the percentage of seismic record which is correctly identified as being blast:

$$\text{TNR} = \frac{\text{TN}}{\text{TN} + \text{FP}}. \quad (18)$$

The quantity 1-specificity is the false positive rate (FPR) and is the percentage of seismic records that are incorrectly identified as being blasts. The sensitivity or true positive rate (TPR) is defined as the percentage of seismic records which is correctly identified as being events:

$$\text{TPR} = \frac{\text{TP}}{\text{TP} + \text{FN}}. \quad (19)$$

The accuracy (ACC) can be expressed as

$$\text{ACC} = \frac{\text{TP} + \text{TN}}{\text{TP} + \text{FN} + \text{FP} + \text{FN}}. \quad (20)$$

3. Results and Discussions

The back-test classification for training samples is calculated using established models. The back-test accuracies of RF, SVM, and NBC are 100%, 100%, and 96.97% for training samples, respectively. The one out cross-validation method was used to validate the methods. Results show that accuracies of RF, SVM (RBF), SVM (liner), and NBC are 100%, 96.97%, and 84.88%, respectively.

The ROC curve is also used to verify and compare the discriminating performance of established models. The established RF model, SVM model, and NBC model were applied to both the training and test samples. The ROC curve is shown in Figure 3. The area under the curve is listed in Table 4. The classification results of test samples using all developed models are presented in Table 5.

In Figure 3, the closer a result from a contingency table is to the upper left corner, the better it predicts, but the distance from the random guess line in either direction or area under curve is the best indicator of how much predictive power a method has.

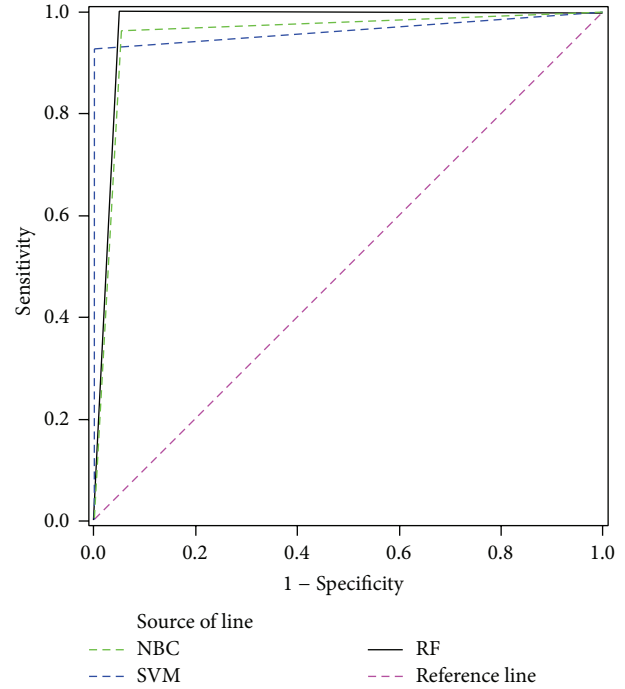


FIGURE 3: ROC of established RF, SVM (RBF), SVM (liner), and NBC models.

As shown in Figure 3 and Table 4, the result of RF method clearly shows the best predictive power with a maximum area of 0.975 among RF, SVM, and NBC. The result of SVM (area: 0.963) is better than that of NBC (area: 0.956).

According to Table 5, we can get the discriminant accuracy of RF, SVM, and NBC for test samples; their accuracy are 92.86%, 85.71%, and 92.86%, respectively. From back test results, one out cross-validation, ROC, and test results, we get the conclusion that RF discriminant model has the best accuracy and discriminant ability. Also, according to weighted values of RF, the most important factors are $Ratio_1$, followed by $Ratio_5$, $Ratio_4$, $Ratio_7$, $Ratio_9$, $Ratio_6$, AD , $Ratio_2$, $Ratio_8$, and $Ratio_3$.

4. Conclusions

RF, SVM, and NBC were applied to seismic event identification. A thorough investigation of the discrimination capabilities of the techniques were undertaken using seismograms from 20 earthquakes and 27 nuclear explosions. Ratios P_1/S_1 , P_2/S_2 , P_g/B , P_g/L_{g1} , $P_g/(R_{g1} + R)$, $P_g/(L_{g1} + R_{g1})$, R/R_{g1} , R_{g1}/L_{g1} , and R_{g2}/L_{g2} within certain velocity windows, as well as average distance, were selected as discriminant indicators.

The classification performance of RF, SVM, and NBC was analyzed and compared based on back test of training samples, one out cross-validation, and ROC curve. The result of RF method clearly shows the best predictive power with a maximum ROC area of 0.975 among RF, SVM, and NBC. The result of SVM (area: 0.963) is better than that of NBC (area: 0.956). Test results show the discriminant accuracies

TABLE 4: Area under the curve.

Test result variable(s)	Area	Std. error ^a	Asymptotic Sig. ^b	Asymptotic 95% confidence interval	
				Lower bound	Upper bound
NBC	0.956	0.035	0.000	0.887	1.026
SVM	0.963	0.030	0.000	0.904	1.022
RF	0.975	0.029	0.000	0.919	1.031

^aUnder the nonparametric assumption.

^bNull hypothesis: true area = 0.5.

TABLE 5: Discriminant results of test samples.

No.	Event	Measured results	NBC			SVM result		RF		
			Prob (N)	Prob (NE)	Result	Prob (N)	Prob (NE)	Result	Prob (N)	Prob (NE)
1	NE20	2	0.1646	0.8354	2	2	0.2354	0.7646	2	
2	NE21	2	0.0276	0.9724	2	2	0.018	0.982	2	
3	NE22	2	0.0041	0.9959	2	2	0.1572	0.8428	2	
4	NE23	2	0.0144	0.9856	2	2	0.0178	0.9822	2	
5	NE24	2	0.2324	0.7676	2	2	0.3342	0.6658	2	
6	NE25	2	0.4416	0.5584	2	2	0.0744	0.9256	2	
7	NE26	2	0.2447	0.7553	2	1*	0.1576	0.8424	2	
8	NE27	2	0.7336	0.2664	1*	1*	0.4752	0.5248	2	
9	E15	1	0.998	0.002	1	1	0.8934	0.1066	1	
10	E16	1	0.9991	0.0009	1	1	0.8214	0.1786	1	
11	E17	1	0.8956	0.1044	1	1	0.7562	0.2438	1	
12	E18	1	0.9807	0.0193	1	1	0.4076	0.5924	2*	
13	E19	1	0.9277	0.0723	1	1	0.8904	0.1096	1	
14	E20	1	0.9725	0.0275	1	1	0.9216	0.0784	1	

Note: result with “*” is incorrect.

of RF, SVM, and NBC are 92.86%, 85.71% and 92.86%, respectively.

From back-test results, one out cross-validation, ROC curve, and test results, we get the conclusion that RF discriminant model has the best accuracy and discriminant ability. Not only can RF discriminant method be applied to seismic identification with high accuracy, but also it can give the weighted sorts of discriminant indicators. In this study, the most important factors are *Ratio*₁, followed by *Ratio*₅, *Ratio*₄, *Ratio*₇, *Ratio*₉, *Ratio*₆, *AD*, *Ratio*₂, *Ratio*₈, and *Ratio*₃.

Conflict of Interests

The authors declare that there is no conflict of interests regarding the publication of this paper.

Acknowledgments

The authors gratefully acknowledge the financial support of the National Natural Science Foundation of China (50934006 and 41272304), National Basic Research (973) Program of China (2010CB732004), China Scholarship Council (CSC), Scholarship Award for Excellent Doctoral Student from Ministry of Education of China (105501010), and Support Program for Cultivating Excellent Ph.D. Thesis of Central South University.

References

- [1] L. Dong and X. Li, “A microseismic/acoustic emission source location method using arrival times of PS waves for unknown velocity system,” *International Journal of Distributed Sensor Networks*, vol. 2013, Article ID 307489, 8 pages, 2013.
- [2] L. Dong and X. Li, “Three-dimensional analytical solution of acoustic emission or microseismic source location under cube monitoring network,” *Transactions of Nonferrous Metals Society of China*, vol. 22, no. 12, pp. 3087–3094, 2012.
- [3] X. B. Li and L. J. Dong, “Comparison of two methods in acoustic emission source location using four sensors without measuring sonic speed,” *Sensor Letters*, vol. 9, no. 5, pp. 2025–2029, 2011.
- [4] L. Dong and X. Li, “Hypocenter relocation for Wenchuan Ms 8.0 and Lushan Ms 7.0 earthquakes using TT and TD methods,” *Disaster Advances*, vol. 6, no. 13, pp. 304–313, 2013.
- [5] Y. Gitterman, V. Pinsky, and A. Shapira, “Spectral discrimination analysis of Eurasian nuclear tests and earthquakes recorded by the Israel Seismic Network and the NORESS array,” *Physics of the Earth and Planetary Interiors*, vol. 113, no. 1–4, pp. 111–129, 1999.
- [6] S. J. Arrowsmith, M. D. Arrowsmith, M. A. H. Hedlin, and B. Stump, “Discrimination of delay-fired mine blasts in Wyoming using an automatic time-frequency discriminant,” *Bulletin of the Seismological Society of America*, vol. 96, no. 6, pp. 2368–2382, 2006.
- [7] A. J. Mendecki, *Seismic Monitoring in Mines*, Chapman & Hall, 1996.

- [8] J. Wuster, "Discrimination of chemical explosions and earthquakes in central Europe—a case study," *Bulletin of the Seismological Society of America*, vol. 83, no. 4, pp. 1184–1212, 1993.
- [9] R. Blandford, "Discrimination between earthquakes and underground explosions," *Annual Review of Earth and Planetary Sciences*, vol. 5, p. 111, 1977.
- [10] A. T. Smith, "Discrimination of explosions from simultaneous mining blasts," *Bulletin of the Seismological Society of America*, vol. 83, no. 1, pp. 160–179, 1993.
- [11] D. R. Baumgardt and G. B. Young, "Regional seismic waveform discriminants and case-based event identification using regional arrays," *Bulletin of the Seismological Society of America*, vol. 80, no. 6, pp. 1874–1892, 1990.
- [12] S. R. Taylor, M. D. Denny, E. S. Vergino, and R. E. Glaser, "Regional discrimination between NTS explosions and western US earthquakes," *Bulletin of the Seismological Society of America*, vol. 79, no. 4, pp. 1142–1176, 1989.
- [13] S. Taylor, M. Denny, and E. Vergino, "Regional m/sub b: M/sub s/discrimination of NTS explosions and western United States earthquakes," Progress Report, Lawrence Livermore National Laboratory, Livermore, Calif, USA, 1986.
- [14] S. G. Kim, Y. Park, and W. Kim, "Discrimination of small earthquakes and artificial explosions in the Korean Peninsula using Pg/Lg ratios," *Geophysical Journal International*, vol. 134, no. 1, pp. 267–276, 1998.
- [15] D. R. Baumgardt and K. A. Ziegler, "Spectral evidence for source multiplicity in explosions: application to regional discrimination of earthquakes and explosions," *Bulletin of the Seismological Society of America*, vol. 78, no. 5, pp. 1773–1795, 1988.
- [16] M. A. H. Hedlin, J. B. Minster, and J. A. Orcutt, "An automatic means to discriminate between earthquakes and quarry blasts," *Bulletin of the Seismological Society of America*, vol. 80, no. 6, pp. 2143–2160, 1990.
- [17] Y. Gitterman and T. van Eck, "Spectra of quarry blasts and microearthquakes recorded at local distances in Israel," *Bulletin of the Seismological Society of America*, vol. 83, no. 6, pp. 1799–1812, 1993.
- [18] A. Booker and W. Mitronovas, "An application of statistical discrimination to classify seismic events," *Bulletin of the Seismological Society of America*, vol. 54, no. 3, pp. 961–971, 1964.
- [19] L. Dong, X. Li, C. Ma, and W. Zhu, "Comparisons of Logistic regression and Fisher discriminant classifier to seismic event identification," *Disaster Advances*, vol. 6, supplement 4, pp. 1–8, 2013.
- [20] L. Breiman, "Random forests," *Machine Learning*, vol. 45, no. 1, pp. 5–32, 2001.
- [21] V. F. Rodriguez-Galiano, B. Ghimire, J. Rogan, M. Chica-Olmo, and J. P. Rigol-Sanchez, "An assessment of the effectiveness of a random forest classifier for land-cover classification," *ISPRS Journal of Photogrammetry and Remote Sensing*, vol. 67, no. 1, pp. 93–104, 2012.
- [22] P. M. Granitto, F. Gasperi, F. Biasoli, E. Trainotti, and C. Furlanello, "Modern data mining tools in descriptive sensory analysis: a case study with a Random forest approach," *Food Quality and Preference*, vol. 18, no. 4, pp. 681–689, 2007.
- [23] R. Genuer, J. Poggi, and C. Tuleau-Malot, "Variable selection using random forests," *Pattern Recognition Letters*, vol. 31, no. 14, pp. 2225–2236, 2010.
- [24] L. J. Dong, X. B. Li, and K. Peng, "Prediction of rockburst classification using Random Forest," *Transactions of Nonferrous Metals Society of China*, vol. 23, no. 2, pp. 472–477, 2013.
- [25] L. Dong and X. Li, "Comprehensive models for evaluating rockmass stability based on statistical comparisons of multiple classifiers," *Mathematical Problems in Engineering*, vol. 2013, Article ID 395096, 10 pages, 2013.
- [26] L. J. Dong, X. B. Li, M. Xu, and Q. Li, "Comparisons of random forest and Support Vector Machine for predicting blasting vibration characteristic parameters," *Procedia Engineering*, vol. 26, pp. 1772–1781, 2011.
- [27] C. Cortes and V. Vapnik, "Support-vector networks," *Machine Learning*, vol. 20, no. 3, pp. 273–297, 1995.
- [28] M. E. Maron, "Automatic indexing: an experimental inquiry," *Journal of the ACM*, vol. 8, no. 3, pp. 404–417, 1961.
- [29] I. Kononenko, "Inductive and Bayesian learning in medical diagnosis," *Applied Artificial Intelligence*, vol. 7, no. 4, pp. 317–337, 1993.
- [30] P. Berchiolla, F. Foltran, and D. Gregori, "Naïve Bayes classifiers with feature selection to predict hospitalization and complications due to objects swallowing and ingestion among European children," *Safety Science*, vol. 51, no. 1, pp. 1–5, 2013.
- [31] R. Powers, M. Goldszmidt, and I. Cohen, "Short term performance forecasting in enterprise systems," in *Proceedings of the 11th ACM SIGKDD International Conference on Knowledge Discovery and Data Mining (KDD '05)*, pp. 801–807, ACM, August 2005.
- [32] Y. Fu and L. Dong, "Bayes discriminant analysis model and its application to the prediction and classification of rockburst," *Journal of China University of Mining and Technology*, vol. 38, no. 4, pp. 56–64, 2009.
- [33] P. Domingos and M. Pazzani, "On the optimality of the simple Bayesian classifier under zero-one loss," *Machine Learning*, vol. 29, no. 2-3, pp. 103–130, 1997.
- [34] A. P. Bradley, "The use of the area under the ROC curve in the evaluation of machine learning algorithms," *Pattern Recognition*, vol. 30, no. 7, pp. 1145–1159, 1997.

Research Article

Hybrid Bernstein Block-Pulse Functions Method for Second Kind Integral Equations with Convergence Analysis

Mohsen Alipour,¹ Dumitru Baleanu,^{2,3,4} and Fereshteh Babaei¹

¹ Faculty of Basic Science, Babol University of Technology, P.O. Box 47148-71167, Babol, Iran

² Department of Mathematics, Cankaya University, Ogretmenler Caddesi 14, Balgat, 06530 Ankara, Turkey

³ Institute of Space Sciences, P.O. Box MG 23, Magurele, 077125 Bucharest, Romania

⁴ Department of Chemical and Materials Engineering, Faculty of Engineering, King Abdulaziz University, P.O. Box 80204, Jeddah 21589, Saudi Arabia

Correspondence should be addressed to Mohsen Alipour; m.alipour2323@gmail.com

Received 22 November 2013; Accepted 9 January 2014; Published 23 February 2014

Academic Editor: Carlo Cattani

Copyright © 2014 Mohsen Alipour et al. This is an open access article distributed under the Creative Commons Attribution License, which permits unrestricted use, distribution, and reproduction in any medium, provided the original work is properly cited.

We introduce a new combination of Bernstein polynomials (BPs) and Block-Pulse functions (BPFs) on the interval $[0, 1]$. These functions are suitable for finding an approximate solution of the second kind integral equation. We call this method Hybrid Bernstein Block-Pulse Functions Method (HBBPFM). This method is very simple such that an integral equation is reduced to a system of linear equations. On the other hand, convergence analysis for this method is discussed. The method is computationally very simple and attractive so that numerical examples illustrate the efficiency and accuracy of this method.

1. Introduction

In recent years, many different basic functions have been used for solving integral equations, such as Block-Pulse functions [1, 2], Triangular functions [3], Haar functions [4], Hybrid Legendre and Block-Pulse functions [5], Hybrid Chebyshev and Block-Pulse functions [6, 7], Hybrid Taylor and Block-Pulse functions [8], and Hybrid Fourier and Block-Pulse functions [9].

Block-Pulse functions were introduced in electrical engineering by Harmuth. After that study, several researchers have discussed applications of Block-Pulse functions [10, 11].

Bernstein polynomials have been applied in various fields of mathematics. For example, some researchers applied the Bernstein polynomials for solving high order differential equations [12], some classes of integral equations [13], partial differential equations, and optimal control problems [14]. Also, we introduced new operational matrices of fractional derivative and integral operators by Bernstein polynomials and then used them for solving fractional differential

equations [15–17], system of fractional differential equations [18], and fractional optimal control problems [19, 20].

In this work, we combine the Bernstein polynomials (BPs) and Block-Pulse functions (BPFs) on the interval $[0, 1]$. Then, we use these bases for finding an approximate solution of the second kind integral equation. We call this method Hybrid Bernstein Block-Pulse Functions Method (HBBPFM). In this method the integral equation is reduced to a system of linear equations. Also, we discuss the convergence analysis for this method. Furthermore, we compare the accuracy of obtained results of BPFs, BPs, and HBBPFM by some examples.

The rest of this paper is as follows. In Section 2, HBBPFs are introduced; therefore we approximate functions by using HBBPFs and also we discuss best approximation and convergence analysis in Section 3. Then we apply HBBPF method to find an approximate solution for the second kind integral equations and we survey error analysis for proposed method in Section 4. Also, we apply the proposed method on some examples. We observe that the accuracy and efficiency of this

method are more than the near methods. Finally, Section 6 concludes our work in this paper.

2. Hybrid of Bernstein and Block-Pulse Functions

In this section, we recall some definitions and properties of Bernstein polynomials and Block-Pulse functions.

Lemma 1 (see [19]). *The Bernstein polynomials (BPs) of m th-degree are defined on the interval $[0, 1]$ as follows:*

$$B_{i,m}(x) = \binom{m}{i} x^i (1-x)^{m-i}, \quad i = 0, 1, \dots, m, \quad (1)$$

where

$$\binom{m}{i} = \frac{m!}{i!(m-i)!}. \quad (2)$$

Then $\{B_{0,m}, B_{1,m}, \dots, B_{m,m}\}$ in Hilbert space $L^2[0, 1]$ is a complete basis. Therefore, any polynomial of degree m can be expanded in terms of linear combination of $B_{i,m}(x)$ ($i = 0, 1, \dots, m$).

Lemma 2. *Let a set of Block-Pulse functions (BPFs) $b_i(t)$, $i = 1, 2, \dots, N$ be on the interval $[0, 1)$ such that.*

$$b_i(t) = \begin{cases} 1, & \frac{i-1}{N} \leq t < \frac{i}{N}, \\ 0, & \text{otherwise.} \end{cases} \quad (3)$$

Then, the following properties for these functions satisfy the following:

- (i) disjointness,
- (ii) orthogonality,
- (iii) completeness.

Proof. The disjointness property can be clearly obtained from the definition of Block-Pulse functions as follows:

$$b_i(t) b_j(t) = \begin{cases} b_i(t), & i = j, \\ 0, & i \neq j, \end{cases} \quad (4)$$

where $i, j = 1, 2, \dots, N$.

The other property is orthogonality. It is clear that

$$\int_0^1 b_i(t) b_j(t) dt = \frac{1}{N} \delta_{ij}, \quad (5)$$

where $i, j = 1, 2, \dots, N$ and δ_{ij} is the Kroneker delta.

The third property is completeness. For every $f \in L^2([0, 1))$, when m approaches the infinity, Parseval's identity holds:

$$\int_0^1 f^2(x) dx = \sum_{i=0}^{\infty} (f_i^2 \|b_i(t)\|^2), \quad (6)$$

where $f_i = N \int_0^1 f(t) b_i(t) dt$. □

Definition 3 (Hybrid Bernstein Block-Pulse Functions (HBBPFs)). $H_{n,m}(t)$, $n = 1, 2, \dots, N$, $m = 0, 1, \dots, M$, have three arguments; n and m are the order of BPFs and BPs, respectively, and t is the normalized time. HBBPFs are defined on the interval $[0, 1)$ as follows:

$$H_{n,m}(t) = \begin{cases} B_{m,M}(Nt - n + 1), & \frac{n-1}{N} \leq t \leq \frac{n}{N}, \\ 0, & \text{otherwise.} \end{cases} \quad (7)$$

In the next section, we deal with the problem of approximation of these functions.

3. Approximation of Functions by Using HBBPFs and Convergence Analysis

Theorem 4. *Suppose that the function $f : [0, 1] \rightarrow R$ is $m + 1$ times continuously differentiable, and $S = \text{Span}\{B_{0,m}, B_{1,m}, \dots, B_{m,m}\}$. Then $c^T B = s_0 = \sum_{i=0}^m c_i B_{i,m} \in S$ is the best approximation f out of $S \subseteq L^2[0, 1]$ with the following inner product:*

$$\begin{aligned} \langle f, B \rangle &= \int_0^1 f(x) B(x)^T dx \\ &= [\langle f, B_{0,m} \rangle, \langle f, B_{1,m} \rangle, \dots, \langle f, B_{m,m} \rangle], \end{aligned} \quad (8)$$

where $B^T = [B_{0,m}, B_{1,m}, \dots, B_{m,m}]$ and $c^T = [c_1, c_2, \dots, c_m]$. Also, one can obtain the following inequality:

$$\|f - c^T B\|_{L^2[0,1]} \leq \frac{\widehat{K}}{(m+1)! \sqrt{2m+3}}, \quad (9)$$

where $\widehat{K} = \max_{x \in [0,1]} |f^{(m+1)}(x)|$.

Proof. We prove that $c^T B$ is the best approximation for f out of S . We can prove that S is a convex subset of a real inner product space $L^2[0, 1]$ (see [21]). Therefore, for any $x \in L^2[0, 1]$, $\widehat{x} \in S$ is its best approximation in S if and only if it satisfies

$$\langle x - \widehat{x}, z - \widehat{x} \rangle \leq 0 \quad \forall z \in S, \quad (10)$$

where the inner product is defined by $\langle f, g \rangle = \int_0^1 f(t)g(t)dt$. Then for any $x \in L^2[0, 1]$, its best approximation is unique. Also, we know that $S \subset L^2[0, 1]$ is a convex and closed finite-dimensional subset of an inner product space $L^2[0, 1]$. Then for any $x \in L^2[0, 1]$, there is a unique element $\widehat{x} \in S$ such that $\|x - \widehat{x}\| = \inf_{z \in S} \|x - z\|$. Therefore, there exist the unique coefficients c_i , $i = 0, 1, \dots, m$ such that

$$f \cong s_0 = \sum_{i=0}^m c_i B_{i,m} = c^T B. \quad (11)$$

On the other hand, we can consider that $\{1, x, \dots, x^m\}$ is a basis for polynomials space of degree m . Therefore we define $y_1(x) = f(0) + x f'(0) + (x^2/2!) f''(0) + \dots + (x^m/m!) f^{(m)}(0)$. Hence, from Taylor expansion we have

$$|f(x) - y_1(x)| = \left| f^{(m+1)}(\xi_x) \frac{x^{m+1}}{(m+1)!} \right|, \quad (12)$$

TABLE 1: Absolute errors by using BPFs for $N = 4$, BPs for $M = 3$, and HBBPFM for $N = 4, M = 3$ in Example 1.

t	Method		
	BPFs $N = 4$	BPs $M = 3$	HBBPFM $N = 4, M = 3$
0	0.159448	0.000252739	2.57612×10^{-7}
0.1	0.0596148	0.0000539886	5.73616×10^{-8}
0.2	0.0392211	0.000110834	1.23088×10^{-7}
0.3	0.118936	0.0000398714	3.42659×10^{-7}
0.4	0.0250381	0.0000566614	2.06685×10^{-7}
0.5	0.167325	0.000106028	1.3331×10^{-6}
0.6	0.0821085	0.0000743689	3.07359×10^{-7}
0.7	0.00253325	0.0000243121	5.58694×10^{-7}
0.8	0.125405	0.000119641	7.24512×10^{-7}
0.9	0.0594347	0.000076931	4.20127×10^{-7}

TABLE 2: Absolute errors by using BPFs for $N = 5$, BPs for $M = 4$, and HBBPFs for $N = 5, M = 4$ in Example 1.

t	Method		
	BPFs $N = 5$	BPs $M = 4$	HBBPFM $N = 5, M = 4$
0	0.120718	0.0000294061	9.38506×10^{-9}
0.1	0.0208845	0.0000117512	4.43327×10^{-10}
0.2	0.124426	4.28074×10^{-6}	7.87196×10^{-9}
0.3	0.0275755	7.98903×10^{-6}	1.13157×10^{-9}
0.4	0.124293	8.7962×10^{-6}	6.2511×10^{-9}
0.5	0.034286	2.23581×10^{-7}	1.14373×10^{-9}
0.6	0.120604	8.9113×10^{-6}	1.22382×10^{-8}
0.7	0.0410285	7.57027×10^{-6}	1.62177×10^{-9}
0.8	0.230475	7.94076×10^{-6}	4.74483×10^{-10}
0.9	0.00358729	0.0000229948	9.2012×10^{-9}

where $\xi_x \in (0, 1)$. Since $c^T B$ is the best approximation f out of S , and we assume that $y_1 \in S$, therefore, we have

$$\begin{aligned} \|f - c^T B\|_{L^2[0,1]}^2 &\leq \|f - y_1\|_{L^2[0,1]}^2 \\ &= \int_0^1 |f(x) - y_1(x)|^2 dx \\ &= \int_0^1 |f^{(m+1)}(\xi_x)|^2 \left(\frac{x^{m+1}}{(m+1)!}\right)^2 dx \quad (13) \\ &\leq \frac{\widehat{K}^2}{(m+1)!^2} \int_0^1 x^{2m+2} dx \\ &= \frac{\widehat{K}^2}{(m+1)!^2 (2m+3)}. \end{aligned}$$

Then by taking square roots, the proof is complete. \square

The previous theorem shows that the error vanishes as $m \rightarrow \infty$.

TABLE 3: Absolute errors by using BPFs for $N = 4$, BPs for $M = 3$, and HBBPFM for $N = 4, M = 3$ in Example 2.

t	Method		
	BPFs $N = 4$	BPs $M = 3$	HBBPFM $N = 4, M = 3$
0	0.134438	0.000939946	2.60043×10^{-6}
0.1	0.0292675	0.000210236	6.00397×10^{-7}
0.2	0.0869644	0.000396173	1.08124×10^{-6}
0.3	0.103935	0.000126329	1.37399×10^{-6}
0.4	0.0380311	0.000213179	7.99831×10^{-7}
0.5	0.216077	0.00037144	4.28735×10^{-6}
0.6	0.0426798	0.000246979	9.89894×10^{-7}
0.7	0.148954	0.0000965353	1.78268×10^{-6}
0.8	0.167943	0.000412916	2.26538×10^{-6}
0.9	0.0661188	0.000254268	1.31873×10^{-6}

TABLE 4: Absolute errors by using BPFs for $N = 5$, BPs for $M = 4$, and HBBPFs for $N = 5, M = 4$ in Example 2.

t	Method		
	BPFs $N = 5$	BPs $M = 4$	HBBPFM $N = 5, M = 4$
0	0.106159	0.0000526416	1.44355×10^{-8}
0.1	0.000988576	0.0000210365	1.12472×10^{-9}
0.2	0.128144	8.80224×10^{-6}	1.65937×10^{-8}
0.3	0.000312002	0.0000141662	1.06195×10^{-9}
0.4	0.155374	0.0000171016	9.87722×10^{-9}
0.5	0.00152224	7.80052×10^{-7}	2.99127×10^{-9}
0.6	0.189012	0.0000166986	4.29645×10^{-8}
0.7	0.00262215	0.0000156271	7.92177×10^{-9}
0.8	0.230475	7.94076×10^{-6}	4.74483×10^{-10}
0.9	0.00358729	0.0000229948	9.2012×10^{-9}

Corollary 5. One can write $c^T \langle B, B \rangle \cong \langle f, B \rangle$, such that one defines $Q = \langle B, B \rangle$ that is a $(m+1) \times (m+1)$ matrix and is said dual matrix of B , and one can obtain

$$\begin{aligned} Q_{i+1,j+1} &= \int_0^1 B_{i,m}(x) B_{j,m}(x) dx \\ &= \frac{\binom{m}{i} \binom{m}{j}}{(2m+1) \binom{2m}{i+j}}, \quad i, j = 0, 1, \dots, m. \end{aligned} \quad (14)$$

Proof. We know

$$f \cong s_0 = \sum_{i=0}^m c_i B_{i,m} = c^T B; \quad (15)$$

therefore, the proof is complete. \square

Corollary 6. A function $f(t) \in L^2([0, 1])$ may be expanded as follows:

$$f(t) = \sum_{n=1}^{\infty} \sum_{m=0}^{\infty} p_{n,m} H_{n,m}(t). \quad (16)$$

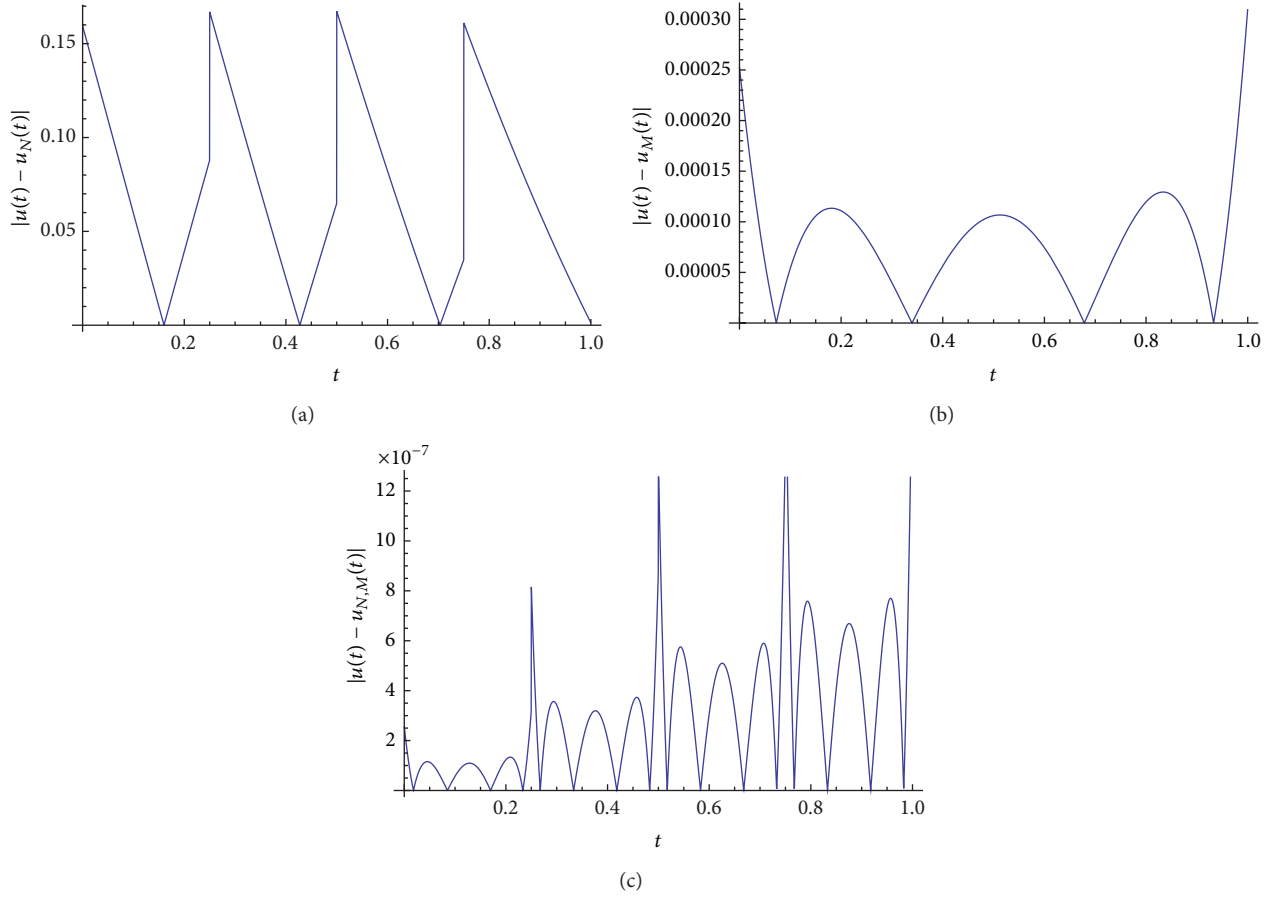


FIGURE 1: Plot of error functions by using BPFs for $N = 4$ (a), BPs for $M = 3$ (b), and HBBPFM for $N = 4, M = 3$ (c) in Example 1.

If the infinite series in (16) is truncated, then we have

$$f(t) \approx \sum_{n=1}^N \sum_{m=0}^M p_{n,m} H_{n,m}(t) = P^T H(t), \quad (17)$$

where

$$H(t) = [H_{1,0}(t), H_{1,1}(t), \dots, H_{1,M}(t), \quad (18)$$

$$H_{2,0}(t), H_{2,1}(t), \dots, H_{N,M}(t)]^T,$$

$$P = [p_{1,0}, p_{1,1}, \dots, p_{1,M}, p_{2,0}, p_{2,1}, \dots, p_{N,M}]^T. \quad (19)$$

Therefore we can get

$$P^T \langle H(t), H(t) \rangle = \langle f(t), H(t) \rangle. \quad (20)$$

Then

$$P = D^{-1} \langle f(t), H(t) \rangle, \quad (21)$$

where

$$D = \langle H(t), H(t) \rangle = \int_0^1 H(t) H^T(t) dt$$

$$= \begin{bmatrix} D_1 & 0 & \cdots & 0 \\ 0 & D_2 & \cdots & 0 \\ \vdots & \vdots & \ddots & \vdots \\ 0 & 0 & \cdots & D_N \end{bmatrix}, \quad (22)$$

where by using (7), D_n ($n = 1, 2, \dots, N$) is defined as follows:

$$(D_n)_{i+1,j+1} = \int_{(n-1)/N}^{n/N} B_{i,M}(Nt - n + 1) B_{j,M}(Nt - n + 1) dt$$

$$= \frac{1}{N} \int_0^1 B_{i,M}(t) B_{j,M}(t) dt$$

$$= \frac{\binom{M}{i} \binom{M}{j}}{N(2M+1) \binom{2M}{i+j}}, \quad i, j = 0, 1, \dots, M. \quad (23)$$

We can also approximate the function $k(t, s) \in L^2([0, 1] \times [0, 1])$ as follows:

$$k(t, s) \approx H^T(t) K H(s), \quad (24)$$

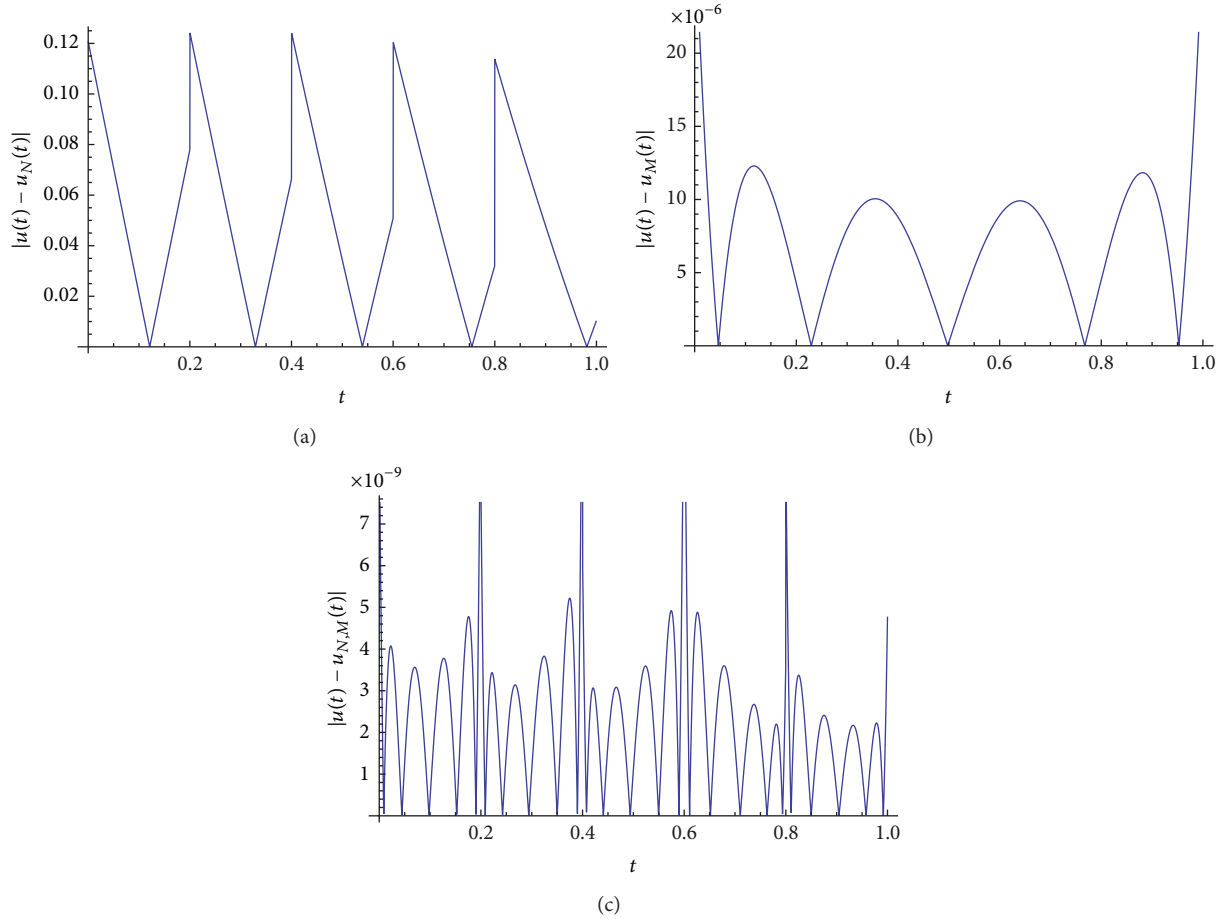


FIGURE 2: Plot of error functions by using BPFs for $N = 5$ (a), BPs for $M = 4$ (b), and HBBPFM for $N = 5, M = 4$ (c) in Example 1.

where K is an $N(M + 1) \times N(M + 1)$ matrix that we can obtain as follows:

$$K = D^{-1} \langle H(t), \langle k(t, s), H(s) \rangle \rangle D^{-1}. \quad (25)$$

Theorem 7. Let the function $f : [0, 1] \rightarrow R$ be $M + 1$ times continuously differentiable; then we have

$$\|f - P^T H\|_{L^2[0,1]} \leq \frac{\tilde{K}}{N^{2M+3} (M + 1)! \sqrt{2M + 3}}, \quad (26)$$

where $\tilde{K} = \max_{t \in [0,1]} |f^{(M+1)}(t)|$.

Proof. By using Theorem 4 we get

$$\begin{aligned} & \|f - P^T H\|_{L^2[0,1]}^2 \\ &= \int_0^1 |f(t) - P^T H(t)|^2 dx \end{aligned}$$

$$\begin{aligned} &= \sum_{n=1}^N \left(\int_{(n-1)/N}^{n/N} \left| f(t) \right. \right. \\ &\quad \left. \left. - \sum_{m=0}^M p_{n,m} B_{m,M}(Nt - n + 1) \right|^2 \right) dt \\ &= \frac{1}{N} \sum_{n=1}^N \int_0^1 \left| f\left(\frac{t+n-1}{N}\right) - \sum_{m=0}^M p_{n,m} B_{n,m}(t) \right|^2 dt \\ &\leq \frac{1}{N^{2M+3}} \sum_{n=1}^N \int_0^1 |f^{(M+1)}(\xi_n)|^2 \frac{t^{2M+2}}{(M+1)!^2} dt \\ &\leq \frac{1}{N^{2M+3}} \sum_{n=1}^N \frac{\widehat{K}_n^2}{(M+1)!^2 (2M+3)} \\ &\leq \frac{\widehat{K}^2}{N^{2M+2} (M+1)!^2 (2M+3)}, \end{aligned} \quad (27)$$

where $\xi_n \in ((n-1)/N, n/N)$ and $\widehat{K}_n = \max_{t \in [(n-1)/N, n/N]} |f^{(M+1)}(t)|$. Therefore by taking square roots, the proof is complete. \square

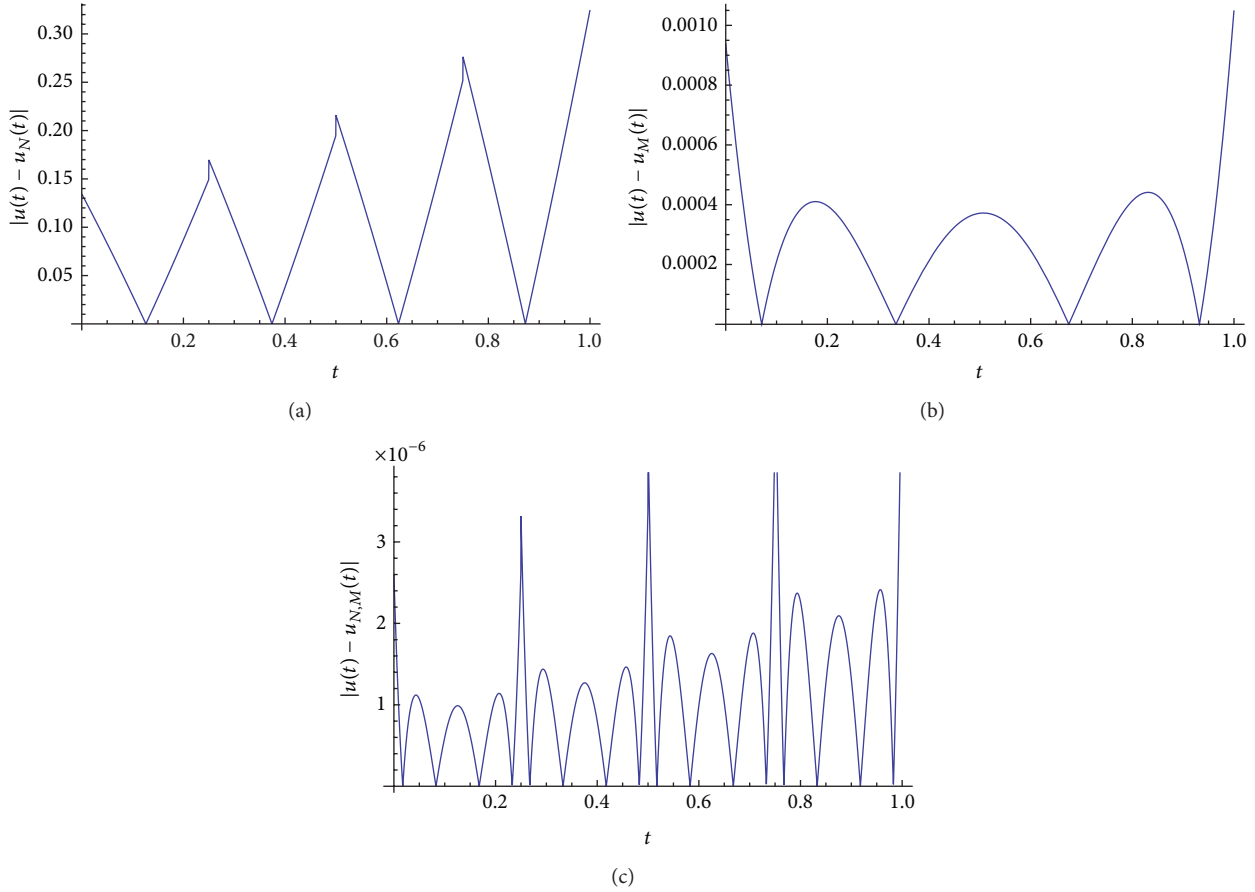


FIGURE 3: Plot of error functions by using BPFs for $N = 4$ (a), BPs for $M = 3$ (b), and HBBPFM for $N = 4, M = 3$ (c) in Example 2.

The above theorem shows that the approximation error vanishes as $M, N \rightarrow \infty$.

4. HBBPFs for the Second Kind Integral Equations and Error Analysis

In this section, we are dealing with the following Fredholm equations of the second kind:

$$u(t) = \int_0^1 k(t,s)u(s)ds + f(t), \tag{28}$$

where $u, f \in L^2([0, 1]), k \in L^2([0, 1] \times [0, 1])$, and $u(t)$ is an unknown function.

Let us approximate u, f , and k by (18) and (25) as follows:

$$\begin{aligned} u(t) &\approx U^T H(t), & f(t) &\approx F^T H(t), \\ k(t,s) &\approx H^T(t)KH(t). \end{aligned} \tag{29}$$

By substituting (29) in (28) we obtain

$$\begin{aligned} H^T(t)U &= \int_0^1 H^T(t)KH(s)H^T(s)U ds + H^T(t)F \\ &= H^T(t)K \left(\int_0^1 H(s)H^T(s)ds \right)U + H^T(t)F \\ &= H^T(t)KDU + H^T(t)F = H^T(t)(KDU + F). \end{aligned} \tag{30}$$

Therefore we have the following linear system:

$$(I - KD)U = F, \tag{31}$$

that by solving this linear system we can obtain the vector U .

Theorem 8. Suppose that $u(t)$ is exact solution of (28) and $u_{N,M}(t)$ is approximate solution by HBBPFs for $u(t)$ and $E_{N,M}(t)$ is perturbation function that depends only on $u_{N,M}(t)$ (i.e., $u_{N,M}(t) = \int_0^1 k(t,s)u_{N,M}(s)ds + f(t) + E_{N,M}(t)$). Let $R = \max_{0 \leq t, s \leq 1} |k(s,t)| < \infty$. Then $E_{N,M}(t) \rightarrow 0$ as $M, N \rightarrow \infty$.

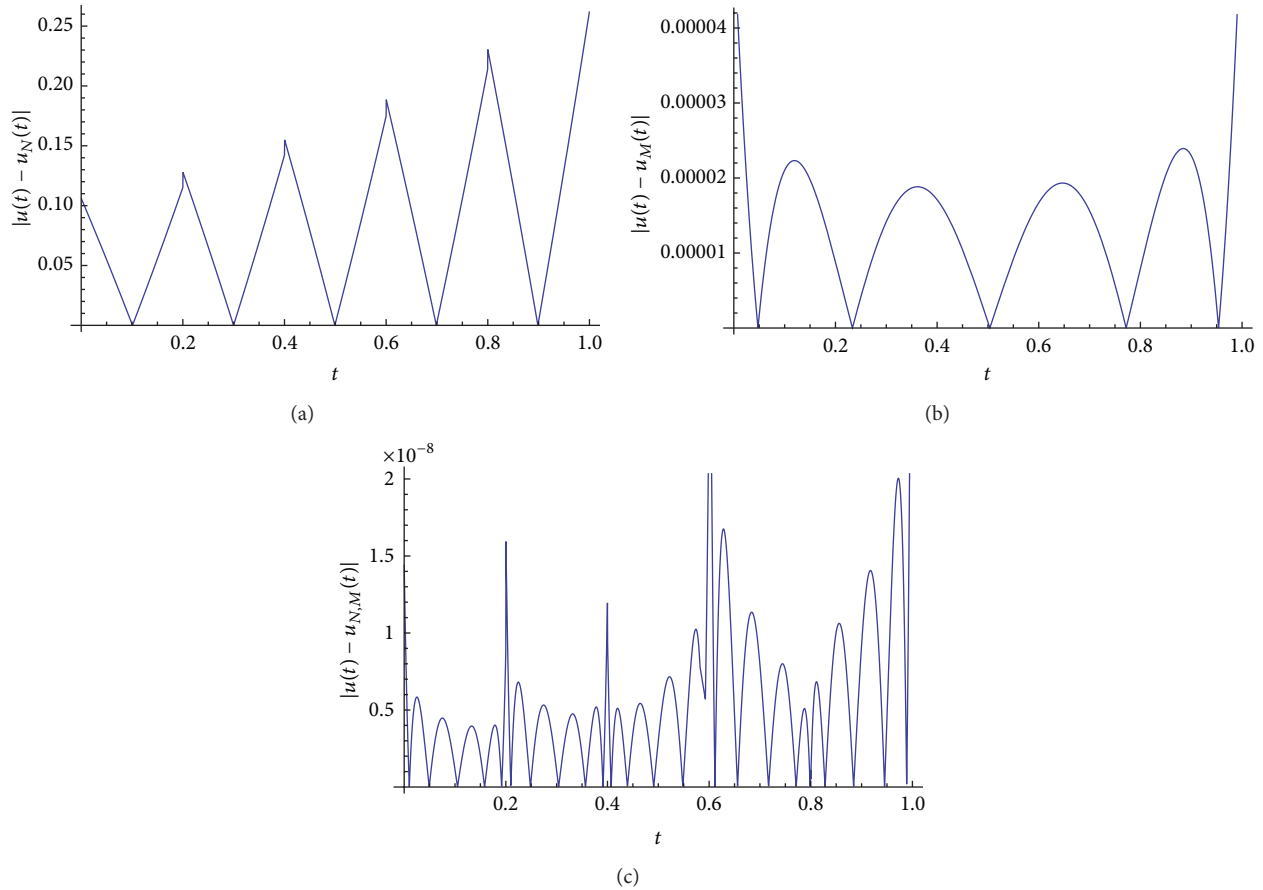


FIGURE 4: Plot of error functions by using BPFs for $N = 5$ (a), BPs for $M = 4$ (b), and HBBPFM for $N = 5, M = 4$ (c) in Example 2.

Proof. Suppose $e_{N,M}(t) = u(t) - u_{N,M}(t)$ is the error function of approximate solution $u_{N,M}(t)$ to the exact solution $u(t)$. Therefore we get

$$e_{N,M}(t) = \int_0^1 k(t,s)e_{N,M}(s) ds - E_{N,M}(t). \quad (32)$$

By taking absolute value and using Holder inequality we get

$$\begin{aligned} |E_{N,M}(t)| &\leq \int_0^1 |k(t,s)| |e_{N,M}(s)| ds + |e_{N,M}(t)| \\ &\leq \left(\int_0^1 |k(t,s)|^2 ds \right)^{1/2} \left(\int_0^1 |e_{N,M}(t)|^2 ds \right)^{1/2} \\ &\quad + |e_{N,M}(t)| \\ &\leq R \|e_{N,M}(t)\|_{L^2[0,1]} + |e_{N,M}(t)|. \end{aligned} \quad (33)$$

Now, by taking norm $L^2([0, 1])$ we obtain

$$\|E_{N,M}(t)\|_{L^2[0,1]} \leq (R + 1) \|e_{N,M}(t)\|_{L^2[0,1]}. \quad (34)$$

Finally, from Theorem 7 we can write

$$\|E_{N,M}(t)\|_{L^2[0,1]} \leq \frac{(R + 1) \bar{K}}{N^{M+1} (M + 1)! \sqrt{2M + 3}}, \quad (35)$$

where $\bar{K} = \max_{t \in [0,1]} |u^{(M+1)}(t)|$.

Therefore, we can show that $E_{N,M}(t) \rightarrow 0$ as $M, N \rightarrow \infty$. \square

5. Numerical Examples

In this section we discuss the implementation of the new method and investigate its accuracy by applying it to different examples. In the following examples, we suppose that $u_N(t)$, $u_M(t)$, and $u_{M,N}(t)$ are approximate solutions by BPFs, BPs, and HBBPFM for the exact solution $u(t)$, respectively.

Example 1. Consider the following integral equation:

$$\begin{aligned} u(t) &= \int_0^1 (t + s) u(s) ds + \sin(t) \\ &\quad - t + (t + 1) \cos(1) - \sin(1). \end{aligned} \quad (36)$$

We know that the exact solution is $u(t) = \sin(t)$. The obtained results of BPFs, BPs, and HBBPFs are reported in Tables 1 and 2 and are plotted in Figures 1 and 2. We compare the obtained results and observe that HBBPFM is very effective and accuracy of approximate solutions in this method is more than methods of BPFs and BPs.

Example 2. Consider the following integral equation:

$$u(t) = \int_0^1 tsu(s) ds + e^t - t, \quad (37)$$

with exact solution $u(t) = e^t$. We obtain the computational by BPFs, BPs, and HBBPFM with $N = 4$, $M = 3$, and $N = 5$, $M = 4$; then we compare them together. The results are reported in Tables 3 and 4 and are plotted in Figures 3 and 4. Similar to the previous example, we see that the method HBBPFM is very effective and accuracy of solution in this method is more than methods of BPFs and BPs.

6. Conclusion

In this paper, HBBPFs are used to solve second kind integral equations we call this method with HBBPFM. This method converts second kind integral equations to systems of linear equations whose answers are coefficient of HBBPFs expansion of the solution of second kind integral equations. Also, by using several lemmas and theorems, we have discussed convergence analysis of the proposed method. Numerical examples show the efficiency and accuracy of the method. Moreover we see that accuracy of solutions in HBBPFM is more satisfactory than the methods of BPFs and BPs.

Conflict of Interests

The authors declare that there is no conflict of interests in this paper.

References

- [1] E. Babolian and Z. Masouri, "Direct method to solve Volterra integral equation of the first kind using operational matrix with block-pulse functions," *Journal of Computational and Applied Mathematics*, vol. 220, no. 1-2, pp. 51-57, 2008.
- [2] K. Maleknejad and B. Rahimi, "Modification of block pulse functions and their application to solve numerically Volterra integral equation of the first kind," *Communications in Nonlinear Science and Numerical Simulation*, vol. 16, no. 6, pp. 2469-2477, 2011.
- [3] F. Mirzaee and S. Piroozfar, "Numerical solution of the linear two-dimensional Fredholm integral equations of the second kind via two-dimensional triangular orthogonal functions," *Journal of King Saud University - Science*, vol. 22, no. 4, pp. 185-193, 2010.
- [4] Y. Ordokhani, "Solution of nonlinear Volterra-Fredholm-Hammerstein integral equations via rationalized Haar functions," *Applied Mathematics and Computation*, vol. 180, no. 2, pp. 436-443, 2006.
- [5] H. R. Marzban, H. R. Tabrizidooz, and M. Razzaghi, "A composite collocation method for the nonlinear mixed Volterra-Fredholm-Hammerstein integral equations," *Communications in Nonlinear Science and Numerical Simulation*, vol. 16, no. 3, pp. 1186-1194, 2011.
- [6] M. Tavassoli Kajani and A. Hadi Vencheh, "Solving second kind integral equations with hybrid Chebyshev and block-pulse functions," *Applied Mathematics and Computation*, vol. 163, no. 1, pp. 71-77, 2005.
- [7] X. T. Wang and Y. M. Li, "Numerical solutions of integrodifferential systems by hybrid of general block-pulse functions and the second Chebyshev polynomials," *Applied Mathematics and Computation*, vol. 209, no. 2, pp. 266-272, 2009.
- [8] K. Maleknejad and Y. Mahmoudi, "Numerical solution of linear Fredholm integral equation by using hybrid Taylor and block-pulse functions," *Applied Mathematics and Computation*, vol. 149, no. 3, pp. 799-806, 2004.
- [9] B. Asady, M. Tavassoli Kajani, A. Hadi Vencheh, and A. Heydari, "Solving second kind integral equations with hybrid Fourier and block-pulse functions," *Applied Mathematics and Computation*, vol. 160, no. 2, pp. 517-522, 2005.
- [10] G. Prasada Rao, *Piecewise Constant Orthogonal Functions and their Application to Systems and Control*, Springer, Berlin, Germany, 1983.
- [11] B. M. Mohan and K. B. Datta, *Orthogonal Functions in Systems and Control*, 1995.
- [12] E. H. Doha, A. H. Bhrawy, and M. A. Saker, "Integrals of Bernstein polynomials: an application for the solution of high even-order differential equations," *Applied Mathematics Letters*, vol. 24, no. 4, pp. 559-565, 2011.
- [13] B. N. Mandal and S. Bhattacharya, "Numerical solution of some classes of integral equations using Bernstein polynomials," *Applied Mathematics and Computation*, vol. 190, no. 2, pp. 1707-1716, 2007.
- [14] S. A. Yousefi and M. Behroozifar, "Operational matrices of Bernstein polynomials and their applications," *International Journal of Systems Science*, vol. 41, no. 6, pp. 709-716, 2010.
- [15] M. Alipour and D. Rostamy, "Solving nonlinear fractional differential equations by Bernstein polynomials operational matrices," *The Journal of Mathematics and Computer Science*, vol. 5, no. 3, pp. 185-196, 2012.
- [16] D. Rostamy, M. Alipour, H. Jafari, and D. Baleanu, "Solving multi-term orders fractional differential equations by operational matrices of BPs with convergence analysis," *Romanian Reports in Physics*, vol. 65, no. 2, pp. 334-349, 2013.
- [17] D. Baleanu, M. Alipour, and H. Jafari, "The Bernstein operational matrices for solving the fractional quadratic Riccati differential equations with the Riemann-Liouville derivative," *Abstract and Applied Analysis*, vol. 2013, Article ID 461970, 7 pages, 2013.
- [18] M. Alipour and D. Baleanu, "Approximate analytical solution for nonlinear system of fractional differential equations by BPs operational matrices," *Advances in Mathematical Physics*, vol. 2013, Article ID 954015, 9 pages, 2013.
- [19] M. Alipour, D. Rostamy, and D. Baleanu, "Solving multi-dimensional fractional optimal control problems with inequality constraint by Bernstein polynomials operational matrices," *Journal of Vibration and Control*, vol. 19, no. 16, pp. 2523-2540, 2013.
- [20] M. Alipour and D. Rostamy, "BPs operational matrices for solving time varying fractional optimal control problems," *The Journal of Mathematics and Computer Science*, vol. 6, pp. 292-304, 2013.
- [21] K. Atkinson and W. Han, *Theoretical Numerical Analysis: A Functional Analysis Framework*, Springer, 2nd edition, 2000.

Research Article

Picard Successive Approximation Method for Solving Differential Equations Arising in Fractal Heat Transfer with Local Fractional Derivative

Ai-Min Yang,^{1,2} Cheng Zhang,³ Hossein Jafari,⁴ Carlo Cattani,⁵ and Ying Jiao⁶

¹ College of Science, Hebei United University, Tangshan, China

² College of Mechanical Engineering, Yanshan University, Qinhuangdao, China

³ School of Civil Engineering and Architecture, Chongqing Jiaotong University, Chongqing 400074, China

⁴ Faculty of Basic Sciences, Department of Mathematics, Ayatollah Amoli Branch, Islamic Azad University, Amol 4615143358, Iran

⁵ Department of Mathematics, University of Salerno, Via Ponte don Melillo, Fisciano, 84084 Salerno, Italy

⁶ Qinggong College, Hebei United University, Tangshan 063000, China

Correspondence should be addressed to Ai-Min Yang; aimin_heut@163.com

Received 12 December 2013; Accepted 1 January 2014; Published 11 February 2014

Academic Editor: Ming Li

Copyright © 2014 Ai-Min Yang et al. This is an open access article distributed under the Creative Commons Attribution License, which permits unrestricted use, distribution, and reproduction in any medium, provided the original work is properly cited.

The Fourier law of one-dimensional heat conduction equation in fractal media is investigated in this paper. An approximate solution to one-dimensional local fractional Volterra integral equation of the second kind, which is derived from the transformation of Fourier flux equation in discontinuous media, is considered. The Picard successive approximation method is applied to solve the temperature field based on the given Mittag-Leffler-type Fourier flux distribution in fractal media. The nondifferential approximate solutions are given to show the efficiency of the present method.

1. Introduction

Engineering problems can be mathematically described by differential equations. Many initial and boundary value problems associated with differential equations can be transformed into problems of solving some approximate integral equations. Heat transfer is described by theory of integral equations. Integral equation arising in heat transfer with smooth condition is valid for continuous media [1–4]. The common methods for solving the equations of heat transfer are purely mathematical are among them; the finite difference techniques (FDT) [5], the regression analysis (RA) [6], the Adomian decomposition method (ADM) [7], the combined Laplace-Adomian method (CLAM) [8], the homotopy analysis method (HAM) [9, 10], the differential transformation method (DTM) [11], the spline-wavelets techniques (SWT) [12], the boundary element method (BEM) [13], the heat-balance integral method (HBIM) [14, 15], the variational iteration method (VIM) [16], the local fractional variational

iteration method (LFVIM) [17], and the Picard successive approximation method (PSAM) [18].

On the other hand, the nanoscale heat problem can be characterized as fractal behaviors. As usual, the materials are called the Cantor materials. Heat transfer in fractal media with nonsmooth conditions is a hot topic. For example, the heat transfer equations in a medium with fractal geometry [19] and fractal domains [20] were considered. The local fractional transient heat conduction equations based upon the Fourier law within local fractional derivative arising in heat transfer from discontinuous media were presented in [21–24].

Fractional calculus was successfully used to deal with the real world problems [25–30]. There is its limit that the operators do not deal with the local fractional continuous functions (nondifferential functions). Hence, the local fractional Fourier flux [21] is not handled by using some approaches from the classical and fractional operators. This paper focuses on analytical solution to local fractional Fourier flux in fractal

media by using Picard’s successive approximation method [18]. This paper is organized as follows. In Section 2, we give notations to local fractional derivative and integrals and investigate the heat transfer in fractal media. Section 3 is devoted to Picard’s successive approximation method based upon local fractional integrals. Analysis solution is shown in Section 4. Conclusions are in Section 5.

2. Heat Transfer in Fractal Media with Local Fractional Derivative

In order to study the non-differential solution for the heat problem in fractal media with local fractional derivative, we here begin with the Fourier flux equation in discontinuous media.

The temperature field reads as [21]

$$T(x, y, z, \tau) = f(x, y, z, \tau) \quad \text{at } \tau > \tau_0 \text{ and in } \Omega, \quad (1)$$

where $f(x, y, z, \tau)$ is local fractional continuous at fractal domain Ω .

For a given temperature field T , a local fractional temperature gradient [21] can be written as follows:

$$\nabla^\alpha T = \frac{\partial^\alpha T}{\partial u_1^\alpha} e_1 + \frac{\partial^\alpha T}{\partial u_2^\alpha} e_2 + \frac{\partial^\alpha T}{\partial u_3^\alpha} e_3, \quad (2)$$

where the local fractional partial derivative is defined by [21–24]

$$\begin{aligned} f_x^{(\alpha)}(x_0, y) &= \left. \frac{\partial^\alpha f(x, y)}{\partial x^\alpha} \right|_{x=x_0} \\ &= \lim_{x \rightarrow x_0} \frac{\Delta^\alpha (f(x, y) - f(x_0, y))}{(x - x_0)^\alpha}, \end{aligned} \quad (3)$$

where $\Delta^\alpha (f(x, y) - f(x_0, y)) \cong \Gamma(1 + \alpha)\Delta(f(x, y) - f(x_0, y))$.

Here, the local fractional derivative is defined on the fractal set like a Cantor set. For example, when we consider the Cantor set, we can find the local fractional derivative of discontinuous function T (however, T is a local fractional continuous function).

We consider the heat flux per unit fractal area \vec{q} is proportional to the temperature gradient in fractal medium. Fourier law of heat conduction in fractal medium with local fractional derivative is expressed by [21]

$$\vec{q}(x, y, z, t) = -K^{2\alpha} \nabla^\alpha T(x, y, z, t), \quad (4)$$

where $K^{2\alpha}$ denotes the thermal conductivity of the fractal material, and it is related to fractal dimensions of materials. It is shown that the fractal dimensions of materials are an important characteristic value. Here, we consider the fractal Fourier flow, which is discontinuous; however, it is found that it is local fractional continuous. Like classical Fourier flow, its thermal conductivity is an approximate value for fractal one when $\alpha = 1$.

Fourier law of one-dimensional heat conduction equation in fractal media reads as [21]

$$q(x, t) = -K^{2\alpha} \frac{d^\alpha T(x, t)}{dx^\alpha}, \quad \text{at } \tau > \tau_0 \text{ and in } A, \quad (5)$$

where $K^{2\alpha}$ denotes the thermal conductivity of the fractal materials.

When $\tau = \tau_0$, from (5) we have

$$q(x) = -K^{2\alpha} \frac{d^\alpha T(x)}{dx^\alpha}, \quad (6)$$

at $\tau > \tau_0$ and in A , where $K^{2\alpha}$ is the thermal conductivity of the fractal materials. Namely, T is a bi-Lipschitz mapping, and shows the fractal characteristic behavior [21].

Local fractional heat conduction equation with heat generation in fractal media can be written as [21]

$$K^{2\alpha} \nabla^{2\alpha} T + g - \rho_\alpha c_\alpha \frac{\partial^\alpha T}{\partial t^\alpha} = 0 \quad \text{at } \tau > \tau_0 \text{ and in } \Omega. \quad (7)$$

Local fractional heat conduction equation with no heat generation in fractal media is suggested as [21, 22]

$$K^{2\alpha} \nabla^{2\alpha} T - \rho_\alpha c_\alpha \frac{\partial^\alpha T}{\partial t^\alpha} = 0 \quad \text{at } \tau > \tau_0 \text{ and in } \Omega, \quad (8)$$

where $\nabla^{2\alpha}$ is a local fractional Laplace operator [21].

3. The Method

In this section, we discuss the Picard successive approximation method. Meanwhile, we transfer the Fourier law of one-dimensional heat conduction equation in fractal media into the local fractional Volterra integral equation of the second kind.

3.1. Picard’s Successive Approximation Method. This method is first proposed in [18]. Here we will give a short introduction to Picard’s successive approximation method within the local fractional calculus.

In this method, we set

$$u_0(x) = f(x). \quad (9)$$

We give the first approximation $u_1(x)$ by

$$u_1(x) = f(x) + \frac{\lambda^\alpha}{\Gamma(1 + \alpha)} \int_0^x K(x, t) u_0(x) (dt)^\alpha, \quad (10)$$

where the local fractional integral of $f(x)$ of order α in the interval $[a, b]$ is defined as follows [21–24]:

$$\begin{aligned} {}_a I_b^{(\alpha)} f(x) &= \frac{1}{\Gamma(1 + \alpha)} \int_a^b f(t) (dt)^\alpha \\ &= \frac{1}{\Gamma(1 + \alpha)} \lim_{\Delta t \rightarrow 0} \sum_{j=0}^{j=N-1} f(t_j) (\Delta t_j)^\alpha \end{aligned} \quad (11)$$

with $\Delta t_j = t_{j+1} - t_j$, $\Delta t = \max\{\Delta t_0, \Delta t_1, \Delta t_2, \dots\}$, and $[t_j, t_{j+1}]$, $j = 0, \dots, N - 1$, $t_0 = a$, and $t_N = b$.

Here, we find that the equality $u_1(x)$ is a local fractional continuous function if $f(x)$, $K(x, t)$ and $u_0(x)$ are local fractional continuous functions.

Continuing in this manner, we have the infinite sequences of functions

$$u_0(x), u_1(x), u_2(x), \dots, u_n(x), \dots \quad (12)$$

such that the recurrence equations are given by

$$u_n(x) = f(x) - \frac{1}{\Gamma(1+\alpha)} \int_0^x K(x,t) u_{n-1}(x) (dt)^\alpha, \quad (13)$$

$$(n = 1, 2, 3, \dots),$$

where $u_0(x)$ is equivalent to any selected function, which is the local fractional continuous function.

Hence, we have successive approximation as follows:

$$u_1(x) = f(x) + \frac{\lambda^\alpha}{\Gamma(1+\alpha)} \int_0^x K(x,t) f(t) (dt)^\alpha,$$

$$\vdots \quad (14)$$

$$u_n(x) = f(x) + \frac{\lambda^\alpha}{\Gamma(1+\alpha)} \int_0^x K(x,t) u_{n-1}(x) (dt)^\alpha.$$

Thus, at the limit, the solution $u(x)$ is written as

$$u(x) = \lim_{n \rightarrow \infty} u_n(x). \quad (15)$$

3.2. *An Alternative Method from Local Fractional Derivative to Local Fractional Volterra Integral Equations.* We directly observe that the local fractional differential equation of α order

$$K^{2\alpha} \frac{d^{\alpha T}}{dx^\alpha} = q(x) \quad (0 \leq x \leq b) \quad (16)$$

can be written immediately as the local fractional Volterra integral equation of the second kind in the form

$$T(x) = T(a) + \frac{\lambda^\alpha}{\Gamma(1+\alpha)} \int_0^x q(t) (dt)^\alpha, \quad (17)$$

where $\lambda = 1/K^2$.

The Mittag-Leffler type Fourier flux distribution in fractal media can be written as follows:

$$q(x) = q_t(t, x) = E_\alpha(x-t)^\alpha T(t) \quad (0 \leq t \leq b). \quad (18)$$

Making use of (18), we can get the local fractional Volterra integral equation of the second kind in the form:

$$T(x) = T(a) + \frac{\lambda^\alpha}{\Gamma(1+\alpha)} \int_0^x E_\alpha(x-t)^\alpha T(t) (dt)^\alpha. \quad (19)$$

4. Approximate Solutions for Local Fractional Volterra Integral Equation of the Second Kind

Let us assume that the zeroth approximation is

$$u_0(x) = 0. \quad (20)$$

Then the first approximation can be written as follows:

$$u_1(x) = f(x) = T(a). \quad (21)$$

Here we obtain the second approximation, which reads as

$$u_2(x) = f(x) + \frac{\lambda^\alpha}{\Gamma(1+\alpha)} \int_0^x E_\alpha(x-t)^\alpha u_1(t) (dt)^\alpha. \quad (22)$$

Proceeding in this manner, we have the third approximation in the following form:

$$u_3(x) = f(x) + \frac{\lambda^\alpha}{\Gamma(1+\alpha)} \int_0^x E_\alpha(x-t)^\alpha u_2(t) (dt)^\alpha. \quad (23)$$

Hence, continuing in this manner, we obtain

$$u_n(x) = f(x) + \frac{\lambda^\alpha}{\Gamma(1+\alpha)} \int_0^x E_\alpha(x-t)^\alpha u_{n-1}(t) (dt)^\alpha$$

$$= f(x) + \frac{\lambda^\alpha}{\Gamma(1+\alpha)}$$

$$\times \int_0^x \left(1 + \dots + \frac{\lambda^{(n-1)\alpha} (x-t)^{(n-1)\alpha}}{\Gamma(1+(n-1)\alpha)} \right)$$

$$\times E_\alpha(x-t)^\alpha f(t) (dt)^\alpha. \quad (24)$$

Taking the limit, we have

$$u(x) = \lim_{n \rightarrow \infty} u_n(x)$$

$$= T(a) + \frac{\lambda^\alpha}{\Gamma(1+\alpha)}$$

$$\times \int_0^x E_\alpha[(x-t)^\alpha (1+\lambda^\alpha)] T(a) (dt)^\alpha \quad (25)$$

$$= T(a) \left\{ \frac{2\lambda^\alpha}{1+\lambda^\alpha} E_\alpha[x^\alpha (1+\lambda^\alpha)] \right\}$$

$$= T(a) \left\{ \frac{2}{K^{2\alpha} + 1} E_\alpha \left[x^\alpha \left(1 + \frac{1}{K^{2\alpha}} \right) \right] \right\},$$

where the term $E_\alpha[x^\alpha(1+\lambda^\alpha)]$ is a Mittag-Leffler type Fourier flux distribution in fractal media, which is related to the fractal coarse-grained mass function [21, 24]. When $K = 1$, we get $u(x) = T(a)E_\alpha[2x^\alpha]$. The nondifferentiable solution of (25) for parameters $K = 1$, $\alpha = \ln 2/\ln 3$, and $T(a) = 1$ is shown in Figure 1; the non-differentiable solution of (25) for parameters $K = 1$, $\alpha = \ln 2/\ln 3$, and $T(a) = 2$ is shown in Figure 2; the non-differentiable solution of (25) for parameters $K = 1$, $\alpha = \ln 2/\ln 3$, and $T(a) = 3$ is shown in Figure 3; the non-differentiable solution of (25) for parameters $K = 1$, $\alpha = \ln 2/\ln 3$, and $T(a) = 4$ is shown in Figure 4.

5. Conclusions

This work studied the Fourier law of one-dimensional heat conduction equation in fractal media. Mittag-Leffler type

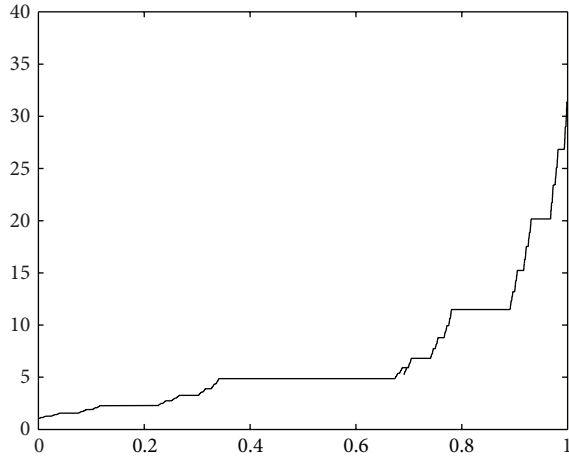


FIGURE 1: The nondifferentiable solution for Mittag-Leffler type Fourier flux distribution for parameters $K = 1$, $\alpha = \ln 2/\ln 3$, and $T(a) = 1$.

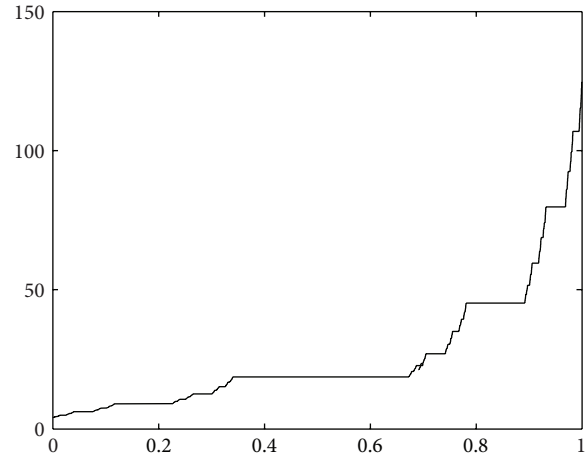


FIGURE 4: The nondifferentiable solution for Mittag-Leffler type Fourier flux distribution for parameters $K = 1$, $\alpha = \ln 2/\ln 3$, and $T(a) = 4$.

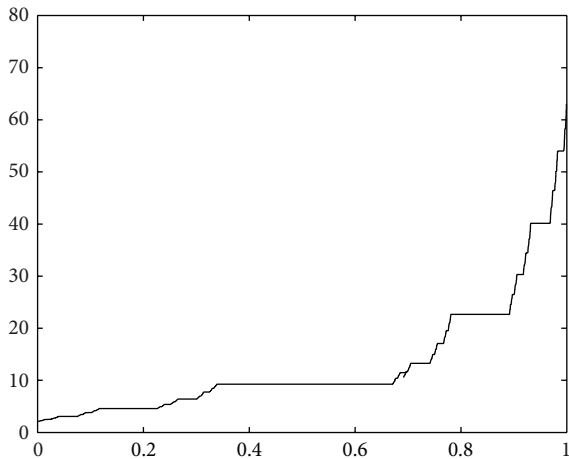


FIGURE 2: The nondifferentiable solution for Mittag-Leffler type Fourier flux distribution for parameters $K = 1$, $\alpha = \ln 2/\ln 3$, and $T(a) = 2$.

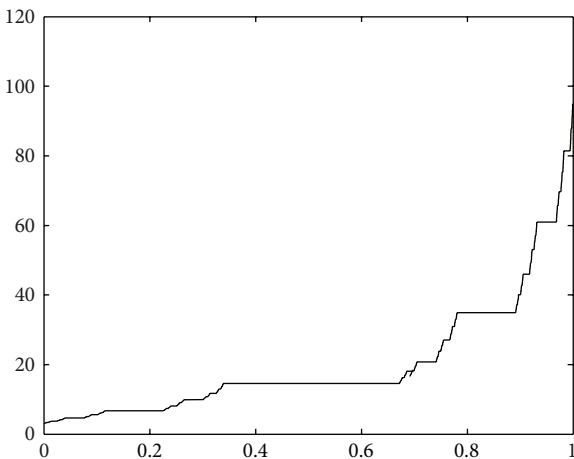


FIGURE 3: The nondifferentiable solution for Mittag-Leffler type Fourier flux distribution for parameters $K = 1$, $\alpha = \ln 2/\ln 3$, and $T(a) = 3$.

Fourier flux distribution in fractal media with temperature field effect was considered. An approximation solution for the local fractional Volterra integral equation of the second kind derived from Fourier law of one-dimensional heat conduction equation for heat conduction in discontinuous media was studied by using Picard's successive approximation method. The non-differential approximate solutions were given to show the efficiency of the present method.

Conflict of Interests

The authors declare that there is no conflict of interests regarding the publication of this paper.

Acknowledgments

This work was supported by National Scientific and Technological Support Projects (no. 2012BAE09B00), the National Natural Science Foundation of China (no. 51274270), and the National Natural Science Foundation of Hebei Province (no. E2013209215).

References

- [1] J. Crank and P. Nicolson, "A practical method for numerical evaluation of solutions of partial differential equations of the heat-conduction type," *Mathematical Proceedings of the Cambridge Philosophical Society*, vol. 43, pp. 50–67, 1947.
- [2] T. M. Shih, "A literature survey on numerical heat transfer," *Numerical Heat Transfer*, vol. 5, no. 4, pp. 369–420, 1982.
- [3] B. C. Choi and S. W. Churchill, "A technique for obtaining approximate solutions for a class of integral equations arising in radiative heat transfer," *International Journal of Heat and Fluid Flow*, vol. 6, no. 1, pp. 42–48, 1985.
- [4] Y. Z. Povstenko, "Fractional heat conduction equation and associated thermal stress," *Journal of Thermal Stresses*, vol. 28, no. 1, pp. 83–102, 2004.

- [5] M. Dehghan, "The one-dimensional heat equation subject to a boundary integral specification," *Chaos, Solitons & Fractals*, vol. 32, no. 2, pp. 661–675, 2007.
- [6] Y. Ioannou, M. M. Fyrillas, and C. Doumanidis, "Approximate solution to Fredholm integral equations using linear regression and applications to heat and mass transfer," *Engineering Analysis with Boundary Elements*, vol. 36, no. 8, pp. 1278–1283, 2012.
- [7] S. Nadeem and N. S. Akbar, "Effects of heat transfer on the peristaltic transport of MHD Newtonian fluid with variable viscosity: application of adomian decomposition method," *Communications in Nonlinear Science and Numerical Simulation*, vol. 14, no. 11, pp. 3844–3855, 2009.
- [8] A.-M. Wazwaz and M. S. Mehanna, "The combined Laplace-Adomian method for handling singular integral equation of heat transfer," *International Journal of Nonlinear Science*, vol. 10, no. 2, pp. 248–252, 2010.
- [9] S. Abbasbandy, "The application of homotopy analysis method to nonlinear equations arising in heat transfer," *Physics Letters A*, vol. 360, no. 1, pp. 109–113, 2006.
- [10] B. Raftari and K. Vajravelu, "Homotopy analysis method for MHD viscoelastic fluid flow and heat transfer in a channel with a stretching wall," *Communications in Nonlinear Science and Numerical Simulation*, vol. 17, no. 11, pp. 4149–4162, 2012.
- [11] A. A. Joneidi, D. D. Ganji, and M. Babaelahi, "Differential transformation method to determine fin efficiency of convective straight fins with temperature dependent thermal conductivity," *International Communications in Heat and Mass Transfer*, vol. 36, no. 7, pp. 757–762, 2009.
- [12] C. Cattani and E. Laserra, "Spline-wavelets techniques for heat propagation," *Journal of Information & Optimization Sciences*, vol. 24, no. 3, pp. 485–496, 2003.
- [13] N. Simões, A. Tadeu, J. António, and W. Mansur, "Transient heat conduction under nonzero initial conditions: a solution using the boundary element method in the frequency domain," *Engineering Analysis with Boundary Elements*, vol. 36, no. 4, pp. 562–567, 2012.
- [14] J. Hristov, "Approximate solutions to fractional sub-diffusion equations: the heat-balance integral method," *The European Physical Journal*, vol. 193, no. 1, pp. 229–243, 2011.
- [15] J. Hristov, "Heat-balance integral to fractional (half-time) heat diffusion sub-model," *Thermal Science*, vol. 14, no. 2, pp. 291–316, 2010.
- [16] D. D. Ganji and H. Sajjadi, "New analytical solution for natural convection of Darcian fluid in porous media prescribed surface heat flux," *Thermal Science*, vol. 15, no. 2, pp. 221–227, 2011.
- [17] X. J. Yang and D. Baleanu, "Fractal heat conduction problem solved by local fractional variation iteration method," *Thermal Science*, vol. 17, no. 2, pp. 625–628, 2013.
- [18] X.-J. Yang, "Picard's approximation method for solving a class of local fractional Volterra integral equations," *Advances in Intelligent Transportation Systems*, vol. 1, no. 3, pp. 67–70, 2012.
- [19] R. R. Nigmatullin, "The realization of the generalized transfer equation in a medium with fractal geometry," *Physica Status Solidi B*, vol. 133, no. 1, pp. 425–430, 1986.
- [20] K. Davey and R. Prosser, "Analytical solutions for heat transfer on fractal and pre-fractal domains," *Applied Mathematical Modelling*, vol. 37, no. 1-2, pp. 554–569, 2013.
- [21] X. J. Yang, *Advanced Local Fractional Calculus and Its Applications*, World Science, New York, NY, USA, 2012.
- [22] Y. Z. Zhang, A. M. Yang, and X.-J. Yang, "1-D heat conduction in a fractal medium: a solution by the local fractional Fourier series method," *Thermal Science*, vol. 17, no. 3, pp. 953–956, 2013.
- [23] M.-S. Hu, D. Baleanu, and X.-J. Yang, "One-phase problems for discontinuous heat transfer in fractal media," *Mathematical Problems in Engineering*, vol. 2013, Article ID 358473, 3 pages, 2013.
- [24] X. J. Yang, *Local Fractional Functional Analysis and Its Applications*, Asian Academic, Hong Kong, 2011.
- [25] M. Li and W. Zhao, "On bandlimitedness and lag-limitedness of fractional Gaussian noise," *Physica A*, vol. 392, no. 9, pp. 1955–1961, 2013.
- [26] M. Li, "Approximating ideal filters by systems of fractional order," *Computational and Mathematical Methods in Medicine*, vol. 2012, Article ID 365054, 6 pages, 2012.
- [27] M. Li and W. Zhao, "On $1/f$ noise," *Mathematical Problems in Engineering*, vol. 2012, Article ID 673648, 23 pages, 2012.
- [28] M. H. Heydari, M. R. Hooshmandasl, F. M. Maalek Ghaini, and M. Li, "Chebyshev wavelets method for solution of nonlinear fractional integro-differential equations in a large interval," *Advances in Mathematical Physics*, vol. 2013, Article ID 482083, 12 pages, 2013.
- [29] S. S. Ray and R. K. Bera, "Analytical solution of a fractional diffusion equation by Adomian decomposition method," *Applied Mathematics and Computation*, vol. 174, no. 1, pp. 329–336, 2006.
- [30] Q. Wang, "Numerical solutions for fractional KdV-Burgers equation by Adomian decomposition method," *Applied Mathematics and Computation*, vol. 182, no. 2, pp. 1048–1055, 2006.

Research Article

A Note on Certain Modular Equations about Infinite Products of Ramanujan

Hong-Cun Zhai

Mathematics College, LuoYang Normal University, LuoYang 471022, China

Correspondence should be addressed to Hong-Cun Zhai; zhai_hc@163.com

Received 17 October 2013; Revised 8 November 2013; Accepted 8 November 2013

Academic Editor: Ming Li

Copyright © 2013 Hong-Cun Zhai. This is an open access article distributed under the Creative Commons Attribution License, which permits unrestricted use, distribution, and reproduction in any medium, provided the original work is properly cited.

Ramanujan proposed additive formulae of theta functions that are related to modular equations about infinite products. Employing these formulae, we derived some identities on infinite products. In the same spirit, we also could present elementary and simple proofs of certain Ramanujan's modular equations on infinite products.

1. Introduction

Q-theory is undoubtedly one of the most famous and useful mathematical theorems, such as Andrews-Askey type integral [1]

$$\int_c^d \frac{(qt/c, qt/d, ft, rst; q)_\infty}{(at, bt, et, st; q)_\infty} {}_3\phi_2 \left[\begin{matrix} r, bt, \frac{c}{g} \\ rst, bc; \end{matrix} \middle| q, sg \right] d_q t$$

$$= \frac{d(1-q)(q, c/d, qd/c, abcd, df, rsd; q)_\infty}{(ac, bc, ad, bd, sd, de; q)_\infty}$$

$$\times \sum_{k=0}^{\infty} \frac{(f/e, ad, sd, bd; q)_k (ce)^k}{(q, df, rsd, abcd; q)_k}$$

$$\times {}_3\phi_2 \left[\begin{matrix} r, bdq^k, \frac{acdq^k}{g} \\ rsdq^k, abcdq^k; \end{matrix} \middle| q, sg \right], \quad (1)$$

Askey-Roy type integral [2]

$$\int_{-\pi}^{\pi} \left(P_n(e^{i\theta}, f) P_m(e^{i\theta}, g) \right. \\ \left. \times \left(\frac{\rho e^{i\theta}}{d}, qde^{-i\theta}, \rho ce^{-i\theta}, \frac{qe^{i\theta}}{(c\rho)}; q \right)_\infty \right)$$

$$\times \left((ae^{i\theta}, be^{i\theta}, ce^{-i\theta}, de^{-i\theta}; q)_\infty \right)^{-1} d\theta$$

$$= \frac{2\pi (af; q)_n (bg; q)_m (abcd, \rho c/d, dq/(c\rho), \rho, q/\rho; q)_\infty}{a^n b^m (q, bc, bd, ac, ad; q)_\infty}$$

$$\times \sum_{k=0}^n \frac{(q^{-n}, ac, ad; q)_k q^k}{(q, af, abcd; q)_k} {}_3\phi_2 \left[\begin{matrix} q^{-m}, bc, bd \\ bg, abcdq^k; \end{matrix} \middle| q, q \right], \quad (2)$$

Moment integrals [3]

$$\int_{-\infty}^{\infty} \frac{P_n(w, c) P_m(w, d)}{(aw, bw; q)_\infty} d\alpha^{(s,t)}(w)$$

$$= \frac{(ac; q)_n (bd; q)_m (abst; q)_\infty}{a^n b^m (as, at, bs, bt; q)_\infty}$$

$$\times \sum_{k=0}^n \frac{(q^{-n}, as, at; q)_k q^k}{(q, ac, abst; q)_k} {}_3\phi_2 \left[\begin{matrix} q^{-m}, bs, bt \\ bd, abstq^k; \end{matrix} \middle| q, q \right], \quad (3)$$

(where $P_n(a, b) = (a-b) \cdots (a-bq^{n-1})$), q -Fractional Calculus Equations [4] and q -Calculus [5]. For more information, please refer to [1-5].

The theta functions are very useful tool in researching q -series, especially in dealing with the form of the equation similar to above formulas, whose left-hand side is summation and right-hand side is integral. The additive identities of

theta are one of the important of Ramanujan’s contributions. Using it, we gave elementary and simple proofs of certain Ramanujan’s modular equations on infinite products. For more information, please refer to [1–7].

In his notebook [8, pages 34–38], Ramanujan defines the following theta functions:

$$f(a, b) := \sum_{n=-\infty}^{\infty} a^{n(n+1)/2} b^{n(n-1)/2} \tag{4}$$

$$= (-a; ab)_{\infty} (-b; ab)_{\infty} (ab; ab)_{\infty}, \quad |ab| < 1,$$

$$\varphi(q) := f(q, q) = \sum_{n=-\infty}^{\infty} q^{n^2} = \frac{(-q; -q)_{\infty}}{(q; -q)_{\infty}}, \tag{5}$$

$$\psi(q) := f(q, q^3) = \sum_{n=1}^{\infty} q^{n(n-1)/2} = \frac{(q^2; q^2)_{\infty}}{(q; q^2)_{\infty}}, \tag{6}$$

where

$$(a; q)_{\infty} := \prod_{n=0}^{\infty} (1 - aq^n), \quad |q| < 1, \tag{7}$$

sometimes written as

$$(a, b, c, \dots; q)_{\infty} = (a; q)_{\infty} (b; q)_{\infty} (c; q)_{\infty} \dots \tag{8}$$

The infinite products are from the Jacobi triple product identity [8, page 35].

In the course of deduction, we used the following simple fact [9, 10]:

$$(a^k; q^k)_{\infty} = (a, a\omega_k, \dots, a\omega_k^{k-1}; q)_{\infty}, \tag{9}$$

$$(a, q)_{\infty} = (a, aq, aq^2, \dots, aq^{k-1}; q^k)_{\infty}.$$

By definition of Ramanujan theta functions one can easily verify the following identities [8, page 45]:

$$\begin{aligned} f(a, b) + f(-a, -b) &= 2f(a^3b, ab^3), \\ f(a, b) - f(-a, -b) &= 2af\left(\frac{b}{a}, \frac{a}{b}a^4b^4\right). \end{aligned} \tag{10}$$

From (4), if $ab = cd = p$, we have

$$f(a, b) f(c, d) = \sum_{m, n=-\infty}^{\infty} p^{(m^2+n^2)/2-(m+n)/2} a^m c^n. \tag{11}$$

Thus setting $m - n = 2j$ and $m + n = 2k$, we find that

$$\begin{aligned} &f(a, b) f(c, d) + f(-a, -b) f(-c, -d) \\ &= \sum_{\substack{n, m=-\infty \\ m, n, \text{even}}}^{+\infty} p^{(m^2+n^2)/2-(m+n)/2} a^m c^n \\ &= 2 \sum_{j, k=-\infty}^{\infty} p^{j^2+k^2-k} a^{j+k} c^{k-j} \tag{12} \\ &= 2 \sum_{j, k=-\infty}^{\infty} p^{k(k-1)} (ac)^k p^{j(j-1)} (bc)^{-j} \\ &= 2f(ac, bd) f(ad, bc). \end{aligned}$$

Thus when $ab = cd$, we have

$$\begin{aligned} &f(a, b) f(c, d) + f(-a, -b) f(-c, -d) \\ &= 2f(ac, bd) f(ad, bc). \end{aligned} \tag{13}$$

Similarly we have that

$$\begin{aligned} &f(a, b) f(c, d) - f(-a, -b) f(-c, -d) \\ &= 2af\left(\frac{b}{c}, \frac{abcd}{b/c}\right) f\left(\frac{b}{d}, \frac{abcd}{b/d}\right). \end{aligned} \tag{14}$$

The special case of these identities can be written as the following form by using Jacobian theta function [6, 7]:

$$\begin{aligned} &2\theta_1(x + y | 2\tau) \theta_1(x - y | 2\tau) \\ &= \theta_3(y | \tau) \theta_4(x | \tau) - \theta_3(x | \tau) \theta_4(y | \tau). \end{aligned} \tag{15}$$

The authors of [6, 7] give simple proofs and very important use of it.

In the above two identities, putting $c = a$ and $d = b$, we easily obtain

$$f^2(a, b) + f^2(-a, -b) = 2f(a^2, b^2) \varphi(ab), \tag{16}$$

$$f^2(a, b) - f^2(-a, -b) = 4af\left(\frac{b}{a}, \frac{a}{b}a^2b^2\right) \psi(a^2b^2). \tag{17}$$

2. Main Results

The sums and products of infinite are used in many domains of mathematics, such as Partition Functions [11–14], Fractal Geometry [9], Fractional Calculus [10], Fractal Time Series [4], and so on. Then the equations of it are concentrated by several mathematicians and engineers [15–18]. At the same time, it can be used in dynamic equations, differential equations [19], and partial differential equations [20].

This paper has two main purposes. The first is to derive the identities as follows: for $|q| < 1$,

$$\frac{(q; q)_{\infty}^2}{(q^3; q^3)_{\infty}^2} + 3 \frac{(-q; q)_{\infty}^2}{(-q^3; q^3)_{\infty}^2} \tag{18}$$

$$= 4\omega \frac{(q; q)_{\infty}^2}{(q^3; q^3)_{\infty}^2} \frac{f(q\omega, q^3\omega^2) f(q\omega^2, q^3\omega)}{f^2(\omega, q\omega^2)},$$

$$\frac{(q; q)_{\infty}^2}{(q^3; q^3)_{\infty}^2} - 3 \frac{(-q; q)_{\infty}^2}{(-q^3; q^3)_{\infty}^2} = 2 \frac{(q; q)_{\infty}^2}{(q^3; q^3)_{\infty}^2} \frac{f(\omega^2, q\omega)}{f^2(\omega, q\omega^2)} \varphi(q), \tag{19}$$

$$\begin{aligned} \frac{(q; q)_{\infty}^2}{(q^5; q^5)_{\infty}^2} - 5 \frac{(-q; q)_{\infty}^2}{(-q^5; q^5)_{\infty}^2} &= \frac{\omega(1-\omega)(1+\omega)(q\omega; q)_{\infty}(q\omega^2; q)_{\infty}}{(1+\omega)(-q\omega; q)_{\infty}(-q\omega^2; q)_{\infty}} \\ &= -\frac{(\omega; q)_{\infty}(q\omega^2; q)_{\infty}}{(-\omega; q)_{\infty}(-q\omega^2; q)_{\infty}} \\ &= -\frac{f(-\omega, -q\omega^2)}{f(\omega, q\omega^2)}. \end{aligned} \tag{20}$$

in which $\omega = \exp(2i\pi/3)$ and $\zeta = \exp(2i\pi/5)$. In the same way, we are able to give the simple and elementary proofs of the following identities of Ramanujan [8, 11, 12]:

$$\frac{(-q; q)_{\infty}^2}{(-q^3; q^3)_{\infty}^2} + \frac{(q; q)_{\infty}^2}{(q^3; q^3)_{\infty}^2} = 2 \frac{(-q^3; q^6)_{\infty}^2}{(q^3; q^6)_{\infty}^2} (-q^2, -q^4; q^6)_{\infty}, \tag{21}$$

$$\frac{(-q; q)_{\infty}^2}{(-q^3; q^3)_{\infty}^2} - \frac{(q; q)_{\infty}^2}{(q^3; q^3)_{\infty}^2} = 4q \frac{(-q^6; q^6)_{\infty}^2}{(q^3; q^6)_{\infty}^2} (-q, -q^5; q^6)_{\infty}, \tag{22}$$

$$\begin{aligned} \frac{(-q; q)_{\infty}^2}{(-q^5; q^5)_{\infty}^2} - \frac{(q; q)_{\infty}^2}{(q^5; q^5)_{\infty}^2} \\ = 4q \frac{(-q, -q^2, -q^3, -q^4, -q^6, -q^7, -q^8, -q^9; q^{10})_{\infty}}{(q^5; q^{10})_{\infty}^4}. \end{aligned} \tag{23}$$

3. Modular Equations of Infinite Productions

In this section, we first give the two sets refinement about the identities (18) and (20).

Theorem 1. For $|q| < 1$,

$$\begin{aligned} \frac{(q; q)_{\infty}}{(q^3; q^3)_{\infty}} - i\sqrt{3} \frac{(-q; q)_{\infty}}{(-q^3; q^3)_{\infty}} &= 2\omega \frac{(q; q)_{\infty}}{(q^3; q^3)_{\infty}} \frac{f(q\omega, q^3\omega^2)}{f(\omega, q\omega^2)}, \\ \frac{(q; q)_{\infty}}{(q^3; q^3)_{\infty}} + i\sqrt{3} \frac{(-q; q)_{\infty}}{(-q^3; q^3)_{\infty}} &= 2 \frac{(q; q)_{\infty}}{(q^3; q^3)_{\infty}} \frac{f(q\omega^2, q^3\omega)}{f(\omega, q\omega^2)}. \end{aligned} \tag{24}$$

Proof. Note that $1 + \omega + \omega^2 = 0$ and $\omega - \omega^2 = i\sqrt{3}$. By (9), we get that

$$\begin{aligned} i\sqrt{3} \frac{(-q; q)_{\infty}}{(-q^3; q^3)_{\infty}} \div \frac{(q; q)_{\infty}}{(q^3; q^3)_{\infty}} \\ = \frac{(\omega - \omega^2)(q\omega; q)_{\infty}(q\omega^2; q)_{\infty}}{(-q\omega; q)_{\infty}(-q\omega^2; q)_{\infty}} \end{aligned}$$

From (10), we have

$$f(\omega, q\omega) - f(-\omega, -q\omega) = 2f(q\omega^2, q^3\omega), \tag{26}$$

$$f(\omega, q\omega) + f(-\omega, -q\omega) = 2\omega f(q\omega, q^3\omega^2). \tag{27}$$

Dividing by $f(\omega, q\omega)$, respectively, and then applying (25), we derive

$$\begin{aligned} i\sqrt{3} \frac{(-q; q)_{\infty}}{(-q^3; q^3)_{\infty}} \div \frac{(q; q)_{\infty}}{(q^3; q^3)_{\infty}} - 1 \\ = -1 - \frac{f(-\omega, -q\omega^2)}{f(\omega, q\omega^2)} = -2\omega \frac{f(q\omega, q^3\omega^2)}{f(\omega, q\omega^2)}, \end{aligned} \tag{28}$$

$$\begin{aligned} i\sqrt{3} \frac{(-q; q)_{\infty}}{(-q^3; q^3)_{\infty}} \div \frac{(q; q)_{\infty}}{(q^3; q^3)_{\infty}} + 1 \\ = 1 - \frac{f(-\omega, -q\omega^2)}{f(\omega, q\omega^2)} = 2 \frac{f(q\omega^2, q^3\omega)}{f(\omega, q\omega^2)}. \end{aligned} \tag{29}$$

Multiplying by $(q; q)_{\infty}/(q^3; q^3)_{\infty}$, respectively, we complete the proofs of (24). \square

Proof of (19). Let $\alpha = \exp(i\pi/6)$; then it is easy to know that $\omega = i\alpha$ and $\alpha + 1/\alpha = -\sqrt{3}$.

One has

$$\begin{aligned} \sqrt{3} \frac{(-q; q)_{\infty}}{(-q^3; q^3)_{\infty}} \div \frac{(q; q)_{\infty}}{(q^3; q^3)_{\infty}} \\ = -\left(\alpha + \frac{1}{\alpha}\right) \frac{(q\omega; q)_{\infty}(q\omega^2; q)_{\infty}}{(-q\omega; q)_{\infty}(-q\omega^2; q)_{\infty}} \\ = -\frac{1}{\alpha} (1 + \alpha^2) \frac{(q\omega; q)_{\infty}(q\omega^2; q)_{\infty}}{(-q\omega; q)_{\infty}(-q\omega^2; q)_{\infty}} \\ = -\frac{1}{\alpha} (1 - i\alpha)(1 + i\alpha) \frac{(q\omega; q)_{\infty}(q\omega^2; q)_{\infty}}{(-q\omega; q)_{\infty}(-q\omega^2; q)_{\infty}} \\ = -\frac{1}{\alpha} (1 - \omega)(1 + \omega) \frac{(q\omega; q)_{\infty}(q\omega^2; q)_{\infty}}{(-q\omega; q)_{\infty}(-q\omega^2; q)_{\infty}} \end{aligned}$$

$$\begin{aligned}
 &= -\frac{1}{\alpha}(1+\omega)^2 \frac{(\omega; q)_\infty (q\omega^2; q)_\infty}{(-\omega; q)_\infty (-q\omega^2; q)_\infty} \\
 &= -\frac{\omega}{\alpha} \frac{f(-\omega, -q\omega^2)}{f(\omega, q\omega^2)} = -i \frac{f(-\omega, -q\omega^2)}{f(\omega, q\omega^2)}.
 \end{aligned}
 \tag{30}$$

Then we obtain that

$$\begin{aligned}
 1 + \sqrt{3} \frac{(-q; q)_\infty}{(-q^3; q^3)_\infty} \div \frac{(q; q)_\infty}{(q^3; q^3)_\infty} &= 1 - i \frac{f(-\omega, -q\omega^2)}{f(\omega, q\omega^2)}, \\
 1 - \sqrt{3} \frac{(-q; q)_\infty}{(-q^3; q^3)_\infty} \div \frac{(q; q)_\infty}{(q^3; q^3)_\infty} &= 1 + i \frac{f(-\omega, -q\omega^2)}{f(\omega, q\omega^2)}.
 \end{aligned}
 \tag{31}$$

In (16), let $a = \omega$ and $b = q\omega^2$ then we have that

$$f^2(\omega, q\omega^2) + f^2(-\omega, -q\omega^2) = 2f(\omega^2, q^2\omega)\varphi(q). \tag{32}$$

Dividing by $f^2(\omega, q\omega^2)$, respectively, we arrive at

$$1 + \frac{f^2(-\omega, -q\omega^2)}{f^2(\omega, q\omega^2)} = \frac{2f(\omega^2, q^2\omega)\varphi(q)}{f^2(\omega, q\omega^2)}. \tag{33}$$

Multiplying (31), combining with (33), and then multiplied by $(q; q)_\infty^2 / (q^3; q^3)_\infty^2$, we are able to obtain (19). \square

Theorem 2. For $|q| < 1$,

$$\begin{aligned}
 &\frac{(q; q)_\infty}{(q^5; q^5)_\infty} - \sqrt{5} \frac{(-q; q)_\infty}{(-q^5; q^5)_\infty} \\
 &= 2\zeta \frac{(q; q)_\infty}{(q^5; q^5)_\infty} \frac{f(q\zeta^2, q\zeta^3) f(\zeta, q^2\zeta^4)}{f(\zeta, q\zeta^4) f(\zeta^2, q\zeta^3)},
 \end{aligned}
 \tag{34}$$

$$\begin{aligned}
 &\frac{(q; q)_\infty}{(q^5; q^5)_\infty} + \sqrt{5} \frac{(-q; q)_\infty}{(-q^5; q^5)_\infty} \\
 &= 2 \frac{(q; q)_\infty}{(q^5; q^5)_\infty} \frac{f(\zeta^3, q^2\zeta^2) f(q\zeta, q\zeta^4)}{f(\zeta, q\zeta^4) f(\zeta^2, q\zeta^3)}.
 \end{aligned}
 \tag{35}$$

Proof. First we recall that $\zeta^5 = 1$, $\zeta + \zeta^4 - \zeta^2 - \zeta^3 = \sqrt{5}$ and $1 + \zeta + \zeta^2 + \zeta^3 + \zeta^4 = 0$. Using (9), we have

$$\begin{aligned}
 &\sqrt{5} \frac{(-q; q)_\infty}{(-q^5; q^5)_\infty} \div \frac{(q; q)_\infty}{(q^5; q^5)_\infty} \\
 &= (\zeta + \zeta^4 - \zeta^2 - \zeta^3) \\
 &\quad \times \frac{(q\zeta; q)_\infty (q\zeta^2; q)_\infty (q\zeta^3; q)_\infty (q\zeta^4; q)_\infty}{(-q\zeta; q)_\infty (-q\zeta^2; q)_\infty (-q\zeta^3; q)_\infty (-q\zeta^4; q)_\infty}
 \end{aligned}$$

$$\begin{aligned}
 &= (\zeta(1-\zeta)(1-\zeta^2)(1+\zeta)(1+\zeta^2) \\
 &\quad \times (q\zeta; q)_\infty (q\zeta^2; q)_\infty (q\zeta^3; q)_\infty (q\zeta^4; q)_\infty) \\
 &\quad \times ((1+\zeta)(1+\zeta^2)(-q\zeta; q)_\infty \\
 &\quad \times (-q\zeta^2; q)_\infty (-q\zeta^3; q)_\infty (-q\zeta^4; q)_\infty)^{-1} \\
 &= -\frac{f(-\zeta, -q\zeta^4) f(-\zeta^2, -q\zeta^3)}{f(\zeta, q\zeta^4) f(\zeta^2, q\zeta^3)}.
 \end{aligned}
 \tag{36}$$

Then we know easily that

$$\begin{aligned}
 1 + \sqrt{5} \frac{(-q; q)_\infty}{(-q^5; q^5)_\infty} \div \frac{(q; q)_\infty}{(q^5; q^5)_\infty} \\
 &= 1 - \frac{f(-\zeta, -q\zeta^4) f(-\zeta^2, -q\zeta^3)}{f(\zeta, q\zeta^4) f(\zeta^2, q\zeta^3)}, \\
 1 - \sqrt{5} \frac{(-q; q)_\infty}{(-q^5; q^5)_\infty} \div \frac{(q; q)_\infty}{(q^5; q^5)_\infty} \\
 &= 1 + \frac{f(-\zeta, -q\zeta^4) f(-\zeta^2, -q\zeta^3)}{f(\zeta, q\zeta^4) f(\zeta^2, q\zeta^3)}.
 \end{aligned}
 \tag{37}$$

In (13) and (14), setting $a = \zeta$, $b = q\zeta^4$, $c = \zeta^2$, and $d = q\zeta^3$, we get that

$$\begin{aligned}
 &f(\zeta, q\zeta^4) f(\zeta^2, q\zeta^3) + f(-\zeta, -q\zeta^4) f(-\zeta^2, -q\zeta^3) \\
 &= 2f(\zeta^3, q^2\zeta^2) f(q\zeta^4, q\zeta), \\
 &f(\zeta, q\zeta^4) f(\zeta^2, q\zeta^3) - f(-\zeta, -q\zeta^4) f(-\zeta^2, -q\zeta^3) \\
 &= 2\zeta f(q\zeta^2, q\zeta^3) f(\zeta, q^2\zeta^4).
 \end{aligned}
 \tag{38}$$

Dividing the above two equations by $f(\zeta, q\zeta^4) f(\zeta^2, q\zeta^3)$, respectively, and then combining with (37), we obtain that

$$\begin{aligned}
 1 + \sqrt{5} \frac{(-q; q)_\infty}{(-q^5; q^5)_\infty} \div \frac{(q; q)_\infty}{(q^5; q^5)_\infty} &= 2 \frac{f(\zeta^3, q^2\zeta^2) f(q\zeta, q\zeta^4)}{f(\zeta, q\zeta^4) f(\zeta^2, q\zeta^3)}, \\
 1 - \sqrt{5} \frac{(-q; q)_\infty}{(-q^5; q^5)_\infty} \div \frac{(q; q)_\infty}{(q^5; q^5)_\infty} &= 2\zeta \frac{f(q\zeta^2, q\zeta^3) f(\zeta, q^2\zeta^4)}{f(\zeta, q\zeta^4) f(\zeta^2, q\zeta^3)}.
 \end{aligned}
 \tag{39}$$

Multiplied by $(q; q)_\infty / (q^5; q^5)_\infty$, the identities (39) and (40) become (34) and (35).

Multiplying the two refinements in Theorems 1 and 2, respectively, we obtain the identities (18) and (20). Using the same method, we can obtain refinement identities of (21) and (22) which are similar to Theorems 1 and 2; then we can deduce (21), (22), and (23) easily. The details of proofs are omitted. \square

The following conclusion can be obtained easily.

Corollary 3. For $|q| < 1$,

$$\begin{aligned} & \frac{(q; q)_{\infty}^4}{(q^3; q^3)_{\infty}^4} - 9 \frac{(-q; q)_{\infty}^4}{(-q^3; q^3)_{\infty}^4} \\ &= 8\omega \frac{(q; q)_{\infty}^4}{(q^3; q^3)_{\infty}^4} \\ & \times \frac{f(\omega^2, q\omega) f(q\omega, q^3\omega^2) f(q\omega^2, q^3\omega)}{f^4(\omega, q\omega^2)} \varphi(q). \end{aligned} \quad (41)$$

Acknowledgments

This work was supported by the National Science Foundation of China, Project nos. 11071107, 11371184, and U1304103. The author would like to thank the referee and editor for many valuable comments and suggestions.

References

- [1] J. Cao, "A note on q -integrals and certain generating functions," *Studies in Applied Mathematics*, vol. 131, pp. 105–118, 2013.
- [2] J. Cao, "Notes on Askey–Roy integral and certain generating functions for q -polynomials," *Journal of Mathematical Analysis and Applications*, vol. 409, no. 1, pp. 435–445, 2014.
- [3] J. Cao, "A note on moment integrals and some applications," *Journal of Mathematical Analysis and Applications*, vol. 410, no. 1, pp. 348–360, 2014.
- [4] M. H. Annaby and Z. S. Mansour, *q -Fractional Calculus and Equations*, vol. 2056 of *Lecture Notes in Mathematics*, Springer, Heidelberg, Germany, 2012.
- [5] T. Ernst, *A Comprehensive Treatment q -Calculus*, Springer, New York, NY, USA, 2001.
- [6] Z.-G. Liu, "Addition formulas for Jacobi theta functions, Dedekind's eta function, and Ramanujan's congruences," *Pacific Journal of Mathematics*, vol. 240, no. 1, pp. 135–150, 2009.
- [7] Z.-G. Liu and X.-M. Yang, "On the Schröter formula for theta functions," *International Journal of Number Theory*, vol. 5, no. 8, pp. 1477–1488, 2009.
- [8] B. C. Berndt, *Ramanujan's Notebooks. Part III*, Springer, New York, NY, USA, 1991.
- [9] C. Cattani and G. Pierro, "On the fractal geometry of DNA by the binary image analysis," *Bulletin of Mathematical Biology*, vol. 75, pp. 1544–1570, 2013.
- [10] C. Cattani, "Fractional calculus and Shannon wavelet," *Mathematical Problems in Engineering*, vol. 2012, Article ID 502812, 26 pages, 2012.
- [11] N. D. Baruah and B. C. Berndt, "Partition identities and Ramanujan's modular equations," *Journal of Combinatorial Theory. Series A*, vol. 114, no. 6, pp. 1024–1045, 2007.
- [12] N. D. Baruah and B. C. Berndt, "Partition identities arising from theta function identities," *Acta Mathematica Sinica*, vol. 24, no. 6, pp. 955–970, 2008.
- [13] R. Blecksmith, J. Brillhart, and I. Gerst, "Parity results for certain partition functions and identities similar to theta function identities," *Mathematics of Computation*, vol. 48, no. 177, pp. 29–38, 1987.
- [14] R. Blecksmith, J. Brillhart, and I. Gerst, "Some infinite product identities," *Mathematics of Computation*, vol. 51, no. 183, pp. 301–314, 1988.
- [15] M. Li, Y.-Q. Chen, J.-Y. Li, and W. Zhao, "Hölder scales of sea level," *Mathematical Problems in Engineering*, vol. 2012, Article ID 863707, 22 pages, 2012.
- [16] M. Li, W. Zhao, and C. Cattani, "Delay bound: fractal traffic passes through network servers," *Mathematical Problems in Engineering*, vol. 2013, Article ID 157636, 15 pages, 2013.
- [17] M. Li and W. Zhao, "On $1/f$ noise," *Mathematical Problems in Engineering*, vol. 2012, Article ID 673648, 23 pages, 2012.
- [18] M. Li, "Fractal time series—a tutorial review," *Mathematical Problems in Engineering*, vol. 2010, Article ID 157264, 26 pages, 2010.
- [19] R. Agarwal, M. Bohner, D. O'Regan, and A. Peterson, "Dynamic equations on time scales: a survey," *Journal of Computational and Applied Mathematics*, vol. 141, no. 1-2, pp. 1–26, 2002, Dynamic equations on time scales.
- [20] M. Bohner and A. Peterson, *Dynamic Equations on Time Scales*, Birkhäuser, Boston, Mass, USA, 2001.

Research Article

On Local Fractional Continuous Wavelet Transform

Xiao-Jun Yang,¹ Dumitru Baleanu,^{2,3,4} H. M. Srivastava,⁵ and J. A. Tenreiro Machado⁶

¹ Department of Mathematics and Mechanics, China University of Mining and Technology, Xuzhou, Jiangsu 221008, China

² Department of Chemical and Materials Engineering, Faculty of Engineering, King Abdulaziz University, P.O. Box 80204, Jeddah 21589, Saudi Arabia

³ Department of Mathematics and Computer Sciences, Faculty of Arts and Sciences, Cankaya University, 06530 Ankara, Turkey

⁴ Institute of Space Sciences, Magurele, 077125 Bucharest, Romania

⁵ Department of Mathematics and Statistics, University of Victoria, Victoria, BC, Canada V8W 3R4

⁶ Department of Electrical Engineering, Institute of Engineering of Porto, Rua Dr. António Bernardino de Almeida 431, 4200-072 Porto, Portugal

Correspondence should be addressed to Xiao-Jun Yang; dyangxiaojun@163.com

Received 25 October 2013; Accepted 10 November 2013

Academic Editor: Carlo Cattani

Copyright © 2013 Xiao-Jun Yang et al. This is an open access article distributed under the Creative Commons Attribution License, which permits unrestricted use, distribution, and reproduction in any medium, provided the original work is properly cited.

We introduce a new wavelet transform within the framework of the local fractional calculus. An illustrative example of local fractional wavelet transform is also presented.

1. Introduction

Wavelet transforms have been applied successfully in the areas of signals analysis, data compression, and sound processing (see, for details, [1–6] and the references cited therein). Although there is scaled and shifted versions of a mother wavelet, the daughter wavelets are structured as follows (see [3–5]):

$$\varphi_{a,b}(t) = \frac{1}{a^{1/2}} \varphi\left(\frac{t-b}{a}\right), \quad (1)$$

where a is the dyadic dilation, b is the dyadic position, and $a^{-1/2}$ is the normalization factor. The expression of a one-dimensional wavelet transform for a given continuous signal $f(t)$ is given by

$$W_\varphi f(a,b) = \int_{-\infty}^{\infty} f(t) \overline{\varphi_{a,b}(t)} dt \quad (2)$$

and the reconstruction formula becomes

$$f(x) = C_\varphi \iint_{-\infty}^{\infty} \frac{1}{a^2} W_\varphi f(a,b) \varphi_{a,b}(t) da db, \quad (3)$$

where

$$C_\varphi = \int_{-\infty}^{\infty} \frac{|f(x)|^2}{|x|} dx. \quad (4)$$

Recently, fractional wavelet transform, as a generalization of the classical wavelet transform, was proposed in [7]. The one-dimensional fractal wavelet transform of a continuous signal $f(t)$ has the following form:

$$W_\varphi f(a,b) = \iint_{-\infty}^{\infty} B(x,t) f(t) \overline{\varphi_{a,b}(x)} dt dx, \quad (5)$$

where $B(x,t)$ denotes a bulk optics kernel.

The reconstructing formula of the input is defined as given by the following expression:

$$f(x) = \frac{1}{C_\varphi} \iint_{-\infty}^{\infty} \frac{1}{a^3} W_\varphi f(a,b) B(x,t) \varphi_{a,b}(t) da db dt dt. \quad (6)$$

We notice that the fractional wavelet transforms was applied to image encryption [8], to the simultaneous spectral analysis in [9], and to the composite signals in [10, 11]. For other definition of fractional wavelet transform, see [12] and the references cited therein.

Keeping in mind the study of the fractal signals (local fractional continuous signals), a new local fractional wavelet transform was developed in [13] based upon the local fractional Fourier transform [14] via local fractional calculus [15–18]. In this paper, we investigate the local fractional Fourier transform to deal with the local fractional wavelet transforms by implementing the local fractional calculus.

The organization of the paper is as follows. Section 2 presents the concept of local fractional Fourier transform and wavelet. Section 3 discusses the derivation of the local fractional continuous wavelet transform. Section 4 studies the wave space and Section 5 present an illustrative example. Finally, Section 6 outlines the main conclusions of our present investigation.

2. Local Fractional Fourier Transform and Wavelet

Let $f(x)$ be local fractional continuous function, which is denoted as follows (see [18]):

$$f(x) \in C_\alpha(-\infty, \infty). \tag{7}$$

The space of local fractional continuous functions $C_{p,\alpha}[a, b]$, under p -norm, is given by (see [13])

$$\|f\|_{p,\alpha} = \left(\frac{1}{\Gamma(1+\alpha)} \int_a^b |f(x)|^p (dx)^\alpha \right)^{1/p}, \quad \text{for } 1 \leq p < \infty, \tag{8}$$

where the operator is local fractional operator.

The space $L_{p,\alpha}[\mathbb{R}]$ norm on $C_{p,\alpha}[\mathbb{R}]$ is defined by

$$\|f\|_{p,\alpha} =: \left(\frac{1}{\Gamma(1+\alpha)} \int_{-\infty}^{\infty} |f(x)|^p (dx)^\alpha \right)^{1/p} < \infty \tag{9}$$

for $1 \leq p < \infty$. This is infinite for a and b .

The local fractional Fourier transforms in fractal space is defined as follows (see [13, 14]):

$$\begin{aligned} F_\alpha \{f(x)\} &= f_\omega^{F,\alpha}(\omega) \\ &:= \frac{1}{\Gamma(1+\alpha)} \int_{-\infty}^{\infty} E_\alpha(-i^\alpha \omega^\alpha x^\alpha) f(x) (dx)^\alpha. \end{aligned} \tag{10}$$

Its inverse is formulated as follows (see [13, 14]):

$$\begin{aligned} f(x) &= F_\alpha^{-1} \left(f_\omega^{F,\alpha}(\omega) \right) \\ &:= \frac{1}{(2\pi)^\alpha} \int_{-\infty}^{\infty} E_\alpha(i^\alpha \omega^\alpha x^\alpha) f_\omega^{F,\alpha}(\omega) (d\omega)^\alpha, \quad x > 0. \end{aligned} \tag{11}$$

Let $\varphi(x) \in L_{2,\alpha}[\mathbb{R}]$ and let

$$\varphi_\omega^{F,\alpha}(\omega) = \frac{1}{\Gamma(1+\alpha)} \int_{-\infty}^{\infty} E_\alpha(-i^\alpha \omega^\alpha x^\alpha) \varphi(x) (dx)^\alpha, \tag{12}$$

$0 < \alpha \leq 1.$

When

$$\varphi_\omega^{F,\alpha}(\omega) = \frac{1}{\Gamma(1+\alpha)} \int_{-\infty}^{\infty} \varphi(x) (dx)^\alpha = 0, \quad 0 < \alpha \leq 1, \tag{13}$$

the function $\varphi(x)$ is called a local fractional wavelet [13].

Let $\varphi(x) \in L_{2,\alpha}[\mathbb{R}]$. Then, we have

$$\begin{aligned} \|\varphi_{a,b,\alpha}(t)\|_{1,\alpha}^2 &= \frac{1}{a^\alpha \Gamma(1+\alpha)} \int_{-\infty}^{\infty} |\varphi_{a,b,\alpha}(t)|^2 (dx)^\alpha \\ &= \frac{1}{\Gamma(1+\alpha)} \int_{-\infty}^{\infty} |\varphi(t)|^2 (dx)^\alpha = \|\varphi\|_{1,\alpha}^2, \end{aligned} \tag{14}$$

so that

$$\varphi_{a,b,\alpha}(t) = \frac{1}{a^{\alpha/2}} \varphi\left(\frac{t-b}{a}\right), \tag{15}$$

where $a, b \in \mathbb{R}$ and $a \neq 0$.

3. Local Fractional Continuous Wavelet Transform

Let $\varphi \in L_{2,\alpha}[\mathbb{R}]$. Then, we arrive at the following relation:

$$\begin{aligned} \|\varphi_{a,b,\alpha}(t)\|_{2,\alpha}^1 &= \frac{1}{a^\alpha \Gamma(1+\alpha)} \int_{-\infty}^{\infty} |\varphi_{a,b,\alpha}(t)|^2 (dt)^\alpha \\ &= \frac{1}{\Gamma(1+\alpha)} \int_{-\infty}^{\infty} |\varphi(t)|^2 (dt)^\alpha = \|\varphi\|_{2,\alpha}^1, \end{aligned} \tag{16}$$

where $\varphi_{a,b,\alpha}(t) = (1/a^{\alpha/2})\varphi((t-b)/a)$, $a, b \in \mathbb{R}$, and $a \neq 0$.

Similarly, we get

$$\|\varphi_{b,\alpha}(t)\|_{2,\alpha}^1 = \|\varphi\|_{2,\alpha}^1. \tag{17}$$

Taking $\varphi_{b,\alpha}(t)$ in place of $\varphi_{a,b,\alpha}(t)E_\alpha(-i^\alpha \omega^\alpha t^\alpha)$, we obtain

$$\begin{aligned} \Theta_{\varphi_{a,b,\alpha}} f(a, b) &= \langle f(t), \varphi_{a,b,\alpha}(t) \rangle \\ &= \frac{1}{\Gamma(1+\alpha)} \int_{-\infty}^{\infty} f(t) \overline{\varphi_{a,b,\alpha}(t)} (dt)^\alpha. \end{aligned} \tag{18}$$

In the special case when $f(t) = 1$, we have the following relation:

$$\Theta_{\varphi_{a,b,\alpha}}(a, b) = \frac{1}{\Gamma(1+\alpha)} \int_{-\infty}^{\infty} \overline{\varphi_{a,b,\alpha}(t)} (dt)^\alpha \tag{19}$$

such that

$$\begin{aligned} &\frac{1}{\Gamma(1+\alpha)} \int_{-\infty}^{\infty} \Theta_{\varphi_{a,b,\alpha}}(a, b) \varphi_{a,b,\alpha}(t) (db)^\alpha \\ &= |a|^\alpha \left[\frac{1}{\Gamma(1+\alpha)} \int_{-\infty}^{\infty} \varphi(t) (dt)^\alpha \right]^2. \end{aligned} \tag{20}$$

Hence, there exists the following relation:

$$\begin{aligned} &\frac{1}{\Gamma^2(1+\alpha)} \iint_{-\infty}^{\infty} a^{-2\alpha} \Theta_{\varphi_{a,b,\alpha}}(a, b) \varphi_{a,b,\alpha}(t) (da)^\alpha (db)^\alpha \\ &= \frac{1}{\Gamma(1+\alpha)} \int_{-\infty}^{\infty} |x|^{-\alpha} (dx)^\alpha. \end{aligned} \tag{21}$$

In general, we also deduce the following identities:

$$\begin{aligned}
 f(x) &= \frac{\int_{-\infty}^{\infty} (|f(x)|^2/|x|^\alpha) (dx)^\alpha}{\Gamma^3(1+\alpha)} \\
 &\times \iint_{-\infty}^{\infty} a^{-2\alpha} \Theta_{\varphi_{a,b,\alpha}} f(a,b) \varphi_{a,b,\alpha}(t) (db)^\alpha (da)^\alpha, \\
 \Theta_{\varphi_{a,b,\alpha}} f(a,b) &= \frac{1}{\Gamma(1+\alpha)} \int_{-\infty}^{\infty} f(t) \overline{\varphi_{a,b,\alpha}(t)} (dt)^\alpha.
 \end{aligned} \tag{22}$$

Now, we establish the following relations:

$$\begin{aligned}
 \Theta_{\varphi_{a,b,\alpha}} \widetilde{f}(a,b) &= \frac{a^{-\alpha/2}}{\Gamma(1+\alpha)} \int_{-\infty}^{\infty} f(t) \overline{\varphi_{a,b,\alpha}(t)} (dt)^\alpha, \\
 &0 < \alpha \leq 1, \\
 f(x) &= \frac{\int_{-\infty}^{\infty} (|f(x)|^2/|x|^\alpha) (dx)^\alpha}{\Gamma^3(1+\alpha)} \\
 &\times \iint_{-\infty}^{\infty} a^{-2\alpha} \Theta_{\varphi_{a,b,\alpha}} \widetilde{f}(a,b) \varphi_{a,b,\alpha} \\
 &\times (t) (da)^\alpha (db)^\alpha.
 \end{aligned} \tag{23}$$

Hence, the local fractional continuous wavelet transform takes the following form (see [13]):

$$W_{\varphi,\alpha} f(a,b) = \frac{a^{-\alpha/2}}{\Gamma(1+\alpha)} \int_{-\infty}^{\infty} f(t) \overline{\varphi_{a,b,\alpha}(t)} (dt)^\alpha, \quad 0 < \alpha \leq 1. \tag{24}$$

And the inversion formula of local fractional continuous wavelet transform is derived as follows (see [14]):

$$\begin{aligned}
 f(x) &= \frac{C_{\varphi,\alpha}}{\Gamma^2(1+\alpha)} \\
 &\times \iint_{-\infty}^{\infty} a^{-2\alpha} W_{\varphi,\alpha} f(a,b) \varphi_{a,b,\alpha}(t) (da)^\alpha (db)^\alpha, \tag{25} \\
 &0 < \alpha \leq 1,
 \end{aligned}$$

where

$$C_{\varphi,\alpha} = \frac{1}{\Gamma(1+\alpha)} \int_{-\infty}^{\infty} \frac{|f(x)|^2}{|x|^\alpha} (dx)^\alpha, \quad 0 < \alpha \leq 1. \tag{26}$$

4. The Wavelet Space

In order to differ the classical wavelets from fractional wavelets, here we formulate a wavelet space as follows. In fact, a wavelet space is defined by

$$\begin{aligned}
 W_{\varphi,\alpha}[\mathbb{R}] &= \left\{ (\varphi, \alpha) : W_{\varphi,\alpha} f(a,b) \right. \\
 &= \left. \frac{a^{-\alpha/2}}{\Gamma(1+\alpha)} \int_{-\infty}^{\infty} f(t) \overline{\varphi_{a,b,\alpha}(t)} (dt)^\alpha, \quad 0 < \alpha \leq 1 \right\}.
 \end{aligned} \tag{27}$$

When the fractal dimension α is equal to 1, from (27), we deduce (see [3–5])

$$\begin{aligned}
 W_{\varphi,1}[\mathbb{R}] &= \left\{ (\varphi, 1) : W_{\varphi,1} f(a,b) \right. \\
 &= \left. a^{-1/2} \int_{-\infty}^{\infty} f(t) \overline{\varphi_{a,b,1}(t)} dt, \quad \alpha = 1 \right\},
 \end{aligned} \tag{28}$$

where $f(t)$ is continuous and $W_{\varphi,1} f(a,b) \in W_{\varphi,1}[\mathbb{R}]$.

Taking the fractal dimension $0 < \alpha < 1$, we derive a formula given by

$$W_{\varphi,\alpha} f(a,b) = \frac{a^{-\alpha/2}}{\Gamma(1+\alpha)} \int_{-\infty}^{\infty} f(t) \overline{\varphi_{a,b,\alpha}(t)} (dt)^\alpha \tag{29}$$

with $W_{\varphi,\alpha} f(a,b) \in W_{\varphi,\alpha}[\mathbb{R}]$, where $f(t)$ is a local fractional continuous function.

5. An Illustrative Example

In order to construct the local fractional continuous wavelet, we suppose that $\phi(t)$ is $m\alpha$ times the local fractional differentiable function.

We define the local fractional wavelet $\varphi(t)$ by means of the following expression:

$$\varphi(t) = \frac{d^{m\alpha} y}{dx^{m\alpha}}, \tag{30}$$

where the differential operator is the local fractional operator proposed by Yang [18] (for other definition, see [19] and the references cited therein).

Then, we get

$$\begin{aligned}
 \frac{1}{\Gamma(1+\alpha)} \int_{-\infty}^{\infty} \varphi(t) \frac{t^{m\alpha}}{\Gamma(1+m\alpha)} (dt)^\alpha \\
 = 0 \quad (m = 0, 1, 2, \dots, m).
 \end{aligned} \tag{31}$$

Let us consider the following nondifferentiable signal, namely,

$$\phi_{H(\alpha)}(t) = \begin{cases} \frac{t^\alpha}{\Gamma(1+\alpha)}, & 0 \leq t < \frac{1}{2}, \\ \frac{(1-t)^\alpha}{\Gamma(1+\alpha)}, & \frac{1}{2} \leq t < 1, \\ 0, & \text{else.} \end{cases} \tag{32}$$

For $0 \leq t < 1/2$, we obtain

$$\frac{d^\alpha \phi_{H(\alpha)}(t)}{dt^\alpha} = \frac{d^\alpha t^\alpha}{dt^\alpha \Gamma(1+\alpha)} = 1. \tag{33}$$

For $1/2 \leq t < 1$, we obtain

$$\frac{d^\alpha \phi_{H(\alpha)}(t)}{dt^\alpha} = \frac{d^\alpha (1-t)^\alpha}{dt^\alpha \Gamma(1+\alpha)} = -1. \tag{34}$$

In view of (33)-(34), we get a local fractional wavelet given by

$$\varphi_{H(\alpha)}(t) = \begin{cases} 1, & 0 \leq t < \frac{1}{2}, \\ -1, & \frac{1}{2} \leq t < 1, \\ 0, & \text{else.} \end{cases} \quad (35)$$

Following (35), we obtain

$$\begin{aligned} \frac{1}{\Gamma(1+\alpha)} \int_{-\infty}^{\infty} \varphi_{H(\alpha)}(t) (dt)^\alpha &= 0, \\ \frac{1}{\Gamma(1+\alpha)} \int_{-\infty}^{\infty} \varphi_{H(\alpha)}^2(t) (dt)^\alpha &= 1. \end{aligned} \quad (36)$$

In view of (15), taking $a = 2^{-j}$ and $b = k2^{-j}$, we have

$$\begin{aligned} \varphi_{a,b,\alpha}(t) &= \frac{1}{a^{\alpha/2}} \varphi\left(\frac{t-b}{a}\right) = \varphi_{j,k,\alpha}(t) \\ &= \varphi_{2^{-j},k2^{-j},\alpha}(t) = 2^{j\alpha/2} \varphi(2^j t - k) \end{aligned} \quad (37)$$

for integers $j, k \in \mathbb{Z}$.

Hence, we get the following equation:

$$\varphi_{H(\alpha)}^{j,k}(t) = 2^{j\alpha/2} \varphi_{H(\alpha)}(2^j t - k). \quad (38)$$

We thus conclude that

$$\begin{aligned} &\frac{1}{\Gamma(1+\alpha)} \int_{-\infty}^{\infty} [\varphi_{H(\alpha)}^{j,k}(t)]^2 (dt)^\alpha \\ &= \frac{1}{\Gamma(1+\alpha)} \int_{-\infty}^{\infty} [2^{j\alpha/2} \varphi_{H(\alpha)}(2^j t - k)]^2 (dt)^\alpha \\ &= 2^{j\alpha} \frac{1}{\Gamma(1+\alpha)} \int_{-\infty}^{\infty} [\varphi_{H(\alpha)}(2^j t - k)]^2 (dt)^\alpha \\ &= \frac{1}{\Gamma(1+\alpha)} \int_{-\infty}^{\infty} [\varphi_{H(\alpha)}(2^j t - k)]^2 (d(2^j t - k))^\alpha \\ &= \frac{1}{\Gamma(1+\alpha)} \int_{-\infty}^{\infty} [\varphi_{H(\alpha)}(t)]^2 (dt)^\alpha \\ &= 1, \\ &\frac{1}{\Gamma(1+\alpha)} \int_{-\infty}^{\infty} \varphi_{H(\alpha)}^{j,k}(t) (dt)^\alpha \\ &= \frac{1}{\Gamma(1+\alpha)} \int_0^{1/2} 2^{j\alpha/2} \varphi_{H(\alpha)}(2^j t - k) (dt)^\alpha \\ &\quad - \frac{1}{\Gamma(1+\alpha)} \int_{1/2}^1 2^{j\alpha/2} \varphi_{H(\alpha)}(2^j t - k) (dt)^\alpha \\ &= 0. \end{aligned} \quad (39)$$

6. Concluding Remarks and Observations

A novel local fractional wavelet transformation was investigated by using Fourier transform based upon local fractional calculus. This transform has been found to be advantageous in dealing with the functions in fractal space. The wave space is considered and an illustrative example is shown.

Conflict of Interests

The authors declare that they have no conflict of interests regarding this paper.

References

- [1] I. Daubechies, "The wavelet transform, time-frequency localization and signal analysis," *IEEE Transactions on Information Theory*, vol. 36, no. 5, pp. 961-1005, 1990.
- [2] R. K. Martinet, J. Morlet, and A. Grossmann, "Analysis of sound patterns through wavelet transforms," *Journal of Pattern Recognition and Artificial Intelligence*, vol. 1, no. 2, pp. 273-302, 1987.
- [3] C. K. Chui, *An Introduction to Wavelets*, Academic Press, San Diego, Calif, USA, 1992.
- [4] L. Debnath, *Wavelet Transforms and Their Application*, Birkhäuser, Boston, Mass, USA, 2002.
- [5] C. Cattani, "Harmonic wavelet solution of Poisson's problem," *Balkan Journal of Geometry and its Applications*, vol. 13, no. 1, pp. 27-37, 2008.
- [6] C. Cattani and J. Rushchitsky, *Wavelet and Wave Analysis as Applied to Materials with Micro or Nanostructure*, World Scientific, 2007.
- [7] D. Mendlovic, Z. Zalevsky, D. Mas, J. García, and C. Ferreira, "Fractional wavelet transform," *Applied Optics*, vol. 36, no. 20, pp. 4801-4806, 1997.
- [8] L. Chen and D. Zhao, "Optical image encryption based on fractional wavelet transform," *Optics Communications*, vol. 254, no. 4-6, pp. 361-367, 2005.
- [9] E. Dinç, F. Demirkaya, D. Baleanu, Y. Kadioglu, and E. Kadioglu, "New approach for simultaneous spectral analysis of a complex mixture using the fractional wavelet transform," *Communications in Nonlinear Science and Numerical Simulation*, vol. 15, no. 4, pp. 812-818, 2010.
- [10] E. Dinç and D. Baleanu, "Fractional wavelet transform for the quantitative spectral resolution of the composite signals of the active compounds in a two-component mixture," *Computers & Mathematics with Applications*, vol. 59, no. 5, pp. 1701-1708, 2010.
- [11] E. Dinç, D. Baleanu, and K. Taş, "Fractional wavelet analysis of the composite signals of two-component mixture by multivariate spectral calibration," *Journal of Vibration and Control*, vol. 13, no. 9-10, pp. 1283-1290, 2007.
- [12] J. Shi, N. Zhang, and X. Liu, "A novel fractional wavelet transform and its applications," *Science China Information Sciences*, vol. 55, no. 6, pp. 1270-1279, 2012.
- [13] X. J. Yang, *Local Fractional Functional Analysis and Its Applications*, Asian Academic publisher, Hong Kong, China, 2011.
- [14] X. J. Yang, D. Baleanu, and J. T. A. Machado, "Mathematical aspects of Heisenberg uncertainty principle within local fractional Fourier analysis," *Boundary Value Problems*, vol. 2013, no. 1, article 131, 2013.
- [15] X. J. Yang and D. Baleanu, "Fractal heat conduction problem solved by local fractional variation iteration method," *Thermal Science*, vol. 17, no. 2, pp. 625-628, 2013.
- [16] A.-M. Yang, X.-J. Yang, and Z.-B. Li, "Local fractional series expansion method for solving wave and diffusion equations on Cantor sets," *Abstract and Applied Analysis*, vol. 2013, Article ID 351057, 5 pages, 2013.

- [17] W.-H. Su, D. Baleanu, X.-J. Yang, and H. Jafari, "Damped wave equation and dissipative wave equation in fractal strings within the local fractional variational iteration method," *Fixed Point Theory and Applications*, vol. 2013, article 89, 2013.
- [18] X. J. Yang, *Advanced Local Fractional Calculus and Its Applications*, World Science, New York, NY, USA, 2012.
- [19] A. A. Kilbas, H. M. Srivastava, and J. J. Trujillo, *Theory and Applications of Fractional Differential Equations*, vol. 204, Elsevier Science, Amsterdam, The Netherlands, 2006.